Numerical methods for dynamic contact and fracture problems

David Doyen

UNIVERSITÉ PARIS-EST

THÈSE

présentée pour l'obtention du titre de

Docteur de l'Université Paris-Est

Spécialité : Mathématiques, Informatique

par **David DOYEN**

Sujet : Méthodes numériques pour des problèmes dynamiques de contact et de fissuration

Soutenue le 2 décembre 2010
devant le jury composé de :

Président :	Jean-Jacques Marigo
Rapporteurs :	Patrick Hild
	Barbara Wohlmuth
Examinateurs :	Thierry Fouquet
	Patrice Hauret
	Yves Renard
Directeurs de thèse :	Alexandre Ern
	Serge Piperno

Méthodes numériques pour des problèmes dynamiques de contact et de fissuration

Résumé : On s'intéresse à la résolution numérique de problèmes de contact et de fissuration en dynamique. Le problème de contact envisagé est le problème de Signorini avec ou sans frottement de Coulomb. Quant au problème de fissuration, il s'agit d'un modèle de zone cohésive avec trajet de fissuration pré-défini. Ces problèmes se caractérisent par la présence d'une condition aux limites non-régulière et se formulent comme des inéquations variationnelles d'évolution ou des inclusions différentielles. Pour les résoudre numériquement, nous combinons, comme il est courant en dynamique des solides, une discrétisation en espace par éléments finis et des schémas d'intégration en temps (de types différences finies). Pour le problème de contact, nous commençons par comparer les principales méthodes proposées dans la littérature. Nous étudions ensuite plus particulièrement la méthode dite de masse modifiée récemment introduite par H. Khenous, P. Laborde et Y. Renard. Nous en proposons une variante semi-explicite. Par ailleurs, nous prouvons un résultat de convergence des solutions semi-discrètes en espace vers une solution continue dans le cas d'un problème de Signorini sans frottement et d'un matériau viscoélastique. Nous analysons également les formulations semi-discrètes en espace et totalement discrètes dans le cas d'un problème de Signorini avec frottement de Coulomb. Pour le problème de fissuration dynamique, la non-régularité de la condition aux limites rend impossible ou peu robuste l'utilisation de schémas totalement explicites. Nous proposons donc des schémas où cette condition aux limites est traitée de façon implicite. Enfin, nous présentons et analysons des méthodes de lagrangien augmenté pour la résolution numérique du problème de fissuration en statique.

Mots-clés : dynamique des solides, contact unilatéral, frottement de Coulomb, modèles de zone cohésive, éléments finis, schémas d'intégration en temps

---

Numerical methods for dynamic contact and fracture problems

Abstract : The present work deals with the numerical solution of dynamic contact and fracture problems. The contact problem is a Signorini problem with or without Coulomb friction. The fracture problem uses a cohesive zone model with a prescribed crack path. These problems are characterized by a non-regular boundary condition and can be formulated with evolutionary variational inequations or differential inclusions. For the numerical solution, we combine, as usual in solid dynamics, a finite element discretization in space and time-integration schemes. For the contact problem, we begin by comparing the main methods proposed in the literature. We then focus on the so-called modified mass method recently introduced by H. Khenous, P. Laborde et Y. Renard, for which we propose a semi-explicit variant. In addition, we prove a convergence result of the space semi-discrete solutions to a continuous solution in the frictionless viscoelastic case. We also analyze the space semi-discrete and fully discrete problems in the friction Coulomb

case. For the dynamic fracture problem, using a fully explicit scheme is impossible or not robust enough. Therefore, we propose time-integration schemes where the boundary condition is treated in an implicit way. Finally, we present and analyze augmented Lagrangian methods for static fracture problems.

Keywords : solid dynamics, unilateral contact, Coulomb friction, cohesive zone models, finite elements, time-integration schemes

Table des matières

1

Introduction

En tant qu'exploitant d'un parc de production électrique, EDF réalise de nombreuses études mécaniques, notamment pour garantir la sûreté et maîtriser la durée de vie de ses installations. Ces études ont naturellement recours à la simulation numérique, ce qui conduit EDF à mener une importante activité de recherche dans le domaine de la mécanique numérique. C'est dans ce contexte industriel que s'inscrit cette thèse.

On s'intéresse à la résolution numérique de deux problèmes. Le premier décrit les déformations d'un solide pouvant entrer en contact avec un obstacle rigide. Le second décrit la fissuration d'un solide le long d'une interface prédéfinie. Ces deux problèmes sont envisagés dans le cadre dynamique, c'est-à-dire que les effets d'inertie ne sont pas négligés. Mathématiquement, le phénomène de contact est représenté par une condition aux limites « non-régulière » sur la frontière du solide. Le phénomène de fissuration introduit une condition aux limites du même genre sur l'interface de fissuration. C'est cette proximité mathématique qui justifie l'étude conjointe de ces deux problèmes. Puisque les modèles de contact et de fissuration que nous étudions sont représentés par des conditions aux limites, on peut les combiner avec différentes lois de comportement

du solide. Par souci de simplicité théorique, mais aussi parce que ces lois sont souvent utilisées en pratique, nous considérons des solides élastiques linéaires ou viscoélastiques linéaires.

L'approche la plus courante pour résoudre un problème de dynamique des solides consiste à combiner une discrétisation spatiale par éléments finis et un schéma d'intégration en temps (de types différences finies). L'application directe de cette approche au problème de contact donne de mauvais résultats : oscillations parasites, mauvais comportement énergétique. Différentes méthodes numériques pour le contact en dynamique ont donc été proposées dans la littérature depuis une vingtaine d'années. Après avoir comparé les principales méthodes (Chapitre 2), nous étudions plus particulièrement la méthode dite de masse modifiée récemment introduite par H. Khenous, P. Laborde et Y. Renard [74, 75]. Nous en proposons une variante semi-explicite (Section 2.7). Nous prouvons un résultat de convergence des solutions semi-discrétisées en espace vers une solution continue dans le cas d'un problème de Signorini sans frottement et d'un matériau viscoélastique (Chapitre 3). Nous analysons également les problèmes semi-discrétisés en espace et totalement discrétisés dans le cas d'un problème de Signorini avec frottement de Coulomb (Chapitre 4). Pour le problème de fissuration dynamique, qui est un phénomène rapide, il semble préférable d'utiliser des schémas en temps explicites, moins coûteux. Malheureusement, la « non-régularité » de la condition aux limites rend impossible ou peu robuste l'utilisation de schémas totalement explicites. Nous proposons donc des schémas où cette condition aux limites est traitée de façon implicite (Chapitre 5). Le Chapitre 6 complète les travaux sur la fissuration, hors du cadre dynamique. Nous y présentons et analysons des méthodes de Lagrangien augmenté pour la résolution numérique du problème de fissuration en statique.

Nous commençons cette introduction avec quelques exemples de problèmes industriels impliquant des phénomènes de fissuration et de contact (Section 1.1). Nous donnons ensuite une formulation mécanique détaillée des modèles étudiés dans cette thèse (Section 1.2). Nous précisons notamment en quoi les conditions aux limites introduites par ces modèles ne sont pas « régulières ». La Section 1.3 introduit quelques outils mathématiques adaptés à l'étude de ces modèles, à savoir les inéquations variationnelles (d'évolution) et les inclusions (différentielles). Dans la Section 1.4, nous abordons la résolution numérique. Après avoir rappelé les méthodes numériques usuelles pour la dynamique des solides linéaires, nous mettons en évidence les difficultés que soulèvent la présence de contact ou d'une interface de fissuration. Un résumé des différents travaux effectués au cours de cette thèse clôt cette introduction (Section 1.5).

1.1 Applications industrielles

Pour commencer, nous présentons deux exemples de problèmes industriels rencontrés par les ingénieurs d'EDF. Le premier concerne l'intégrité des cuves des réacteurs nucléaires et fait intervenir des phénomènes de fissuration dynamique. Le second concerne l'insertion des barres de commande dans un réacteur nucléaire et fait intervenir des phénomènes dynamiques de contact et de frottement.

1.1.1 Cuves des réacteurs nucléaires

EDF exploite actuellement 58 réacteurs nucléaires à eau pressurisée (REP) et souhaite prolonger leur durée d'exploitation. Cette démarche repose sur une meilleure analyse de la durée

de vie des composants sensibles, notamment les cuves des réacteurs. La cuve d'un REP est une

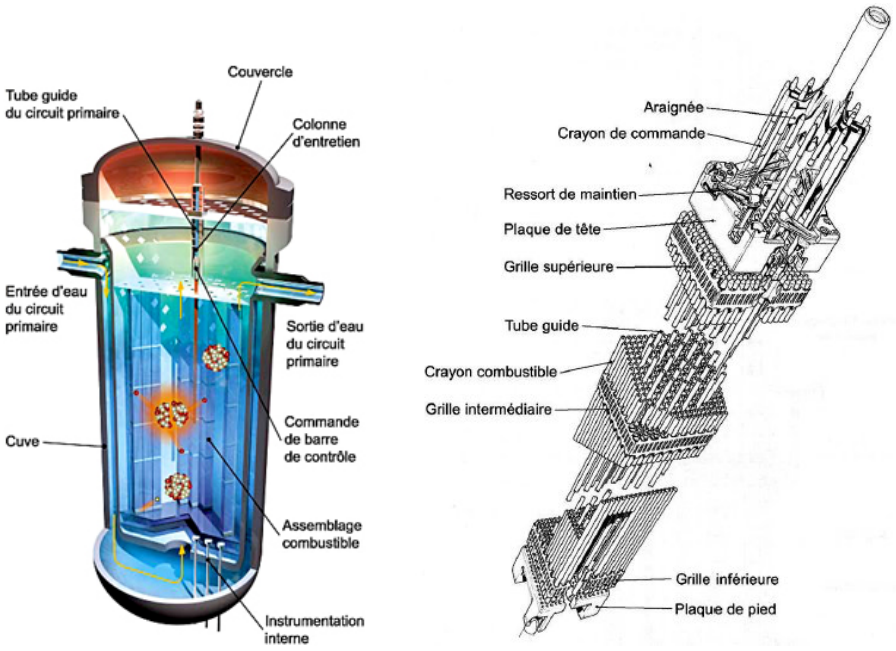

Figure 1.1. Cuve d'un réacteur à eau pressurisée (gauche). Assemblage combustible avec sa grappe de commande (droite). Source : CEA.

enveloppe étanche en acier d'environ 12m de hauteur et 20cm d'épaisseur. Elle contient le cœur du réacteur, les structures de supportage du cœur et les structures de guidage des barres de commande (voir Figure 1.1 à gauche). La cuve n'est pas remplaçable. En fonctionnement, elle est remplie d'eau pressurisée à 300°C. En cas d'accident de perte de refroidissement primaire, il est prévu d'y injecter une grande quantité d'eau froide. Il s'ensuit un choc thermomécanique dans les parois de la cuve, ce qui pourrait provoquer l'amorçage et la propagation dynamique d'une fissure. Pour garantir l'intégrité de la cuve, il est donc important de pouvoir simuler un tel phénomène.

1.1.2 Barres de commande dans un réacteur nucléaire

Les grappes de commandes sont constituées d'une vingtaine de crayons absorbeurs de neutrons. Elles peuvent s'insérer dans les assemblages combustible, qui disposent à cet effet d'emplacements creux occupés par des tubes guides (voir Figure 1.1 à droite). Les tubes guides font environ 4m. On utilise ces grappes de commande pour régler la puissance du réacteur (en les insérant plus ou moins profondément) ou pour arrêter en urgence le réacteur (en les lâchant complètement). Il est essentiel que l'insertion ou la chute des grappes de commande se fasse à la vitesse prévue. En particulier, la chute des barres de commande doit pouvoir se faire en moins de 2s. Les tubes guides n'étant pas parfaitement droits, l'insertion ou la chute des grappes de commande peuvent être ralenties par des phénomènes dynamiques de contact et de

frottement. La simulation numérique de ces phénomènes permet de mieux comprendre l'influence de la déformation du tube guide.

1.2 Modèles mécaniques

Les problèmes étudiés dans cette thèse combinent deux ingrédients : un modèle de dynamique des solides et une condition aux limites qui décrit le phénomène de contact ou de fissuration. Dans cette section, nous commençons par présenter les modèles de dynamique des solides utilisés, à savoir le modèle élastique linéaire et le modèle viscoélastique linéaire de type Kelvin-Voigt. Puis nous présentons les modèles de contact unilatéral et de frottement de Coulomb, ainsi que les modèles de zone cohésive. Nous précisons en quoi les conditions aux limites introduites par ces modèles ne sont pas « régulières ».

1.2.1 Elastodynamique et viscoélastodynamique linéaire

On se place dans le cadre des petits déplacements. On considère un solide occupant le domaine $\Omega \subset \mathbb{R}^d$ ($d = 2$ ou $d = 3$) durant un intervalle de temps $[0, T]$ (voir Figure 1.2). Le principe fondamental de la dynamique s'écrit :

$$\rho\ddot{u} - \operatorname{div}\sigma = f \quad \text{dans } \Omega \times (0,T), \tag{1.1}$$

où ρ désigne la densité de masse, u le déplacement, σ le champ de contrainte, f les forces volumiques extérieures et les points les dérivées temporelles. La frontière $\partial\Omega$ est divisée en deux parties disjointes Γ^D et Γ^N, où sont imposées, respectivement, des conditions de Dirichlet et de Neumann :

$$u = u_D \quad \text{sur } \Gamma^D \times (0,T), \qquad \sigma \cdot \nu = f_N \quad \text{sur } \Gamma^N \times (0,T), \tag{1.2}$$

où ν désigne la normale extérieure à $\partial\Omega$, alors que u_D et f_N sont des données. On prescrit les conditions initiales suivantes :

$$u(0) = u_0, \quad \dot{u}(0) = v_0 \quad \text{sur } \Omega. \tag{1.3}$$

Le tenseur des déformations linéarisées s'écrit :

$$\epsilon = \frac{1}{2}(\nabla u + {}^{\mathrm{T}}\nabla u). \tag{1.4}$$

On suppose que le solide a un comportement viscoélastique linéaire de type Kelvin-Voigt si bien que le tenseur des contraintes est relié au tenseur des déformations par l'expression :

$$\sigma = \mathcal{A} : \epsilon + \mathcal{B} : \dot{\epsilon}, \tag{1.5}$$

où $\mathcal{A}$ est le tenseur d'élasticité et $\mathcal{B}$ est le tenseur de viscosité. Si le tenseur de viscosité est nul, on parle de matériau purement élastique. On peut définir l'énergie totale du solide à l'instant t comme la somme de l'énergie cinétique et de l'énergie élastique :

$$E(t) = \frac{1}{2}\int_\Omega \rho|\dot{u}(t)|^2 + \frac{1}{2}\int_\Omega \epsilon(t) : \mathcal{A} : \epsilon(t). \tag{1.6}$$

Un matériau purement élastique et un matériau viscoélastique ont des comportements assez différents. Dans un matériau purement élastique, l'énergie se conserve (en l'absence de forces extérieures) et il peut y avoir des ondes de choc, c'est-à-dire des discontinuités de vitesse et de contrainte. Au contraire, dans un matériau viscoélastique, il y a une dissipation de l'énergie et les chocs sont lissés.

Dans un matériau isotrope, le tenseur d'élasticité peut s'exprimer à l'aide de deux paramètres seulement : le module de Young E et le coefficient de Poisson ν_P. On définit alors des vitesses caractéristiques associées aux ondes de compression (*dilatational waves*) et de cisaillement (*shear waves*),

$$c_d = \sqrt{\frac{E(1-\nu_P)}{\rho(1+\nu_P)(1-2\nu_P)}}, \qquad c_s = \sqrt{\frac{E}{2\rho(1+\nu_P)}}. \tag{1.7}$$

À titre d'exemple, dans un acier ($E = 200$ GPa, $\nu = 0.3$, $\rho = 8000$ kg·m^{-3}) les ondes de compression se propagent à environ 5 800 m·s^{-1} et les ondes de cisaillement à 3 100 m·s^{-1}.

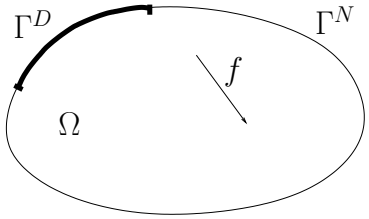

Figure 1.2. Dynamique linéaire des solides. Domaine Ω.

Remarque 1.1. *L'équation (1.1) est l'équation générale de la dynamique des solides. Quand on néglige le terme d'inertie $\rho\ddot{u}$ dans cette équation, on parle de problème statique (lorsque les données et les lois de comportement sont indépendantes du temps) ou quasi-statique (lorsque celles-ci dépendent du temps).*

1.2.2 Contact unilatéral

Il existe une grande variété de problèmes de contact sur le plan géométrique : contact entre plusieurs corps, contact en grandes déformations, auto-contact, etc... De même il existe différentes lois de contact : contact unilatéral, contact *compliant*, contact avec frottement, érosion, etc... Pour une présentation des différents problèmes de contact, on renvoie par exemple à Kikuchi & Oden [76] ou à Wriggers [124]. Dans cette thèse, nous considérons le problème dit de Signorini, qui décrit le contact unilatéral d'un solide déformable et d'un obstacle rigide dans le cadre des petits déplacements. Dans certains cas, nous ajoutons également du frottement de Coulomb. Le contact unilatéral prescrit les conditions suivantes :

- le solide ne peut pénétrer l'obstacle ;
- quand le corps n'est pas en contact avec l'obstacle, il ne subit aucune pression de la part de l'obstacle ;

– quand le corps est en contact avec l'obstacle, il subit une pression de la part de l'obstacle qui tend à le comprimer.

Puisque l'on est dans le cadre des petits déplacements, il est raisonnable de fixer *a priori* en chaque point de la frontière la direction selon laquelle peut avoir lieu le contact avec l'obstacle (on choisit généralement la normale à la frontière du solide). L'écart à l'obstacle est alors le déplacement du solide dans cette direction moins la distance initiale à l'obstacle selon cette direction. Cette condition linéarisée de contact unilatéral est appelée condition de Signorini. Pour une discussion plus détaillée, nous renvoyons à [76]. Le frottement de Coulomb prescrit les conditions suivantes :

– il n'y a pas de glissement du solide le long de l'obstacle tant que la contrainte tangentielle est strictement inférieure à un certain seuil ;
– quand la contrainte tangentielle atteint ce seuil, il y a glissement dans la direction opposée à cette contrainte ;
– ce seuil dépend de la pression de contact.

Les conditions de contact unilatéral et de frottement de Coulomb sont illustrées sur la Figure 1.3.

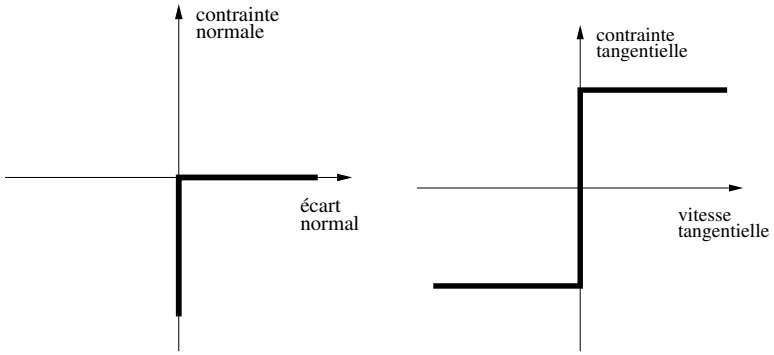

Figure 1.3. Contact unilatéral et frottement de Coulomb.

Formulons maintenant précisément le problème de Signorini avec frottement de Coulomb. On considère un solide viscoélastique occupant le domaine $\Omega \subset \mathbb{R}^d$ durant un intervalle de temps $[0,T]$ (Figure 1.4). La frontière $\partial\Omega$ est divisée maintenant en trois parties disjointes Γ^D, Γ^N et $\Gamma^{\rm c}$. Comme précédemment, des conditions de Dirichlet et de Neumann sont imposées sur Γ^D et Γ^N. Sur $\Gamma^{\rm c}$, on impose le contact unilatéral et le frottement de Coulomb. On note $u_\nu := u_{|\partial\Omega} \cdot \nu$ et $u_\tau := u_{|\partial\Omega} - u_\nu \nu$ les déplacements normal et tangentiel sur $\partial\Omega$. On note $\sigma_\nu(u) := \nu \cdot \sigma(u)_{|\partial\Omega} \cdot \nu$ et $\sigma_\tau(u) := \sigma(u)_{|\partial\Omega} \cdot \nu - \sigma(u)_\nu \nu$ les contraintes normale et tangentielle sur $\partial\Omega$. Remarquons que u_ν et $\sigma_\nu(u)$ sont des scalaires tandis que u_τ et $\sigma_\tau(u)$ sont des vecteurs de $\mathbb{R}^d$. Le problème de Signorini avec frottement de Coulomb consiste à chercher un champ de déplacement u vérifiant (1.1)-(1.5) et

$$u_\nu \le g, \quad \sigma_\nu(u) \le 0, \quad \sigma_\nu(u)(u_\nu - g) = 0 \qquad \text{sur } \Gamma^{\rm c} \times (0,T), \tag{1.8}$$

$$|\sigma_\tau(u)| \le \mu |\sigma_\nu(u)| \qquad \text{sur } \Gamma^{\rm c} \times (0,T), \tag{1.9}$$

$$\sigma_\tau(u) = -\mu |\sigma_\nu(u)| \frac{\dot{u}_\tau}{|\dot{u}_\tau|} \quad \text{si } \dot{u}_\tau \neq 0 \qquad \text{sur } \Gamma^{\rm c} \times (0,T), \tag{1.10}$$

où g est l'écart initial à l'obstacle, μ est le coefficient de frottement et $|\cdot|$ est la norme euclidienne.

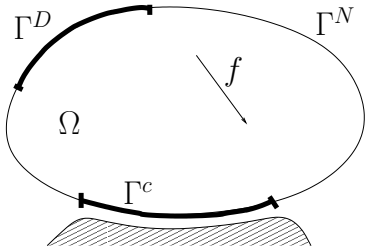

Figure 1.4. Problème de Signorini. Domaine Ω.

La condition de contact unilatéral (1.8) n'est pas une condition aux limites classique comme une condition de Dirichlet ou de Neumann. Elle s'écrit comme une alternative. Sur la partie de la frontière où il y a contact, elle est équivalente à une condition de Dirichlet, tandis que sur la partie où il n'y a pas contact, elle est équivalente à une condition de Neumann. Bien entendu, on ne connaît pas à l'avance la partie de la frontière où il y a contact. Dans son article fondateur sur l'étude mathématique du contact unilatéral [47], G. Fichera parle d'ailleurs de « *ambigue condizioni al contorno* ». On peut également formaliser la condition de contact unilatéral à l'aide d'une fonction multivaluée, c'est-à-dire une fonction qui associe à une variable un ensemble de valeurs (zéro, une ou plusieurs). En effet, quand l'écart à l'obstacle est négatif, il n'y a aucune contrainte admissible ; quand l'écart est nul, toutes les contraintes négatives sont admissibles ; quand l'écart est positif, seule une contrainte nulle est admissible. La contrainte est donc reliée à l'écart à l'obstacle par une fonction multivaluée. De la même manière, les conditions de frottement de Coulomb (1.9)-(1.10) s'écrivent comme une alternative ou à l'aide d'une fonction multivaluée.

Remarque 1.2. *On parle de contact unilatéral par opposition au contact bilatéral. Deux corps en contact bilatéral ne peuvent se séparer, ils peuvent seulement glisser l'un contre l'autre.*

Remarque 1.3. *Dans le modèle de frottement de Coulomb, le seuil de glissement dépend de la pression de contact. Il existe un modèle de frottement plus simple dans lequel le seuil de frottement est fixé à l'avance, c'est le modèle de Tresca.*

1.2.3 Modèles de zone cohésive

Les mécanismes physiques mis en jeu dans les phénomènes de fissuration (voir un essai de fissuration à la Figure 1.5) varient selon le type de matériau et le type de sollicitation. Dans tous les cas, il s'agit d'un phénomène complexe. Par exemple, lors de la fissuration dynamique d'un acier, on observe en pointe de fissure des micro-fissures, des phénomènes de plasticité, de l'échauffement. En général, les modèles ne décrivent pas à ce niveau de détails les processus qui conduisent à la création de la fissure. Le phénomène de fissuration est réduit à une loi ou à un critère assez simple et est caractérisé par un ou deux paramètres. Parmi les grands familles de modèles, citons :

- les modèles à critère de propagation (Lawn [90], Bui [19])
- les modèles de zone cohésive (Elices et al. [43]),
- les modèles de type endommagement volumique (Mazars [96]),
- et les modèles variationnels (Bourdin, Francfort & Marigo [12]).

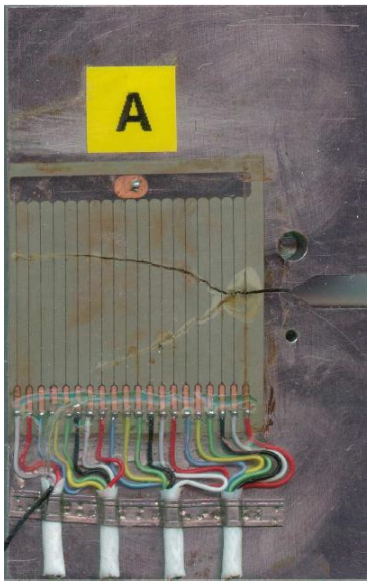

Figure 1.5. Essai de fissuration. L'éprouvette d'acier est équipée d'une jauge électrique pour mesurer l'avancée de la fissure (la fissure coupe les différents fils de la jauge au cours de son avancée). Dans cet essai, la fissure s'est initiée à partir de l'entaille (située à droite) et s'est rapidement divisée en deux branches. Source : EDF.

Ici, nous considérons un modèle de fissuration reposant sur deux hypothèses. 1. La fissure ne peut apparaître que le long d'une surface connue à l'avance (interface de fissuration). 2. le processus de séparation le long de l'interface obéit à un modèle de zone cohésive. Le fait de définir à l'avance la surface où le matériau peut fissurer peut apparaître comme une restriction importante du modèle. Néanmoins, cette hypothèse est raisonnable pour de nombreuses applications (petite propagation de fissure, fissure à l'interface entre deux matériaux). De plus, les modèle de fissuration s'affranchissant de cette hypothèse ne sont pas encore, à notre avis, suffisamment robustes, notamment pour des applications industrielles. Les modèles de zone cohésive sont utilisés pour une large gamme de matériaux (béton, acier, etc...) et de types de fissuration (rupture fragile, rupture ductile, fatigue, rupture dynamique). Un des intérêts de ces modèles est qu'ils peuvent être facilement enrichis avec d'autres phénomènes physiques (corrosion, contact et frottement après décohésion). De plus, ces modèles se combinent plutôt bien avec des méthodes d'éléments finis. Pour toutes ces raisons, ces modèles sont largement utilisés dans les codes de calcul. Les modèles de zone cohésive relient les contraintes mécaniques à l'interface au saut de déplacement à l'interface. Typiquement, un modèle de zone cohésive prescrit les conditions suivantes :

- le saut de déplacement normal à l'interface est positif ou nul ;
- la séparation intervient seulement après qu'un seuil critique a été atteint ;
- quand la séparation se produit, il reste des forces cohésives qui décroissent avec l'ouverture et finissent par s'annuler.

Ces conditions sont illustrées sur la Figure 1.6. Les phénomènes de fissuration sont généralement irréversibles ; une fois qu'un matériau est fissuré, il ne se recolle pas ! On peut introduire cette irréversibilité en faisant dépendre la loi cohésive de l'ouverture maximale passée. Dans le cas dynamique, les simulations numériques avec des modèles dépendant uniquement de l'ouverture donnent des vitesses de propagation de la fissure bien supérieures à celles observées dans les expériences. Pour mieux rendre compte des expériences, on peut faire dépendre la loi cohésive

de la vitesse d'ouverture comme cela est proposé par Zhou, Molinari & Shioya [126]. Dans le Chapitre 5, nous considérons un modèle de zone cohésive qui dépend de l'ouverture, de l'ouverture maximale passée et de la vitesse d'ouverture. Dans le Chapitre 6, nous considérons un modèle qui dépend seulement de l'ouverture.

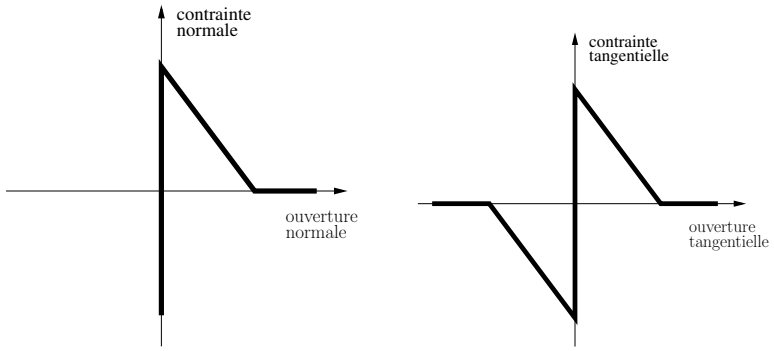

Figure 1.6. Un modèle de zone cohésive.

Formulons maintenant précisément le problème de fissuration. On considère un solide viscoélastique occupant le domaine $\Omega \subset \mathbb{R}^d$ durant un intervalle de temps $[0,T]$ (Figure 1.7). La frontière $\partial\Omega$ est divisée en deux parties disjointes Γ^D et Γ^N. Des conditions de Dirichlet et de Neumann sont imposées sur Γ^D et Γ^N. On considère aussi une interface de fissuration Γ, qui est une surface régulière de dimension $d-1$ incluse dans Ω. Sur Γ on impose un modèle de zone cohésive. On peut fixer une orientation et définir un côté positif et un côté négatif. La trace d'un champ de déplacement v sur le côté positif est notée v^+, celle sur le côté négatif est notée v^-. On note ν le vecteur normal à Γ pointant vers le côté positif. Le saut à l'interface est défini comme $[\![v]\!] := v^+ - v^-$. Le problème de fissuration consiste à chercher un champ de déplacement u vérifiant (1.1)-(1.5) et

$$\sigma^- \cdot \nu = -\sigma^+ \cdot \nu =: \lambda, \tag{1.11}$$

$$\lambda \in R_\Gamma([\![u]\!]), \tag{1.12}$$

où R_Γ est l'opérateur multivalué qui donne la force cohésive.

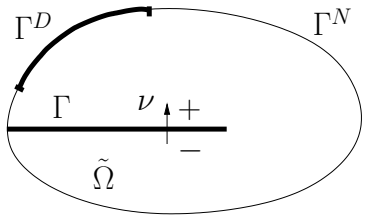

Figure 1.7. Problème de fissuration. Domaine Ω.

1.3 Cadre mathématique

Pour étudier mathématiquement les problèmes de contact et de fissuration décrits précédemment, on dispose essentiellement de deux outils : les inclusions et les inéquations variationnelles. L'objet de cette partie est d'introduire ces deux concepts et de donner quelques résultats de la littérature sur l'existence et l'unicité pour les problèmes de contact et de fissuration.

1.3.1 Contact unilatéral

Nous commençons par étudier le problème de Signorini en élastostatique. On définit $V := \{v \in H^1(\Omega)^d;\ v = 0 \text{ sur } \Gamma^D\}$ l'espace des déplacements admissibles, et $K := \{v \in V;\ v_n \geq g\}$, le sous-ensemble des déplacements vérifiant la condition de non-interpénétration avec l'obstacle. L'espace V est un espace de Hilbert et l'ensemble K est convexe. On définit la forme bilinéaire et la forme linéaire suivantes,

$$a : V \times V \ni (v, w) \longmapsto \int_\Omega \epsilon(v) : \mathcal{A} : \epsilon(w),$$
$$l : V \ni v \longmapsto \int_\Omega f \cdot v + \int_{\Gamma^N} f_N \cdot v.$$

À ces formes bilinéaire et linéaire, on associe, grâce au théorème de Riesz, l'opérateur $A : V \to V$ et le vecteur $L \in V$ tels que

$$(Av, w) = a(v, w) \quad \forall (v, w) \in V \times V,$$
$$(L, v) = l(v), \quad \forall v \in V,$$

où $(\cdot, \cdot)$ désigne le produit scalaire de V. Pour décrire le contact, on introduit la fonctionnelle

$$I_K(v) = \begin{cases} 0 & \text{si } v \in K, \\ +\infty & \text{si } v \notin K. \end{cases}$$

Cette fonctionnelle n'est pas différentiable. Cependant, elle est convexe et on peut donc définir son sous-gradient [1] $\partial I_K : K \to \mathcal{P}(V)$ défini comme

$$\partial I_K(v) := \{g \in V;\ 0 \geq (g, w - v)\ \forall w \in K\}. \tag{1.14}$$

Quand v appartient à l'intérieur de K, $\partial I_K(v)$ est réduit au singleton $\{0\}$. Quand v appartient à la frontière de K, $\partial I_K(v)$ est le cône normal extérieur à K. Quand v n'appartient pas à K, $\partial I_K(v)$ n'est pas défini. Notons que l'opérateur ∂I_K est monotone [2].

1. Soit V un espace de Hilbert muni du produit scalaire $(\cdot, \cdot)$. Soit $J : V \to \mathbb{R} \cup \{+\infty\}$ une fonction convexe et $D(J) := \{v \in V;\ J(v) < +\infty\}$ son domaine. On définit le sous-gradient de J comme l'application multivaluée $\partial J : D(J) \to \mathcal{P}(V)$ telle que

$$\forall v \in D(J), \quad \partial J(v) := \{\gamma \in V;\ J(w) - J(v) \geq (\gamma, w - v),\ \forall w \in D(J)\}, \tag{1.13}$$

où $\mathcal{P}(V)$ désigne l'ensemble des parties de V.

2. Soit V un espace de Hilbert muni du produit scalaire $(\cdot, \cdot)$. Un opérateur multivalué $P : D(P) \to \mathcal{P}(V)$ ($D(P)$ désigne le domaine de P) est dit monotone si pour tout $x_1,\ x_2 \in D(V)$, $(y_1 - y_2, x_1 - x_2) \geq 0, \quad \forall y_1 \in P(x_1),\ \forall y_2 \in P(x_2)$.

On peut formuler le problème de Signorini statique comme une inclusion ou une inéquation variationnelle.

Problème 1.1 (Inclusion). Chercher $u \in K$ tel que

$$Au - L + \partial I_K(u) \ni 0. \tag{1.15}$$

Le membre de gauche est à comprendre comme l'ensemble $\partial I_K(u)$ translaté par le vecteur $Au-L$.

Problème 1.2 (Inéquation variationnelle). Chercher $u \in K$ tel que

$$a(u, v-u) \geq l(v-u), \quad \forall v \in K. \tag{1.16}$$

Ces deux formulations sont équivalentes. De plus, une solution de ces problèmes vérifie au sens faible le problème de Signorini [76]. On peut montrer que ces problèmes admettent une et une seule solution en utilisant le théorème de Stampacchia (voir Brézis [15]), qui est l'analogue du théorème de Lax-Milgram pour les inéquations, ou la théorie des opérateurs monotones (voir Brézis [14]). Il existe une troisième façon équivalente d'écrire le problème de Signorini, à savoir sous la forme d'une minimisation.

Problème 1.3 (Minimisation). Chercher u tel que

$$u = \arg\min_{v \in V} \frac{1}{2} a(v,v) - l(v) + I_K(v), \tag{1.17}$$

ou, ce qui est équivalent,

$$u = \arg\min_{v \in K} \frac{1}{2} a(v,v) - l(v). \tag{1.18}$$

L'inclusion (1.15) et l'inéquation variationnelle (1.16) sont en effet les conditions d'optimalité des problèmes de minimisation (1.18) et (1.17). Avec cette nouvelle formulation, on obtient une autre façon de montrer l'existence et l'unicité d'une solution. Il s'agit en effet de la minimisation d'une fonctionnelle strictement convexe sur un ensemble convexe (voir Brézis [15] ou Ekeland & Temam [42]).

Les inclusions et les inéquations se généralisent aux problèmes en temps. On parle alors d'inclusions différentielles et d'inéquations d'évolution. On peut mettre sous cette forme le problème de Signorini élastodynamique.

Problème 1.4. Chercher u tel que $u(t) \in K$ pour tout $t \in [0,T]$ et

$$\rho \ddot{u}(t) + Au(t) - L(t) + \partial I(u(t)) \ni 0, \quad \text{p.p. sur } (0,T), \tag{1.19}$$

avec $u(0) = u_0$, $\dot{u}(0) = v_0$.

Problème 1.5. Chercher u tel que $u(t) \in K$ pour tout $t \in [0,T]$ et

$$\langle \rho \ddot{u}(t), v \rangle + a(u(t), v-u(t)) \geq l(t, v-u(t)), \quad \forall v \in K, \text{ p.p. sur } (0,T), \tag{1.20}$$

avec $u(0) = u_0$, $\dot{u}(0) = v_0$.

Par souci de simplicité, nous sommes restés assez vagues sur le cadre fonctionnel des formulations (1.19) et (1.20), notamment sur la régularité de l'accélération. Ces problèmes ont été posés dès les années 1960, mais l'existence et l'unicité d'une solution restent des problèmes ouverts (sauf dans le cas d'un domaine 1D). En ajoutant un terme de viscosité de type Kelvin-Voigt, on peut montrer l'existence d'une solution, mais pas l'unicité. On trouvera une revue des résultats d'existence sur les problèmes de contact en dynamique dans Eck, Jarušek & Krbec [41].

1.3.2 Autres modèles

Le frottement de Coulomb et les modèles de zone cohésive se formulent également avec des inclusions ou des inéquations. Notons que l'opérateur qui décrit le frottement de Coulomb n'est pas monotone et ne dérive pas d'une énergie. L'opérateur qui décrit la zone cohésive n'est pas non plus monotone. Beaucoup de modèles de zone cohésive dérivent d'une énergie, mais cette énergie n'est jamais convexe. On peut résumer les caractéristiques mathématiques des différents modèles dans le Tableau 1.1.

Modèle	contact unilatéral	frottement de Tresca	frottement de Coulomb	zone cohésive
Energie	convexe	convexe	pas d'énergie associée	non-convexe
Opérateur	monotone	monotone	non-monotone	non-monotone

Tableau 1.1. Caractéristiques mathématiques des modèles

Remarque 1.4. *De nombreux problèmes issus de la mécanique, de la physique ou de la finance peuvent s'écrire mathématiquement comme des inéquations variationnelles ou des inclusions : plasticité [40], asservissement thermique [40], problème de Stefan [78], pricing d'options américaines [71], etc... De manière générale, les systèmes gouvernés par des lois qui changent quand un seuil est atteint ou dépassé peuvent s'écrire ainsi.*

1.4 Résolution numérique

Nous abordons maintenant la résolution numérique des modèles de contact et de zone cohésive. Nous commençons par rappeler les méthodes numériques usuelles pour la dynamique des solides linéaires. Pour une présentation plus complète, on renvoie à Hughes [70]. Puis nous mettons en évidence les difficultés que soulèvent la présence de contact ou d'une interface de fissuration.

1.4.1 Elastodynamique linéaire

Pour résoudre les problèmes de dynamique linéaire, on combine généralement une discrétisation par éléments finis et un schéma d'intégration en temps. Par simplicité, nous restreignons la discussion au cas de l'élastodynamique. Commençons par discrétiser le problème en espace. On obtient le système d'équations différentielles ordinaires :

$$M\ddot{u}(t) + Ku(t) = L(t), \quad \forall t \in]0,T[, \tag{1.21}$$

où M est la matrice de masse, K la matrice de rigidité, et $L(t)$ le vecteur des forces extérieures. Le système différentiel (1.21) est un système linéaire du second ordre. On peut le résoudre par des méthodes de différences finies qu'on appelle schémas d'intégration en temps. Pour ce faire, l'intervalle de temps est subdivisé en pas de temps de longueur Δt, pris constant pour simplifier. On pose $t^n := n\Delta t$. On note u^n, $\dot{u}^n$, $\ddot{u}^n$, les approximations respectives de $u(t^n)$, $\dot{u}(t^n)$, $\ddot{u}(t^n)$. Il existe de nombreuses méthodes pour résoudre les équations différentielles. En élastodynamique, on utilise le plus souvent des méthodes linéaires à un pas. À chaque pas de temps, il faut donc trouver u^{n+1}, $\dot{u}^{n+1}$ et $\ddot{u}^{n+1}$ tels que

$$M\ddot{u}^{n+1} + Ku^{n+1} = L(t^{n+1}), \tag{1.22}$$

$$u^{n+1} = \alpha\ddot{u}^{n+1} + \Psi_\alpha(u^n, \dot{u}^n, \ddot{u}^n), \tag{1.23}$$

$$\dot{u}^{n+1} = \beta\ddot{u}^{n+1} + \Psi_\beta(\dot{u}^n, \ddot{u}^n). \tag{1.24}$$

Quand $\alpha = \beta = 0$, on dit que le schéma est explicite. Autrement, on parle de schéma implicite. Dans un schéma implicite, à chaque pas de temps on doit résoudre un système linéaire. Dans un schéma explicite, si la matrice de masse standard est remplacée par une approximation diagonale (matrice condensée), le coût du système linéaire à résoudre devient négligeable. Un schéma explicite est donc beaucoup moins coûteux. On dit qu'un schéma est inconditionnellement stable s'il est stable pour n'importe quel pas de temps, aussi grand soit-il. Il n'existe pas de schéma linéaire explicite et inconditionnellement stable. Dans le cas de l'élastodynamique linéaire, la condition de stabilité des schémas explicites est de la forme $\Delta t \leq C c_d \Delta x$, où Δx est le diamètre du plus petit élément du maillage, c_d une vitesse caractéristique (ici la vitesse des ondes de compression) et C est une constante numérique. Cette condition est appelée condition de Courant-Friedrichs-Lewy (condition CFL). Ainsi, les schémas explicites sont plutôt adaptés aux problèmes où le phénomène d'intérêt est rapide (et où le maillage ne contient pas d'éléments trop petits). Pour une analyse plus complète des schémas en temps pour l'élastodynamique (stabilité, ordre de convergence), on renvoie, entre autres, à Raviart & Thomas [106].

L'élastodynamique décrit un phénomène vibratoire. Il est donc parfois pratique d'adopter un point de vue spectral. On introduit alors les modes propres et les fréquences propres associés à l'opérateur de l'élastodynamique (ou à sa discrétisation en espace). Les modes propres associés aux hautes fréquences du problème continu sont très mal approchés par le problème discrétisé en espace. Avec un point de vue spectral, on peut caractériser plus finement l'erreur commise par un schéma en temps [70, §9.1.3]. On dit qu'un schéma est dispersif quand il modifie les fréquences propres par rapport à celles du problème semi-discrétisé en espace. On dit qu'il est dissipatif quand il introduit un amortissement artificiel. Puisque les hautes fréquences sont mal représentées dans le problème discrétisé en espace, il est parfois intéressant d'avoir des schémas dissipatifs dans les hautes fréquences.

Le problème (1.21) n'est pas un système différentiel quelconque dans la mesure où il jouit de plusieurs propriétés remarquables. En l'absence de force extérieure et de conditions de Dirichlet, il conserve une énergie, la quantité de mouvement, le moment angulaire ; de plus, son flot est symplectique. Il est souvent préférable de choisir des schémas qui possèdent de telles propriétés. Cela assure notamment un meilleur comportement en temps long (voir Hairer, Lubich & Wanner [59]).

Parmi les schémas en temps les plus utilisés en dynamique des solides, on trouve les schémas de Newmark, les schémas HHT, le schéma du point-milieu, le schéma des différences centrées, les schémas de Chung-Hulbert, les schémas de Tchamwa-Wielgosz. Leurs caractéristiques principales sont résumées dans le Tableau 1.2.

Newmark (trapèze)	Point-milieu	HHT	Différences centrées	Chung-Hulbert	Tchamwa-Wielgosz
2nd ordre	2nd ordre	2nd ordre	2nd ordre	2nd ordre	1er ordre
implicite	implicite	implicite	explicite	explicite	explicite
stable	stable	stable	stable sous CFL	stable sous CFL	stable sous CFL
conservatif	conservatif	dissipatif	quasi-conservatif	dissipatif	dissipatif

Tableau 1.2. Schémas en temps usuels pour la dynamique des solides.

1.4.2 Contact unilatéral et frottement de Coulomb

Comme on vient de le voir dans la section 1.4.1, la semi-discrétisation en espace du problème de l'élastodynamique linéaire aboutit à un système d'équations différentielles ordinaires. En présence de contact unilatéral, le situation se complique. Considérons par exemple l'impact d'une barre unidimensionnelle contre un sol rigide. La vitesse initiale de la barre est uniforme et notée v_0. On ne tient pas compte de la gravité. Discrétisons la barre avec un unique élément fini linéaire (Figure 1.8). On obtient un système à 4 degrés de liberté (vitesse et position des points A et B). Jusqu'à l'impact, à l'instant t_i, le mouvement du système est déterminé de manière unique. En particulier, $v_A = v_B = v_0$. Après l'impact (instant t_i^+), le point B peut s'immobiliser ou repartir avec n'importe quelle vitesse positive. Dans tous les cas, les conditions de Signorini auront été respectées. Pour sélectionner une solution, il faut introduire une loi supplémentaire, une loi qui donne la vitesse avec laquelle repart un point après un impact.

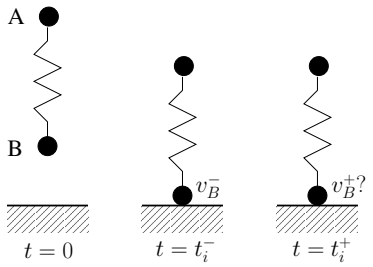

Figure 1.8. Impact d'une barre élastique.

Si l'on ne tient pas compte de cette loi d'impact et que l'on discrétise naïvement en temps le problème, on s'expose à quelques désagréments. Par exemple, si l'on considère les cas tests de l'impact d'une barre contre un obstacle rigide ou des rebonds de cette barre (ces cas tests seront amplement décrits au Chapitre 2), on observe des oscillations parasites durant les phases de contact (Figure 1.9 à gauche) et une mauvaise conservation de l'énergie (Figure 1.10 à gauche). Pour surmonter ces problèmes, de nombreuses solutions ont été proposées dans la littérature depuis une vingtaine d'années.

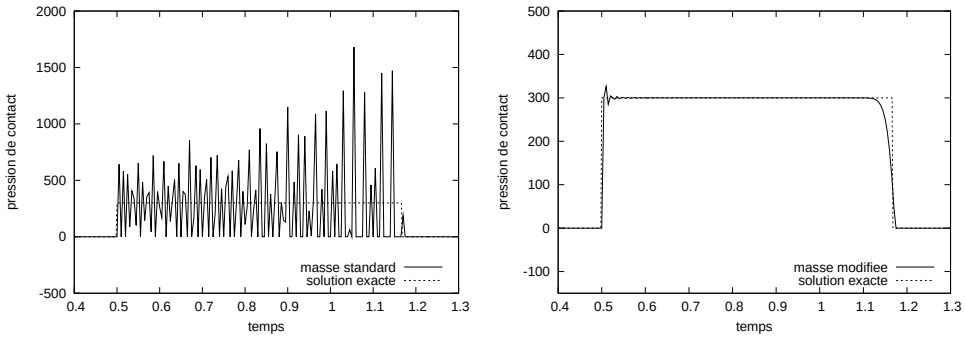

Figure 1.9. Simulation numérique de l'impact d'une barre élastique. Pression de contact. Schéma de Newmark avec masse standard (gauche) et avec masse modifiée (droite).

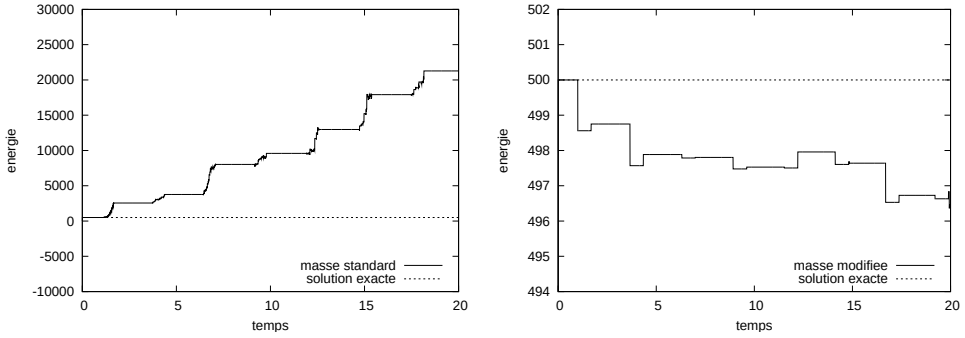

Figure 1.10. Simulation numérique des rebonds d'une barre élastique. Evolution de l'énergie. Schéma de Newmark avec masse standard (gauche) et avec masse modifiée (droite). Avec la masse standard, la situation se dégrade considérablement après plusieurs rebonds.

La méthode de masse modifiée apparaît comme l'une des méthodes les plus performantes pour les problèmes de contact unilatéral en dynamique. Introduite dans Khenous, Laborde & Renard [74, 75] pour les problèmes de contact sans frottement, elle repose sur une formulation semi-discrète en espace dans laquelle la matrice de masse a été modifiée. Dans sa version la plus simple, les coefficients de la matrice de masse associés aux déplacements (normaux) à la frontière de contact sont mis à zéro. Le problème semi-discrétisé en espace est équivalent à un système d'équations différentielles ordinaires lipschitzien et est, par conséquent, bien posé [75]. La variation d'énergie est égale au travail des forces extérieures ; les forces de contact ne travaillent pas [75]. Le problème semi-discret peut ensuite être discrétisé en temps avec divers schémas d'intégration. La méthode élimine les oscillations parasites (Figure 1.9 à droite). De plus, avec un schéma convenable comme le schéma de Newmark (méthode du trapèze), un bon comportement énergétique et un bon comportement en temps long sont observés (Figure 1.10 à droite). Enfin, soulignons que cette méthode ne nécessite ni étape de calcul supplémentaire ni paramètres supplémentaires. La méthode de masse modifiée a depuis été appliquée à des problèmes de contact avec frottement (Hager, Hüeber & Wohlmuth [57, 58]). D'autres façons de construire la matrice de masse modifiée ont également été proposées. Il est en effet intéressant, dans certaines situations, de construire des matrices de masse modifiées qui conservent certains invariants de la matrice de masse standard, notamment la masse totale. Cela est fait en résolvant

un problème d'optimisation sous contrainte dans [75] et par des formules de quadrature dans [57]. Avec cette matrice construite par quadrature et un schéma de Newmark, on obtient une convergence quadratique de la méthode pour l'élastodynamique linéaire sans contact (Hager & Wohlmuth [58]). Dans Renard [107] et Hauret [62], la méthode de masse modifiée est interprétée et généralisée comme une formulation mixte vitesse-déplacement. Cette généralisation permet notamment d'appliquer la méthode de masse modifiée à un problème de membrane avec obstacle [107].

1.4.3 Modèles de zone cohésive

Dans les problèmes de fissuration dynamique, la vitesse de la pointe de fissure est en général élevée, du même ordre que la vitesse des ondes. Par conséquent, des petits pas de temps sont nécessaires pour capter précisément le phénomène de fissuration et il est naturel de vouloir utiliser des schémas en temps explicites. Le schéma explicite le plus courant en dynamique des solides, le schéma des différences centrées, s'écrit

$$M\left(\frac{u^{n+1}-2u^n+u^{n-1}}{\Delta t^2}\right)+F_{int}(u^n)=F_{ext}(t^n), \tag{1.25}$$

où F_{int} désigne les forces intérieures et F_{ext} désigne les forces extérieures. Dans notre modèle de fissuration, F_{int} est une fonction multivaluée (Figure 1.6), ce qui pose essentiellement deux problèmes. Tout d'abord, l'opérateur F_{int} n'est pas défini pour tous les champs de déplacement : il n'est pas défini quand le saut de déplacement normal à l'interface est négatif (Figure 1.6 à gauche). De plus, même quand l'opérateur F_{int} est bien défini partout, les branches verticales rendent ce schéma peu robuste (Figure 1.6 à droite). Numériquement, on observe en effet des oscillations de part et d'autre des branches verticales.

Une première solution pour utiliser un schéma explicite consiste à régulariser le modèle de zone cohésive pour en faire une fonction classique. Malheureusement, une condition de non-interpénétration régularisée dégrade fortement la condition CFL du schéma des différences centrées. De plus, échanger une branche verticale contre une branche quasi-verticale ne résout pas vraiment le problème des oscillations. Une seconde solution consiste à traiter la partie multivaluée du problème de façon implicite. Cette approche a déjà été utilisée pour le contact (Paoli & Schatzman [111, 102, 103]) et le frottement (Glowinski et al. [54, 55]). C'est cette approche que nous retenons dans le cadre de cette thèse.

Remarque 1.5. *La méthode de masse modifiée permet d'utiliser naturellement une approche explicite avec les problèmes de contact (Section 2.7). Avec les modèles de zone cohésive, il n'est pas possible d'utiliser directement la méthode de masse modifiée. En effet, les modèles de zone cohésive n'étant pas monotones, en l'absence de terme d'inertie, le problème est mal posé. De plus la méthode de masse modifiée ne règle pas le problème des oscillations de part et d'autre des branches verticales des modèles de zone cohésive.*

1.5 Résumé des travaux

Les travaux réalisés au cours de cette thèse s'organisent en deux parties. La première concerne les problèmes de contact. La seconde concerne les problèmes de fissuration.

1.5.1 Contact unilatéral et frottement de Coulomb

Dans cette thèse, nous comparons les principales méthodes numériques pour le contact en dynamique (Chapitre 2) et nous proposons une méthode de masse modifiée avec un schéma en temps semi-explicite (Section 2.7). Enfin, nous complétons l'analyse de la méthode de masse modifiée dans deux directions. Nous prouvons un résultat de convergence vers le problème continu dans le cas d'un problème de Signorini sans frottement et d'un matériau viscoélastique (Chapitre 3) et, par ailleurs, nous analysons la méthode de masse modifiée dans le cas d'un problème de Signorini avec frottement de Coulomb (Chapitre 4).

Comparaison des méthodes numériques pour le contact en dynamique [36]

La discrétisation du problème de Signorini implique essentiellement trois choix : (i) l'espace d'éléments finis ; (ii) la façon d'imposer la condition de contact ; (iii) le schéma en temps. Nous avons classé les différentes discrétisations proposées dans la littérature en 4 groupes. Les trois premiers groupes correspondent à trois façons d'imposer la condition de contact : condition de contact exacte, pénalisation, condition de contact en vitesse. La quatrième approche repose sur une modification de la matrice de masse et peut être vue comme une modification dans l'approximation par éléments finis. À ces quatre approches correspondent quatre formulations semi-discrètes en espace, qui peuvent être ensuite discrétisées en temps avec différents schémas. Nous sélectionnons des discrétisations représentatives de chaque classe et nous examinons leurs principales propriétés : présence d'oscillations parasites, comportement énergétique, et stabilité pour les schémas explicites. Pour illustrer ces propriétés, des simulations numériques sur deux cas tests avec solution analytique ont été réalisées. Le premier cas test, l'impact d'une barre élastique, est bien connu dans la littérature et met en évidence les éventuelles oscillations parasites. Le second, les rebonds d'une barre élastique avec multiples impacts, met en avant le comportement énergétique. Il s'agit, à notre connaissance, d'un nouveau cas test, pour lequel nous fournissons la solution analytique.

Méthode de masse modifiée semi-explicite [36, 38]

Jusqu'à maintenant, la méthode de masse modifiée a été utilisée avec des schémas implicites [75, 57]. Nous proposons une méthode de masse modifiée semi-explicite pour les problèmes de contact sans frottement. Cette méthode s'obtient naturellement en discrétisant le problème semi-discret avec un schéma des différences centrées. À chaque pas de temps, les déplacements des nœuds de l'intérieur sont calculés d'une façon explicite, tandis que les déplacements des nœuds de la frontière de contact sont calculés en résolvant un problème non-linéaire. Numériquement, nous observons la même condition de stabilité pour cette méthode que pour le schéma des différences centrées sans contact. Nous observons également un très bon comportement énergétique.

Convergence des solutions semi-discrètes en espace vers une solution du problème continu [35]

Nous prouvons un résultat de convergence vers le problème continu dans le cas d'un problème de Signorini sans frottement et d'un matériau viscoélastique. Plus précisément, nous mon-

trons la convergence, à une sous-suite près, des solutions semi-discrètes en espace vers une solution du problème continu. L'existence d'une solution au problème continu dans le cas d'un matériau purement élastique est toujours un problème ouvert, et la convergence des solutions semi-discrètes semble pour l'instant hors de portée. Dans le cas viscoélastique, l'existence d'une solution a été montrée en utilisant une méthode de pénalisation [41, §4.2.2] ; l'unicité est toujours un problème ouvert. Notre preuve de convergence s'appuie sur des arguments relativement classiques, à savoir estimations *a priori* sur les solutions semi-discrètes et arguments de compacité, mais la modification de la masse nécessite une attention particulière lors du passage à la limite. Les estimations *a priori* sur la vitesse fournies par le terme de viscosité jouent un rôle crucial dans la preuve, de sorte que celle-ci n'est plus valable quand la viscosité disparaît.

Analyse de la méthode de masse modifiée pour le frottement de Coulomb [34]

Nous analysons la méthode de masse modifiée dans le cas d'un problème de Signorini avec frottement de Coulomb. Nous prouvons que le problème semi-discrétisé en espace est équivalent à une inclusion différentielle semi-continue supérieure avec condition de Lipschitz et est donc bien posé. De plus, nous montrons que la variation d'énergie du système semi-discrétisé en espace est égale au travail des forces extérieures et des forces de frottement. Pour la discrétisation en temps, nous considérons un schéma implicite. Chaque pas de temps nécessite alors la résolution d'un problème non-linéaire semblable à un problème de frottement en statique. Il est bien connu qu'un tel problème peut avoir plusieurs solutions. Ici, nous prouvons que, sous une certaine condition sur les paramètres de discrétisation de type CFL, le problème discrétisé en espace et en temps est bien posé. Pour une discrétisation en espace fixée, nous prouvons également que les solutions discrètes en espace et en temps convergent vers la solution semi-discrétisée en espace lorsque le pas de temps tend vers zéro.

1.5.2 Modèles de zone cohésive

Schémas quasi-explicites pour les problèmes de fissuration dynamique

Nous étudions des schémas en temps quasi-explicites pour des problèmes dynamiques de fissuration avec des modèles de zone cohésive. Ces schémas utilisent un schéma en temps des différences centrées pour la partie élastodynamique. Dans un premier schéma, les forces à l'interface de fissuration sont imposés de façon totalement implicite. Dans un second schéma, seule la partie multivaluée est imposée de façon implicite. De plus, les forces à l'interface sont condensées. Ainsi, à chaque pas de temps, les déplacements des nœuds de l'intérieur du domaine sont calculés de façon explicite, tandis que les déplacements de chaque nœud à l'interface sont calculés en résolvant un problème non-linéaire local. Cette approche permet de traiter de façon générale et robuste les différents modèles de zone cohésive multivalués tout en conservant des coûts de calcul modérés.

Méthodes de Lagrangien augmenté pour les problèmes de fissuration statique [37]

Nous analysons des méthodes de Lagrangien augmenté pour le problème de fissuration statique. Nous commençons par l'analyse mathématique du problème continu. Celui-ci peut s'écrire

comme la minimisation sous contrainte d'une énergie non-convexe. Nous reformulons le problème à l'aide d'un Lagrangien augmenté à trois champs : déplacement dans le volume, contrainte et déplacement sur la frontière cohésive. Nous discrétisons le problème avec des éléments finis mixtes. Pour pouvoir utiliser des méthodes de collocation, nous approchons le déplacement sur la frontière cohésive par des éléments finis discontinus. Nous obtenons pour ces approximations une estimation d'erreur en s'inspirant notamment des analyses faites pour le contact dans Hüeber & Wohlmuth [69] et Hild & Laborde [66]. Par ailleurs, nous présentons et nous analysons deux méthodes itératives de résolution : une méthode de type Uzawa avec une approche de décomposition-coordination et une méthode de Newton. Finalement, des résultats numériques illustrent l'analyse théorique.

Part I

Unilateral contact

2

Time-integration schemes for the finite element dynamic Signorini problem

This chapter is submitted to *SIAM Journal on Scientific Computing* [36]. See also [38].

2.1 Introduction

The design of robust and efficient numerical methods for dynamic contact problems has motivated a large amount of work over the last two decades and remains a challenging issue. Here, we focus on the dynamic Signorini problem, which models the infinitesimal deformations of a solid body that can come into contact with a rigid obstacle. This problem is the simplest dynamic contact problem, but also the first step toward more complex situations, such as multi-body problems, large deformation problems, contact with friction, etc... For an overview of the different contact problems, we refer to [76, 87, 124].

In structural dynamics, the usual space-time discretization combines finite elements in space and a time-stepping scheme. In this framework, the discretization of the dynamic Signorini problem involves mainly three choices: (i) the finite element space; (ii) the enforcement of the contact condition; (iii) the time-stepping scheme. The combination of these three ingredients presents some difficulties. For instance, it is well-known that the combination of an exact enforcement of the contact condition and an implicit Newmark scheme yields spurious oscillations as well as poor energy behavior, that is, sizeable deviations from the exact value. Moreover, the combination of an exact enforcement and an explicit scheme is not straightforward, whereas the use of a penalty contact condition tightens the stability condition of explicit schemes. Consequently, various alternative discretizations have been designed for the dynamic Signorini problem. The aim of this work is to classify the different discretizations and to illustrate numerically their main properties.

We classify the discretizations into four groups. The first three groups correspond to different ways of enforcing the contact condition: exact enforcement [22, 33, 72, 89, 102, 103, 118, 121], enforcement with penalty [2, 9, 63], and enforcement with contact condition in velocity [4, 9, 88]. The fourth approach is based on a modification of the mass matrix [57, 75]; it can be seen as an alternative choice of the finite element space. These four classes yield different space semi-discrete problems which in turn can be discretized in time using various time-stepping schemes, either implicit or semi-explicit. We select representative discretizations within each class and examine

their main properties: presence of spurious oscillations, energy behavior after multiple impacts, and stability in the case of explicit schemes. By energy conservation we mean that the variation of the energy is equal to the work of the external forces (the contact forces should not work). To illustrate these properties, numerical simulations on two 1D benchmarks have been performed. The first benchmark, the impact of an elastic bar on a rigid surface, is well-known and allows to detect spurious oscillations. The second one, for which we derive the exact solution, deals with the bounces of an elastic bar and is geared toward assessing energy behavior, in so far as multiple impacts occur. It is to our knowledge a new benchmark. Additionally, some of the schemes are assessed on a 2D benchmark (without analytical solution) associated with the impact and multiple bounces of a disk on a rigid surface. Some of the presented Newmark-based schemes are also compared in 3D in [80]. The mathematical analysis of the different methods is beyond the scope of this article, but we mention, whenever they exist, the theoretical results (well-posedness of the discrete problems and convergence of the discrete solutions). Dynamic contact problems yield shock waves, and spurious oscillations appear near the shock in the numerical solutions, owing to the so-called Gibbs phenomenon (see, e.g., [56] and references therein). These oscillations can be eliminated using dissipative schemes (or, equivalently, by filtering). This issue, being important but not specific to dynamic contact problems, is not further addressed here (see also Remark 2.4).

The material is organized as follows. We formulate the dynamic Signorini problem in the continuous setting (Section 2.1) and we introduce the main ingredients for its approximation (Sections 2.2 and 2.3). We present the two 1D benchmark problems with their analytical solutions (Section 3). We describe the four classes of discretizations together with numerical results in 1D: exact enforcement of the contact condition (Section 4), enforcement with penalty contact condition (Section 5), enforcement with contact condition in velocity (Section 6), and modification of the mass matrix (Section 7). Finally, we present numerical results on the 2D benchmark for selected schemes (Section 2.8) and draw some conclusions (Section 2.9).

2.2 The dynamic Signorini problem

2.2.1 Governing equations

We consider the infinitesimal deformations of a body occupying a reference domain $\Omega \subset \mathbb{R}^d$ ($d \in \{1,2,3\}$) during a time interval $[0,T]$. The tensor of elasticity is denoted by $\mathcal{A}$ and the mass density is denoted by ρ. An external load f is applied to the body. Let $u : (0,T)\times\Omega \to \mathbb{R}^d$, $\epsilon(u) : (0,T)\times\Omega \to \mathbb{R}^{d,d}$ and $\sigma(u) : (0,T)\times\Omega \to \mathbb{R}^{d,d}$ be the displacement field, the linearized strain tensor and the stress tensor, respectively. Denoting time-derivatives by dots, the momentum conservation equation reads

$$\rho\ddot{u} - \operatorname{div}\sigma = f, \quad \sigma = \mathcal{A} : \epsilon, \quad \epsilon = \frac{1}{2}(\nabla u +^{\mathrm{T}} \nabla u) \quad \text{in } \Omega\times(0,T). \tag{2.1}$$

The boundary $\partial\Omega$ is partitioned into three disjoint open subsets Γ^D, Γ^N and Γ^c. Dirichlet and Neumann conditions are prescribed on Γ^D and Γ^N, respectively, $u = u_D$ on $\Gamma^D\times(0,T)$ and $\sigma\cdot n = f_N$ on $\Gamma^N\times(0,T)$, where n denotes the outward unit normal to Ω. We set $u_n := u_{|\partial\Omega}\cdot n$

and $\sigma_n := n \cdot \sigma_{|\partial\Omega} \cdot n$, the normal displacement and the normal stress on $\partial\Omega$, respectively. On Γ^c, a unilateral contact condition, also called Signorini condition, is imposed,

$$u_n \leq 0,\ \sigma_n(u) \leq 0,\ \sigma_n(u)u_n = 0 \quad \text{on } \Gamma^c \times (0,T). \tag{2.2}$$

At the initial time, the displacement and velocity fields are prescribed. The above problem is an evolution partial differential equation under unilateral constraints. Here, the equation is second-order in time and the constraint holds on the displacement; this is not the most favorable case. The existence and uniqueness of a solution has only been proven in 1D, when the contact boundary is reduced to a point [91, 41]. In 1D, it has also been proven that the variation of energy is equal to the work of the external forces; the contact force does not work [91, 41]. In higher dimension, the existence of a solution is proven in the case of a viscoelastic material [41], while existence and uniqueness is proven for the wave equation under certain assumptions.

2.2.2 Basic time-integration schemes in linear elastodynamics

In this section, we briefly recall some basic facts about time-integration schemes in linear elastodynamics; most of this material can be found in [70]. Firstly, we discretize the problem in space with a finite element method. To alleviate the notation, we still denote by u the space semi-discrete displacement. The number of degrees of freedom is denoted by N_d. Let K, M, and $F(t)$ be the stiffness matrix, the mass matrix, and the column vector of the external forces, respectively. The space semi-discrete problem consists in seeking $u : [0,T] \to \mathbb{R}^{N_d}$ such that, for all $t \in [0,T]$,

$$M\ddot{u}(t) + Ku(t) = F(t), \tag{2.3}$$

with the initial conditions $u(0) = u^0$ and $\dot{u}(0) = v^0$. For solving such a system of ordinary differential equations (ODEs), linear one-step schemes are the most frequently used. For simplicity, the interval $[0,T]$ is divided into equal subintervals of length Δt. We set $t^n = n\Delta t$ and denote by u^n, $\dot{u}^n$, and $\ddot{u}^n$ the approximations of $u(t^n)$, $\dot{u}(t^n)$, and $\ddot{u}(t^n)$, respectively. We define the convex combination $\square^{n+\omega} := (1-\omega)\square^n + \omega\square^{n+1}$, where $\square$ stands for u, $\dot{u}$, $\ddot{u}$ or t, and $\omega \in [0,1]$. We use a slightly different definition for the external load, namely $F^{n+\alpha} := F(t^{n+\alpha})$; for instance, $F^{n+\frac{1}{2}} = F(t^{n+\frac{1}{2}})$ generally differs from $\frac{1}{2}(F^n + F^{n+1})$. Moreover, at time t^n, the energy of the system is $\mathcal{E}^n := \frac{1}{2}{}^{\mathrm{T}}\dot{u}^n M \dot{u}^n + \frac{1}{2}{}^{\mathrm{T}}u^n K u^n$. Now we can formulate some of the most common time-stepping schemes in linear elastodynamics.

Discretization 2.2.1 (HHT-Newmark) *Seek $u^{n+1},\ \dot{u}^{n+1},\ \ddot{u}^{n+1} \in \mathbb{R}^{N_d}$ such that*

$$M\ddot{u}^{n+1} + Ku^{n+1+\alpha} = F^{n+1+\alpha}, \tag{2.4}$$

$$u^{n+1} = u^n + \Delta t\ \dot{u}^n + \frac{\Delta t^2}{2}\ \ddot{u}^{n+2\beta}, \tag{2.5}$$

$$\dot{u}^{n+1} = \dot{u}^n + \Delta t\ \ddot{u}^{n+\gamma}, \tag{2.6}$$

where α, β, γ are real parameters. The choice $\alpha = 0$ yields Newmark schemes while the choice $\alpha \in [-1/3, 0]$, $\beta = 1/4(1-\alpha)^2$, and $\gamma = 1/2 - \alpha$ yields HHT schemes.

Discretization 2.2.2 (Midpoint) *Seek $u^{n+1},\ \dot{u}^{n+1},\ \ddot{u}^{n+\frac{1}{2}} \in \mathbb{R}^{N_d}$ such that*

$$M\ddot{u}^{n+\frac{1}{2}} + Ku^{n+\frac{1}{2}} = F^{n+\frac{1}{2}}, \tag{2.7}$$

$$u^{n+1} = u^n + \Delta t\ \dot{u}^{n+\frac{1}{2}}, \tag{2.8}$$

$$\dot{u}^{n+1} = \dot{u}^n + \Delta t\ \ddot{u}^{n+\frac{1}{2}}. \tag{2.9}$$

Discretization 2.2.3 (Central differences) *Seek $u^{n+1} \in \mathbb{R}^{N_d}$ such that*

$$M\left(\frac{u^{n+1} - 2u^n + u^{n-1}}{\Delta t^2}\right) + Ku^n = F^n. \tag{2.10}$$

HHT schemes are implicit, unconditionally stable, second-order accurate, and dissipative in the high frequencies. The amount of dissipation is controlled by the parameter α. Newmark schemes do not, in general, conserve the energy; such schemes instead conserve the quadratic form $\mathcal{E}^n_{\beta,\gamma} := \mathcal{E}^n + \frac{\Delta t^2}{2}\left(\beta - \frac{1}{2}\gamma\right)^{\mathrm{T}} \ddot{u}^n M \ddot{u}^n$ since there holds [82]

$$\begin{aligned}\mathcal{E}^{n+1}_{\beta,\gamma} - \mathcal{E}^n_{\beta,\gamma} =^{\mathrm{T}} & \left(\frac{1}{2}(F^{n+1} + F^n) + \left(\gamma - \frac{1}{2}\right)(F^{n+1} - F^n)\right)(u^{n+1} - u^n) \\ & - \left(\gamma - \frac{1}{2}\right)\left({}^{\mathrm{T}}(u^{n+1} - u^n)K(u^{n+1} - u^n) + \left(\beta - \frac{1}{2}\gamma\right)^{\mathrm{T}}(\ddot{u}^{n+1} - \ddot{u}^n)M(\ddot{u}^{n+1} - \ddot{u}^n)\right).\end{aligned}$$

The quadratic form $\mathcal{E}^n_{\beta,\gamma}$ coincides with the energy only if $\beta = \frac{1}{2}\gamma$. For $\beta \neq \frac{1}{2}\gamma$, we refer to $\mathcal{E}^n_{\beta,\gamma}$ as a shifted energy; the sign of the difference between $\mathcal{E}^n_{\beta,\gamma}$ and $\mathcal{E}^n$ only depends on the sign of $(\beta - \frac{1}{2}\gamma)$. The particular choice $\beta = 1/4$, $\gamma = 1/2$ yields an implicit, unconditionally stable, and second-order accurate scheme. It is energy-conserving in the sense that

$$\mathcal{E}^{n+1} - \mathcal{E}^n =^{\mathrm{T}} \left(\frac{F^{n+1} + F^n}{2}\right)(u^{n+1} - u^n).$$

The midpoint scheme is implicit, unconditionally stable, and second-order accurate. It is energy-conserving in the sense that

$$\mathcal{E}^{n+1} - \mathcal{E}^n =^{\mathrm{T}} F^{n+\frac{1}{2}}(u^{n+1} - u^n).$$

The central difference scheme is explicit (lumping the mass matrix avoids solving any linear system), conditionally stable and second-order accurate. Here it is written as a two-step linear scheme involving only the displacement but it can be formulated as a one-step scheme. Actually, it is a Newmark scheme with parameters $\beta = 0$, $\gamma = 1/2$; the velocity and acceleration are then $\dot{u}^n = \frac{1}{2\Delta t}(u^{n+1} - u^{n-1})$ and $\ddot{u}^n = \frac{1}{\Delta t^2}(u^{n+1} - 2u^n + u^{n-1})$. The central difference scheme does not conserve the energy $\mathcal{E}^n$ but the shifted energy $\mathcal{E}^n_{0,\frac{1}{2}}$ in the sense that

$$\mathcal{E}^{n+1}_{0,\frac{1}{2}} - \mathcal{E}^n_{0,\frac{1}{2}} =^{\mathrm{T}} \left(\frac{F^{n+1} + F^n}{2}\right)(u^{n+1} - u^n).$$

There exist also explicit schemes with high-frequency dissipation, such as the Chung-Hulbert or Tchamwa-Wielgosz schemes (see [100] and references therein).

2.2.3 Enforcing the contact condition

The enforcement of a contact condition in a finite element setting has been widely studied in the case of the static Signorini problem [76]. We assume that the mesh is compatible with the partition of the boundary. Let N_c be the number of nodes lying on the contact boundary. We define the linear normal trace operator on Γ^c, $g : v \longmapsto -v_{|\Gamma} \cdot n$ and the associated matrix G. Note that the dimension of G is $N_c \times N_d$. We denote by $\{G_i\}_{1 \leq i \leq N_c}$ the rows of the matrix G. Thus, $G_i u$ yields the value of the normal displacement at the ith node of the contact boundary. With an exact enforcement, the static Signorini problem consists in seeking a displacement $u \in \mathbb{R}^{N_d}$ and a contact pressure $r \in \mathbb{R}^{N_c}$ such that

$$Ku = F + {}^{\mathrm{T}} Gr, \tag{2.11}$$

$$Gu \geq 0, \quad r \geq 0, \quad {}^{\mathrm{T}} rGu = 0. \tag{2.12}$$

Here the problem is formulated as a complementarity problem. Other formalisms can be found in the literature, e.g., variational inequality, Lagrangian formulation, and formulation with sub-derivatives. If the matrix K is positive definite, problem (2.11)-(2.12) has a unique solution. For solving this problem, a large variety of methods has been developed [76, 124]: Uzawa algorithms, active set methods, semi-smooth Newton methods, Lemke algorithm, monotone multigrid method, etc...

Penalty formulations are another classical way of dealing with constrained problems. We have to define a penalty function $R_\epsilon : \mathbb{R}^{N_c} \to \mathbb{R}^{N_c}$. For instance we can choose $R_\epsilon(v) = \frac{1}{\epsilon}(v)^-$, where $(v)^-$ denotes the negative part of v. The penalized static Signorini problem consists now in seeking $u \in \mathbb{R}^{N_d}$ such that

$$Ku = F + {}^{\mathrm{T}} GR_\epsilon(Gu). \tag{2.13}$$

A third way of enforcing the contact condition, specific to the dynamic problem, is to replace the Signorini condition by an approximation involving the velocity instead of the displacement [41, 97]. Assume that $u_n = 0$ at a certain time t^c. Then, on a short time interval afterwards, $u_n \approx (t - t^c)\dot{u}_n$. This motivates the following contact condition in velocity,

$$\dot{u}_n \leq 0, \ \sigma_n(u) \leq 0, \ \sigma_n(u)\dot{u}_n = 0, \quad \text{on } \Gamma^c. \tag{2.14}$$

It must be stressed that the above condition condition is applicable only during contact phases. This condition is not applicable during non-contact phases because a positive normal velocity is not allowed.

2.3 1D benchmark problems

To compare the different methods, we test them on two 1D problems. Both problems can be formulated in the same setting. We consider an elastic bar dropped against a rigid ground. The bar is dropped, undeformed, from a height h_0, with an initial velocity $-v_0$, under a gravity acceleration $g_0 \geq 0$. The length of the bar is denoted by L, the Young modulus by E, and the density by ρ. Let $c_0 := \sqrt{\frac{E}{\rho}}$ denote the wave speed. The reference domain is $\Omega = [0, L]$. In this

context, the governing equations presented in Section 2.2.1 for the continuous problem take the form

$$\rho\ddot{u} - E\frac{\partial^2 u}{\partial x^2} = -\rho g_0 + r, \quad \text{in } \Omega \times (0,T), \tag{2.15}$$

$$u(0,t) \geq 0,\ r(t) \geq 0,\ r(t)u(0,t) = 0 \quad \text{on } (0,T), \tag{2.16}$$

$$\frac{\partial u}{\partial x}(L,t) = 0 \quad \text{on } (0,T), \quad u(\cdot,0) = h_0, \quad \dot{u}(\cdot,0) = -v_0, \tag{2.17}$$

where u is the scalar-valued displacement of the bar and r the contact pressure equal to the normal stress $-E\frac{\partial u}{\partial x}$ at $x = 0$. Problem (2.15)-(2.17) has a unique solution and the variation of the energy is equal to the work of the gravity force [91],

$$\frac{d}{dt}\left(\frac{1}{2}\int_\Omega \rho\dot{u}^2 + \frac{1}{2}\int_\Omega E\left|\frac{\partial u}{\partial x}\right|^2\right) = \int_\Omega -\rho g_0 \dot{u}, \quad \forall t \in [0,T]. \tag{2.18}$$

In the first problem, $v_0 > 0$ and $g_0 = 0$ so that there is a single impact. This benchmark has been widely used in the literature (see, e.g., [124]). It enables us to examine the possible spurious oscillations triggered by the numerical schemes. In the second problem, $v_0 = 0$ and $g_0 > 0$, so that the bar can make several bounces. With a suitable choice of parameters, the motion of the bar is periodic in time and we can calculate the exact solution. It enables us to examine the time evolution of energy after multiple impacts. This benchmark is, to our knowledge, new.

2.3.1 Impact of an elastic bar

Let us describe the solution of the first problem (Figure 2.1). Before the impact, the bar is undeformed and has a uniform velocity $-v_0$. The bar reaches the ground at time $t_1 := \frac{h_0}{v_0}$. After the impact, the bar stays in contact with the ground. A shock wave travels from the bottom of the bar to the top. Above the shock wave, the velocity is $-v_0$; below, the velocity is zero. Then, the shock wave travels from the top to the bottom. Above the shock wave, the velocity is v_0; below, the velocity is still zero. As soon as the wave reaches the bottom, the bar takes off, undeformed, with a uniform velocity v_0. The speed of the shock wave is c_0. Thus, the wave takes a time $\tau_w := \frac{L}{c_0}$ to travel along the bar, and the bar takes off at time $t_2 := t_1 + 2\tau_w$. The

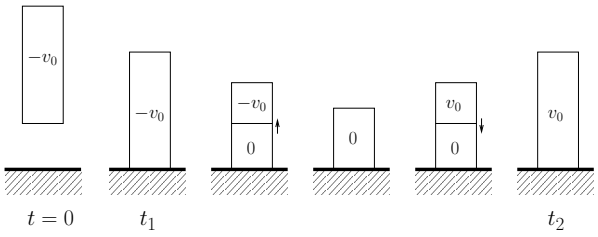

Fig. 2.1. Impact of an elastic bar.

analytical solution can be easily expressed using travelling wave solutions. Defining the auxiliary function $H_v(x,t) = -v\min(x/c_0, \tau_w - |t - \tau_w|)$, the exact solution is

$$u(x,t) = \begin{cases} h_0 - v_0 t & \text{if } t \le t_1 \\ H_{v_0}(x, t - t_1) & \text{if } t_1 < t \le t_2 \\ v_0(t - t_2) & \text{if } t_2 < t \end{cases}$$

In particular, the displacement at the bottom of the bar and the contact pressure are:

$$u(0,t) = \begin{cases} h_0 - v_0 t & \text{if } t \le t_1 \\ 0 & \text{if } t_1 < t \le t_2 \\ v_0(t - t_2) & \text{if } t_2 < t \end{cases} \qquad r(t) = \begin{cases} 0 & \text{if } t \le t_1 \\ \frac{E v_0}{c_0} & \text{if } t_1 < t \le t_2 \\ 0 & \text{if } t_2 < t \end{cases}$$

These two quantities are represented in Figure 2.2 (with the parameters chosen in Section 2.3.3).

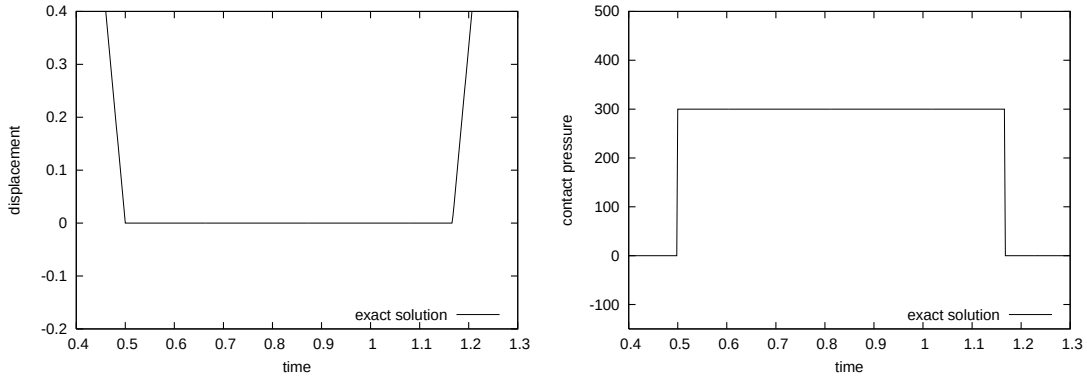

Fig. 2.2. Impact of an elastic bar. Displacement at the bottom of the bar (left) and contact pressure (right).

2.3.2 Bounces of an elastic bar

In the second problem (Figure 2.3), the bar is dropped, undeformed, with a zero initial velocity. It takes a time $\tau_f := \sqrt{\frac{2h_0}{g_0}}$ to reach the ground. At the impact, at time $t_1 := \tau_f$, the bar is undeformed and has uniform velocity $-v_f$, where $v_f := \sqrt{2h_0 g_0}$. After the impact, as in the previous benchmark, the bar stays in contact with the ground during a time $2\tau_w$. During this contact phase, the response of the bar is the superposition of a shock wave due to velocity at the impact and a vibration due to the gravity as reflected by the series S_1 and S_2 below. When the bar takes off, at time $t_2 := t_1 + 2\tau_w$, it has a uniform velocity v_f but it is compressed (by symmetry, $u(x,t_2) = \tilde{u}(x) := \frac{g_0}{c_0^2}(x^2 - 2Lx)$ is twice the static deformation with homogeneous Dirichlet and Neumann conditions at $x = 0$ and $x = L$ respectively). Consequently, during the flight phase, the response of the bar is the superposition of a rigid parabolic motion (due to the gravity and the velocity) and a vibration (due to the initial deformation). If we choose $\tau_f = p\tau_w$ for a positive integer p (for instance, $\tau_f = 3\tau_w$), we can ensure that the bar reaches the ground with uniform velocity $-v_f$ and with displacement field $\tilde{u}$. By doing so, the second impact occurs at time $t_3 := t_2 + 2\tau_f = t_2 + 6\tau_w$. When the bar takes off again, at time $t_4 :=$

$t_3+2\tau_w$, it is undeformed and has a uniform velocity v_f. The next flight phase is a rigid parabolic movement. Then, this sequence of two contact phases and two flight phases repeats periodically. To compute the analytical solution, we use a decomposition on the eigenmodes in addition to the

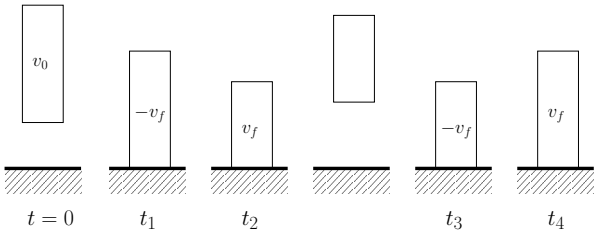

Fig. 2.3. Bounces of an elastic bar.

travelling wave solutions. We set $t_{4k+1} = 3\tau_w + 16k\tau_w$, $t_{4k+2} = t_{4k+1} + 2\tau_w$, $t_{4k+3} = t_{4k+1} + 8\tau_w$ and $t_{4k+4} = t_{4k+1} + 10\tau_w$. We define also the auxiliary functions $P(x,t) = h_0 - \frac{1}{2}g_0(t-\tau_f)^2$, $S_1(x,t) = \sum_{n=1}^{\infty} a_n(1 - cos(c_0\nu_n t))sin(\nu_n x)$, $S_2(x,t) = -\frac{2g_0L^2}{3c_0^2} + \sum_{n=1}^{\infty} b_n cos(c_0\lambda_n t)cos(\lambda_n x)$, where $a_n = \frac{-2g_0}{c_0^2 L\nu_n^3}$, $\nu_n = (n-\frac{1}{2})\frac{\pi}{L}$, $b_n = \frac{4g_0}{c_0^2\lambda_n^2}$, $\lambda_n = n\frac{\pi}{L}$. The function S_1 corresponds to the vibration of a bar, clamped at its bottom, initially at rest, under a gravity g_0. The function S_2 corresponds to the vibration of a bar, free at its two extremities, with the initial displacement $\tilde{u}$, a zero initial velocity and without external force. The computation of the series S_1 and S_2 is standard; see [29] for instance. The exact solution is

$$u(x,t) = \begin{cases} P(x,t+\tau_f) & \text{if } t \le t_1 \\ H_{v_f}(x,t-t_{4k+1}) + S_1(x,t-t_{4k+1}) & \text{if } t_{4k+1} < t \le t_{4k+2} \\ P(x,t-t_{4k+2}) + S_2(x,t-t_{4k+2}) & \text{if } t_{4k+2} < t \le t_{4k+3} \\ H_{v_f}(x,t_{4k+4}-t) + S_1(x,t_{4k+4}-t) & \text{if } t_{4k+3} < t \le t_{4k+4} \\ P(x,t-t_{4k+4}) & \text{if } t_{4k+4} < t \le t_{4(k+1)+1} \end{cases}$$

The displacement at the bottom of the bar is represented in Figure 2.4 (with the parameters chosen in Section 2.3.3).

2.3.3 Numerical simulations

The parameters used in the numerical simulations are $E = 900$, $\rho = 1$, $L = 10$, $h_0 = 5$. In the first benchmark, $v_0 = 10$, $g_0 = 0$; in the second benchmark, $v_0 = 0$, $g_0 = 10$. The bar is discretized with a uniform mesh size Δx and linear finite elements are used. We define $\nu_c := c_0\frac{\Delta t}{\Delta x}$ the Courant number, which is the relevant ratio to link the mesh size and the time step. In particular, central difference schemes with lumped mass matrix are stable in the linear case under the condition $\nu_c \le 1$. In what follows, we take $\nu_c = 1.5$ for unconditionally stable schemes and $\nu_c = 0.75$ (thereby halving the time step) for central difference schemes. To describe the numerical results, we consider the following quantities: the displacement at the bottom node of the bar (denoted by u_0^n), the stress at the bottom node of the bar (denoted by $(Ku^n)_0$), the contact pressure r^n, and the energy $\mathcal{E}^n - {}^{\mathrm{T}} Fu^n$ (the load vector being time-independent, we

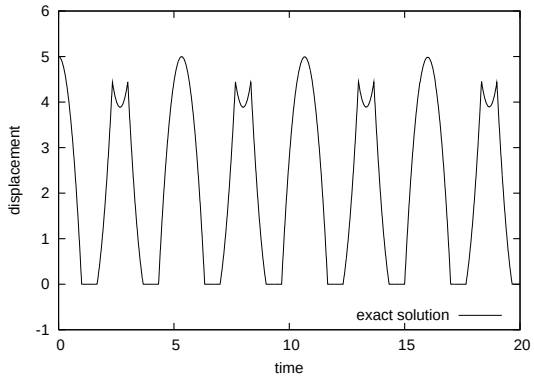

Fig. 2.4. Bounces of an elastic bar. Displacement at the bottom of the bar.

denote it by F). Note that, because of the finite element discretization, the stress at the bottom node and the contact pressure are not equal.

2.4 Discretizations with exact enforcement of the contact condition

In this section we combine standard finite elements in space and an exact enforcement of the contact condition at each node of the contact boundary. This leads to the semi-discrete problem,

$$M\ddot{u}(t) + Ku(t) = F(t) + {}^{\mathrm{T}}Gr(t), \tag{2.19}$$

$$Gu(t) \geq 0, \quad r(t) \geq 0, \quad {}^{\mathrm{T}}r(t)Gu(t) = 0. \tag{2.20}$$

Problem (2.19)-(2.20) is a system of differential equations under unilateral constraints. The same kind of formulation arises in rigid-body dynamics with impact [18, 116], so the mathematical results and the numerical methods developed in this framework can in general be applied to our problem. Mathematically, problem (2.19)-(2.20) turns out to be delicate. Firstly, the functional framework is not obvious. Due to the unilateral constraints, the velocity can be discontinuous and there is in general no strong solution (i.e. twice differentiable in time) to this problem. One possibility is to look for a weak solution such that the displacement u is continuous in time, the velocity $\dot{u}$ is a function with bounded variation in time, the acceleration $\ddot{u}$ and the contact pressure r are measures (they contain impulses). Secondly, this weak solution is in general not unique. Consider the simple example of a point mass impacting a rigid foundation. Before the impact, the motion of the point mass is uniquely determined. After the impact, an infinity of velocities and trajectories are admissible. To recover uniqueness, an additional condition, specifying the velocity after an impact, is needed. Denoting by v^- the normal velocity before the impact and by v^+ the normal velocity after the impact, an usual approach is to prescribe $v^+ = -ev^-$, where e is a non-negative parameter. In the present space semi-discrete setting, it seems reasonable to take $e = 0$. Indeed, in the dynamic Signorini problem, the unilateral constraint holds on the boundary and the boundary does not bounce after an impact. We can now formulate the semi-discrete problem in a rigorous way.

Problem 2.1. Seek a displacement $u : [0,T] \to \mathbb{R}^{N_d}$ and a contact pressure $r : [0,T] \to \mathbb{R}^{N_c}$ such that

$$M\ddot{u} + Ku = F + {}^{\mathrm{T}}Gr, \tag{2.21}$$

$$Gu \geq 0, \quad r \geq 0, \quad {}^{\mathrm{T}}rGu = 0, \tag{2.22}$$

$${}^{\mathrm{T}}r_i(t)G_i\dot{u}(t^+) = 0 \quad \text{if} \quad G_iu(t) = 0, \tag{2.23}$$

with the initial conditions $u(0) = u^0$ and $\dot{u}(0) = v^0$.

Equation (2.23) constitutes the impact law. Most of the mathematical terms in equations (2.21)-(2.23) must be understood in the sense of measures. In particular ${}^{\mathrm{T}}rGu$ and ${}^{\mathrm{T}}r_i(t)G_i\dot{u}(t^+)$ should be defined with suitable duality products. For more details, we refer to [18, 116].

Remark 2.1. *The impact law* (2.23) *is a consequence of the discretization in space. Indeed, the continuous problem does not need an impact law to have a unique solution. This fact is proven in 1D [41, 91]; in higher dimension, uniqueness is still an open problem, but the difficulty does not seem to come from the absence of an impact law.*

Remark 2.2. *Another difference to the continuous solution is that the semi-discrete solution does not conserve the energy since there is a loss of energy at each impact of a node. Actually, energy is conserved for $e = 1$, but this is not satisfactory since the contact is never established for a time interval of nonzero length.*

Remark 2.3. *The impact law is different from the concept of persistency condition sometimes encountered in the literature [2, 87, 88, 89]. The persistency condition is defined in the continuous setting and in the fully discrete setting. It requires that the contact force does not work. Note that in the continuous problem, the persistency condition seems to be a consequence of the Signorini condition (it is at least proven in 1D).*

2.4.1 Implicit schemes

We consider first dissipative schemes and then schemes dealing with the impact.

Dissipative schemes

To motivate the discussion, let us begin with an ill-founded discretization. We choose a Newmark scheme (trapezoidal rule) for the elastodynamics part and we enforce the contact condition (2.22) at a certain time, say t^{n+1}. We pay no attention to the impact law (2.23). This choice corresponds to Discretization 2.4.1 with $\alpha = 0$, $\beta = 1/4$, $\gamma = 1/2$.

Discretization 2.4.1 (HHT-Newmark) *Seek u^{n+1}, $\dot{u}^{n+1}$, $\ddot{u}^{n+1} \in \mathbb{R}^{N_d}$, and $r^{n+1} \in \mathbb{R}^{N_c}$ such that*

$$M\ddot{u}^{n+1} + Ku^{n+1+\alpha} = F^{n+1+\alpha} + {}^{\mathrm{T}}Gr^{n+1}, \tag{2.24}$$

$$Gu^{n+1} \geq 0, \quad r^{n+1} \geq 0, \quad {}^{\mathrm{T}}r^{n+1}Gu^{n+1} = 0, \tag{2.25}$$

$$u^{n+1} = u^n + \Delta t\dot{u}^n + \frac{\Delta t^2}{2}\ \ddot{u}^{n+2\beta}, \tag{2.26}$$

$$\dot{u}^{n+1} = \dot{u}^n + \Delta t\ \ddot{u}^{n+\gamma}. \tag{2.27}$$

At each time step, Problem (2.24)-(2.27) is equivalent to a linear complementarity problem and is well-posed. In contrast to the static case, the matrix K does not need to be positive definite for the problem to be well-posed (Dirichlet boundary conditions are not needed). When this scheme is tested on the first benchmark, we observe large spurious oscillations on the contact pressure and small spurious oscillations on the displacement during the contact phase (Figure 2.5). On the second benchmark, we observe a poor displacement and a poor energy behavior (Figure 2.6). Let us try to explain what happens exactly. Suppose there is contact at the ith node of the contact boundary at time t^{n+1} (i.e. $G_i u^{n+1} = 0$), then

$$G_i\dot{u}^{n+1} = -\frac{\gamma}{\beta\Delta t}G_i u^n + \left(1 - \frac{\gamma}{\beta}\right)G_i\dot{u}^n + \Delta t\frac{2\beta - \gamma}{2\beta}G_i\ddot{u}^n, \tag{2.28}$$

$$G_i\ddot{u}^{n+1} = -\frac{1}{\beta\Delta t^2}G_i u^n - \frac{1}{\beta\Delta t}G_i\dot{u}^n - \frac{1 - 2\beta}{2\beta}G_i\ddot{u}^n. \tag{2.29}$$

Thus, the impact law is not satisfied since we expect that after an impact, $G_i\dot{u}^{n+1} = G_i\ddot{u}^{n+1} = 0$. During a contact phase following an impact, the velocity and the acceleration oscillate. In the simple case of an impact without initial acceleration and initial velocity v_i, the magnitude of the acceleration oscillations after the impact is $\frac{v_i}{\Delta t}$. These oscillations trigger oscillations of magnitude $\frac{m_i v_i}{\Delta t}$ on the contact pressure, where m_i is the mass associated with the node i (Figure 2.5). Moreover, the energy balance takes the form

$$\mathcal{E}^{n+1} - \mathcal{E}^n = {}^{\mathrm{T}}\left(\frac{r^{n+1} + r^n}{2}\right)(Gu^{n+1} - Gu^n) + {}^{\mathrm{T}}\left(\frac{F^{n+1} + F^n}{2}\right)(u^{n+1} - u^n),$$

so that the contact force works when a node changes status. When a node comes into contact ($G_i u^n > 0$, $r^n = 0$, $G_i u^{n+1} = 0$, $r^{n+1} > 0$), the work is negative; when a node is released ($G_i u^n = 0$, $r^n > 0$, $G_i u^{n+1} > 0$, $r^{n+1} = 0$), the work is positive. As the contact pressure is polluted by large oscillations, this strongly perturbs the rest of the structure (Figure 2.6). The poor behavior of the Newmark scheme can be summarized as follows: large oscillations of the acceleration at the contact boundary $\Rightarrow$ large oscillations of the contact pressure $\Rightarrow$ perturbation of the whole structure. In themselves the oscillations of the acceleration at the contact boundary are not a problem. The oscillations of the contact pressure are more troublesome if a Lagrangian method is used for solving the linear complementarity problem at each time step (the Lagrange multiplier being equal to the contact pressure). Of course, the perturbation of the whole structure must be avoided. Several options can be considered to design better algorithms. The first option consists in using dissipative schemes, such as HHT schemes (Discretization 2.4.1). The spurious oscillations are then damped (Figure 2.7), but at the expense of poor energy behavior (Figure 2.8). The selected value $\alpha = -0.2$ achieves here a reasonable compromise between dissipation of spurious oscillations and energy. First-order schemes like θ-schemes, which are implicit, unconditionally stable, dissipative schemes, yield the same kind of results (Discretization 2.4.2).

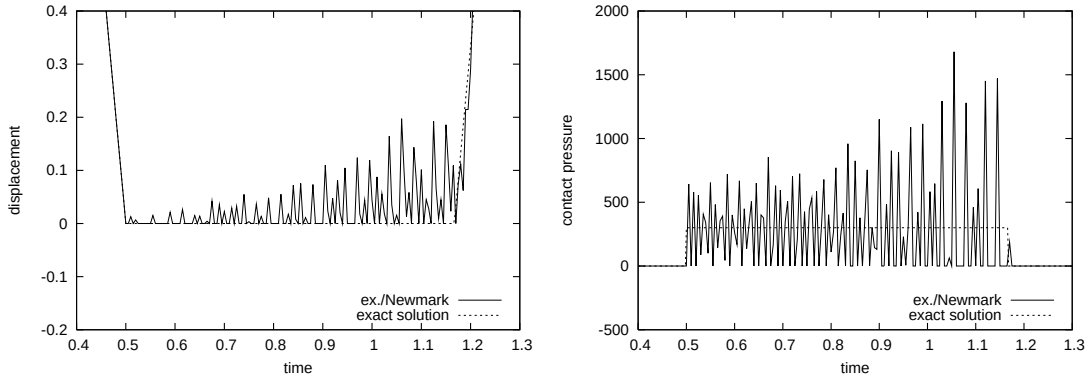

Fig. 2.5. Impact of an elastic bar. Displacement u_0^n (left) and contact pressure r^n (right). Discretization 2.4.1 with $\alpha = 0$, $\beta = 1/4$ and $\gamma = 1/2$. $\Delta x = 0.1$, $\Delta t = 0.005$, $\nu_c = 1.5$.

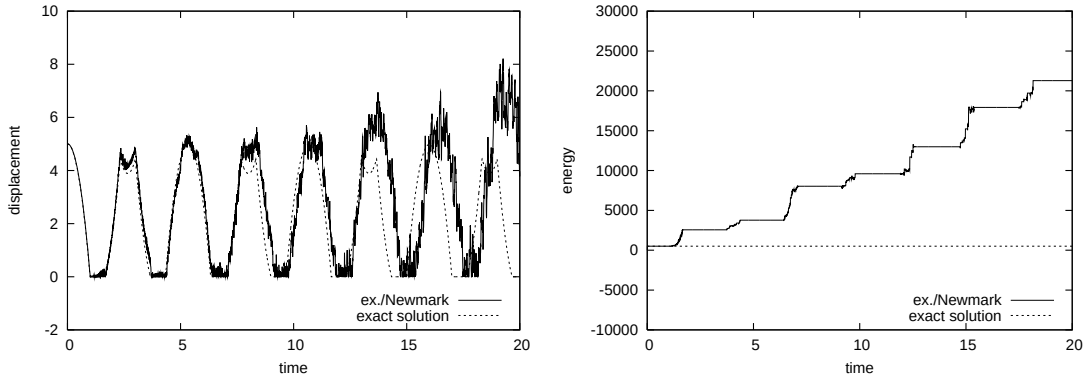

Fig. 2.6. Bounces of an elastic bar. Displacement u_0^n (left) and energy $\mathcal{E}^n - {}^{\mathrm{T}} F u^n$ (right). Discretization 2.4.1 with $\alpha = 0$, $\beta = 1/4$ and $\gamma = 1/2$. $\Delta x = 0.1$, $\Delta t = 0.005$, $\nu_c = 1.5$.

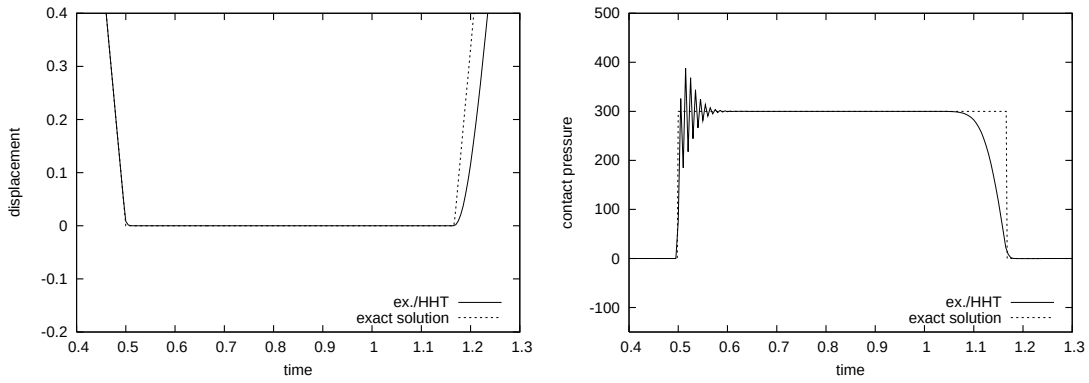

Fig. 2.7. Impact of an elastic bar. Displacement u_0^n (left) and contact pressure r^n (right). Discretization 2.4.1 with $\alpha = -0.2$, $\beta = 1/4(1-\alpha)^2$, $\gamma = 1/2 - \alpha$. $\Delta x = 0.1$, $\Delta t = 0.005$, $\nu_c = 1.5$.

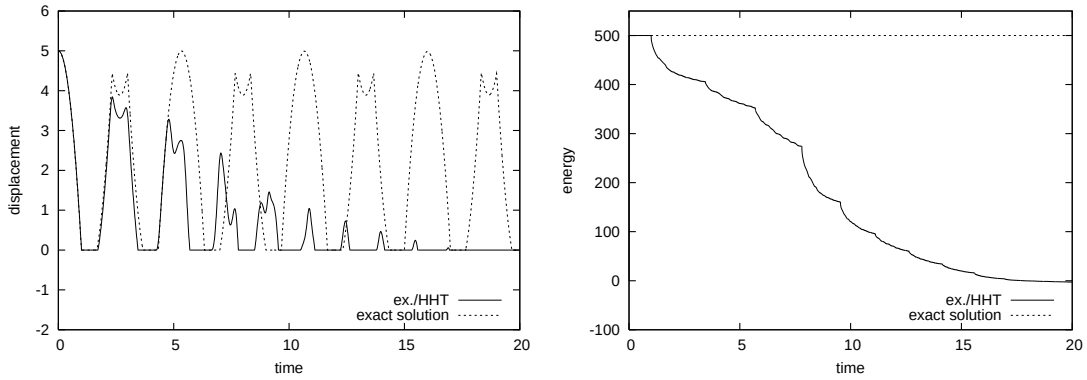

Fig. 2.8. Bounces of an elastic bar. Displacement u_0^n (left) and energy $\mathcal{E}^n - {}^{\mathrm{T}} F u^n$ (right). Discretization 2.4.1 with $\alpha = -0.2$, $\beta = 1/4(1-\alpha)^2$, $\gamma = 1/2 - \alpha$. $\Delta x = 0.1$, $\Delta t = 0.005$, $\nu_c = 1.5$.

Discretization 2.4.2 (θ-schemes [121]) *Seek* $u^{n+1},\ \dot{u}^{n+1} \in \mathbb{R}^{N_d}$, *and* $r^{n+1} \in \mathbb{R}^{N_c}$ *such that*

$$M\ddot{u}^{n+\frac{1}{2}} + Ku^{n+\theta} = F^{n+\theta} + {}^{\mathrm{T}} G r^{n+1}, \tag{2.30}$$

$$Gu^{n+1} \geq 0, \quad r^{n+1} \geq 0, \quad {}^{\mathrm{T}} r^{n+1} G u^{n+1} = 0, \tag{2.31}$$

$$u^{n+1} = u^n + \Delta t\ \dot{u}^{n+\theta}, \tag{2.32}$$

$$\dot{u}^{n+1} = \dot{u}^n + \Delta t\ \ddot{u}^{n+\frac{1}{2}}. \tag{2.33}$$

Remark 2.4. *It is sometimes advocated in the literature that first-order schemes must be preferred to second-order schemes for dynamic contact problems, due to the non-smoothness of the solution. We must distinguish two issues: the treatment of the contact condition and the treatment of the shock waves induced by the contact. As discussed previously, a proper treatment of the contact condition is not related to the order of the scheme. As for the shock waves, they require a scheme with dissipation and there exist second-order accurate schemes with dissipation, such as the HHT or Chung-Hulbert schemes. Note also that the amount of dissipation needed to treat the shock waves in the bulk is much smaller than that needed to dissipate the oscillations caused by the contact condition.*

Schemes dealing with the impact

First we briefly discuss a naive stabilized Newmark scheme where an extra-step is used to enforce the impact law (Discretization 2.4.3). Then, we consider two schemes with dissipative contact using a midpoint (Discretization 2.4.4) or a Newmark (Discretization 2.4.5) scheme. Finally, an improvement of these schemes based on the velocity-update method introduced in [89] can be considered; in the case of the Newmark scheme, this yields Discretization 2.4.6. An alternative approach to prevent the oscillations of the acceleration from transferring to the contact pressure consists in removing the mass at the contact boundary. This approach will be developed in Section 2.7.

To motivate the discussion, let us look for a scheme which satisfies the impact law or, more precisely, a scheme which enforces the acceleration to be zero during the contact phases.

No implicit Newmark scheme achieves this. An extra-step is needed to enforce the impact law (Discretization 2.4.3).

Discretization 2.4.3 (naive stabilized Newmark)
1. Seek $u^{n+1} \in \mathbb{R}^{N_d}$, $\dot{u}^{n+1} \in \mathbb{R}^{N_d}$, $\ddot{u}^{n+1} \in \mathbb{R}^{N_d}$, *and* $r^{n+1} \in \mathbb{R}^{N_c}$ *satisfying (2.24)-(2.27).*
2. If $G_i u^n \geq 0$ *and* $G_i u^{n+1} = 0$, *then* $\dot{u}^{n+1}$ *and* $\ddot{u}^{n+1}$ *are modified so that* $G_i \dot{u}^{n+1} = 0$ *and* $G_i \ddot{u}^{n+1} = 0$.

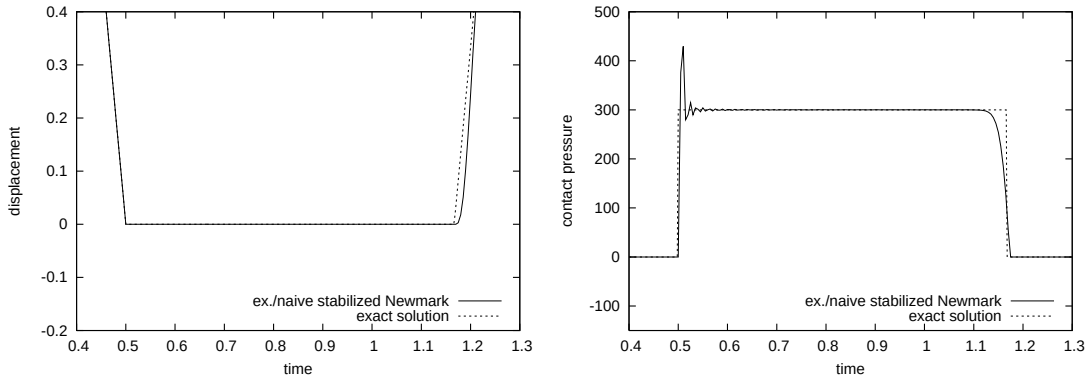

Fig. 2.9. Impact of an elastic bar. Displacement u_0^n (left) and contact pressure r^n (right). Discretization 2.4.3 with $\alpha = 0$, $\beta = 1/4$ and $\gamma = 1/2$. $\Delta x = 0.1$, $\Delta t = 0.005$, $\nu_c = 1.5$.

As illustrated in Figure 2.9, the large spurious oscillations have disappeared. However, this stabilization takes effect only one step after the impact, which explains the peak in the contact pressure just after the impact. A possible remedy consists in finding a time discretization where the contact force does not work or is at least dissipative. For instance, the midpoint scheme with an enforcement of the contact condition at time t^{n+1} (Discretization 2.4.4) achieves the following energy balance,

$$\mathcal{E}^{n+1} - \mathcal{E}^n =^{\mathrm{T}} r^{n+1}(Gu^{n+1} - Gu^n) +^{\mathrm{T}} F^{n+\frac{1}{2}}(u^{n+1} - u^n).$$

It is easy to check that the work of the contact force is always non-positive. As illustrated in Figure 2.10, the contact pressure still oscillates but the stress is practically free of oscillations. The oscillations of the stress after the bar has taken off are due to vibrations. However, energy losses, even if they are not substantial, do have an impact on the solution (Figure 2.11). It can also be noticed that energy losses do not vanish as Δt approaches zero, but this losses decrease with the mesh size.

Discretization 2.4.4 (Midpoint-implicit contact) *Seek* u^{n+1}, $\dot{u}^{n+1} \in \mathbb{R}^{N_d}$, *and* $r^{n+1} \in \mathbb{R}^{N_c}$ *such that*

$$M\ddot{u}^{n+\frac{1}{2}} + Ku^{n+\frac{1}{2}} = F^{n+\frac{1}{2}} +^{\mathrm{T}} Gr^{n+1}, \tag{2.34}$$

$$Gu^{n+1} \geq 0, \quad r^{n+1} \geq 0, \quad {}^{\mathrm{T}}r^{n+1}Gu^{n+1} = 0, \tag{2.35}$$

$$u^{n+1} = u^n + \Delta t\ \dot{u}^{n+\frac{1}{2}}, \tag{2.36}$$

$$\dot{u}^{n+1} = \dot{u}^n + \Delta t\ \ddot{u}^{n+\frac{1}{2}}. \tag{2.37}$$

Another scheme with dissipative contact has been proposed in [72]. The Newmark scheme with parameters $\beta = 1/2$ and $\gamma = 1$ and with an enforcement of the contact condition at time t^{n+1} yields the following energy balance

$$\mathcal{E}^{n+1} - \mathcal{E}^n =^{\mathrm{T}} r^{n+1}(Gu^{n+1} - Gu^n) - \frac{1}{2}{}^{\mathrm{T}}(u^{n+1} - u^n)K(u^{n+1} - u^n) +^{\mathrm{T}} F^{n+1}(u^{n+1} - u^n).$$

The work of the contact force is always non-positive, but there is a strong bulk dissipation. To remove this dissipation, one can, as proposed in [72], discretize the acceleration coming from the contact forces with the dissipative parameters ($\beta = 1/2$ and $\gamma = 1$) and the acceleration coming from the elastic forces with a trapezoidal rule ($\beta = 1/4$ and $\gamma = 1/2$). This yields Discretization 2.4.5. With such a discretization, the energy balance is

$$\mathcal{E}^{n+1} - \mathcal{E}^n =^{\mathrm{T}} r^{n+1}(Gu^{n+1} - Gu^n) +^{\mathrm{T}} F^{n+1}(u^{n+1} - u^n).$$

The numerical results are similar to those obtained with Discretization 2.4.4.

Discretization 2.4.5 (Newmark with dissipative contact [72]) *Seek* u^{n+1}, $\dot{u}^{n+1}$, $\ddot{u}_{int}^{n+1}$, $\ddot{u}_{con}^{n+1} \in \mathbb{R}^{N_d}$, *and* $r^{n+1} \in \mathbb{R}^{N_c}$ *such that*

$$M\ddot{u}^{n+1} + Ku^{n+1} = F^{n+1} +^{\mathrm{T}} Gr^{n+1}, \tag{2.38}$$

$$Gu^{n+1} \geq 0, \quad r^{n+1} \geq 0, \quad {}^{\mathrm{T}}r^{n+1}Gu^{n+1} = 0, \tag{2.39}$$

$$u^{n+1} = u^n + \Delta t\dot{u}^n + \frac{\Delta t^2}{2}\ddot{u}_{int}^{n+2\beta} + \frac{\Delta t^2}{2}\ddot{u}_{con}^{n+1}, \tag{2.40}$$

$$\dot{u}^{n+1} = \dot{u}^n + \Delta t\ddot{u}_{int}^{n+\gamma} + \Delta t\ddot{u}_{con}^{n+1}, \tag{2.41}$$

where $\ddot{u}^{n+1} = \ddot{u}_{int}^{n+1} + \ddot{u}_{con}^{n+1}$ *and* $M\ddot{u}_{con}^{n+1} =^{\mathrm{T}} Gr^{n+1}$.

To compensate energy losses in schemes with dissipative contact, the so-called velocity-update method can be considered [89]. Applied to Discretization 2.4.4, this procedure does not improve significantly the solution on our second benchmark. In [33], the authors add to Discretization

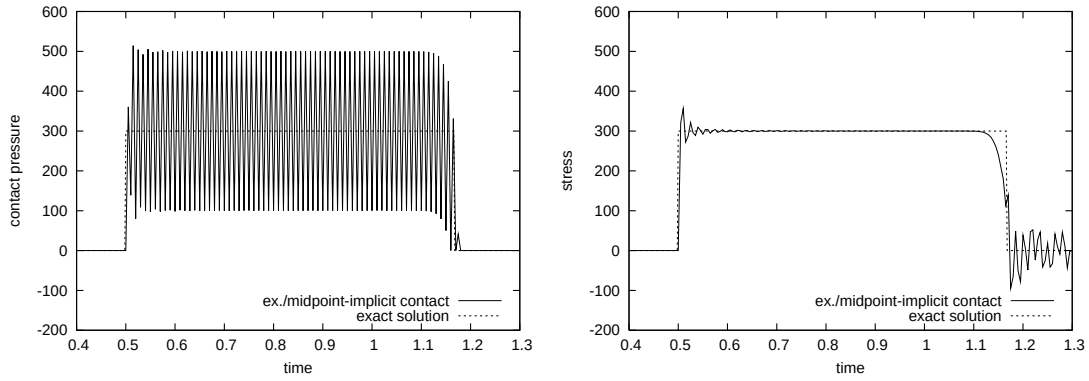

Fig. 2.10. Impact of an elastic bar. Contact pressure r^n (left) and stress $(Ku^n)_0$ (right). Discretization 2.4.4. $\Delta x = 0.1$, $\Delta t = 0.005$, $\nu_c = 1.5$.

2.4.5 a stabilization procedure (Discretization 2.4.6); see also [79] for further developments on this approach.

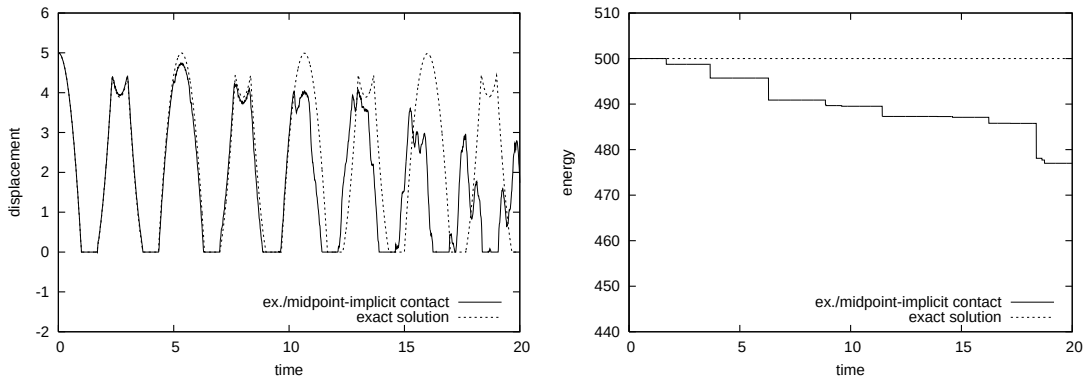

Fig. 2.11. Bounces of an elastic bar. Displacement u_0^n (left) and energy $\mathcal{E}^n - {}^{\mathrm{T}} F u^n$ (right). Discretization 2.4.4. $\Delta x = 0.1$, $\Delta t = 0.005$, $\nu_c = 1.5$.

Discretization 2.4.6 (stabilized Newmark [33])
1. Seek $u_{pred}^{n+1} \in \mathbb{R}^{N_d}$ *and* $\lambda^{n+1} \in \mathbb{R}^{N_c}$ *such that*

$$M u_{pred}^{n+1} = M u^n + \Delta t M \dot{u}^n, \tag{2.42}$$

$$G u_{pred}^{n+1} \geq 0, \quad \lambda^{n+1} \geq 0, \quad {}^{\mathrm{T}}\lambda^{n+1} G u_{pred}^{n+1} = 0. \tag{2.43}$$

2. Seek $u^{n+1}, \dot{u}^{n+1}, \ddot{u}_{int}^{n+1}$, $\ddot{u}_{con}^{n+1} \in \mathbb{R}^{N_d}$, *and* $r^{n+1} \in \mathbb{R}^{N_c}$ *satisfying* (2.38), (2.39), *and* (2.41), *while* (2.40) *is replaced by*

$$u^{n+1} = u_{pred}^{n+1} + \frac{\Delta t^2}{2} \ddot{u}_{int}^{n+2\beta} + \frac{\Delta t^2}{2} \ddot{u}_{con}^{n+1}. \tag{2.44}$$

The additional step required by Discretization 2.4.6 is not expensive compared with the main step, especially if the mass matrix is lumped. With this scheme, the contact pressure is now almost free of oscillations (Figure 2.12). Although the impact law is not fulfilled, there holds that if $G_i u^{n+1} = G_i u_{pred}^{n+1} = 0$, then $G_i \ddot{u}_{int}^{n+2\beta} + G_i \ddot{u}_{con}^{n+1} = 0$. Energy losses still remain sizeable in the second benchmark (Figure 2.13).

2.4.2 Semi-explicit schemes

Now, we try to discretize the elastodynamics part of the problem with an explicit scheme, such as the central difference scheme. It is not possible to enforce an explicit exact contact condition. Nevertheless, the contact condition can be enforced implicitly as in [102, 103].

Discretization 2.4.7 (Central differences-implicit contact [102, 103]) *Seek* $u^{n+1} \in \mathbb{R}^{N_d}$ *and* $r^{n+1} \in \mathbb{R}^{N_c}$ *such that*

$$M \left(\frac{u^{n+1} - 2u^n + u^{n-1}}{\Delta t^2} \right) + K u^n = F^n + {}^{\mathrm{T}} G r^{n+1}, \tag{2.45}$$

$$G u^{n+1} \geq 0, \quad r^{n+1} \geq 0, \quad {}^{\mathrm{T}} r^{n+1} G u^{n+1} = 0. \tag{2.46}$$

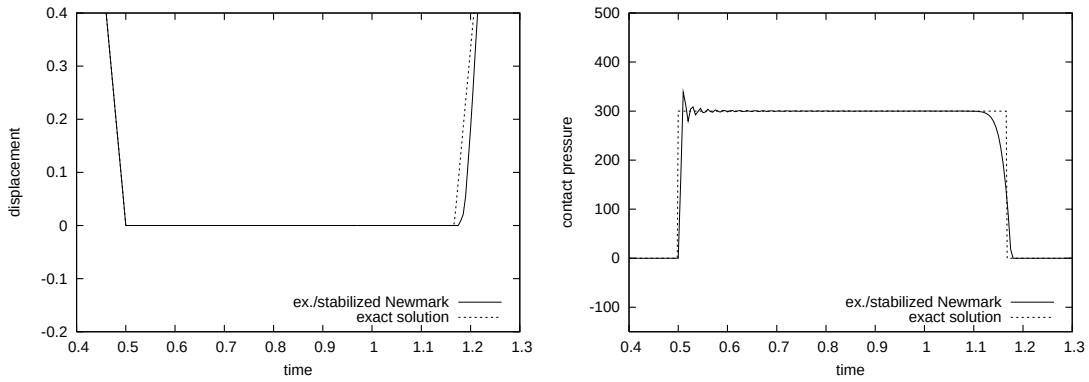

Fig. 2.12. Impact of an elastic bar. Displacement u_0^n (left) and contact pressure r^n (right). Discretization 2.4.6 with $\beta = 1/4$ and $\gamma = 1/2$ (lumped mass matrix). $\Delta x = 0.1$, $\Delta t = 0.005$, $\nu_c = 1.5$.

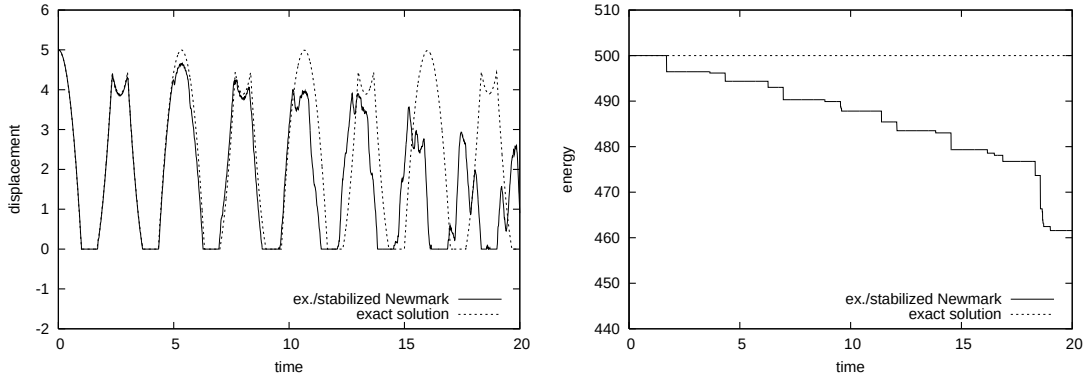

Fig. 2.13. Bounces of an elastic bar. Displacement u_0^n (left) and energy $\mathcal{E}^n = {}^{\mathrm{T}} F u^n$ (right). Discretization 2.4.6 with $\beta = 1/4$ and $\gamma = 1/2$ (lumped mass matrix). $\Delta x = 0.1$, $\Delta t = 0.005$, $\nu_c = 1.5$.

With a lumped mass matrix, this scheme is equivalent to that proposed in [22] where the contact condition is enforced by a projection step in the following semi-explicit way (observe that the first step is explicit):
1. Seek $u^{n+1} \in \mathbb{R}^{N_d}$ such that

$$M \left(\frac{u^{n+1} - 2u^n + u^{n-1}}{\Delta t^2} \right) + K u^n = F^n. \tag{2.47}$$

2. If $G_i u^{n+1} < 0$, then u^{n+1} is modified so that $G_i u^{n+1} = 0$.
It is easy to check that with Discretization 2.4.7, the acceleration at the contact boundary vanishes during a contact phase (after two steps). Indeed, if $G_i u^{n+1} = G_i u^n = G_i u^{n-1} = 0$, then $G_i \ddot{u}^n = G_i \left(\frac{u^{n+1} - 2u^n + u^{n-1}}{\Delta t^2} \right) = 0$. Consequently, there are (almost) no spurious oscillations (Figure 2.14). The shifted energy balance reads

$$\mathcal{E}^{n+1}_{0,\frac{1}{2}} - \mathcal{E}^n_{0,\frac{1}{2}} = {}^{\mathrm{T}} \left(\frac{r^{n+2} + r^{n+1}}{2} \right) (G u^{n+1} - G u^n) + {}^{\mathrm{T}} \left(\frac{F^{n+1} + F^n}{2} \right) (u^{n+1} - u^n).$$

Energy losses, although moderate, affect the quality of the solution after some impacts (Figure 2.15). In 1D, the convergence of the discrete solutions to the continuous solution, provided a

stability condition is met (the same as in the linear case), has been established in [111]. The convergence of the discrete solutions to a semi-discrete solution has been proven in [102, 103].

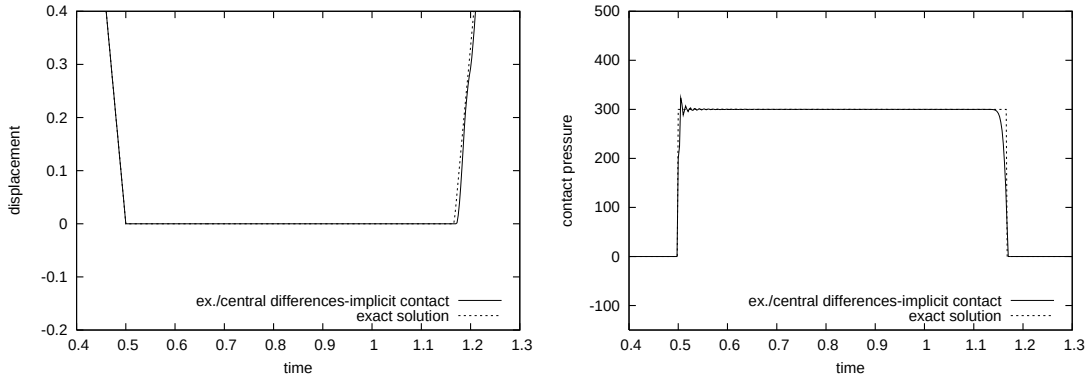

Fig. 2.14. Impact of an elastic bar. Displacement u_0^n (left) and contact pressure r^n (right). Discretization 2.4.7 (lumped mass matrix). $\Delta x = 0.1$, $\Delta t = 0.0025$, $\nu_c = 0.75$.

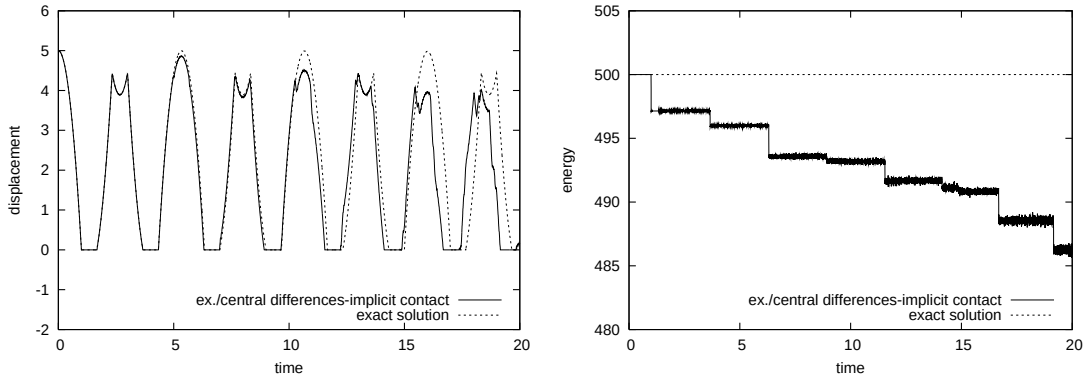

Fig. 2.15. Bounces of an elastic bar. Displacement u_0^n (left) and energy $\mathcal{E}^n - {}^{\mathrm{T}} F u^n$ (right). Discretization 2.4.7 (lumped mass matrix). $\Delta x = 0.1$, $\Delta t = 0.0025$, $\nu_c = 0.75$.

2.5 Discretizations with penalty contact condition

In this part we combine standard finite elements in space and a penalty approximation of the contact condition (the penalty parameter is denoted by ϵ). Then, the semi-discrete problem is a mere system of ODEs.

Problem 2.2. Seek a displacement $u : [0,T] \to \mathbb{R}^{N_d}$ such that, $\forall t \in [0,T]$,

$$M\ddot{u}(t) + Ku(t) = f(t) + {}^{\mathrm{T}} G R_\epsilon(Gu(t)), \tag{2.48}$$

with the initial conditions $u(0) = u^0$ and $\dot{u}(0) = v^0$.

Problem 2.2 being a system of ODEs with a Lipschitz continuous right-hand side, has one and only one solution, which is furthermore twice differentiable in time.

2.5.1 Implicit schemes

To begin with, we discretize Problem 2.2 with an implicit Newmark scheme.

Discretization 2.5.1 (Newmark) *Seek* $u^{n+1},\ \dot{u}^{n+1},\ \ddot{u}^{n+1} \in \mathbb{R}^{N_d}$, *such that*

$$M\ddot{u}^{n+1} + Ku^{n+1} = F^{n+1} +^{\mathrm{T}} GR_\epsilon(Gu^{n+1}), \tag{2.49}$$

$$u^{n+1} = u^n + \Delta t\dot{u}^n + \frac{\Delta t^2}{2}\ddot{u}^{n+2\beta}, \tag{2.50}$$

$$\dot{u}^{n+1} = \dot{u}^n + \Delta t\ddot{u}^{n+\gamma}. \tag{2.51}$$

We observe that the penalty formulation tends to reduce spurious oscillations (Figure 2.16). Nevertheless, the oscillations grow with $1/\epsilon$ (Figure 2.17). This is not surprising since the penalty contact condition tends to the exact contact condition when $1/\epsilon$ tends to infinity. If the oscillations are too large, stabilization procedures can be used (see for instance the procedure described in [2]). With the addition of a penalty term, the Newmark scheme (trapezoidal rule) no longer conserves the energy. The energy losses are moderate but not so marginal (Figure 2.18); the energy behavior is poorer when $1/\epsilon$ grows. In [2, 63], the authors proposed a discretization of the penalty term which enables to recover energy control by conserving an augmented energy (Discretization 2.5.2). It is based on a midpoint scheme. On our benchmark problems, it does not yield significantly better results.

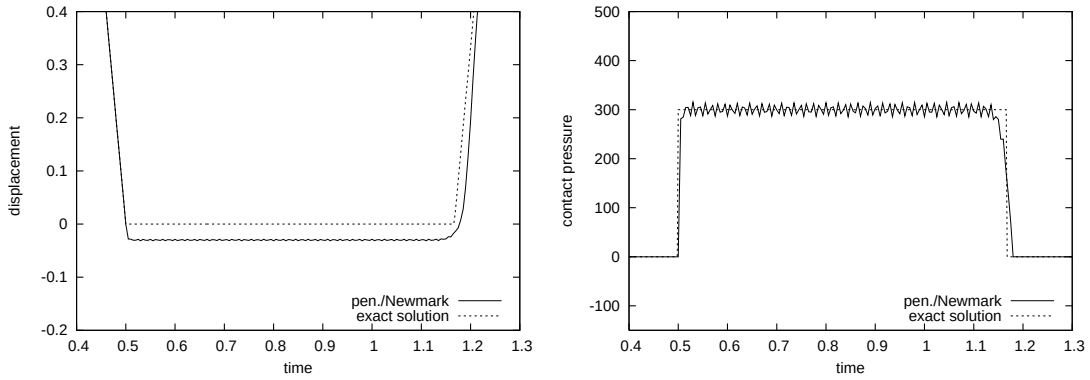

Fig. 2.16. Impact of an elastic bar. Displacement u_0^n (left) and contact pressure ${}^{\mathrm{T}}GR_\epsilon(Gu^n)$ (right). Discretization 2.5.1 with $\alpha = 0$, $\beta = 1/4$, $\gamma = 1/2$, $\epsilon = 10^{-4}$. $\Delta x = 0.1$, $\Delta t = 0.005$, $\nu_c = 1.5$.

Discretization 2.5.2 (Energy-controlling midpoint [2, 63]) *Seek* $u^{n+1},\ \dot{u}^{n+1} \in \mathbb{R}^{N_d}$, *such that*

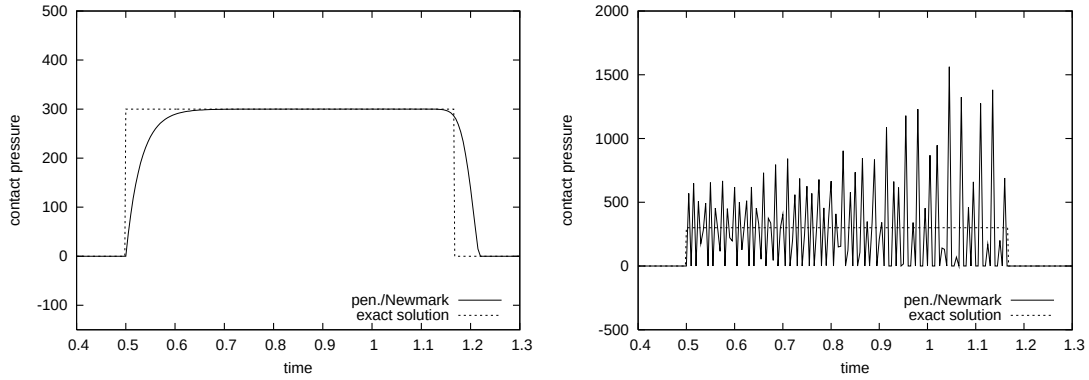

Fig. 2.17. Impact of an elastic bar. Contact pressure ${}^{\mathrm{T}}GR_\epsilon(Gu^n)$. Discretization 2.5.1 with $\alpha = 0$, $\beta = 1/4$ and $\gamma = 1/2$. $\Delta x = 0.1$, $\Delta t = 0.005$, $\nu_c = 1.5$. $\epsilon = 10^{-3}$ (left) and $\epsilon = 10^{-5}$ (right).

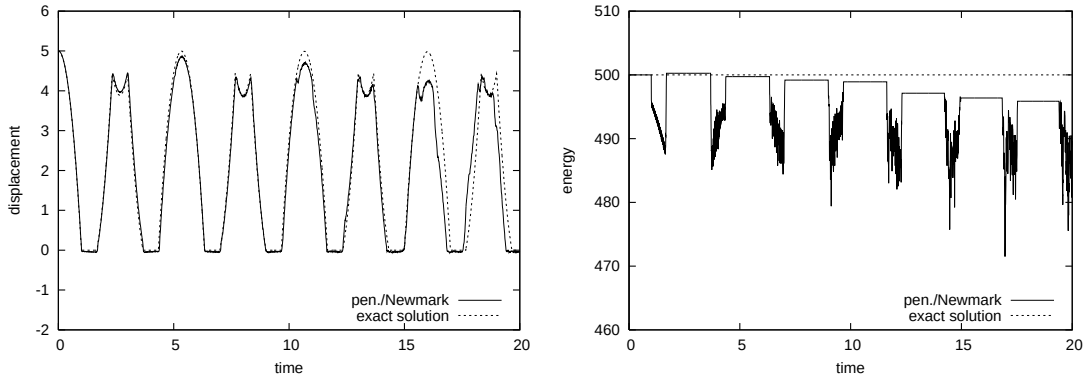

Fig. 2.18. Bounces of an elastic bar. Displacement u_0^n (left) and energy $\mathcal{E}^n -^{\mathrm{T}} Fu^n$ (right). Discretization 2.5.1 with $\alpha = 0$, $\beta = 1/4$ and $\gamma = 1/2$, $\epsilon = 10^{-4}$. $\Delta x = 0.1$, $\Delta t = 0.005$, $\nu_c = 1.5$.

$$M\ddot{u}^{n+\frac{1}{2}} + Ku^{n+\frac{1}{2}} = F^{n+\frac{1}{2}} +^{\mathrm{T}} G\tilde{R}_\epsilon(Gu^{n+1}, Gu^n), \tag{2.52}$$

$$u^{n+1} = u^n + \Delta t\dot{u}^{n+\frac{1}{2}}, \tag{2.53}$$

$$\dot{u}^{n+1} = \dot{u}^n + \Delta t\ddot{u}^{n+\frac{1}{2}}, \tag{2.54}$$

where

$$(\tilde{R}_\epsilon(Gu^{n+1}, Gu^n))_i = \begin{cases} \frac{1}{2\epsilon}\frac{((G_iu^{n+1})^-)^2 - ((G_iu^n)^-)^2}{G_iu^{n+1} - G_iu^n} & \text{if } G_iu^n \neq G_iu^{n+1} \\ 0 & \text{if } G_iu^n = G_iu^{n+1} \geq 0 \\ \frac{1}{2\epsilon}(Gu^{n+1} + Gu^n) & \text{if } G_iu^n = G_iu^{n+1} < 0 \end{cases} \tag{2.55}$$

Defining the augmented energy $\mathcal{E}_{pen}^n := \mathcal{E}^n + \frac{1}{2\epsilon}((Gu^n)^-)^2$, there holds

$$\mathcal{E}_{pen}^{n+1} - \mathcal{E}_{pen}^n =^{\mathrm{T}} F^{n+\frac{1}{2}}(u^{n+1} - u^n).$$

Since $\mathcal{E}_{pen}^n$ is an upper bound of $\mathcal{E}^n$, controlling $\mathcal{E}_{pen}^n$ allows one to control $\mathcal{E}^n$.

2.5.2 Explicit schemes

We can also use an explicit scheme for Problem 2.2.

Discretization 2.5.3 (Central differences) *Seek* $u^{n+1} \in \mathbb{R}^{N_d}$ *such that*

$$M\left(\frac{u^{n+1}-2u^n+u^{n-1}}{\Delta t^2}\right)+Ku^n=F^n+^{\mathrm{T}}GR_\epsilon(Gu^n). \tag{2.56}$$

The results are similar to those obtained with the implicit approach. Unfortunately, the penalty term stiffens the system of ODEs, which limits the stability domain of the schemes. More precisely, it introduces a constraint on the time step of the form $\Delta t \leq O(\sqrt{\rho\epsilon\Delta x_c})$, where Δx_c is the mesh size near the contact boundary [9].

2.6 Discretizations with contact condition in velocity

In this part, standard finite elements in space are combined with an approximation of the contact condition involving the velocity.

Problem 2.3. Seek a displacement $u : [0,T] \to \mathbb{R}^{N_d}$ and a contact pressure $r : [0,T] \to \mathbb{R}^{N_c}$ such that, for almost every $t \in [0,T]$,

$$M\ddot{u}(t)+Ku(t)=f(t)+^{\mathrm{T}}Gr(t), \tag{2.57}$$

$$G\dot{u}(t)\geq 0, \quad r(t)\geq 0, \quad {}^{\mathrm{T}}r(t)G\dot{u}(t)=0, \tag{2.58}$$

with the initial conditions $u(0)=u^0$ and $\dot{u}(0)=v^0$.

With this contact condition in velocity, the semi-discrete problem is much simpler than (2.19)-(2.20). Problem 2.3 is still a system of ODEs under unilateral constraints, but the constraint involves now the velocity instead of the displacement. The general theory developed in [16, 53] applies to Problem 2.3. The solution u is unique [16]. Furthermore, u is continuous and $\dot{u}$ is differentiable in time almost everywhere, so that the equations have a sense at almost every time. The time discretization has been extensively studied in [53].

Unfortunately, the contact condition in velocity is not equivalent to the Signorini condition as discussed in Section 2.2.3. The strategy adopted is the following: if a node satisfies the non-interpenetration condition, then at the next iteration no constraint is enforced on this node; if a node breaks the non-interpenetration condition, then at the next iteration the contact condition in velocity will be applied to this node. This approach allows for slight interpenetration. At each time step, we define the matrix G^n whose rows G_i^n are

$$G_i^n=\begin{cases}(0\dots 0) & \text{if } G_iu^n\geq 0\\ G_i & \text{if } G_iu^n<0\end{cases} \tag{2.59}$$

This approach based on a contact condition in velocity has also been widely used in rigid-body dynamics with impacts (see, e.g., [116]).

2.6.1 Implicit schemes

A midpoint scheme with contact condition in velocity has been proposed in [88]; see also [74] for the contact condition.

Discretization 2.6.1 (Midpoint [88]) *Seek* $u^{n+1},\ \dot{u}^{n+1} \in \mathbb{R}^{N_d}$, *and* $r^{n+1} \in \mathbb{R}^{N_c}$ *such that*

$$M\ddot{u}^{n+\frac{1}{2}} + Ku^{n+\frac{1}{2}} = F^{n+\frac{1}{2}} +^{\mathrm{T}} G^n r^{n+\frac{1}{2}}, \tag{2.60}$$

$$G^n \dot{u}^{n+\frac{1}{2}} \geq 0, \quad r^{n+\frac{1}{2}} \geq 0, \quad {}^{\mathrm{T}}r^{n+\frac{1}{2}} G^n \dot{u}^{n+\frac{1}{2}} = 0, \tag{2.61}$$

$$u^{n+1} = u^n + \Delta t\ \dot{u}^{n+\frac{1}{2}}, \tag{2.62}$$

$$\dot{u}^{n+1} = \dot{u}^n + \Delta t\ \ddot{u}^{n+\frac{1}{2}}. \tag{2.63}$$

An interesting feature of this scheme is to be energy-conserving,

$$\mathcal{E}^{n+1} - \mathcal{E}^n =^{\mathrm{T}} F^{n+\frac{1}{2}}(u^{n+1} - u^n).$$

The contact pressure does not perturb the structure despite its oscillations (Figure 2.19). Energy is preserved, and the solution for the second benchmark is quite satisfactory, although not as accurate as with Discretization 2.5.1 after several impacts (Figure 2.20).

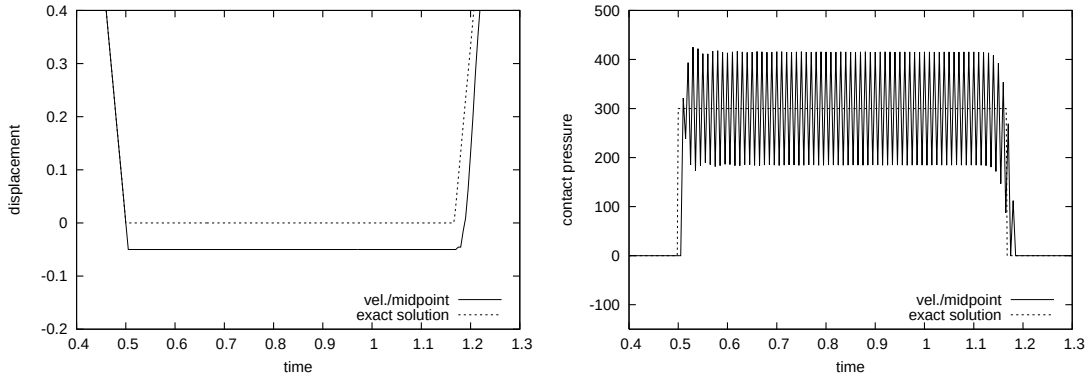

Fig. 2.19. Impact of an elastic bar. Displacement u_0^n (left) and stress (right). Discretization 2.6.1 with $\alpha = 0$, $\beta = 1/4$ and $\gamma = 1/2$. $\Delta x = 0.1$, $\Delta t = 0.005$, $\nu_c = 1.5$.

2.6.2 Semi-explicit schemes

A semi-explicit scheme with contact condition in velocity has been proposed in [9].

Discretization 2.6.2 (Central differences [9]) *Seek* $u^{n+1} \in \mathbb{R}^{N_d}$ *and* $r^{n+1} \in \mathbb{R}^{N_c}$ *such that*

$$M\left(\frac{u^{n+1} - 2u^n + u^{n-1}}{\Delta t^2}\right) + Ku^n = F^n +^{\mathrm{T}} G^n r^{n+1}, \tag{2.64}$$

$$G^n(u^{n+1} - u^n) \geq 0, \quad r^{n+1} \geq 0, \quad {}^{\mathrm{T}}r^{n+1} G^n(u^{n+1} - u^n) = 0. \tag{2.65}$$

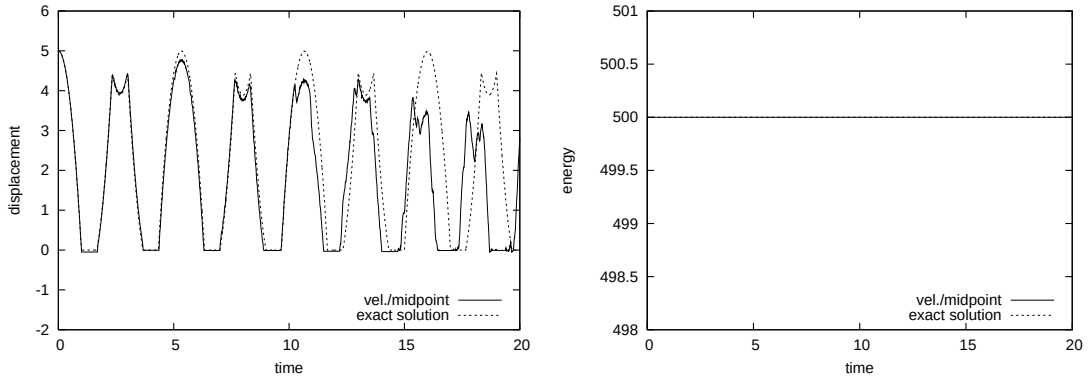

Fig. 2.20. Bounces of an elastic bar. Displacement u_0^n (left) and energy $\mathcal{E}^n - {}^{\mathrm{T}} F u^n$ (right). Discretization 2.6.1 with $\alpha = 0$, $\beta = 1/4$ and $\gamma = 1/2$. $\Delta x = 0.1$, $\Delta t = 0.005$, $\nu_c = 1.5$.

Numerical simulations suggest that the stability condition of the central difference scheme is not tightened by the contact condition. The results are similar to those obtained with Discretization 2.4.7 (Figures 2.21 and 2.22).

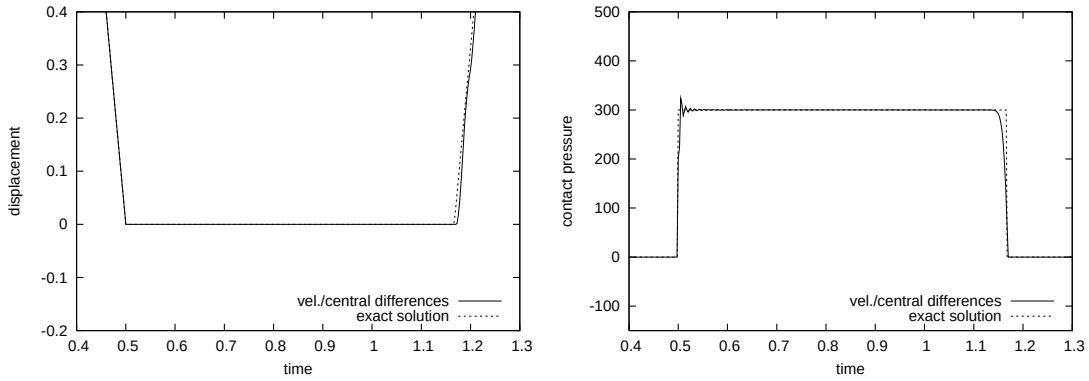

Fig. 2.21. Impact of an elastic bar. Displacement u_0^n (left) and contact pressure r^n (right). Discretization 2.6.2 (lumped mass matrix). $\Delta x = 0.1$, $\Delta t = 0.0025$, $\nu_c = 0.75$.

2.7 Discretizations with modified mass

In the previous three parts, we have considered various ways of enforcing the contact condition. Here we describe methods based on a modification of the mass matrix. Such methods are thus compatible with any enforcement of the contact condition. For brevity, we restrict ourselves to an exact enforcement of the contact condition. In the modified mass matrix, the entries associated with the normal displacements at the contact boundary are set to zero. The motivation for this modification is very simple: if the mass is removed, the inertial forces and the oscillations are eliminated. This approach has been introduced in [75].

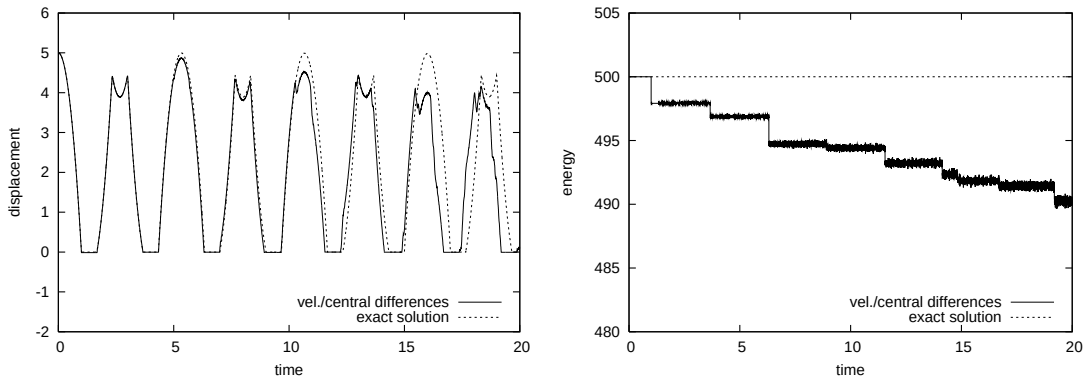

Fig. 2.22. Bounces of an elastic bar. Displacement u_0^n (left) and energy $\mathcal{E}^n - {}^{\mathrm{T}} F u^n$ (right). Discretization 2.6.2 (lumped mass matrix). $\Delta x = 0.1$, $\Delta t = 0.0025$, $\nu_c = 0.75$.

Set $N_d^* := N_d - N_c$. For the sake of simplicity, suppose that the degrees of freedom associated with normal displacements at the contact boundary are numbered from $N_d^* + 1$ to N_d. The modified mass matrix is defined as

$$M^* = \begin{pmatrix} M_{**} & 0 \\ 0 & 0 \end{pmatrix}.$$

Many choices are possible to build the block M_{**}. In [57, 75], the authors devise various methods to preserve some features of the standard mass matrix (the total mass, the center of gravity, and the moments of inertia); see also [107] for further results. We can also simply keep the corresponding block in the standard mass matrix (and this is what we will do in our numerical simulations below). The modified problem reads

$$M^* \ddot{u}(t) + Ku(t) = F(t) + {}^{\mathrm{T}} G r(t), \tag{2.66}$$

$$Gu(t) \geq 0, \quad r(t) \geq 0, \quad {}^{\mathrm{T}} r(t) G u(t) = 0. \tag{2.67}$$

If we set $u(t) = \begin{pmatrix} u_*(t) \\ u_c(t) \end{pmatrix}$, $K = \begin{pmatrix} K_{**} & K_{*c} \\ K_{c*} & K_{cc} \end{pmatrix}$, $F(t) = \begin{pmatrix} F_*(t) \\ F_c(t) \end{pmatrix}$, and $G = (0 \; G_c)$, then equations (2.66) and (2.67) can be recast as

$$M_{**} \ddot{u}_*(t) + K_{**} u_*(t) + K_{*c} u_c(t) = F_*(t), \tag{2.68}$$

$$K_{c*} u_*(t) + K_{cc} u_c(t) = F_c(t) + {}^{\mathrm{T}} G_c r(t), \tag{2.69}$$

$$G_c u_c(t) \geq 0, \quad r(t) \geq 0, \quad {}^{\mathrm{T}} r(t) G_c u_c(t) = 0. \tag{2.70}$$

For given t and $u_*(t)$, there exists one and only one $u_c(t)$ satisfying (2.69) and (2.70). Denote by $Q : [0,T] \times \mathbb{R}^{N_d^*} \to \mathbb{R}^{N_c}$ the nonlinear map such that $u_c(t) = Q(t, u_*(t))$.

Problem 2.4. Seek a displacement $u : [0,T] \to \mathbb{R}^{N_d}$ such that, for all $t \in [0,T]$,

$$M_{**} \ddot{u}_*(t) + K_{**} u_*(t) + K_{*c} Q(t, u_*(t)) = F_*(t), \tag{2.71}$$

$$u_c(t) = Q(t, u_*(t)), \tag{2.72}$$

with the initial conditions $u(0) = u^0$ and $\dot{u}(0) = v^0$.

The operator $Q(t,\cdot)$ is Lipschitz continuous at each time t, so that equation (2.71) is a Lipschitz system of ODEs. Therefore, it has a unique solution u_*, twice differentiable in time. Owing to (2.72), u_c is differentiable in time almost everywhere. The detailed mathematical analysis of the space semi-discrete modified mass formulation can be found in [75, 35]. A result of convergence of the space semi-discrete solutions to a continuous solution is proven for viscoelastic materials in [35].

Remark 2.5. *In contrast to the semi-discrete problem with standard mass matrix, the semi-discrete problem with modified mass matrix does not require an impact law and conserves a modified energy where the mass modification is accounted for in the kinetic energy [75].*

2.7.1 Implicit schemes

A HHT-Newmark scheme can be used for Problem 2.4.

Discretization 2.7.1 (HHT-Newmark [75]) *Seek* $u^{n+1} \in \mathbb{R}^{N_d}$, $\dot{u}_*^{n+1} \in \mathbb{R}^{N_d}$ *and* $\ddot{u}_*^{n+1} \in \mathbb{R}^{N_d}$ *such that*

$$M_{**}\ddot{u}_*^{n+1} + K_{**}u_*^{n+1+\alpha} + K_{*c}Q(t^{n+1+\alpha}, u_*^{n+1+\alpha}) = F_*^{n+1+\alpha}, \tag{2.73}$$

$$u_c^{n+1+\alpha} = Q(t^{n+1+\alpha}, u_*^{n+1+\alpha}), \tag{2.74}$$

$$u_*^{n+1} = u_*^n + \Delta t\dot{u}_*^n + \frac{\Delta t^2}{2}\ddot{u}_*^{n+2\beta}, \tag{2.75}$$

$$\dot{u}_*^{n+1} = \dot{u}_*^n + \Delta t\ddot{u}_*^{n+\gamma}. \tag{2.76}$$

The equations can be recast as a linear complementarity problem,

$$M^*\ddot{u}^{n+1} + Ku^{n+1+\alpha} = F^{n+1+\alpha} +^{\mathrm{T}} Gr^{n+1}, \tag{2.77}$$

$$Gu^{n+1} \geq 0, \quad r^{n+1} \geq 0, \quad {}^{\mathrm{T}}r^{n+1}Gu^{n+1} = 0, \tag{2.78}$$

$$u^{n+1} = u^n + \Delta t\dot{u}^n + \frac{\Delta t^2}{2}\ddot{u}^{n+2\beta}, \tag{2.79}$$

$$\dot{u}^{n+1} = \dot{u}^n + \Delta t\ddot{u}^{n+\gamma}. \tag{2.80}$$

In spite of the modification of the mass matrix, the problem is well posed. In practice, we use this set of equations to compute the solution. As expected, the large oscillations have disappeared during the contact phase (Figure 2.23). The energy behavior is also very satisfactory (Figure 2.24), since there holds

$$\mathcal{E}_*^{n+1} - \mathcal{E}_*^n = {}^{\mathrm{T}}\left(\frac{r^{n+1}+r^n}{2}\right)(Gu^{n+1} - Gu^n) + {}^{\mathrm{T}}\left(\frac{F^{n+1}+F^n}{2}\right)(u^{n+1} - u^n),$$

where the modified energy $\mathcal{E}_*^n$ has the same expression as $\mathcal{E}^n$, except that M is replaced by M^*. The displacement after several impacts is quite satisfactory, although not as accurate as with Discretization 2.5.1 (Figure 2.24).

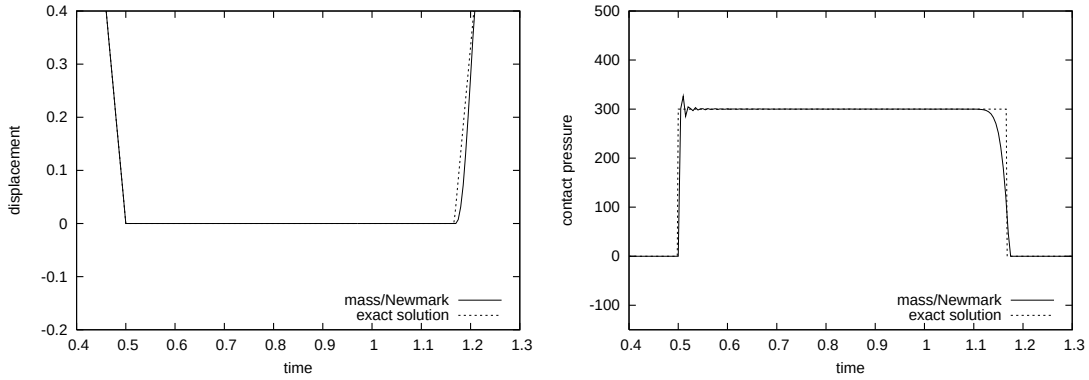

Fig. 2.23. Impact of an elastic bar. Displacement u_0^n and contact pressure r^n. Discretization 2.7.1 with $\alpha = 0$, $\beta = 1/4$ and $\gamma = 1/2$. $\Delta x = 0.1$, $\Delta t = 0.005$, $\nu_c = 1.5$.

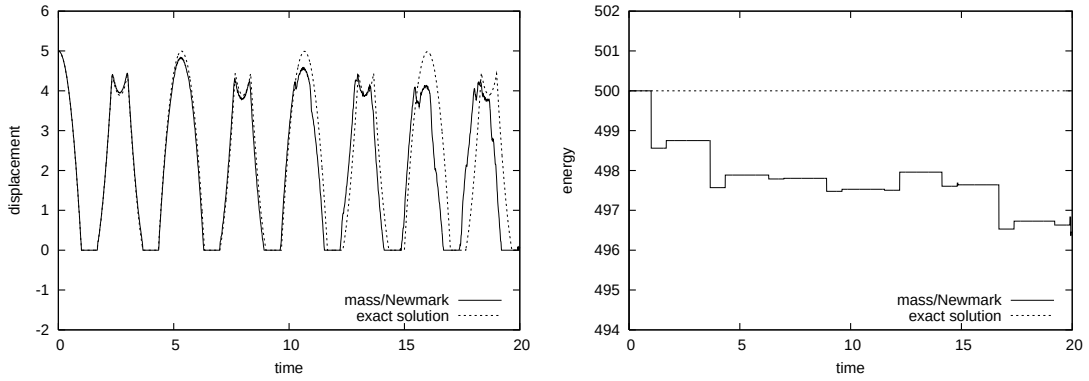

Fig. 2.24. Bounces of an elastic bar. Displacement u_0^n (left) and modified energy $\mathcal{E}_*^n - {}^{\mathrm{T}} F u^n$ (right). Discretization 2.7.1 with $\alpha = 0$, $\beta = 1/4$ and $\gamma = 1/2$. $\Delta x = 0.1$, $\Delta t = 0.005$, $\nu_c = 1.5$.

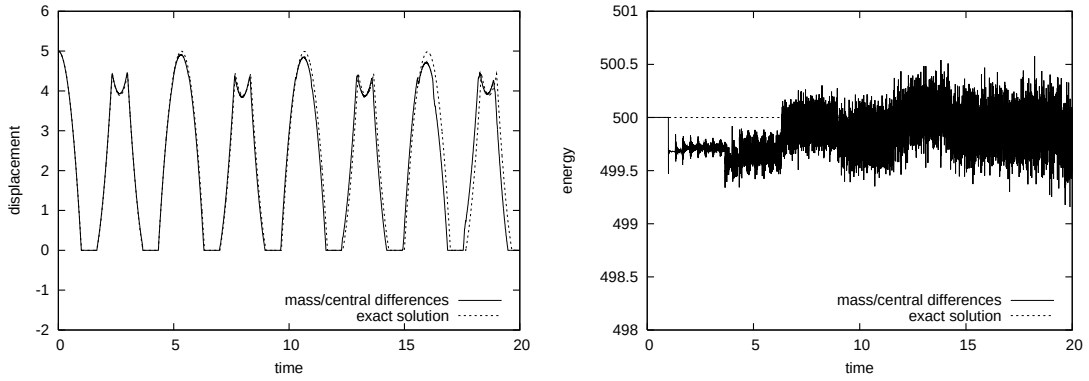

Fig. 2.25. Bounces of an elastic bar. Displacement u_0^n (left) and modified energy $\mathcal{E}_*^n - {}^{\mathrm{T}} F u^n$ (right). Discretization 2.7.2 (lumped mass matrix). $\Delta x = 0.1$, $\Delta t = 0.0025$, $\nu_c = 0.75$.

2.7.2 Semi-explicit schemes

We can discretize Problem 2.4 with an explicit scheme, such as the central difference scheme. This yields a semi-explicit scheme.

Discretization 2.7.2 (Central differences [38]) *Seek $u^{n+1} \in \mathbb{R}^{N_d}$ such that*

$$M_{**}\left(\frac{u_*^{n+1}-2u_*^n+u_*^{n-1}}{\Delta t^2}\right)+K_{**}u_*^n+K_{*c}Q(t^n,u_*^n)=F_*^n, \tag{2.81}$$

$$u_c^{n+1}=Q(t^{n+1},u_*^{n+1}). \tag{2.82}$$

In practice, the equations are solved as follows: 1. Seek $u_*^{n+1} \in \mathbb{R}^{N_d}$ such that

$$M_{**}\left(\frac{u_*^{n+1}-2u_*^n+u_*^{n-1}}{\Delta t^2}\right)+K_{**}u_*^n+K_{*c}u_c^n=F_*^n. \tag{2.83}$$

2. Seek $u_c^{n+1} \in \mathbb{R}^{N_d^*}$ and $r^{n+1} \in \mathbb{R}^{N_c}$ such that

$$K_{c*}u_*^{n+1}+K_{cc}u_c^{n+1}=F_c^{n+1}+^{\mathrm{T}}G_c r^{n+1}, \tag{2.84}$$

$$G_c u_c^{n+1} \geq 0, \quad r^{n+1} \geq 0, \quad {}^{\mathrm{T}}rG_c u_c^{n+1}=0. \tag{2.85}$$

The first step is explicit, and the mass matrix M_{**} can be lumped. The second step is a constrained problem on the variable u_c^{n+1} only. Discretization 2.7.2 amounts to

$$M^*\left(\frac{u^{n+1}-2u^n+u^{n-1}}{\Delta t^2}\right)+Ku^n=F^n+^{\mathrm{T}}Gr^n,$$

$$Gu^n \geq 0, \quad r^n \geq 0, \quad {}^{\mathrm{T}}r^nGu^n=0,$$

and yields the modified shifted energy balance

$$\mathcal{E}_{0,\frac{1}{2}*}^{n+1}-\mathcal{E}_{0,\frac{1}{2}*}^{n}=^{\mathrm{T}}\left(\frac{r^{n+1}+r^n}{2}\right)(Gu^{n+1}-Gu^n)+^{\mathrm{T}}\left(\frac{F^{n+1}+F^n}{2}\right)(u^{n+1}-u^n),$$

where $\mathcal{E}_{0,\frac{1}{2}*}^{n}$ has the same expression than $\mathcal{E}_{0,\frac{1}{2}}^{n}$, except that M is replaced by M^*. We observe numerically that the stability condition on the time step is the same as in the linear case. Compared with Discretizations 2.4.7 and 2.6.2, the semi-explicit modified mass method shows a better energy behavior and a better solution (Figure 2.25). Additional tests show that the amplitude of energy oscillations decreases at least linearly with Δt at fixed Courant number. Results on the first benchmark are similar to those with the implicit scheme.

2.8 A 2D benchmark

We consider the bounces of an elastic disk against a rigid ground (Figure 2.26). The reference configuration is the undeformed disk touching the ground. The disk is dropped, undeformed, with a zero initial velocity, under a gravity acceleration g_0, the displacement of its center being initially h_0. The disk has radius R. The material is supposed to be linear elastic (plane strain)

with a Young modulus E, a Poisson ratio ν, and a mass density ρ. The contact boundary Γ^c is the lower half part of the disk boundary. We define the contact condition using the normal vector to the ground. The parameters are $E = 4000$, $\nu = 0.2$, $\rho = 100$, $g_0 = 5$, $R = 1$, $h_0 = 0.1$. The disk is meshed with triangles (100 edges on the boundary, 1804 triangles, 953 vertices, see Figure 2.26) and we use linear finite elements. The number of nodes lying on the contact boundary is 51. Simulations are performed using FreeFem++ [65]. The Courant number is defined as $\nu_c := c_d \frac{\Delta x}{\Delta t}$ where $c_d = \frac{20}{3}$ is the speed of dilatational waves and $\Delta x = 0.0628$ the length of boundary edges.

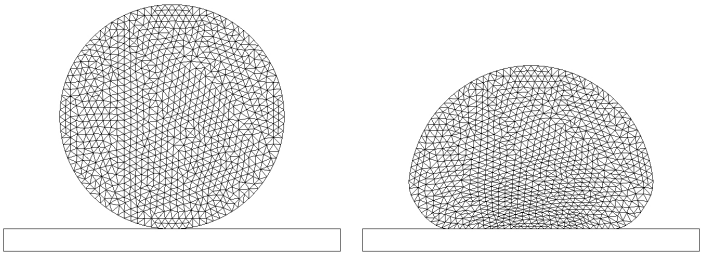

Fig. 2.26. Bounces of an elastic disk. Reference configuration (left), mesh (middle), and deformed configuration after the first impact (right).

Results are presented for the implicit Discretizations 2.4.6, 2.6.1, and 2.7.1 (Figure 2.27) and for the semi-explicit Discretizations 2.4.7 and 2.7.2 (Figure 2.28). For the semi-explicit schemes, the observed stability condition is $\nu_c \leq 0.65$. In all cases, the trajectory of the disk center is rather well captured, with some discrepancies appearing after five bounces. The energy behaviors remain consistent with those observed in 1D. Note that the present choice of parameters is somewhat severe for energy behavior because of the relatively high impact velocity and low Young modulus.

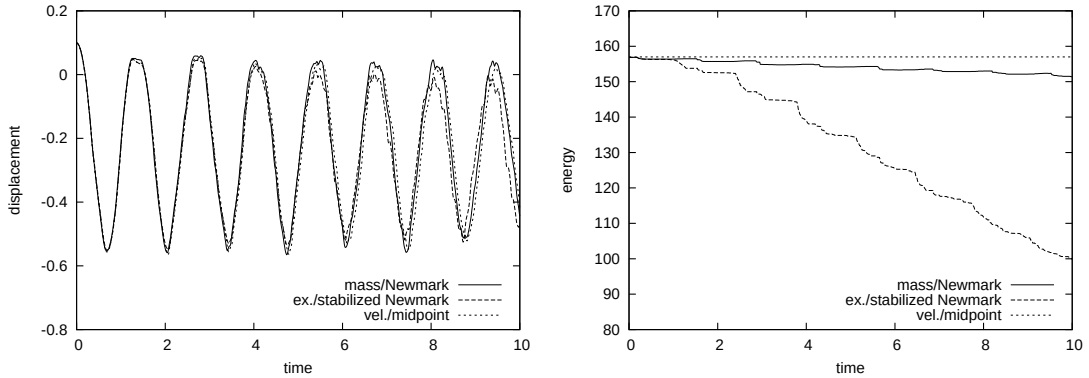

Fig. 2.27. Bounces of an elastic disk. Displacement of its center (left) and energy or modified energy (right). Discretizations 2.4.6, 2.6.1, and 2.7.1. $\Delta t = 0.01$, $\nu_c = 1.06$.

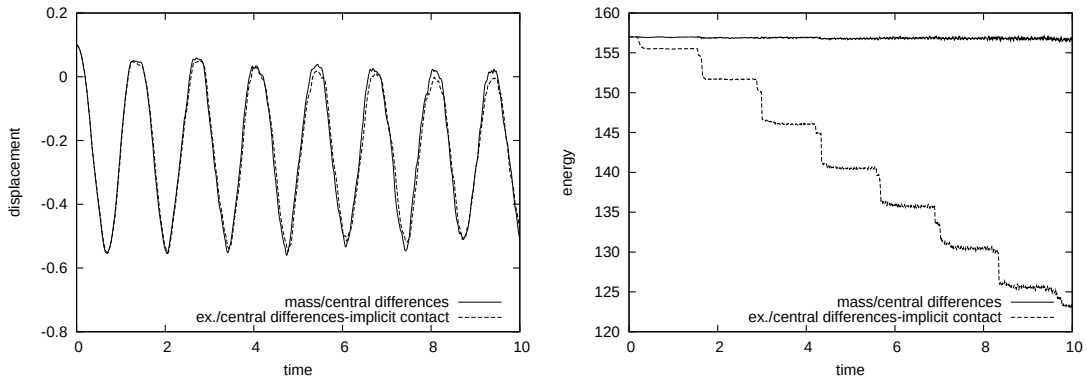

Fig. 2.28. Bounces of an elastic disk. Displacement of its center (left) and energy or modified energy (right). Discretizations 2.4.7 and 2.7.2. $\Delta t = 0.005$, $\nu_c = 0.53$.

2.9 Conclusions

In this work, we have reviewed various time-integration schemes for the finite element dynamic Signorini problem. We have classified the schemes into four groups, the first three depending on the way the contact condition is enforced while the fourth group corresponds to modifying the mass matrix at the contact boundary. We have assessed in detail the various schemes on two 1D benchmarks, both with analytical solution. The second benchmark is new and allows one to study the energy behavior within multiple impacts. Some selected schemes with favorable properties have been further compared on a 2D benchmark. All in all, we believe that the schemes with modified mass matrix, either implicit or semi-explicit, offer attractive properties, including ease of implementation, robustness, and relatively firm mathematical ground. The semi-explicit scheme with modified mass is new and stems from the combination of two existing ideas. We hope that the present results will stimulate further interest in the analysis and testing of these schemes.

3

Convergence of a modified mass method for the dynamic Signorini problem

This chapter has been published in *Communications in Mathematical Sciences* [35].

3.1 Introduction

The dynamic Signorini problem models the infinitesimal deformations of a solid body which can come into contact with a rigid obstacle. Many textbooks dealing with the mathematical theory of contact mechanics have appeared recently; see, e.g., [41, 81, 115] and references therein. Usual space-time discretizations for this problem combine finite element space approximation and time-stepping schemes. In this framework, most methods exhibit spurious oscillations and/or poor behavior in long time. The modified mass method proposed by Khenous, Laborde and Renard in [75] is a space semi-discrete formulation overcoming these two difficulties: the mass term is modified (the mass associated with the nodes at the contact boundary is set to zero), and the contact condition is enforced by a variational inequality. Owing to the mass modification, inertial forces cannot trigger spurious oscillations at the boundary. Furthermore, the system conserves an energy, which ensures a good behavior in long time.

The purpose of the present work is to strengthen the mathematical foundations of the modified mass method. Our main result is the convergence, up to a subsequence, of the space semi-discrete solutions to a solution of the continuous dynamic Signorini problem in the case of a visco-elastic material. In the elastic case, that is, in the absence of viscosity, it is already known [75] that the space semi-discrete problem is equivalent to a Lipschitz system of ordinary differential equations (ODEs) and is, therefore, well-posed (such a result cannot be established when using a standard mass term). However, the existence of a continuous solution is still an open problem in the elastic case, and the convergence proof of the space semi-discrete solutions is still out of reach. Instead, in the visco-elastic case, the existence of a continuous solution has been proven using a penalty method [41, §4.2.2]; the uniqueness of the solution is still an open problem. Our convergence proof takes a fairly standard path, namely *a priori* estimates on the space semi-discrete solutions and compactness arguments, but the mass modification at the contact boundary requires special care when passing to the limit. In both cases (penalty method or finite-dimensional variational inequality), the *a priori* estimate on the velocity delivered by the viscosity term plays a crucial role in the proof; as such, the argument cannot be extended to

the vanishing viscosity limit. Incidentally, the present convergence proof provides an alternate, albeit more complex, way to prove the existence of a continuous solution.

3.2 Continuous formulation

Consider the infinitesimal deformations of a body occupying a reference domain $\Omega \subset \mathbb{R}^d$ ($d = 2$ or $d = 3$) during a time interval $[0, T]$. We use the following assumptions and notation. The boundary of the domain Ω is piecewise smooth, so that its outward normal, n, is well defined almost everywhere at the boundary. The material is linear visco-elastic (Kelvin–Voigt model). The tensors of elasticity and viscosity, denoted by $\mathcal{A}$ and $\mathcal{B}$ respectively, are symmetric positive definite and taken to be constant for simplicity. The mass density, denoted by $\rho : \Omega \to \mathbb{R}$, is bounded by below by a constant $\rho_0 > 0$. An external load f is applied to the body. The boundary $\partial\Omega$ is partitioned into three disjoint open subsets Γ^D, Γ^N and Γ^c (the measure of Γ^D is positive). Homogeneous Dirichlet and Neumann conditions are prescribed on Γ^D and Γ^N, respectively. On Γ^c, a unilateral contact condition is imposed. Let $u : (0,T) \times \Omega \to \mathbb{R}^d$, $\epsilon(u) : (0,T) \times \Omega \to \mathbb{R}^{d,d}$ and $\sigma(u) : (0,T) \times \Omega \to \mathbb{R}^{d,d}$ be the displacement field, the linearized strain tensor and the stress tensor, respectively. Let $u_n := u_{|\partial\Omega} \cdot n$ and $\sigma_{nn} := n \cdot \sigma_{|\partial\Omega} \cdot n$ respectively denote the normal displacement and the normal stress on $\partial\Omega$. At the initial time, the displacement and velocity fields are u^0 and v^0. Denoting time-derivatives by dots, the strong formulation of the dynamic Signorini problem is

$$\rho\ddot{u} - \operatorname{div}\sigma = f, \quad \sigma = \mathcal{A} : \epsilon + \mathcal{B} : \dot{\epsilon}, \quad \epsilon = \frac{1}{2}(\nabla u + \nabla u^{\mathrm{T}}) \quad \text{in } \Omega \times (0,T), \tag{3.1}$$

$$u_n \le 0,\ \sigma_{nn} \le 0,\ \sigma_{nn} u_n = 0 \quad \text{on } \Gamma^c \times (0,T), \tag{3.2}$$

$$\sigma \cdot n = 0 \quad \text{on } \Gamma^N \times (0,T), \quad u = 0 \quad \text{on } \Gamma^D \times (0,T), \tag{3.3}$$

$$u(0) = u^0, \quad \dot{u}(0) = v^0 \quad \text{in } \Omega. \tag{3.4}$$

Consider the functional spaces $V = H^1_0(\Omega, \Gamma^D)^d = \{v \in H^1(\Omega)^d;\ v = 0 \text{ a.e. on } \Gamma^D\}$ and $M = L^2(\Omega)^d$, and the closed convex cone $K = \{v \in V;\ v_{|\partial\Omega} \cdot n \le 0 \text{ a.e. on } \Gamma^c\}$. The space M and its topological dual space are identified. Standard notation is used for spaces of time-dependent functions valued in a Banach space B, e.g., $C^k([0,T]; B)$ and so on; see [92, 119]. We assume the following regularity on the data: $f \in C^0([0,T]; M)$, $\rho \in L^\infty(\Omega)$, $u^0 \in K$ and $v^0 \in M$. Define the following bilinear and linear forms

$$m : M \times M \ni (v, w) \longmapsto \int_\Omega \rho v \cdot w, \tag{3.5}$$

$$a : V \times V \ni (v, w) \longmapsto \int_\Omega \epsilon(v) : \mathcal{A} : \epsilon(w), \tag{3.6}$$

$$b : V \times V \ni (v, w) \longmapsto \int_\Omega \epsilon(v) : \mathcal{B} : \epsilon(w), \tag{3.7}$$

$$l : [0,T] \times V \ni (t, v) \longmapsto \int_\Omega f(t) \cdot v. \tag{3.8}$$

Owing to Korn's first inequality and the assumptions on $\mathcal{A}$ and $\mathcal{B}$, the bilinear forms a and b are V-elliptic. We consider the following variational formulation of equations (3.1)-(3.4) (see [41] for its derivation).

Problem 3.1. Seek $u \in L^2(0,T;K) \cap H^1(0,T;V) \cap C^1([0,T];M)$ such that for all $v \in L^2(0,T;K) \cap H^1(0,T;M)$,

$$\int_0^T \Big\{ -m(\dot{u}, \dot{v}-\dot{u}) + a(u, v-u) + b(\dot{u}, v-u) \Big\} dt + m(\dot{u}(T), v(T)-u(T)) - m(v^0, v(0)-u^0) \geq \int_0^T l(t, v-u) dt. \tag{3.9}$$

Remark 3.1. *Since the space $H^1(0,T;M)$ is continuously imbedded in $C^0([0,T];M)$, the quantities $v(0)$ and $v(T)$ are well defined in (3.9).*

3.3 Semi-discrete formulation

For the sake of simplicity, we assume that in 2D (resp., in 3D) the domain Ω is a polygon (resp., a polyhedron) and the contact boundary Γ^c is a straight line (resp., a polygon). The outward normal to Γ^c is then constant and is denoted by n_c. We also suppose that $\overline{\Gamma^D} \cap \overline{\Gamma^c} = \emptyset$. Let $(\mathcal{T}_k)_{k\in\mathbb{N}}$ be a quasi-uniform family of simplicial meshes over Ω (triangles in 2D and tetrahedra in 3D). The meshes are possibly unstructured, but supposed to be compatible with the partition of the boundary. The notation $A \lesssim B$ means that $A \leq cB$ with a constant c independent of k. The space V is approximated by the usual conforming space of linear finite elements,

$$V_k = \{v_k \in C^0(\overline{\Omega})^d;\ v_{k|T} \in (\P_1)^d,\ \forall T \in \mathcal{T}_k, \ \text{ and } v_k = 0 \text{ on } \Gamma^D\}. \tag{3.10}$$

Let $\{x_{i,k}\}_{i\in\mathcal{N}_k}$ be the nodes of the mesh not lying on $\overline{\Gamma^D}$ and $\{\phi_{i,k}\}_{i\in\mathcal{N}_k}$ the associated scalar basis functions. Let $\{e_\alpha\}_{1\leq\alpha\leq d}$ be the canonical basis of $\mathbb{R}^d$. The space V_k is spanned by $\{\phi_{i,k}e_\alpha\}_{i\in\mathcal{N}_k, 1\leq\alpha\leq d}$. Denote by $\mathcal{N}_k^c$ the set of indices of nodes lying on $\overline{\Gamma^c}$, and by $\mathcal{N}_k^*$ the complementary of $\mathcal{N}_k^c$ in $\mathcal{N}_k$. We set $V_k^* = \mathrm{span}(\{\phi_{i,k}e_\alpha\}_{i\in\mathcal{N}_k^*, 1\leq\alpha\leq d})$ and $V_k^c = \mathrm{span}(\{\phi_{i,k}e_\alpha\}_{i\in\mathcal{N}_k^c, 1\leq\alpha\leq d})$. The space V_k is clearly the direct sum of V_k^* and V_k^c so that any discrete function $v_k \in V_k$ can be decomposed as

$$v_k = v_k^* + v_k^c \quad \text{with} \quad v_k^* \in V_k^*,\ v_k^c \in V_k^c. \tag{3.11}$$

Let $\mathcal{T}_k^c$ be the set of elements such that at least one vertex belongs to $\overline{\Gamma^c}$, and let $\mathcal{T}_k^*$ be its complement in $\mathcal{T}_k$. We set $\Omega_k^c = \mathrm{int}\left(\cup_{T\in\mathcal{T}_k^c}\overline{T}\right)$ and $\Omega_k^* = \mathrm{int}\left(\cup_{T\in\mathcal{T}_k^*}\overline{T}\right)$ (see Fig. 3.1). We observe that V_k^* is the subset of functions in V_k that vanish on Γ^c, while V_k^c is the subset of functions in V_k that vanish in Ω_k^*. The constraint set K is approximated by the set $K_k := \{v_k \in V_k;\ v_k \cdot n_c \leq 0 \text{ on } \Gamma^c\} = \{v_k \in V_k;\ v_k(x_{i,k}) \cdot n_c \leq 0,\ \forall i \in \mathcal{N}_k^c\}$.

As mentioned in the introduction, the key idea is to remove the mass associated with the nodes at the contact boundary. We consider an approximate mass term m_k such that

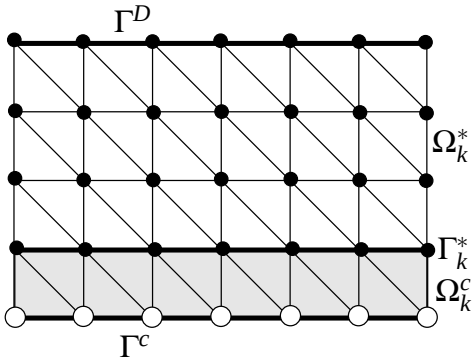

Fig. 3.1. Decomposition of the domain Ω; bullets (resp., circles) indicate nodes indexed by elements of the set $\mathcal{N}_k^*$ (resp., $\mathcal{N}_k^c$).

$$m_k(\phi_{i,k}e_\alpha, w_k) = m_k(w_k, \phi_{i,k}e_\alpha) = 0, \quad \forall i \in \mathcal{N}_k^c,\ \forall \alpha \in \{1,..,d\},\ \forall w_k \in V_k. \tag{3.12}$$

Many choices are possible to build the rest of the mass term. In [57, 75], the authors devise various methods to preserve some features of the standard mass term (the total mass, the center of gravity and the moments of inertia). Here we will focus for simplicity on the choice

$$m_k : V_k \times V_k \ni (v_k, w_k) \longmapsto \int_{\Omega_k^*} \rho v_k \cdot w_k. \tag{3.13}$$

In the elastic case, owing to the property (3.12), the semi-discrete problem reduces to a system of ODEs. To keep this property in the visco-elastic case also, we also modify the viscosity term at the boundary by setting

$$b_k : V_k \times V_k \ni (v_k, w_k) \longmapsto \int_{\Omega_k^*} \epsilon(v_k) : \mathcal{B} : \epsilon(w_k). \tag{3.14}$$

It is also convenient to modify the external load term at the boundary as

$$l_k : [0,T] \times V_k \ni (t, v_k) \longmapsto \int_{\Omega_k^*} f(t) \cdot v_k. \tag{3.15}$$

The modification of the viscosity and external load terms is convenient from a theoretical viewpoint. In practice, it is probably not needed. Owing to the above definitions, there holds for all $v_k^c \in V_k^c$ and all $w_k \in V_k$,

$$m_k(v_k^c, w_k) = m_k(w_k, v_k^c) = b_k(v_k^c, w_k) = b_k(w_k, v_k^c) = l_k(t, v_k^c) = 0. \tag{3.16}$$

The approximate initial values u_k^0 and v_k^0 are chosen such that $u_k^0 \in K_k$, $v_k^0 \in V_k$, and

$$u_k^0 \to u^0 \text{ in } V, \quad v_k^0 \to v^0 \text{ in } M. \tag{3.17}$$

If the initial data are continuous, such values can be built by Lagrange interpolation. We now formulate the space semi-discrete problem and examine its properties.

Problem 3.2. Seek $u_k \in C^0([0,T];K_k)$ such that $u_k^* \in C^2([0,T];V_k^*)$ and for all $v_k \in K_k$ and all $t \in [0,T]$,

$$m_k(\ddot{u}_k^*, v_k - u_k) + a(u_k, v_k - u_k) + b_k(\dot{u}_k^*, v_k - u_k) \geq l_k(t, v_k - u_k), \tag{3.18}$$

with the initial conditions $u_k^*(0) = u_k^{0*}$ and $\dot{u}_k^*(0) = \mathrm{v}_k^{0*}$ in Ω.

Proposition 3.1. *(i) The variational inequality (3.18) is equivalent to*

$$m_k(\ddot{u}_k^*, v_k^*) + a(u_k^* + q_k(u_k^*), v_k^*) + b_k(\dot{u}_k^*, v_k^*) = l_k(t, v_k^*), \quad \forall v_k^* \in V_k^*,\ \forall t \in [0,T], \tag{3.19}$$

$$u_k^c = q_k(u_k^*), \qquad \forall t \in [0,T], \tag{3.20}$$

where $q_k : V_k^* \to V_k^c$ is a Lipschitz function.
(ii) There exists a unique solution u_k to Problem 3.2. Moreover, $u_k \in W^{1,\infty}(0,T;V_k)$.
(iii) The value of u_k at the initial time is $u_k(0) = u_k^{0*} + q_k(u_k^{0*})$ and $\|u_k(0)\|_V \lesssim \|u_k^0\|_V$.
(iv) For all $t_0 \in [0,T]$, the following energy balance holds,

$$E_k(u_k(t_0)) - E_k(u_k(0)) = \int_0^{t_0} \Big\{ l_k(t, \dot{u}_k^*(t)) - b_k(\dot{u}_k^*(t), \dot{u}_k^*(t)) \Big\} dt, \tag{3.21}$$

where $E_k(v_k) = \frac{1}{2}\left(m_k(\dot{v_k}^*, \dot{v_k}^*) + a(v_k, v_k)\right)$.

Proof. (i) The variational inequality (3.18) is clearly equivalent to the following system

$$m_k(\ddot{u}_k^*, v_k^*) + a(u_k, v_k^*) + b_k(\dot{u}_k^*, v_k^*) = l_k(t, v_k^*), \quad \forall v_k^* \in V_k^*,\ \forall t \in [0,T], \tag{3.22}$$

$$a(u_k, v_k^c - u_k^c) \geq 0, \qquad \forall v_k^c \in V_k^c \cap K_k,\ \forall t \in [0,T]. \tag{3.23}$$

Consider (3.23). If we fix $u_k^* \in V_k^*$, there exists a unique u_k^c satisfying the variational inequality (3.23) (indeed it is equivalent to the minimization of a strictly convex functional over a convex set). Denote $q_k : V_k^* \to V_k^c$ to be the map such that for a given $u_k^* \in V_k^*$, $u_k^c = q_k(u_k^*)$ is the unique solution of (3.23). The system (3.22)-(3.23) is then equivalent to the system (3.19)-(3.20). Now we study the regularity of q_k. Let $v_k^*, w_k^* \in V_k^*$. Set $v_k^c = q_k(v_k^*)$ and $w_k^c = q_k(w_k^*)$. Owing to (3.23), it follows that

$$a(v_k^c - w_k^c, v_k^c - w_k^c) \leq a(v_k^* - w_k^*, w_k^c - v_k^c).$$

The bilinear form a being continuous and elliptic, a straightforward calculation yields $\|v_k^c - w_k^c\|_V \lesssim \|v_k^* - w_k^*\|_V$, which proves that q_k is Lipschitz continuous.

(ii) The system of ODEs (3.19) is globally Lipschitz. Owing to the Cauchy–Lipschitz theorem, there exists a unique solution $u_k^* \in C^2(0,T;V_k^*)$ satisfying the initial conditions of Problem 3.2. From (3.20), $u_k = u_k^* + u_k^c = u_k^* + q_k(u_k^*)$. Therefore, Problem (3.2) has a unique solution $u_k \in C^0(0,T;K_k)$. Rademacher's theorem [45] states that in finite dimension a Lipschitz function is differentiable almost everywhere; hence, $u_k \in W^{1,\infty}(0,T;V_k)$.

(iii) The value of u_k at the initial time is $u_k(0) = u_k^{0*} + q_k(u_k^{0*})$. Since $u_k^0 \in K_k$, we can apply (3.23) with $v_k^c = u_k^{0c}$, so that $a(u_k(0), u_k^{0c} - u_k^c(0)) \geq 0$. Since $u_k^*(0) = u_k^{0*}$, $a(u_k(0), u_k^0 - u_k(0)) =$

$a(u_k(0), u_k^{0c} - u_k^c(0)) \geq 0$. Hence, $\|u_k(0)\|_V \lesssim \|u_k^0\|_V$.

(iv) Without loss of generality, we assume that $e_1 = n_c$. Recalling that the family $\{\phi_{i,k} e_\alpha\}_{i \in \mathcal{N}_k^c, 1 \leq \alpha \leq d}$ is a basis of V_k^c, we decompose u_k^c on this basis yielding $u_k^c = \sum_{i \in \mathcal{N}_k^c} \sum_{\alpha=1}^d u_{k,i}^\alpha \phi_{k,i} e_\alpha$. The normal and tangential components of u_k^c at the node indexed by $i \in \mathcal{N}_k^c$ are given by $N_{k,i} u_k^c = u_{k,i}^1 \phi_{k,i} n_c$ and $T_{k,i} u_k^c = \sum_{\alpha=2}^d u_{k,i}^\alpha \phi_{k,i} e_\alpha$, so that $u_k^c = \sum_{i \in \mathcal{N}_k^c} (T_{k,i} u_k^c + N_{k,i} u_k^c)$. Owing to (3.23), $a(u_k, T_{k,i} \dot{u}_k^c) = 0$. Moreover, define $C_i^0 := \{t \in [0,T];\ u_{k,i}^1 = 0\}$ and $C_i^- := \{t \in [0,T];\ u_{k,i}^1 < 0\}$. The sets C_i^0 and C_i^- are respectively closed and open, and they form a partition of $[0,T]$. On $\mathrm{int}(C_i^0)$, $N_{k,i} \dot{u}_k^c = 0$. Owing to (3.23), $a(u_k, N_{k,i} \dot{u}_k^c) = 0$ on C_i^-. Finally, $a(u_k, N_{k,i} \dot{u}_k^c) = 0$ on $\mathrm{int}(C_i^0) \cup C_i^-$, and hence almost everywhere (since an open set in $\mathbb{R}$ is a countable union of open intervals, so that its boundary has zero measure). Hence,

$$a(u_k, \dot{u}_k^c) = 0, \quad \text{a.e. on }]0,T[. \tag{3.24}$$

Setting $v_k^* = \dot{u}_k^*$ in (3.22) and using (3.24), we obtain

$$m_k(\ddot{u}_k^*, \dot{u}_k^*) + a(u_k, \dot{u}_k) + b_k(\dot{u}_k^*, \dot{u}_k^*) = l_k(t, \dot{u}_k^*), \quad \text{a.e. on }]0,T[. \tag{3.25}$$

The energy balance (3.21) readily follows by integrating in time. The equality holds for all time since the energy is continuous in time.

3.4 Convergence of the semi-discrete solutions

This section is organized as follows. First we establish *a priori* estimates on the space semi-discrete solutions (Lemma 3.3). Owing to these estimates and using compactness arguments, we extract a weakly convergent subsequence (Lemma 3.4). Then we check that this weak limit is a solution of the continuous problem (Theorem 3.1). In the sequel, to alleviate the notation, we do not renumber subsequences.

We first recall two useful results on time-dependent functional spaces; for their proof, see respectively [92] and [119, §III.2]. For two Banach spaces B_1 and B_2, let $\mathcal{W}(B_1, B_2) := \{v : (0,T) \to B_1; v \in L^2(0,T;B_1),\ \dot{v} \in L^2(0,T;B_2)\}$, equipped with the norm $v \mapsto \|v\|_{L^2(0,T;B_1)} + \|\dot{v}\|_{L^2(0,T;B_2)}$.

Lemma 3.1 (Lions-Magenes). *Let $V_1 \subset V_2$ be two Hilbert spaces. Assume that V_1 is continuously imbedded in V_2. Then, $\mathcal{W}(V_1, V_2)$ is continuously imbedded in $C^0([0,T]; [V_1, V_2]_{\frac{1}{2}})$, where $[V_1, V_2]_{\frac{1}{2}}$ is the interpolation space of exponent $\frac{1}{2}$.*

Lemma 3.2 (Aubin). *Let $B_1 \subset B \subset B_2$ be three reflexive Banach spaces. Assume that B_1 is compactly imbedded in B and B is continuously imbedded in B_2. Then, $\mathcal{W}(B_1, B_2)$ is compactly imbedded in $L^2(0,T;B)$.*

Owing to the modifications in the space semi-discrete formulation, *a priori* estimates are obtained only on restrictions of $\dot{u}_k$ and $\ddot{u}_k$ to Ω_k^*. Let $\Gamma_k^* := \mathrm{int}(\partial\Omega_k^* \cap \partial\Omega_k^c)$ (see Fig. 3.1) and set $W = H_0^1(\Omega, \Gamma^D \cup \Gamma^c)^d$. Define the cut-off operators $\chi_k : M \to M$ such that

$$\chi_k v = v \text{ on } \Omega_k^*, \qquad \chi_k v = 0 \text{ on } \Omega_k^c. \tag{3.26}$$

Of course, $\|\chi_k v\|_M = \|v_{|\Omega_k^*}\|_{M(\Omega_k^*)}$. Furthermore, for any node index $i \in \mathcal{N}_k^c$, pick a node $x_{i^*,k}$ of the same element as $x_{i,k}$ and lying on $\overline{\Gamma_k^*}$, and define the operator $\xi_k : V_k \to V_k$ such that

$$\xi_k v_k = v_k \text{ on } \Omega_k^*, \qquad \forall i \in \mathcal{N}_k^c,\ \xi_k v_k(x_{i,k}) = \xi_k v_k(x_{i^*,k}). \tag{3.27}$$

Using standard finite element techniques (details are skipped for brevity) yields $\|\xi_k v_k\|_V \lesssim \|v_{k|\Omega_k^*}\|_{V(\Omega_k^*)}$.

Lemma 3.3. *Let $(u_k)_{k\in\mathbb{N}}$ be the sequence of solutions to Problem 3.2. Then, the following estimates hold:*

$$\|u_k\|_{C^0([0,T];V)} + \|\xi_k u_k\|_{H^1(0,T;V)} + \|\chi_k \dot{u}_k\|_{C^0([0,T];M)} + \|\chi_k \ddot{u}_k\|_{L^2(0,T;W')} \lesssim 1. \tag{3.28}$$

Proof. (i) Let $t_0 \in [0,T]$. The energy balance (3.21) implies

$$\begin{aligned} \|\chi_k \dot{u}_k(t_0)\|_M^2 + \|u_k(t_0)\|_V^2 + \int_0^{t_0} \|\dot{u}_{k|\Omega_k^*}(t)\|_{V(\Omega_k^*)}^2 dt \\ \lesssim \int_0^{t_0} \|f(t)\|_M \|\dot{u}_{k|\Omega_k^*}(t)\|_{M(\Omega_k^*)} dt + \|u_k(0)\|_V^2 + \|\chi_k \dot{u}_k(0)\|_M^2. \end{aligned} \tag{3.29}$$

Since $u_k^0 \to u^0$ in V and $v_k^0 \to v^0$ in M, we obtain $\|u_k^0\|_V \lesssim \|u^0\|_V$ and $\|v_k^0\|_M \lesssim \|v^0\|_M$. Hence, $\|u_k(0)\|_V \lesssim \|u^0\|_V$ and $\|\chi_k \dot{u}_k(0)\|_M \lesssim \|v^0\|_M$. Then, owing to (3.29) and using $\|\cdot\|_{M(\Omega_k^*)} \lesssim \|\cdot\|_{V(\Omega_k^*)}$ together with Young's inequality yields

$$\|\chi_k \dot{u}_k(t_0)\|_M^2 + \|u_k(t_0)\|_V^2 + \int_0^{t_0} \|\dot{u}_{k|\Omega_k^*}(t)\|_{V(\Omega_k^*)}^2 dt \lesssim \int_0^{t_0} \|f(t)\|_M^2 dt + \|u^0\|_V^2 + \|v^0\|_M^2.$$

The first three estimates in (3.28) are readily deduced from this inequality.

(ii) Let $v \in S_W := \{v \in W; \|v\|_V = 1\}$. The bilinear form m defines a scalar product on V_k^*. Let $\pi_k^* v$ be the m-orthogonal projection of v onto V_k^*. The mesh family being quasi-uniform and using standard finite element techniques (see, e.g., [44, §1.6.3]) yields the following stability property:

$$\|\pi_k^* v\|_V \lesssim \|v\|_V. \tag{3.30}$$

Owing to (3.19),

$$\begin{aligned} \langle \rho \chi_k \ddot{u}_k(t), v\rangle_{W',W} &= m(\chi_k \ddot{u}_k(t), v) = m(\chi_k \ddot{u}_k(t), \pi_k^* v) \\ &= m_k(\chi_k \ddot{u}_k(t), \pi_k^* v) = l_k(t, \pi_k^* v) - a(u_k, \pi_k^* v) - b_k(\dot{u}_{k|\Omega_k^*}, \pi_k^* v). \end{aligned}$$

Using the stability property (3.30), it is inferred that

$$\begin{aligned}\langle \rho\chi_k\ddot{u}_k(t), v\rangle_{W',W} &\lesssim \|f(t)\|_M\|\pi_k^* v\|_M + \|u_k\|_V\|\pi_k^* v\|_V + \|\dot{u}_{k|\Omega_k^*}\|_{V(\Omega_k^*)}\|\pi_k^* v\|_V\\ &\lesssim \|f(t)\|_M + \|u_k\|_V + \|\dot{u}_{k|\Omega_k^*}\|_{V(\Omega_k^*)}.\end{aligned}$$

Using the definition of the norm W' and since ρ is uniformly bounded from below,

$$\|\chi_k\ddot{u}_k(t)\|_{W'} = \sup_{v\in S_W} |\langle \chi_k\ddot{u}_k(t), v\rangle_{W',W}| \lesssim \|f(t)\|_M + \|u_k(t)\|_V + \|\dot{u}_{k|\Omega_k^*}(t)\|_{V(\Omega_k^*)}.$$

Hence,

$$\|\chi_k\ddot{u}_k\|_{L^2(0,T;W')} \lesssim \|f\|_{L^2(0,T;M)} + \|u_k\|_{L^2(0,T;V)} + \|\dot{u}_{k|\Omega_k^*}\|_{L^2(0,T;V(\Omega_k^*))}.$$

This proves the fourth estimate in (3.28).

Lemma 3.4. *There exists $u \in L^2(0,T;K)\cap H^1(0,T;V)\cap C^1([0,T];M)$ such that, up to a subsequence,*

$$u_k \rightharpoonup u \text{ weakly in } L^2(0,T;V), \tag{3.31}$$
$$\chi_k\dot{u}_k \to \dot{u} \text{ in } L^2(0,T;M), \tag{3.32}$$
$$u_k(0) \to u^0 \text{ in } V, \tag{3.33}$$
$$\chi_k\dot{u}_k(0) \to v^0 \text{ in } M, \tag{3.34}$$
$$u_k(T) \rightharpoonup u(T) \text{ weakly in } V, \tag{3.35}$$
$$u_k(T) \to u(T) \text{ in } M, \tag{3.36}$$
$$\chi_k\dot{u}_k(T) \rightharpoonup \dot{u}(T) \text{ weakly in } M. \tag{3.37}$$

Proof. (i) Closed bounded sets in reflexive Banach spaces are weakly compact. Therefore, owing to estimates (3.28), there exists $u \in L^2(0,T;V)$, $u_1 \in H^1(0,T;V)$, $v \in L^2(0,T;M)$ and $w \in L^2(0,T;W')$ such that, up to a subsequence,

$$u_k \rightharpoonup u \text{ weakly in } L^2(0,T;V), \tag{3.38}$$
$$\xi_k u_k \rightharpoonup u_1 \text{ weakly in } H^1(0,T;V), \tag{3.39}$$
$$\chi_k\dot{u}_k \rightharpoonup v \text{ weakly in } L^2(0,T;M), \tag{3.40}$$
$$\chi_k\ddot{u}_k \rightharpoonup w \text{ weakly in } L^2(0,T;W'). \tag{3.41}$$

Let $\phi \in \mathcal{D}(\Omega\times]0,T[)$. Since ϕ has compact support, beyond a certain index k, there holds $\langle u_k,\phi\rangle = \langle \xi_k u_k,\phi\rangle$. Therefore, $(u_k)_{k\in\mathbb{N}}$ and $(\xi_k u_k)_{k\in\mathbb{N}}$ have the same limit in $\mathcal{D}'(\Omega\times]0,T[)$; hence, $u = u_1$. The same argument yields that $(\chi_k\dot{u}_k)_{k\in\mathbb{N}}$ and $(\dot{u}_k)_{k\in\mathbb{N}}$ have the same limit in $\mathcal{D}'(\Omega\times]0,T[)$. Continuity of the differentiation in $\mathcal{D}'(\Omega\times]0,T[)$ yields $\dot{u}_k \to \dot{u}$ in $\mathcal{D}'(\Omega\times]0,T[)$, and thus $v = \dot{u}$. The equality $w = \ddot{u}$ is obtained similarly. Moreover, it is clear that $\xi_k\dot{u}_k \rightharpoonup \dot{u}$ weakly in $L^2(0,T;V)$.

(ii) Regularity of the limit u. We have just established that $u \in H^1(0,T;V)$ and $\ddot{u} \in L^2(0,T;W')$. Hence, owing to Lemma 3.1, $\dot{u} \in C^0([0,T];[V,W']_{\frac{1}{2}}) = C^0([0,T];M)$ (for the proof of the equality $[V,W']_{\frac{1}{2}} = M$, see [92]). Furthermore, the set $L^2(0,T;K)$ is convex and closed in $L^2(0,T;V)$. Therefore, $L^2(0,T;K)$ is weakly closed. The sequence $(u_k)_{k\in\mathbb{N}}$ being in $L^2(0,T;K)$, the weak

limit u is also in $L^2(0,T;K)$. Hence, $u \in L^2(0,T;K) \cap H^1(0,T;V) \cap C^1([0,T];M)$.

(iii) Proof of (3.32). Let $\epsilon > 0$. The functions $\chi_k \dot{u}$ and $\dot{u}$ only differ on a set whose measure tends to zero as $k \to +\infty$. Since both sequences are bounded in $L^2(0,T;M)$, it is inferred, up to a subsequence, that there exists $k_0 \in \mathbb{N}$ such that $\|\chi_{k_0}\dot{u} - \dot{u}\|_{L^2(0,T;M)} \leq \epsilon/3$. The same argument shows that k_0 can be chosen so that for all $k \geq k_0$, $\|\chi_{k_0}\dot{u}_k - \chi_k \dot{u}_k\|_{L^2(0,T;M)} \leq \epsilon/3$. The index k_0 now being fixed, we define $W(\Omega_{k_0}^*) = H_0^1(\Omega_{k_0}^*, \Gamma^D \cup \Gamma_{k_0}^*)^d$, $V(\Omega_{k_0}^*) = H_0^1(\Omega_{k_0}^*, \Gamma^D)^d$ and $M(\Omega_{k_0}^*) = L^2(\Omega_{k_0}^*)^d$, and proceeding as in the proof of Lemma 3.3 leads to the *a priori* estimate

$$\|\dot{u}_{k|\Omega_{k_0}^*}\|_{L^2(0,T;V(\Omega_{k_0}^*))} + \|\ddot{u}_{k|\Omega_{k_0}^*}\|_{L^2(0,T;W(\Omega_{k_0}^*)')} \lesssim 1,$$

where the constant can depend on k_0 (but not on k). We then use Lemma 3.2 with $B_1 = V(\Omega_{k_0}^*)$, $B = M(\Omega_{k_0}^*)$, and $B_2 = W(\Omega_{k_0}^*)'$, to infer that, up to a subsequence, there holds $\dot{u}_{k|\Omega_{k_0}^*} \to v_{k_0}$ in $L^2(0,T;M(\Omega_{k_0}^*))$. As previously, we prove that $v_{k_0} = \dot{u}_{|\Omega_{k_0}^*}$. This implies that there is $k_1 \in \mathbb{N}$ such that for all $k \geq k_1$, $\|\chi_{k_0}\dot{u}_k - \chi_{k_0}\dot{u}\|_{L^2(0,T;M)} \leq \epsilon/3$. Collecting the above bounds, it is inferred that for all $k \geq \max(k_0, k_1)$,

$$\begin{aligned}\|\chi_k \dot{u}_k - \dot{u}\|_{L^2(0,T;M)} \leq & \|\chi_k \dot{u}_k - \chi_{k_0}\dot{u}_k\|_{L^2(0,T;M)} + \|\chi_{k_0}\dot{u}_k - \chi_{k_0}\dot{u}\|_{L^2(0,T;M)} \\ & + \|\chi_{k_0}\dot{u} - \dot{u}\|_{L^2(0,T;M)} \leq \epsilon,\end{aligned}$$

which proves (3.32).

(iv) Proof of (3.33) and (3.34). Let $\epsilon > 0$. Since $u_k(0)$ and u_k^0 only differ on a set whose measure tends to zero as $k \to +\infty$ and since both sequences are bounded in V, the sequence $(u_k(0) - u_k^0)_{k\in\mathbb{N}}$ converges to zero in V, whence (3.33) is deduced owing to (3.17). Moreover, (3.34) is a straightforward consequence of (3.17).

(v) Proof of (3.35), (3.36) and (3.37). Owing to estimate (3.28), there exists $u_T \in V$, $v_T \in M$ such that, up to a subsequence,

$$u_k(T) \rightharpoonup u_T \text{ weakly in } V, \tag{3.42}$$

$$\chi_k \dot{u}_k(T) \rightharpoonup v_T \text{ weakly in } M. \tag{3.43}$$

Since $\xi_k u_k \rightharpoonup u$ weakly in $H^1(0,T;V)$, it is inferred that $\xi_k u_k(T) \rightharpoonup u(T)$ weakly in V. The uniqueness of the limit in the sense of distributions implies that $u_T = u(T)$ and $v_T = \dot{u}(T)$. Since the imbedding $V \hookrightarrow M$ is compact, $u_k(T) \to u(T)$ in M.

Theorem 3.1. *The limit u identified in Lemma 3.4 is a solution to Problem 3.1.*

Proof. (i) Integrating by parts (3.18) yields for all $v_k \in C^0([0,T];K_k) \cap C^1([0,T];V_k)$,

$$\begin{aligned}&\int_0^T \Big\{ - m_k(\dot{u}_k, \dot{v}_k - \dot{u}_k) + a(u_k, v_k - u_k) + b_k(\dot{u}_k, v_k - u_k)\Big\} dt \\ &+ m_k(\dot{u}_k(T), v_k(T) - u_k(T)) - m_k(\dot{u}_k(0), v_k(0) - u_k(0)) \geq \int_0^T l_k(t, v_k - u_k) dt.\end{aligned} \tag{3.44}$$

(ii) Let $v \in L^2(0,T;K) \cap H^1(0,T;M)$ be a test function in Problem 3.1. We can generate a sequence $(v_k)_{k\in\mathbb{N}}$ such that $v_k \in C^0([0,T];K_k) \cap C^1([0,T];V_k)$ and

$$\begin{aligned} &v_k \to v \text{ in } L^2(0,T;V),\\ &\dot{v}_k \to \dot{v} \text{ in } L^2(0,T;M),\\ &v_k(0) \to v(0) \text{ in } M,\\ &v_k(T) \to v(T) \text{ in } M. \end{aligned}$$

To this purpose, we first consider an interpolation operator $I_k : V \to V_k$ preserving positivity on the boundary. Such an operator can be built by giving local mean-values to the nodal values (see, e.g., the operators described [99] which preserve positivity on the whole domain and not only on the boundary). Setting $w_k = I_k v$ yields $w_k \in L^2(0,T;K_k) \cap H^1(0,T;V_k)$, $w_k \to v$ in $L^2(0,T;V)$, $\dot{w}_k \to \dot{v}$ in $L^2(0,T;M)$, $w_k(0) \to v(0)$ in M, $w_k(T) \to v(T)$ in M. Finally, to obtain a sequence $(v_k)_{k\in\mathbb{N}}$ that is smooth in time, the sequence $(w_k)_{k\in\mathbb{N}}$ is regularized by convolution in time. This preserves positivity on the boundary as well as the convergence properties.

(iii) The last step is to pass to the limit in the inequality (3.44) with the sequence $(v_k)_{k\in\mathbb{N}}$ defined above. The bilinear form a being V-elliptic, the function $v \mapsto a(v,v)$ is convex and thus lower semi-continuous in V. Using (3.31) then yields

$$\liminf_{k\to+\infty} \int_0^T a(u_k,u_k)dt \geq \int_0^T a(u,u)dt.$$

For the viscosity term, we observe that

$$\begin{aligned} \int_0^T b_k(\dot{u}_k,u_k)dt =& b_k(u_k(T),u_k(T)) - b_k(u_k(0),u_k(0))\\ =& b(u_k(T),u_k(T)) + [b_k(u_k(T),u_k(T)) - b(u_k(T),u_k(T))]\\ &- b(u_k(0),u_k(0)) - [b_k(u_k(0),u_k(0)) - b(u_k(0),u_k(0))]. \end{aligned}$$

Owing to a convexity argument and (3.35), $\liminf b(u_k(T),u_k(T)) \geq b(u(T),u(T))$, and, owing to the strong convergence (3.33), $\lim b(u_k(0),u_k(0)) = b(u^0,u^0)$. The two other terms tend to zero since $(u_k(0))_{k\in\mathbb{N}}$ and $(u_k(T))_{k\in\mathbb{N}}$ are bounded in V. Hence,

$$\liminf_{k\to+\infty} \int_0^T b_k(\dot{u}_k,u_k)dt \geq b(u(T),u(T)) - b(u(0),u(0)) = \int_0^T b(\dot{u},u)dt.$$

For the inertia term, using (3.32) yields

$$\lim_{k\to+\infty} \int_0^T m_k(\dot{u}_k,\dot{u}_k)dt = \lim_{k\to+\infty} \int_0^T m(\chi_k\dot{u}_k,\chi_k\dot{u}_k)dt = \int_0^T m(\dot{u},\dot{u})dt.$$

Moreover, (3.36) and (3.37) imply that

$$\lim_{k\to+\infty} m_k(\dot{u}_k(T),u_k(T)) = m(\dot{u}(T),u(T)),$$

while (3.33) and (3.34) yield

$$\lim_{k\to+\infty} m_k(\dot{u}_k(0), u_k(0)) = m(v^0, u^0).$$

The limits involving $(v_k)_{k\in\mathbb{N}}$ are straightforward owing to the strong convergence properties of the sequence $(v_k)_{k\in\mathbb{N}}$. Collecting the above limits leads to the variational inequality (3.9).

Remark 3.2. *The strong convergence of $(\chi_k \dot{u}_k)$ in $L^2(0,T;M)$, i.e., property (3.32), plays a key role in the proof. We restate that without the viscosity term, the velocity is not necessarily bounded in V, and the required compactness argument no longer holds.*

Remark 3.3. *If the solution to Problem 3.1 were proven to be unique, we could conclude that the whole sequence $(u_k)_{k\in\mathbb{N}}$ converged to u.*

Acknowledgment. The authors are thankful to R. Monneau (CERMICS) for stimulating discussions.

4

Analysis of the modified mass method for the dynamic Signorini problem with Coulomb friction

This chapter is submitted for publication [34].

4.1 Introduction

The modified mass method is a new approach for solving computationally dynamic problems with unilateral contact. Introduced in [75] for frictionless contact problems, it is based on a space semi-discrete formulation in which the mass matrix is modified (the entries of the mass matrix associated with the (normal) displacements at the contact boundary are set to zero). This modified semi-discrete problem can then be discretized with various time-integration schemes. The modified mass method eliminates the large spurious oscillations on the contact pressure, which can appear with a standard mass matrix, while ensuring an exact enforcement of the contact condition. Moreover, with a suitable scheme such as the Newmark scheme (trapezoidal rule), a tight energy conservation and a good behavior in long-time are observed. In addition, the method does not require extra steps or extra parameters and can easily be implemented. Since its introduction, the modified mass method has been developed in several directions: alternative ways of building the modified mass matrix [57, 107, 62], use of semi-explicit time-integration schemes [38, 36], application to contact with friction [73, 57, 58], application to thin structures [107]. For a comparison of the modified mass method with other popular methods, we refer to [73, 36, 80].

Up to date, no theoretical analysis has been carried out for the modified mass method in the frictional case. In the frictionless case with an elastic material, interesting results have been proven. The space semi-discrete problem is equivalent to a Lipschitz system of ordinary differential equations and is, therefore, well-posed [75]. The variation of energy is equal to the work of the external forces; the contact forces do not work [75]. Convergence of the semi-discrete solutions to a continuous solution is proven for viscoelastic materials in [35]. An error analysis of the modified mass matrix has been performed in [58] for linear elastodynamics without contact.

The aim of the present work is to analyze the modified mass method for the dynamic Signorini problem with Coulomb friction. Implementation and numerical simulations are extensively discussed in [57, 58, 80]. We prove that the space semi-discrete problem is equivalent to an upper semi-continuous one-sided Lipschitz differential inclusion [31, 114] and is, therefore, well-posed

(Theorem 4.2). Furthermore, the variation of energy is equal to the work of the external forces and friction forces (Theorem 4.3). For the time discretization, we consider an implicit scheme. Each time step requires solving a nonlinear problem similar to a static friction problem. It is well-known that such a problem can have several solutions [67]. Here we prove that, under a certain condition on the discretization parameters of CFL-type, the fully discrete problem is well-posed (Theorem 4.4). For a fixed discretization in space, we prove also that the fully discrete solutions converge to the space semi-discrete solution when the time step tends to zero (Theorem 4.5).

With a standard mass term, proving the existence of a semi-discrete solution to a dynamic contact problem is quite delicate. It is necessary to add an impact law and to work with BV and measures spaces [18, 116, 5]. The modification of the mass term greatly simplifies the analysis. Indeed, the unilateral contact condition can be eliminated and replaced by a Lipschitz continuous term in the momentum equation [75]. Moreover, static and quasi-static Coulomb friction problems can have several solutions [67]. Uniqueness is only obtained for small friction coefficients (see [76, Theorem 11.4] for the static case and [60, Theorem 7.2.1] for the quasi-static case). It is worthwhile to notice that in the dynamic case, uniqueness is recovered. Finally, we do not examine herein the convergence of the discrete solutions to a solution of the continuous problem. Nevertheless, it seems possible to extend the convergence result in [35] to the case of a non-local Coulomb friction (the non-local Coulomb friction is a regularization of Coulomb friction [76, 27]).

This paper is organized as follows. In Section 2, we formulate the continuous problem. Sections 3 and 4 are devoted to the space semi-discrete and fully discrete problems, respectively. In Section 5, we examine the convergence of the fully discrete solutions to the space semi-discrete solution. Conclusions are drawn in Section 4.6.

4.2 Continuous problem

We consider the infinitesimal deformations of a body occupying a reference domain $\Omega \subset \mathbb{R}^d$ ($d \in \{2,3\}$) during a time interval $[0,T]$. Let ν be the outward unit normal to Ω. The elasticity tensor is denoted by $\mathcal{A}$ and the mass density by ρ. An external load f is applied to the body. Let $u : (0,T) \times \Omega \to \mathbb{R}^d$, $\epsilon(u) : (0,T) \times \Omega \to \mathbb{R}^{d,d}$, and $\sigma(u) : (0,T) \times \Omega \to \mathbb{R}^{d,d}$ be the displacement field, the linearized strain tensor, and the stress tensor, respectively. Denoting time-derivatives by dots, the momentum conservation equation reads

$$\rho\ddot{u} - \operatorname{div}\sigma = f, \qquad \sigma = \mathcal{A} : \epsilon, \qquad \epsilon = \frac{1}{2}(\nabla u +^{\mathrm{T}} \nabla u) \quad \text{in } \Omega \times (0,T). \tag{4.1}$$

The boundary $\partial\Omega$ is partitioned into three disjoint open subsets Γ^D, Γ^N, and Γ^{c}. Dirichlet and Neumann conditions are prescribed on Γ^D and Γ^N, respectively,

$$u = u_D \quad \text{on } \Gamma^D \times (0,T), \qquad \sigma \cdot \nu = f_N \quad \text{on } \Gamma^N \times (0,T). \tag{4.2}$$

In what follows, we assume $f \in W^{1,\infty}(0,T;L^2(\Omega)^d)$ and $f_N \in W^{1,\infty}(0,T;L^2(\Gamma^N)^d)$.

We let $u_\nu := u_{|\partial\Omega} \cdot \nu$ and $u_\tau := u_{|\partial\Omega} - u_\nu \nu$ the normal and tangential displacements on $\partial\Omega$, respectively. We also let $\sigma_\nu(u) := \nu \cdot \sigma(u)_{|\partial\Omega} \cdot \nu$ and $\sigma_\tau(u) := \sigma(u)_{|\partial\Omega} \cdot \nu - \sigma(u)_\nu \nu$ be the normal and tangential stress on $\partial\Omega$, respectively. Note that u_ν and $\sigma_\nu(u)$ are scalars while u_τ and $\sigma_\tau(u)$

are vectors in $\mathbb{R}^d$. Let $|\cdot|$ denote the Euclidean norm in $\mathbb{R}^m$, $m \geq 1$. On Γ^c, a unilateral contact condition, also called Signorini condition, and a Coulomb friction (see Fig. 4.1) are enforced

$$u_\nu \leq g,\ \sigma_\nu(u) \leq 0,\ \sigma_\nu(u)(u_\nu - g) = 0 \qquad \text{on } \Gamma^c \times (0,T), \tag{4.3}$$

$$|\sigma_\tau(u)| \leq \mu|\sigma_\nu(u)| \qquad \text{on } \Gamma^c \times (0,T), \tag{4.4}$$

$$\sigma_\tau(u) = -\mu|\sigma_\nu(u)|\frac{\dot{u}_\tau}{|\dot{u}_\tau|} \quad \text{if } \dot{u}_\tau \neq 0 \qquad \text{on } \Gamma^c \times (0,T), \tag{4.5}$$

where $\mu > 0$ is the friction coefficient (taken to be constant for simplicity) and g is the initial gap. At the initial time, the displacement and velocity fields are prescribed,

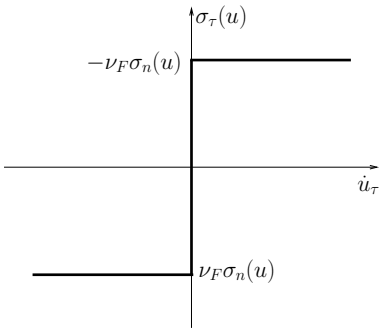

Fig. 4.1. Coulomb condition ($d = 2$).

$$u(0) = u^0, \quad \dot{u}(0) = v^0 \quad \text{in } \Omega. \tag{4.6}$$

The mathematical analysis of the above time-dependent problem entails substantial difficulties [41]. The existence of a weak solution is only proven for a viscoelastic material and a non-local Coulomb friction law [27].

4.3 Space semi-discrete formulation

In this section, we formulate the space semi-discrete problem and prove existence and uniqueness of a solution. We also establish an energy balance. In the frictionless case, the semi-discrete problem is equivalent to a Lipschitz ordinary differential equation, and existence and uniqueness are deduced from the Cauchy-Lipschitz theorem. With friction, the situation is more complicated. We choose to model the friction term as a set-valued map. The semi-discrete problem is then equivalent to a differential inclusion, for which generalizations of the Cauchy-Lipschitz theorem are available [31, 114].

4.3.1 Preliminaries

To begin with, we introduce some notions needed for the formulation of our problem as a differential inclusion.

- Given a set E, we define $\mathcal{P}(E)$ as the set of all subsets of E, and $\mathcal{P}^*(E) := \mathcal{P}(E) \setminus \{\emptyset\}$.
- A set-valued map is said to be closed convex if its images are closed convex sets.
- Various notions of continuity can be defined for set-valued maps. One of them is upper semi-continuity [1]. A set-valued map F is said to be upper semi-continuous at x if, for every open set V containing $F(x)$, there exists a neighborhood U of x such that $F(U) \subset V$. Consider, for instance, the following set-valued maps:

$$F_1(x) = \begin{cases} [-1,1] & \text{if } x = 0, \\ \{0\} & \text{if } x \neq 0, \end{cases} \quad \text{and} \quad F_2(x) = \begin{cases} \{0\} & \text{if } x = 0, \\ [-1,1] & \text{if } x \neq 0. \end{cases}$$

  It is easy to verify that F_1 is upper semi-continuous for all $x \in \mathbb{R}$, whereas F_2 is not upper semi-continuous at $x = 0$. Here is another example of set-valued-map, closely related to the Coulomb friction term,

$$F_3(x,y) = \begin{cases} \{-|x|\} & \text{if } y < 0, \\ [-|x|, |x|] & \text{if } y = 0, \\ \{|x|\} & \text{if } y > 0. \end{cases}$$

  It is easy to verify that this map is upper semi-continuous for all $(x,y) \in \mathbb{R}^2$. Finally, we observe that upper semi-continuity applied to single-valued functions is equivalent to continuity. For more details on set-valued maps, we refer to [3].
- The existence theorem for differential inclusions we use does not provide continuously differentiable solutions in time. The solutions are only absolutely continuous in time. For brevity, we do not define this concept and refer to [109]. For our purpose, it suffices to know that an absolutely continuous function y is continuous, differentiable almost everywhere and is equal to the integral of its derivative:

$$y(t_0) = y(0) + \int_0^{t_0} \dot{y}(t)dt.$$

  Lipschitz continuous functions are absolutely continuous. In what follows, we denote by $AC([0,T];\mathbb{R}^m)$, the space spanned by absolutely continuous functions from $[0,T]$ to $\mathbb{R}^m$.
- The set-valued maps which appear in our space semi-discrete problem are subgradients and for completeness, we define this notion. Let $J : \mathbb{R}^m \to \mathbb{R} \cup \{+\infty\}$ be a convex function and $D(J) := \{v \in \mathbb{R}^m;\ J(v) < +\infty\}$ its domain. We define the subgradient of J as the set-valued map $\partial J : D(J) \to \mathcal{P}^*(\mathbb{R}^m)$ such that

$$\forall v \in D(J), \quad \partial J(v) := \{\gamma \in \mathbb{R}^m;\ J(w) - J(v) \geq (\gamma, w - v),\ \forall w \in D(J)\}, \tag{4.7}$$

  where $(\cdot,\cdot)$ denotes the canonical inner product on $\mathbb{R}^m$. It is easy to prove that the subgradient of a convex function is well-defined and is a closed convex set-valued map. For more details on subgradients, we refer to [26, 68].

We can now state the main result we use for asserting the well-posedness of a problem posed in the form of a differential inclusion.

1. This notion of upper semi-continuity is distinct from the upper semi-continuity for single-valued functions.

Theorem 4.1. *Let $P : [0,T] \times \mathbb{R}^m \to \mathcal{P}^*(\mathbb{R}^m)$ be a closed convex set-valued map. Let $x_0 \in \mathbb{R}^m$ and consider the following problem: Find $x \in AC([0,T];\mathbb{R}^m)$ such that*

$$\dot{x}(t) \in P(t, x(t)), \tag{4.8}$$
$$x(0) = x_0. \tag{4.9}$$

Assume that

1. *the set-valued map $P(t,\cdot)$ is upper semi-continuous for almost all $t \in [0,T]$;*
2. *for any $x \in \mathbb{R}^m$, there exists a measurable function $p(\cdot, x)$ satisfying $p(t,x) \in P(t,x)$ for almost all $t \in [0,T]$;*
3. *there exists a function $b \in L^1(0,T;\mathbb{R}^m)$ such that $|p(t,x)| \leq b(t)$ for almost all $t \in [0,T]$.*

Then, there exists a solution to (4.8)-(4.9). Furthermore, assume the following one-sided Lipschitz condition: there exists $K \in \mathbb{R}$ such that, for all $t \in [0,T]$, for all x_1, $x_2 \in \mathbb{R}^m$,

$$(y_1 - y_2, x_1 - x_2) \leq K\|x_1 - x_2\|^2, \quad \forall y_1 \in P(t,x_1),\ \forall y_2 \in P(t,x_2). \tag{4.10}$$

Then, the solution is unique.

Proof. For the existence, see [114, Theorem 4.7] or [31, Theorem 5.2]. Uniqueness is straightforward owing to the one-sided Lipschitz condition since it implies that two solutions x_1 and x_2 satisfy $\frac{1}{2}\frac{d}{dt}(\|x_1 - x_2\|^2) \leq K\|x_1 - x_2\|^2$.

Remark 4.1. *In the single-valued case ($P : [0,T] \times \mathbb{R}^m \to \mathbb{R}^m$), the hypotheses of Theorem 4.1 become*

1. *$P(t,\cdot)$ is continuous for almost all $t \in [0,T]$;*
2. *for any $x \in \mathbb{R}$, $P(\cdot, x)$ is measurable;*
3. *there exists a function $b \in L^1(0,T;\mathbb{R})$ such that $|P(t,x)| \leq b(t)$ for almost all $t \in [0,T]$;*

We recover Caratheodory's existence theorem for ordinary differential equations [48]. Furthermore, the one-sided Lipschitz condition means that $P(t,\cdot)$ is Lipschitz continuous for all $t \in [0,T]$ (uniformly).

Remark 4.2. *If P is a monotone operator, i.e., for all $t \in [0,T]$, for all x_1, $x_2 \in \mathbb{R}^m$,*

$$(y_1 - y_2, x_1 - x_2) \geq 0, \quad \forall y_1 \in P(t,x_1),\ \forall y_2 \in P(t,x_2),$$

then $-P$ satisfies the one-sided Lipschitz condition.

4.3.2 The discrete setting

For simplicity, we suppose that Ω is a polyhedron. Let $\mathcal{T}$ be a simplicial mesh of Ω (triangles in 2D and tetrahedra in 3D). Let $\{x_i\}_{i\in\mathcal{N}}$ and $\{\phi_i\}_{i\in\mathcal{N}}$ be the nodes of the mesh and the associated scalar basis functions (continuous and piecewise affine), respectively. We denote by $\mathcal{N}^D$ the set of indices where a Dirichlet condition is enforced, and we set $\tilde{\mathcal{N}} := \mathcal{N} \setminus \mathcal{N}^D$. The space of admissible displacements is approximated by the space

$$V = \{v \in C^0(\overline{\Omega})^d;\ v_{|T} \in (\mathbb{P}_1)^d,\ \forall T \in \mathcal{T},\ \text{and } v(x_i) = 0,\ \forall i \in \mathcal{N}^D\}.$$

The space V is spanned by $\{\phi_i e_\alpha\}_{i\in\tilde{\mathcal{N}},1\le\alpha\le d}$, where $\{e_\alpha\}_{1\le\alpha\le d}$ is the canonical basis of $\mathbb{R}^d$. Denote by $\mathcal{N}^{\rm c}$ the set of indices of contact nodes (that is, the nodes located on $\Gamma^{\rm c}$ which is fixed *a priori*) and by $\mathcal{N}^{\rm i} := \tilde{\mathcal{N}} \setminus \mathcal{N}^{\rm c}$ the set of indices of the remaining nodes (see Fig. 4.2). Let $\{\nu_i\}_{i\in\mathcal{N}^{\rm c}}$ and $\{\tau_{i,\alpha}\}_{i\in\mathcal{N}^{\rm c},1\le\alpha\le d-1}$ be the contact normal vectors and tangential vectors, respectively. We set

$$V^{\rm i} = \mathrm{span}(\{\phi_i e_\alpha\}_{i\in\mathcal{N}^{\rm i},1\le\alpha\le d}),$$

$$V^{\rm c} = \mathrm{span}(\{\phi_i \nu_i\}_{i\in\mathcal{N}^{\rm c}}) \quad \text{and} \quad V^{\rm f} = \mathrm{span}(\{\phi_i \tau_{i,\alpha}\}_{i\in\mathcal{N}^{\rm c},1\le\alpha\le d-1}).$$

Clearly, $V = V^{\rm i} \oplus V^{\rm c} \oplus V^{\rm f}$, so that any discrete function $v \in V$ can be decomposed as

$$v = v_{\rm i} + v_{\rm c} + v_{\rm f} \quad \text{with} \quad v_{\rm i} \in V^{\rm i},\ v_{\rm c} \in V^{\rm c},\ v_{\rm f} \in V^{\rm f}.$$

We also introduce the space $V^* := V^{\rm i} \oplus V^{\rm f}$, so that any discrete function $v \in V$ can also be decomposed as

$$v = v_* + v_{\rm c} \quad \text{with} \quad v_* \in V^*,\ v_{\rm c} \in V^{\rm c}.$$

Let $(\cdot,\cdot)$ denote the L^2 inner product on V. Let $\|\cdot\|$ denote the norm associated with $(\cdot,\cdot)$. Herein, we always work in finite dimension on a fixed spatial mesh; the specific choice of the norm is therefore not critical. The present choice is made for simplicity.

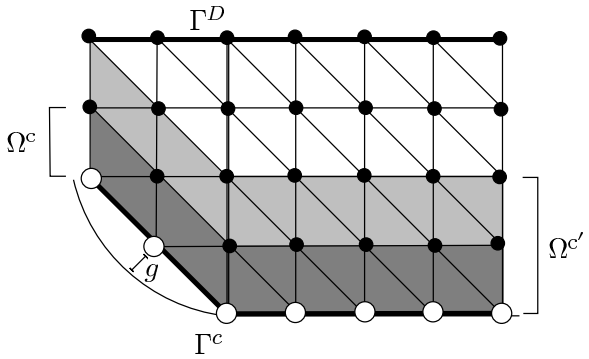

Fig. 4.2. Decomposition of the domain Ω; bullets (resp., circles) indicate nodes indexed by elements of the set $\mathcal{N}^{\rm i}$ (resp., $\mathcal{N}^{\rm c}$). The open sets Ω^c and $\Omega^{c'}$ are defined in Section 3.

The standard mass term stems from the bilinear form

$$m : L^2(\Omega)^d \times L^2(\Omega)^d \ni (v,w) \longmapsto \int_\Omega \rho v \cdot w \in \mathbb{R}.$$

The key idea in the modified mass method is to remove the mass associated with the normal components at the contact nodes. We consider an approximate mass term associated with the bilinear form m^* such that

$$m^*(\phi_i\nu_i, w) = m^*(w, \phi_i\nu_i) = 0, \quad \forall i \in \mathcal{N}^{\rm c},\ \forall w \in V. \tag{4.11}$$

Many choices are possible to build the rest of the mass term. In [57, 75], the authors devise various methods to preserve some features of the standard mass term (the total mass, the center

of gravity, and the moments of inertia); see also [107] for further results. Here, we focus for simplicity on the choice

$$m^* : V \times V \ni (v, w) \longmapsto m(v_*, w_*) \in \mathbb{R}.$$

We define the associated operator $M^* : V^* \to V^*$ such that,

$$(M^* v_*, w_*) = m^*(v_*, w_*) \quad \forall (v_*, w_*) \in V^* \times V^*.$$

We define the bilinear and linear forms

$$a : H^1(\Omega)^d \times H^1(\Omega)^d \ni (v, w) \longmapsto \int_\Omega \epsilon(v) : \mathcal{A} : \epsilon(w),$$
$$l : [0, T] \times H^1(\Omega)^d \ni (t, v) \longmapsto \int_\Omega f(t) \cdot v + \int_{\Gamma^N} f_N(t) \cdot v.$$

We define the linear operator $A : V \to V$ and the vector $L(t) \in V$ such that for all $v \in V$ and $w \in V$, and for all $t \in [0, T]$,

$$(Av, w) = a(v, w), \qquad (L(t), w) = l(t, w).$$

We also need $A^{\mathrm{c}} : V \to V^{\mathrm{c}}$ and $L^{\mathrm{c}}(t) \in V^{\mathrm{c}}$ such that for all $v \in V$ and all $w_{\mathrm{c}} \in V^{\mathrm{c}}$, and for all $t \in [0, T]$,

$$(A^{\mathrm{c}} v, w_{\mathrm{c}}) = a(v, w_{\mathrm{c}}), \qquad (L^{\mathrm{c}}(t), w_{\mathrm{c}}) = l(t, w_{\mathrm{c}}),$$

and, similarly, $A^* : V \to V^*$ and $L^*(t) \in V^*$ such that for all $v \in V$ and all $w_* \in V^*$, and for all $t \in [0, T]$,

$$(A^* v, w_*) = a(v, w_*), \qquad (L^*(t), w_{\mathrm{c}}) = l(t, w_*).$$

We define the constraint set

$$K := \{v \in V;\ v(x_i) \cdot \nu_i \leq g(x_i),\ \forall i \in \mathcal{N}^{\mathrm{c}}\},$$

and the unilateral contact term $I_K : V^{\mathrm{c}} \to \mathbb{R} \cup \{+\infty\}$ such that

$$I_K(v_{\mathrm{c}}) = \begin{cases} 0 & \text{if } v_{\mathrm{c}} \in K, \\ +\infty & \text{if } v_{\mathrm{c}} \notin K. \end{cases}$$

The function I_K is non-differentiable, but convex since K is convex. Therefore, it is possible to define its subgradient $\partial I_K : V^{\mathrm{c}} \cap K \to \mathcal{P}^*(V^{\mathrm{c}})$,

$$\partial I_K(v_{\mathrm{c}}) := \{\gamma \in V^{\mathrm{c}};\ 0 \geq (\gamma, w_{\mathrm{c}} - v_{\mathrm{c}})\ \forall w_{\mathrm{c}} \in V^{\mathrm{c}} \cap K\}.$$

Now, we define the friction term $j : V \times V^{\mathrm{f}} \to \mathbb{R}$ such that

$$j(v, w_{\mathrm{f}}) = \int_{\Gamma^{\mathrm{c}}} \mu |\sigma_\nu(v)||w_{\mathrm{f}}|. \tag{4.12}$$

The function j is non-differentiable with respect to its second argument, but convex, and its domain is V^{f}. We can define its subgradient with respect to its second argument such that for all $z \in V$, $\partial_2 j(z, \cdot) : V^{\mathrm{f}} \to \mathcal{P}^*(V^{\mathrm{f}})$ with

$$\partial_2 j(z, v_{\mathrm{f}}) := \left\{\gamma \in V^{\mathrm{f}};\ j(z, w_{\mathrm{f}}) - j(z, v_{\mathrm{f}}) \geq (\gamma, w_{\mathrm{f}} - v_{\mathrm{f}})\ \forall w_{\mathrm{f}} \in V^{\mathrm{f}}\right\}. \tag{4.13}$$

4.3.3 Formulation of the semi-discrete problem

We can now formulate the semi-discrete problem. Let $u_*^0 \in V^*$ and $v_*^0 \in V^*$ be suitable approximations of the initial displacement and velocity u^0 and v^0, respectively.

Problem 4.1. Seek $u \in C^0([0,T];K)$ such that $u_* \in C^1([0,T];V^*)$, $\dot{u}_* \in AC([0,T];V^*)$, and the following differential inclusion holds true

$$M^*\ddot{u}_* \in -Au - \partial_2 j(u,\dot{u}_{\rm f}) - \partial I_K(u_{\rm c}) + L(t) \quad \text{a.e. in } [0,T], \tag{4.14}$$

with the initial conditions $u_*(0) = u_*^0$ and $\dot{u}_*(0) = v_*^0$ in Ω.

Remark 4.3. *The velocity $\dot{u}_*$ is absolutely continuous. Therefore, it is differentiable almost everywhere, and the acceleration $\ddot{u}_*$ in (4.14) is well-defined. Moreover, $u_{\rm c} \in K$ so that $\partial I_K(u_{\rm c})$ is well-defined.*

To explicitate the link between the space semi-discrete Problem 4.1 and the continuous problem formulated in Section 2, we observe that (4.14) means that, for almost all $t \in [0,T]$, there exist $\lambda_{\rm c} \in \partial I_K(u_{\rm c})$ and $\lambda_{\rm f} \in \partial_2 j(u,\dot{u}_{\rm f})$ such that

$$M^*\ddot{u}_* + Au + \lambda_{\rm c} + \lambda_{\rm f} = L(t).$$

Therefore, the vectors $\lambda_{\rm c}$ and $\lambda_{\rm f}$ are discrete counterparts of the normal and tangential contact stresses. Furthermore, lumping the mass matrices, it is easy to verify that the definitions of $\partial I_K(u_{\rm c})$ and $\partial_2 j(u,\dot{u}_{\rm f})$ imply that, for all $i \in \mathcal{N}^{\rm c}$,

$$u_{\rm c}(x_i)\cdot\nu_i \le g(x_i),\ \lambda_{\rm c}(x_i) \le 0,\ \lambda_{\rm c}(x_i)(u_{\rm c}(x_i)\cdot\nu_i - g(x_i)) = 0, \tag{4.15}$$

$$|\lambda_{\rm f}(x_i)| \le \mu|\sigma_\nu(u)(x_i)|, \tag{4.16}$$

$$\lambda_{\rm f}(x_i) = -\mu|\sigma_\nu(u)(x_i)|\frac{\dot{u}_{\rm f}(x_i)}{|\dot{u}_{\rm f}(x_i)|} \quad \text{if } \dot{u}_{\rm f}(x_i) \neq 0. \tag{4.17}$$

Thus, we recover the discrete counterpart of the contact and friction conditions (4.3)-(4.5).

4.3.4 Main results

This section contains our main results concerning the space semi-discrete problem. We define the map $q : [0,T] \times V^* \to V^{\rm c} \cap K$ such that for all $t \in [0,T]$ and for all $v_* \in V^*$, $v_{\rm c} = q(t,v_*) \in V^{\rm c} \cap K$ solves the following variational inequality

$$a(v_{\rm c}, w_{\rm c} - v_{\rm c}) \ge l(t, w_{\rm c} - v_{\rm c}) - a(v_*, w_{\rm c} - v_{\rm c}) \quad \forall w_{\rm c} \in V^{\rm c} \cap K. \tag{4.18}$$

This variational inequality is well-posed since it is equivalent to the minimization of a strictly convex functional over a convex set. We first examine the properties of the map q.

Lemma 4.1. *For all $v_* \in V^*$, the map $t \mapsto q(t,v_*)$ is Lipschitz continuous, and its Lipschitz constant is uniformly bounded in v_*. For all $t \in [0,T]$, the map $v_* \mapsto q(t,v_*)$ is Lipschitz continuous, and its Lipschitz constant is uniformly bounded in t.*

Proof. Let $t_1, t_2 \in [0,T]$ and $v_*, w_* \in V^*$. Set $v_\mathrm{c} = q(t_1, v_*)$ and $w_\mathrm{c} = q(t_2, w_*)$. Owing to (4.18),

$$a(v_\mathrm{c} - w_\mathrm{c}, v_\mathrm{c} - w_\mathrm{c}) \le a(v_* - w_*, w_\mathrm{c} - v_\mathrm{c}) + l(t_1, v_\mathrm{c} - w_\mathrm{c}) - l(t_2, v_\mathrm{c} - w_\mathrm{c}). \tag{4.19}$$

Since $l(t, v_\mathrm{c} - w_\mathrm{c}) = \int_\Omega f(t)\cdot(v_\mathrm{c} - w_\mathrm{c}) + \int_{\Gamma^N} f_N(t)\cdot(v_\mathrm{c} - w_\mathrm{c})$ and since since $f \in W^{1,\infty}(0,T;L^2(\Omega)^d)$ and $f_N \in W^{1,\infty}(0,T;L^2(\Gamma^N)^d)$, there exists a constant c_l such that

$$l(t_1, v_\mathrm{c} - w_\mathrm{c}) - l(t_2, v_\mathrm{c} - w_\mathrm{c}) \le c_l |t_1 - t_2| \|v_\mathrm{c} - w_\mathrm{c}\|.$$

Moreover, the bilinear form a being continuous (with constant c_a) and elliptic (with constant α) for the norm $\|\cdot\|$, a straightforward calculation yields

$$\alpha \|v_\mathrm{c} - w_\mathrm{c}\| \le c_a \|v_* - w_*\| + c_l |t_1 - t_2|,$$

which proves the desired regularity for q.

We now reformulate the differential inclusion (4.14) using the map q.

Lemma 4.2. *The differential inclusion (4.14) is equivalent to*

$$M^* \ddot{u}_* \in -A^*(u_* + q(t,u_*)) - \partial_2 j(u_* + q(t,u_*), \dot{u}_\mathrm{f}) + L^*(t), \qquad \text{a.e. in } [0,T], \tag{4.20}$$

$$u_\mathrm{c} = q(t,u_*), \qquad \forall t \in [0,T], \tag{4.21}$$

Proof. Distinguishing components in V^* and V^c, the inclusion (4.14) is equivalently split into the following inclusions

$$M^* \ddot{u}_* \in -A^* u - \partial_2 j(u, \dot{u}_\mathrm{f}) + L^*(t) \qquad \text{a.e. in } [0,T], \tag{4.22}$$

$$0 \in -A^\mathrm{c} u - \partial I_K(u_\mathrm{c}) + L^\mathrm{c}(t) \qquad \text{a.e. in } [0,T]. \tag{4.23}$$

Consider (4.23). By continuity, the inclusion (4.23) is valid for all $t \in [0,T]$. For convenience, we recast it as a variational inequality,

$$a(u, v_\mathrm{c} - u_\mathrm{c}) \ge l(t, v_\mathrm{c} - u_\mathrm{c}) \quad \forall t \in [0,T],\ \forall v_\mathrm{c} \in V^\mathrm{c} \cap K, \tag{4.24}$$

or, equivalently,

$$a(u_\mathrm{c}, v_\mathrm{c} - u_\mathrm{c}) \ge l(t, v_\mathrm{c} - u_\mathrm{c}) - a(u_*, v_\mathrm{c} - u_\mathrm{c}) \quad \forall t \in [0,T],\ \forall v_\mathrm{c} \in V^\mathrm{c} \cap K. \tag{4.25}$$

Hence $u_\mathrm{c} = q(t, u_*)$ so that the system (4.22)-(4.23) is equivalent to the system (4.20)-(4.21).

We can now state our main existence result for Problem 4.1.

Theorem 4.2. *There exists a unique solution u to Problem 4.1. Furthermore, $u_\mathrm{c} \in W^{1,\infty}(0,T;V^\mathrm{c})$.*

Proof. (i) To prove the existence of a solution, we rewrite the second-order differential inclusion (4.14) as a first-order differential inclusion. We define the single-valued map $S : [0,T] \times V^* \times V^* \to V^* \times V^*$ such that, for all $t \in [0,T]$, for all $v_*, w_* \in V^*$,

$$S(t, v_*, w_*) = \begin{pmatrix} w_* \\ -A^*(v_* + q(t, v_*)) + L^*(t) \end{pmatrix},$$

and the set-valued map $P : [0,T] \times V^* \times V^* \to \{0\} \times \mathcal{P}^*(V^*)$ such that

$$P(t, v_*, w_*) = \begin{pmatrix} 0 \\ -\partial_2 j(v_* + q(t, v_*), w_{\rm f}) \end{pmatrix}.$$

We define also the linear single-valued map $D : V^* \times V^* \to V^* \times V^*$ such that

$$D(v_*, w_*) = \begin{pmatrix} v_* \\ M^* w_* \end{pmatrix}.$$

Setting $X(t) = \begin{pmatrix} u_*(t) \\ \dot{u}_*(t) \end{pmatrix} \in V^* \times V^*$, the differential inclusion (4.20) can be recast as

$$D\dot{X}(t) \in S(t, X(t)) + P(t, X(t)). \tag{4.26}$$

We equip the product space $V^* \times V^*$ with the product norm.

(ii) The operator S is a single-valued map. Since $q(t, \cdot)$ is continuous and $q(\cdot, x)$ is Lipschitz continuous, the operator S satisfies the hypotheses of Theorem 4.1 (see Remark 4.1).

(iii) We now examine the operator P. This operator is a closed convex set-valued map (owing to the properties of the subgradients of convex functions). Since $q(t, \cdot)$ is continuous and $\partial_2 j(\cdot, \cdot)$ is upper semi-continuous (see the example given by (4.3.1)), the map $P(t, \cdot)$ is upper semi-continuous. Hence, Hypothesis 1 of Theorem 4.1 holds true. Since $q(\cdot, x)$ is Lipschitz continuous, Hypotheses 2 and 3 of this theorem are also satisfied. Next, we check the one-sided Lipschitz condition (4.10). Let $(u_*^1, u_*^2, v_*^1, v_*^2) \in (V^*)^4$ and let $t \in [0,T]$. Set $u^1 = u_*^1 + q(t, u_*^1)$ and $u^2 = u_*^2 + q(t, u_*^2)$. Let $\gamma_1 \in -\partial_2 j(u^1, v_{\rm f}^1)$ and let $\gamma_2 \in -\partial_2 j(u^2, v_{\rm f}^2)$. Using the definition of the subgradient, a reverse triangle inequality, norm equivalence in finite dimension, and the fact that $q(t, \cdot)$ is Lipschitz, we infer

$$\begin{aligned}
(\gamma_2 - \gamma_1, v_*^1 - v_*^2) &\le j(u^1, v_{\rm f}^1) - j(u^1, v_{\rm f}^2) + j(u^2, v_{\rm f}^2) - j(u^2, v_{\rm f}^1) \\
&\le \int_{\Gamma^{\rm c}} \mu \left(|\sigma_\nu(u^1)| - |\sigma_\nu(u^2)| \right) \left(|v_{\rm f}^1| - |v_{\rm f}^2| \right) \\
&\le \int_{\Gamma^{\rm c}} \mu \left| |\sigma_\nu(u^1)| - |\sigma_\nu(u^2)| \right| \left| |v_{\rm f}^1| - |v_{\rm f}^2| \right| \\
&\le \int_{\Gamma^{\rm c}} \mu |\sigma_\nu(u^1) - \sigma_\nu(u^2)| |v_*^1 - v_*^2| \\
&\lesssim \|u^1 - u^2\| \|v_*^1 - v_*^2\| \\
&\lesssim \left(\|u_*^1 - u_*^2\| + \|q(t, u_*^1) - q(t, u_*^2)\| \right) \|v_*^1 - v_*^2\| \\
&\lesssim \|u_*^1 - u_*^2\| \|v_*^1 - v_*^2\| \lesssim \|u_*^1 - u_*^2\|^2 + \|v_*^1 - v_*^2\|^2.
\end{aligned}$$

Therefore, P satisfies the one-sided Lipschitz condition.

(iv) Owing to Theorem 4.1, there exists a unique $X \in AC([0,T]; V^* \times V^*)$ satisfying (4.26) with the initial condition $X(0) = \begin{pmatrix} u_*^0 \\ v_*^0 \end{pmatrix}$. Therefore, there exists a unique $u_* \in C^1(0,T; V^*)$ such

that $\dot{u}_* \in AC([0,T];V^*)$ satisfying (4.20) with the initial conditions $u_*(0) = u_*^0$ and $\dot{u}_*(0) = v_*^0$. Owing to (4.21), $u = u_* + u_c = u_* + q(t,u_*)$. Therefore, Problem 4.1 has a unique solution and it is clear that $u_c = q(t,u_*) \in W^{1,\infty}(0,T;V^c)$.

We conclude this section with the energy balance.

Theorem 4.3. *For all $t_0 \in [0,T]$, the following energy balance holds true:*

$$E(u(t_0)) - E(u(0)) = \int_0^{t_0} \Big\{ l(t,\dot{u}(t)) - j(u(t),\dot{u}_f(t)) \Big\} dt, \tag{4.27}$$

where $E(v) = \frac{1}{2}\left(m(\dot{v}_*,\dot{v}_*) + a(v,v)\right)$.

Proof. We recast the differential inclusion (4.20) as a variational inequality,

$$m(\ddot{u}_*, v_* - \dot{u}_*) + a(u, v_* - \dot{u}_*) + j(u,v_f) - j(u,\dot{u}_f) \\ \geq l(t, v_* - \dot{u}_*) \quad \forall v_* \in V^*, \text{ a.e. in } [0,T]. \tag{4.28}$$

Taking $v_* = 0$ and then $v_* = 2\dot{u}_*$ in the above inequality, we obtain

$$m(\ddot{u}_*, \dot{u}_*) + a(u,\dot{u}_*) + j(u,\dot{u}_f) = l(t,\dot{u}_*) \quad \text{a.e. on } [0,T]. \tag{4.29}$$

Recalling that the family $\{\phi_i\nu_i\}_{i\in\mathcal{N}^c}$ is a basis of V^c, we decompose u_c on this basis yielding $u_c = \sum_{i\in\mathcal{N}^c} u_i\phi_i\nu_i$. Define $C_i^0 := \{t \in [0,T];\ u_i = 0\}$ and $C_i^- := \{t \in [0,T];\ u_i < 0\}$. The sets C_i^0 and C_i^- are respectively closed and open, and they form a partition of $[0,T]$. On $\mathrm{int}(C_i^0)$, $\dot{u}_i\phi_i\nu_i = 0$ so that $a(u,\dot{u}_i\phi_i\nu_i) = 0 = l(t,\dot{u}_i\phi_i\nu_i)$. On C_i^-, $a(u,\dot{u}_i\phi_i\nu_i) = l(t,\dot{u}_i\phi_i\nu_i)$ owing to (4.23). Finally, $a(u,\dot{u}_i\phi_i\nu_i) = l(t,\dot{u}_i\phi_i\nu_i)$ on $\mathrm{int}(C_i^0)\cup C_i^-$, and hence almost everywhere (since an open set in $\mathbb{R}$ is a countable union of open intervals, so that its boundary has zero measure). Hence,

$$a(u,\dot{u}_c) = l(t,\dot{u}_c) \quad \text{a.e. on } [0,T]. \tag{4.30}$$

Using (4.30), we obtain

$$m(\ddot{u}_*, \dot{u}_*) + a(u,\dot{u}) + j(u,\dot{u}_f) = l(t,\dot{u}) \quad \text{a.e. on } [0,T]. \tag{4.31}$$

Since $\dot{u}$ is absolutely continuous in time, by integrating in time (4.31), we obtain (4.27).

4.4 Fully discrete formulation

In this section, we discretize the space semi-discrete problem with an implicit time scheme. We discretize the elastodynamics part with an implicit Newmark scheme (trapezoidal rule), while the unilateral contact and friction conditions are enforced in an implicit way. This choice of time discretization is very common. It is for instance employed in [57]. At each time step, we have thus to solve a nonlinear problem similar to a static friction problem. It is well-known that such a problem may have several solutions. Here we prove that, under a certain condition on the discretization parameters of CFL-type, the fully discrete problem is well-posed. We also derive the energy balance of this time-integration scheme.

For simplicity, the interval $[0,T]$ is divided into N equal subintervals of length Δt. We set $t^n = n\Delta t$ and denote by u^n, v^n, and a^n the approximations of $u(t^n)$, $\dot{u}(t^n)$, and $\ddot{u}(t^n)$, respectively. We define the convex combination $\square^{n+\alpha} := (1-\alpha)\square^n + \alpha\square^{n+1}$, where $\square$ stands for u, v, a or t, and $\alpha \in [0,1]$. In this section, the notation $A \lesssim B$ means that $A \le cB$ with a constant c independent of h and Δt.

Let $\mathcal{T}^{\rm c} \subset \mathcal{T}$ be the set of simplices such that at least one vertex is a contact node. We set $\Omega^{\rm c} = \mathrm{int}\left(\cup_{T\in\mathcal{T}^{\rm c}}\overline{T}\right)$. Let $\mathcal{T}^{c'} \subset \mathcal{T}$ be the set of simplices such that at least one vertex belongs to $\overline{\Omega^{\rm c}}$. We set $\Omega^{c'} = \mathrm{int}\left(\cup_{T\in\mathcal{T}^{c'}}\overline{T}\right)$(see Fig. 4.2). We define

$$h_{\rm c} = \min_{T\in\mathcal{T}^{\rm c}} \mathrm{diam}(T) \quad \text{and} \quad h_{c'} = \min_{T\in\mathcal{T}^{c'}} \mathrm{diam}(T),$$

where $\mathrm{diam}(T)$ denotes the diameter of the simplex T. Observe that $h_{\rm c}$ and $h_{c'}$ are defined using a minimum.

Let us recall some classical discrete trace and inverse inequalities (see, e.g., [122] and [44]). For all $v_{\rm c} \in V^{\rm c}$,

$$\|v_{\rm c}\|_{L^2(\Gamma^{\rm c})^d} \le \frac{1}{\sqrt{h_{\rm c}}}\|v_{\rm c}\|_{L^2(\Omega^{\rm c})^d}, \tag{4.32}$$

$$|v_{\rm c}|_{H^1(\Omega^{\rm c})^d} = \|\nabla v_{\rm c}\|_{L^2(\Omega^{\rm c})^{d\times d}} \le \frac{1}{h_{\rm c}}\|v_{\rm c}\|_{L^2(\Omega^{\rm c})^d}. \tag{4.33}$$

The same inequalities hold when $\Omega^{\rm c}$ is replaced by $\Omega^{\rm c'}$, and $h_{\rm c}$ by $h_{\rm c'}$. We define the operator $q^n : V^* \to V^{\rm c}$, such that for all $0 \le n \le N$,

$$q^n(v_*) = q(t^n, v_*) \quad \forall v_* \in V^*, \tag{4.34}$$

where the map q is defined in Section 4.3.4.

Lemma 4.3. *The function $q^n : V^* \to V^{\rm c}$ is Lipschitz continuous. More precisely,*

$$|q^n(v_*) - q^n(w_*)|_{H^1(\Omega^{\rm c})^d} \lesssim |v_* - w_*|_{H^1(\Omega^{c'})^d} \quad \forall v_*, w_* \in V^*. \tag{4.35}$$

Proof. Let $v_*, w_* \in V^*$. Set $v_{\rm c} = q^n(v_*)$ and $w_{\rm c} = q^n(w_*)$. Owing to (4.19),

$$a(v_{\rm c} - w_{\rm c}, v_{\rm c} - w_{\rm c}) \le a(v_* - w_*, w_{\rm c} - v_{\rm c}).$$

Since $v_{\rm c}$ and $w_{\rm c}$ are zero outside $\Omega^{\rm c}$, $a(v_{\rm c} - w_{\rm c}, v_{\rm c} - w_{\rm c}) \gtrsim |v_{\rm c} - w_{\rm c}|^2_{H^1(\Omega^{\rm c})^d}$, and

$$a(v_* - w_*, w_{\rm c} - v_{\rm c}) = a((v_* - w_*)1_{\Omega^{c'}}, w_{\rm c} - v_{\rm c}) \lesssim |v_* - w_*|_{H^1(\Omega^{c'})^d}|v_{\rm c} - w_{\rm c}|_{H^1(\Omega^{\rm c})^d},$$

whence the assertion.

We can now formulate the fully discrete problem.

Problem 4.2. Seek $u^{n+1} \in V$, $\mathrm{v}_*^{n+1} \in V^*$, and $\mathrm{a}_*^{n+1} \in V^*$ such that

$$M^*\mathrm{a}_*^{n+1} \in -A^*u^{n+1} - \partial_2 j(u^{n+1}, \mathrm{v}_{\rm f}^{n+1}) + L^*(t^{n+1}), \tag{4.36}$$

$$u_{\rm c}^{n+1} = q^{n+1}(u_*^{n+1}), \tag{4.37}$$

$$u_*^{n+1} = u_*^n + \Delta t\ \mathrm{v}_*^n + \frac{\Delta t^2}{2}\mathrm{a}_*^{n+\frac{1}{2}}, \tag{4.38}$$

$$\mathrm{v}_*^{n+1} = \mathrm{v}_*^n + \Delta t\ \mathrm{a}_*^{n+\frac{1}{2}}. \tag{4.39}$$

To begin with, we reformulate Problem 4.2 by eliminating v_*^{n+1} and a_*^{n+1}. We set $\delta_*^n := -u_*^n - \frac{\Delta t}{2} v_*^n$ and $\varepsilon_*^n := -u_*^n - \Delta t v_*^n - \frac{\Delta t^2}{4} a_*^n$, and we rewrite v_*^{n+1} and a_*^{n+1} as

$$v_*^{n+1} = \frac{2}{\Delta t}(u_*^{n+1} + \delta_*^n),$$
$$a_*^{n+1} = \frac{4}{\Delta t^2}(u_*^{n+1} + \varepsilon_*^n).$$

Next, we define the linear operator $\tilde{A}^* : V^* \to V^*$ and the vector $\tilde{L}^{n+1} \in V^*$ such that, $\forall v_* \in V^*$,

$$\tilde{A}^* v_* := A^* v_* + \frac{1}{4\Delta t^2} M^* v_*,$$
$$\tilde{L}^{n+1} := L^*(t^{n+1}) - \frac{1}{4\Delta t^2} M^* \varepsilon_*^n.$$

Then, using (4.37), it is straightforward to turn (4.36) into

$$0 \in \tilde{A}^* u_*^{n+1} + \partial_2 j \left(u_*^{n+1} + q^{n+1}(u_*^{n+1}), \frac{2}{\Delta t}(u_{\mathrm{f}}^{n+1} + \delta_{\mathrm{f}}^n) \right) - \tilde{L}^{n+1} + A^* q^{n+1}(u_*^{n+1}). \tag{4.40}$$

Observe that the last term on the right-hand side of (4.40) involves the operator A^* (and not $\tilde{A}^*$) owing to (4.11) and the fact that $q^{n+1}(u_*^{n+1}) \in V^{\mathrm{c}}$.

Theorem 4.4. *Problem 4.2 has a unique solution under the CFL-type condition*

$$\frac{\Delta t}{h_{c'}} \lesssim 1. \tag{4.41}$$

Proof. Define the map $\Phi^n : V^* \to V^*$ such that for all $\hat{v}_* \in V^*$, $v_* = \Phi^n(\hat{v}_*)$ satisfies

$$0 \in \tilde{A}^* v_* + \partial_2 j \left(\hat{v}, \frac{2}{\Delta t}(v_{\mathrm{f}} + \delta_{\mathrm{f}}^n) \right) - \tilde{L}^{n+1} + A^* \hat{v}_{\mathrm{c}}, \tag{4.42}$$

where $\hat{v}_{\mathrm{c}} := q^{n+1}(\hat{v}_*)$ and $\hat{v} := \hat{v}_* + \hat{v}_{\mathrm{c}}$, so that (4.40) amounts to seeking a fixed-point for Φ^n. Setting $y_* := \frac{2}{\Delta t}(v_* + \delta_*^n)$, we rewrite the above inclusion as a variational inequality,

$$\tilde{a}(v_*, z_* - y_*) + j(\hat{v}, z_{\mathrm{f}}) - j(\hat{v}, y_{\mathrm{f}}) \geq l^{n+1}(z_* - y_*) - a(\hat{v}_{\mathrm{c}}, z_* - y_*), \ \forall z_* \in V^*, \tag{4.43}$$

where we have set $\tilde{a}(v_*, w_*) := (\tilde{A}^* v_*, w_*)$ and $l^{n+1}(v_*) := (L(t^{n+1}), v_*)$. Taking $z_* := \frac{2}{\Delta t}(w_* + \delta_*^n)$ in (4.43), then dividing by $\frac{2}{\Delta t}$, we obtain for all $w_* \in V^*$,

$$\tilde{a}(v_*, w_* - v_*) + j(\hat{v}, w_{\mathrm{f}} + \delta_{\mathrm{f}}^n) - j(\hat{v}, v_{\mathrm{f}} + \delta_{\mathrm{f}}^n) \geq l^{n+1}(w_* - v_*) - a(\hat{v}_{\mathrm{c}}, w_* - v_*). \tag{4.44}$$

The variational inequality (4.44) has one and only one solution. Indeed, it is equivalent to the minimization of a strictly convex functional. The map Φ^n is thus well-defined. Now we shall prove that Φ^n is a contraction under the CFL condition (4.41). Let $\hat{v}_* \in V^*$ and $\hat{w}_* \in V^*$. Set $v_* := \Phi^n(\hat{v}_*)$ and $w_* := \Phi^n(\hat{w}_*)$. Using (4.44), a straightforward calculation yields

$$\begin{aligned} \tilde{a}(v_* - w_*, v_* - w_*) \leq\ & j(\hat{v}, w_{\mathrm{f}} + \delta_{\mathrm{f}}^n) - j(\hat{w}, w_{\mathrm{f}} + \delta_{\mathrm{f}}^n) \\ & - j(\hat{v}, v_{\mathrm{f}} + \delta_{\mathrm{f}}^n) + j(\hat{w}, v_{\mathrm{f}} + \delta_{\mathrm{f}}^n) - a(\hat{v}_{\mathrm{c}} - \hat{w}_{\mathrm{c}}, v_* - w_*). \end{aligned} \tag{4.45}$$

Using the ellipticity of m and a,

$$\tilde{a}(v_* - w_*, v_* - w_*) \gtrsim \frac{4}{\Delta t^2}\|v_* - w_*\|^2_{L^2(\Omega)^d} + |v_* - w_*|^2_{H^1(\Omega)^d}. \tag{4.46}$$

Using a reverse triangle inequality,

$$\begin{aligned} j(\hat{v}, w_\mathrm{f} + \delta^n_\mathrm{f}) - j(\hat{w}, w_\mathrm{f} + \delta^n_\mathrm{f}) - j(\hat{v}, v_\mathrm{f} + \delta^n_\mathrm{f}) + j(\hat{w}, v_\mathrm{f} + \delta^n_\mathrm{f}) \\ &\leq \int_{\Gamma^\mathrm{c}} \mu \left|\sigma_\nu(\hat{v}) - \sigma_\nu(\hat{w})\right| \left| |w_\mathrm{f} + \delta^n_\mathrm{f}| - |v_\mathrm{f} + \delta^n_\mathrm{f}| \right| \\ &\leq \int_{\Gamma^\mathrm{c}} |\mu||\sigma_\nu(\hat{v}) - \sigma_\nu(\hat{w})||v_\mathrm{f} - w_\mathrm{f}| \\ &\lesssim \int_{\Gamma^\mathrm{c}} |\sigma_\nu(\hat{v}) - \sigma_\nu(\hat{w})||v_\mathrm{f} - w_\mathrm{f}|. \end{aligned}$$

Using the Cauchy-Schwarz inequality and the trace inequality (4.32),

$$\begin{aligned} j(\hat{v}, w_\mathrm{f} + \delta^n_\mathrm{f}) - j(\hat{w}, w_\mathrm{f} + \delta^n_\mathrm{f}) - j(\hat{v}, v_\mathrm{f} + \delta^n_\mathrm{f}) + j(\hat{w}, v_\mathrm{f} + \delta^n_\mathrm{f}) \\ &\lesssim \|\sigma_\nu(\hat{v}) - \sigma_\nu(\hat{w})\|_{L^2(\Gamma^\mathrm{c})}\|v_\mathrm{f} - w_\mathrm{f}\|_{L^2(\Gamma^\mathrm{c})^d} \\ &\lesssim \frac{1}{h_\mathrm{c}}\|\sigma_\nu(\hat{v}) - \sigma_\nu(\hat{w})\|_{L^2(\Omega^\mathrm{c})}\|v_* - w_*\|_{L^2(\Omega^\mathrm{c})^d} \\ &\lesssim \frac{1}{h_\mathrm{c}}|\hat{v} - \hat{w}|_{H^1(\Omega^\mathrm{c})^d}\|v_* - w_*\|_{L^2(\Omega^\mathrm{c})^d}. \end{aligned} \tag{4.47}$$

Furthermore, using (4.35) and the inverse inequality (4.33),

$$\begin{aligned} |\hat{v} - \hat{w}|_{H^1(\Omega^\mathrm{c})^d} &= |\hat{v}_\mathrm{c} - \hat{w}_\mathrm{c}|_{H^1(\Omega^\mathrm{c})^d} + |\hat{v}_* - \hat{w}_*|_{H^1(\Omega^\mathrm{c})^d} \\ &= |q^{n+1}(\hat{v}_*) - q^{n+1}(\hat{w}_*)|_{H^1(\Omega^\mathrm{c})^d} + |\hat{v}_* - \hat{w}_*|_{H^1(\Omega^\mathrm{c})^d} \\ &\lesssim |\hat{v}_* - \hat{w}_*|_{H^1(\Omega^{\mathrm{c}'})^d} + |\hat{v}_* - \hat{w}_*|_{H^1(\Omega^\mathrm{c})^d} \\ &\lesssim |\hat{v}_* - \hat{w}_*|_{H^1(\Omega^{\mathrm{c}'})^d} \lesssim \frac{1}{h_{\mathrm{c}'}}\|\hat{v}_* - \hat{w}_*\|_{L^2(\Omega^{\mathrm{c}'})^d}. \end{aligned} \tag{4.48}$$

Collecting inequalities (4.47) and (4.48), and since $h_{\mathrm{c}'} \leq h_\mathrm{c}$,

$$\begin{aligned} j(\hat{v}, w_\mathrm{f} + \delta^n_\mathrm{f}) - j(\hat{w}, w_\mathrm{f} + \delta^n_\mathrm{f}) - j(\hat{v}, v_\mathrm{f} + \delta^n_\mathrm{f}) + j(\hat{w}, v_\mathrm{f} + \delta^n_\mathrm{f}) \\ \leq \frac{1}{h^2_{\mathrm{c}'}}\|\hat{v}_* - \hat{w}_*\|_{L^2(\Omega)^d}\|v_* - w_*\|_{L^2(\Omega^\mathrm{c})^d}. \end{aligned}$$

Using the boundedness of a, Lemma 4.3, and the inverse inequality (4.33),

$$a(\hat{v}_\mathrm{c} - \hat{w}_\mathrm{c}, w_* - v_*) \lesssim \frac{1}{h^2_{\mathrm{c}'}}\|\hat{w}_* - \hat{v}_*\|_{L^2(\Omega)^d}\|v_* - w_*\|_{L^2(\Omega)^d}.$$

Collecting these different estimates,

$$\|\Phi^n(\hat{v}_*) - \Phi^n(\hat{w}_*)\|_{L^2(\Omega)^d} = \|v_* - w_*\|_{L^2(\Omega)^d} \lesssim \left(\frac{\Delta t}{h_{\mathrm{c}'}}\right)^2 \|\hat{v}_* - \hat{w}_*\|_{L^2(\Omega)^d}.$$

Hence, if the ratio $\frac{\Delta t}{h_{\mathrm{c}'}}$ is sufficiently small, the mapping Φ^n is a contraction. The Banach fixed-point theorem guarantees that the problem has a unique solution.

Remark 4.4. *In the above proof, the inertial term is essential. By strengthening the coercivity of $\tilde{a}$, it enables to prove that Φ^n is a contraction (for a time step sufficiently small). In the static case, without the help of the inertial term, this fixed-point proof works only for a certain range of physical parameters, for instance when the Young modulus is large compared with the friction coefficient [76, Theorem 11.4].*

To conclude this part, we formulate the energy balance. We define the energy at time t^n as

$$E^n := \frac{1}{2}(Au^n, u^n) + \frac{1}{2}(M^* v^n, v^n). \tag{4.49}$$

At each time t^n, there exist $\lambda_{\rm c}^n \in \partial I_K(u_{\rm c}^n)$ and $\lambda_{\rm f}^n \in \partial_2 j(u^n, v_{\rm f}^n)$ such that

$$M^* a_*^n + Au^n + \lambda_{\rm c}^n + \lambda_{\rm f}^n = L(t^n). \tag{4.50}$$

Proceeding as in [82], it is readily shown that

$$\begin{aligned} E^{n+1} - E^n = &-\frac{1}{2}(\lambda_{\rm c}^n + \lambda_{\rm c}^{n+1}, u^{n+1} - u^n) - \frac{1}{2}(\lambda_{\rm f}^n + \lambda_{\rm f}^{n+1}, u^{n+1} - u^n) \\ &+ \frac{1}{2}(L^n + L^{n+1}, u^{n+1} - u^n). \end{aligned} \tag{4.51}$$

4.5 Convergence of the fully discrete solutions

We fix the space discretization and we build the approximate solutions $\omega^{\Delta t} : [0,T] \to V$ as follows:

$$\omega^{\Delta t}(t) := u^n + v_*^n(t - t^n) + \frac{1}{2} a_*^{n+\frac{1}{2}}(t - t^n)^2 \qquad \forall t \in [t^n, t^{n+1}), \tag{4.52}$$

$$\omega^{\Delta t}(T) := u^N. \tag{4.53}$$

It is readily verified that, by construction, $\omega^{\Delta t} \in C^0([0,T];V)$ and $\omega_*^{\Delta t} \in C^1([0,T];V^*)$. Furthermore, $\omega^{\Delta t} \in W^{1,\infty}(0,T;V)$. We are now going to prove the convergence of these approximate solutions to the semi-discrete solution u of Problem 4.1. In this section, the notation $A \lesssim B$ means that $A \le cB$ with a constant c independent of Δt, but which can depend on h. We assume without loss of generality that $\Delta t \le 1$.

Lemma 4.4. *Let (u^n, v^n, a^n) solve, for all $n \in \{0, \dots, N\}$, Problem 4.2. Then, for Δt small enough,*

$$\|u^n\| \lesssim 1, \quad \|v_*^n\| \lesssim 1, \quad \|a_*^n\| \lesssim 1. \tag{4.54}$$

Proof. (i) Let $n \in \{0, \dots, N\}$. From (4.50) we deduce $A^{\rm c} u^n + \lambda_{\rm c}^n = L^{\rm c}(t^n)$, and then, $\|\lambda_{\rm c}^n\| \lesssim \|u^n\| + \|L(t^n)\|$. Owing to the inequality (4.16), we obtain $\|\lambda_{\rm f}^n\| \lesssim \|u^n\|$. Hence, owing to the equilibrium equation (4.50), $\|a_*^n\| \lesssim \|u^n\| + \|L(t^n)\|$.

(ii) Using the energy balance (4.51), it follows that

$$E^{n+1} - E^n \lesssim \big(\|u^n\| + \|u^{n+1}\| + \|L(t^n)\| + \|L(t^{n+1})\|\big)\, \|u^{n+1} - u^n\|.$$

Observing by (4.19) that $\|q^{n+1}(u_*^n) - q^n(u_*^n)\| \lesssim \|L(t^{n+1}) - L(t^n)\|$, we infer

$$\begin{aligned}\|u^{n+1} - u^n\| &\le \|u_*^{n+1} - u_*^n\| + \|q^{n+1}(u_*^{n+1}) - q^{n+1}(u_*^n)\| + \|q^{n+1}(u_*^n) - q^n(u_*^n)\| \\ &\lesssim \|u_*^{n+1} - u_*^n\| + \|L(t^{n+1}) - L(t^n)\| \\ &\lesssim \|u_*^{n+1} - u_*^n\| + \|L(t^{n+1})\| + \|L(t^n)\|,\end{aligned}$$

we infer

$$\begin{aligned}E^{n+1} - E^n \lesssim \left(\|u^n\| + \|u^{n+1}\| + \|L(t^n)\| + \|L(t^{n+1})\|\right) \\ \left(\|u_*^{n+1} - u_*^n\| + \|L(t^{n+1})\| + \|L(t^n)\|\right).\end{aligned} \tag{4.55}$$

Using (4.38),

$$\begin{aligned}E^{n+1} - E^n \lesssim \Delta t \left(\|u^n\| + \|u^{n+1}\| + \|L(t^n)\| + \|L(t^{n+1})\|\right) \\ \left(\|v_*^n\| + \frac{\Delta t}{2}\|a_*^{n+\frac{1}{2}}\| + \|L(t^{n+1})\| + \|L(t^n)\|\right).\end{aligned} \tag{4.56}$$

Thus, using the previous bound on $\|a_*^n\|$ and $\|a_*^{n+1}\|$, and since $\Delta t \le 1$,

$$\begin{aligned}E^{n+1} - E^n \lesssim \Delta t \left(\|u^n\| + \|u^{n+1}\| + \|L(t^n)\| + \|L(t^{n+1})\|\right) \\ \left(\|v_*^n\| + \|u^n\| + \|u^{n+1}\| + \|L(t^{n+1})\| + \|L(t^n)\|\right).\end{aligned} \tag{4.57}$$

Now, using Young's inequality and the coercivity of the energy E^n,

$$E^{n+1} - E^n \le C_1 \Delta t\ E^{n+1} + C_2 \Delta t\ E^n + C_3 \Delta t \left(\|L(t^n)\|^2 + \|L(t^{n+1})\|^2\right),$$

where C_1, C_2, C_3 are three constants independent of Δt. Next,

$$E^{n+1} - E^n \le C_1 \Delta t\ (E^{n+1} - E^n) + (C_1 + C_2)\Delta t\ E^n + C_3 \Delta t \left(\|L(t^n)\|^2 + \|L(t^{n+1})\|^2\right),$$

For $\Delta t \le 1/(2C_1)$,

$$\frac{1}{2}(E^{n+1} - E^n) \le (C_1 + C_2)\Delta t\ E^n + C_3 \Delta t \left(\|L(t^n)\|^2 + \|L(t^{n+1})\|^2\right),$$

so that

$$E^{n+1} - E^n \lesssim \Delta t \left(E^n + \|L(t^n)\|^2 + \|L(t^{n+1})\|^2\right).$$

Finally, using a discrete Gronwall lemma,

$$E^n \lesssim E^0 + \sum_{j=0}^{n} \Delta t \|L(t^j)\|^2 \lesssim 1.$$

Then, it is straightforward to obtain the estimates (4.54).

Theorem 4.5. *The following convergence results hold true as $\Delta t \to 0$,*

$$\begin{aligned}&\omega^{\Delta t} \to u \quad \text{in } C^0([0,T];V), \\ &\dot{\omega}_*^{\Delta t} \to \dot{u}_* \text{ in } C^0([0,T];V^*), \\ &\ddot{\omega}_*^{\Delta t} \to \ddot{u}_* \text{ weakly} * \text{ in } L^\infty(0,T;V^*),\end{aligned}$$

where u solves Problem 4.1.

Proof. (i) From the estimates (4.54), we deduce that

$$\|\omega^{\Delta t}\|_{L^\infty(0,T;V)} \lesssim 1, \quad \|\dot\omega^{\Delta t}\|_{L^\infty(0,T;V)} \lesssim 1,$$
$$\|\dot\omega_*^{\Delta t}\|_{L^\infty(0,T;V^*)} \lesssim 1, \quad \|\ddot\omega_*^{\Delta t}\|_{L^\infty(0,T;V^*)} \lesssim 1.$$

(ii) Using standard compactness arguments [119], there exists $\omega \in C^0(0,T;V)$ such that $\dot\omega_* \in C^0(0,T;V^*)$, $\ddot\omega_* \in L^\infty(0,T;V^*)$, and, up to a subsequence,

$$\omega^{\Delta t} \to \omega \ \text{ in } C^0([0,T];V),$$
$$\dot\omega_*^{\Delta t} \to \dot\omega_* \text{ in } C^0([0,T];V^*),$$
$$\ddot\omega_*^{\Delta t} \rightharpoonup \ddot\omega_* \text{weakly} * \text{ in } L^\infty(0,T;V^*).$$

(iii) Next, we introduce the auxiliary (piecewise constant in time) approximate solutions $\underline{\omega}^{\Delta t} : [0,T] \to V$ and $\zeta_*^{\Delta t} : [0,T] \to V^*$ such that

$$\zeta_*^{\Delta t}(t) := v_*^{n+1} \quad \forall t \in [t^n, t^{n+1}), \qquad \zeta_*^{\Delta t}(T) := v_*^N,$$
$$\underline{\omega}^{\Delta t}(t) := u^{n+1} \quad \forall t \in [t^n, t^{n+1}), \qquad \underline{\omega}^{\Delta t}(T) := u^N.$$

By definition of the approximate solutions $\omega^{\Delta t}$ and $\underline{\omega}^{\Delta t}$, and using relation (4.38), $\forall n \in \{0,\dots,N\}$, $\forall t \in [t^n, t^{n+1})$,

$$\|\omega^{\Delta t}(t) - \underline{\omega}^{\Delta t}(t)\| \le \|u^{n+1} - u^n\| + \Delta t \|v_*^n\| + \frac{1}{2}\Delta t^2 \|a_*^{n+\frac12}\|$$
$$\le 2\Delta t \|v_*^n\| + \Delta t^2 \|a_*^{n+\frac12}\|.$$

Hence, using estimates (4.54),

$$\|\omega^{\Delta t}(t) - \underline{\omega}^{\Delta t}(t)\| \lesssim \Delta t \quad \text{a.e. in } [0,T].$$

We deduce that $\underline{\omega}^{\Delta t} \to \omega$ in $L^\infty(0,T;V)$. In the same way, we prove that $\zeta_*^{\Delta t} \to \dot\omega_*$ in $L^\infty(0,T;V^*)$. We define an approximate external force vector,

$$\underline{L}^{\Delta t}(t) := L(t^{n+1}) \quad \forall t \in [t^n, t^{n+1}), \qquad \underline{L}^{\Delta t}(T) := L(t^N).$$

Since $t \mapsto L(t)$ is Lipschitz continuous, $\underline{L}^{\Delta t} \to L$ in $L^\infty(0,T;V)$.
(iv) Owing to (4.36), the approximate solutions satisfy

$$M^*\ddot\omega_*^{\Delta t} \in -A^*\underline{\omega}^{\Delta t} - \partial_2 j(\underline{\omega}^{\Delta t}, \zeta_{\rm f}^{\Delta t}) + \underline{L}^{\Delta t *}(t) \qquad \text{a.e. in } [0,T],$$

so that

$$m^*(\ddot\omega_*^{\Delta t}, v_* - \zeta_*^{\Delta t}) + a(\underline{\omega}^{\Delta t}, v_* - \zeta_*^{\Delta t}) + j(\underline{\omega}^{\Delta t}, v_{\rm f}) - j(\underline{\omega}^{\Delta t}, \zeta_{\rm f}^{\Delta t})$$
$$\ge \big(\underline{L}^{\Delta t}, v_* - \zeta_*^{\Delta t}\big) \quad \forall v_* \in V^*, \text{ a.e. in } [0,T].$$

Passing to the limit,

$$m^*(\ddot\omega_*, v_* - \dot\omega_*) + a(\omega, v_* - \dot\omega_*) + j(\omega, v_{\rm f}) - j(\omega, \dot\omega_{\rm f})$$
$$\ge l(t, v_* - \dot\omega_*) \quad \forall v_* \in V^*, \text{ a.e. in } [0,T],$$

and hence

$$M^*\ddot\omega_* \in -A^*\omega - \partial_2 j(\omega, \dot\omega_{\rm f}) + L^*(t) \qquad \text{a.e. in } [0,T].$$

By uniqueness of the solution, we conclude that $\omega = u$. This uniqueness also implies that the whole sequence $(\omega^{\Delta t})$ converges, not only a subsequence.

4.6 Conclusions

In this work, we have established three results on the numerical analysis of the modified mass method for dynamic Signorini problems with Coulomb friction: the well-posedness of the space semi-discrete problem, the well-posedness of the fully discrete problem under a CFL-type condition on the mesh size and the time step, and the convergence of the fully discrete solution to the space semi-discrete solution as the time step tends to zero. These results contribute to the theoretical foundations of a computationally attractive method for which various numerical results and implementation aspects are discussed in [57, 58, 80]. Further work can examine the convergence of the space semi-discrete problem and deriving upper bounds on the approximation error.

Part II

Cohesive zone models

5

Quasi-explicit time-integration schemes for dynamic fracture with set-valued cohesive zone models

5.1 Introduction

Cohesive zone models have been introduced in the late 50s [6, 7, 39]. They can be applied to a large range of materials (concrete, steel, etc...) and fracture processes (brittle fracture, ductile fracture, fatigue, dynamic fracture) and they can be easily enriched with more complex physical behaviors (contact and friction after decohesion, corrosion, etc...). Moreover, cohesive zone models fit quite well within the framework of finite elements. For all these reasons, they are now widely used in engineering simulations. A cohesive zone model describes the mechanical forces along the fracture interface — it can be simply viewed as a boundary condition. The interface forces depend at least on the opening (displacement jump at the interface). In a typical cohesive zone model, the separation occurs at the interface only after a critical stress has been reached. When the separation has occurred, cohesive forces remain. These forces decrease when the opening increases and tend to vanish (softening behavior). Physically, the cohesive forces represent the weakening of the material in the fracture process zone ahead of the crack tip. Furthermore, real cracks cannot health in general. To take into account this irreversibility, one can introduce a history parameter, such as the maximal opening. For quasi-static fracture, cohesive zone models depending on opening and maximal opening are well established and in good agreement with experiments. In the dynamic case, numerical simulations with such cohesive zone models predict often crack speeds far higher than those observed in the experiments. For instance, for mode I fracture in brittle materials, numerical crack tip speeds are close to the Rayleigh wave speed, while experimental crack tip speeds nearly reach half of this value (see for instance [112, 105]). To remedy this, cohesive zone models depending on the opening rate have been designed [110, 126]. Such models are called rate-dependent.

Since the crack tip speed is high, typically of the same order as the wave speeds, small time steps are needed to capture accurately the fracture phenomenon. Therefore, it seems natural to consider an explicit time-integration scheme. For cohesive zone models in which the interface forces are related to the opening by a classical function, the use of an explicit time-integration scheme is straightforward [125]. However, in most cohesive zone models, the interface forces are not related to the opening by a classical function, but by a set-valued map. Indeed, most cohesive zone models feature perfect initial adhesion, contact or rigid unloading. There are two main difficulties in using fully explicit schemes in such a context. Firstly, the interface forces are not defined for negative normal opening (see Figure 5.1, left). Secondly, the interface forces are

discontinuous with respect to the opening (see Figure 5.1, right), and this can cause oscillations. A first option consists in regularizing the set-valued map to turn it into a single-valued map. Unfortunately, the regularization of a non-interpenetration condition deteriorates substantially the stability condition of explicit schemes. Moreover, replacing a discontinuity by a very stiff slope does not really improve the problem. Alternatively, some *ad hoc* procedures have also been developed to treat the set-valued parts of the interface forces: allowing the separation only after a failure criterion has been reached [21, 101, 46], *a posteriori* enforcement of the non-interpenetration condition [21, 46], tolerance parameter on the tangential opening [46].

In the present work, we focus on dynamic fracture models where the material can only crack along a prescribed surface (fracture interface). In other words, the crack path is known in advance. This assumption may appear as a major limitation. However, fracture models predicting the crack path are not yet robust enough, especially for industrial applications. Moreover, for a large range of applications (interfacial crack, small propagation crack), postulating *a priori* the crack path is reasonable (see [93] for a further discussion). We assume that the bulk behavior is governed by linear elastodynamic equations and that the separation process at the interface fracture obeys a cohesive zone model. We consider an abstract cohesive zone model depending on the opening, the opening rate, and the maximal opening. This abstract model encompasses most of the usual cohesive zone models. Space semi-discretization is achieved using P_1 finite elements. We propose time-integration schemes that combine a central difference scheme with a partially or fully implicit enforcement of the interface forces. The central difference scheme is a standard scheme for elastodynamics [70]. The implicit enforcement of the interface forces provides a general and robust way of treating the set-valued cohesive zone model. In order to keep a moderate computational cost, we use lumping techniques for the mass term and the interface forces. We thus obtain quasi-explicit methods: at each time step, the displacements of the nodes in the interior of the domain are computed in an explicit way, while the displacements of each node at the interface are computed by solving a small nonlinear problem (this can generally be achieved in an analytical way). First, we consider a fully implicit enforcement of the interface forces. However, staggering in time the force at the fracture interface can have a sizeable effect on the energy behavior and the accuracy of the time-integration scheme. Consequently, we propose a second time-integration scheme, in which we split the interface forces into a set-valued monotone part and a single-valued softening part. The former is treated in an implicit way, the latter in an explicit way. This improves the accuracy and the energy behavior. Note that some of the *ad hoc* procedures described above can be interpreted as an implicit enforcement of the set valued part of the cohesive zone model (failure criterion, *a posteriori* enforcement of the contact condition).

We begin by presenting the abstract cohesive zone model and examples which fit into this framework (Section 5.2). We then formulate the continuous problem of dynamic fracture (Section 5.3). Sections 5.4 and 5.5 are devoted to the finite element discretization in space and to the time-integration schemes, respectively. We discuss the implementation of the schemes in Section 5.6. Finally, numerical simulations on 2D examples are presented in Section 5.7.

5.2 Cohesive zone model

We consider an abstract cohesive zone model. The forces at the fracture interface are described by a set-valued map which depends on the opening, the opening rate, and the maximal effective opening (we define below what we call effective opening).

5.2.1 Abstract model

Let $(\cdot,\cdot)$ denote the usual scalar product in $\mathbb{R}^n$ ($n \geq 1$) and let $|\cdot|$ denote the corresponding Euclidean norm. Let $\mathcal{P}(\mathbb{R}^n)$ denote the set of all subsets of $\mathbb{R}^n$. In a d-dimensional problem ($d = 2$ or $d = 3$), the cohesive zone model is characterized by a set-valued map $R : \mathbb{R}^d \times \mathbb{R}^d \times \mathbb{R}^d \to \mathcal{P}(\mathbb{R}^d)$. The arguments of R are the maximal effective opening, the opening rate, and the opening, respectively. For each triplet (δ, z, p), the map $R(\delta, z, p)$ yields a set of vectors, which are the admissible interaction forces. The first component of $\lambda \in R(\delta, z, p)$ is the normal force at the interface and the second and third ones are the tangential forces. For an opening $p \in \mathbb{R}^3$ (resp. $p \in \mathbb{R}^2$), the corresponding effective opening is defined as $\bar{\delta}(p) = (p_1, |p_2|, |p_3|)$ (resp. $\bar{\delta}(p) = (p_1, |p_2|)$).

Since a cohesive zone model describes a softening behavior, the set-valued map R is not monotone with respect to the opening. However, we make the following reasonable assumption on R. This assumption is, in particular, useful to establish the well-posedeness of our first time-integration scheme (see Proposition 5.1).

Assumption 5.1. *The operator R satisfies the following one-sided Lipschitz condition : there is a real number c_s such that, for all $\delta \in \mathbb{R}^d$, for all $z \in \mathbb{R}^d$, for all p_1, $p_2 \in \mathbb{R}^d$,*

$$(\lambda_1 - \lambda_2, p_1 - p_2) \geq -c_s |p_1 - p_2|^2, \qquad \forall \lambda_1 \in R(\delta, z, p_1),\ \forall \lambda_2 \in R(\delta, z, p_2). \tag{5.1}$$

This condition means that the slope of the softening part is bounded. Furthermore, in most models, the operator $R(\delta, z, \cdot)$ is built as the differential (in a generalized sense) of an energy. This operator being non-monotone, the associated cohesive energy is non-convex.

The present abstract model encompasses for instance the Camacho-Ortiz law [21] and the Talon-Curnier law [117], but not the rectangular law (because of the infinite slope of the softening part).

5.2.2 Examples

This section collects some examples of cohesive zone models fitting the above framework. The first two examples can be viewed as simplified variants of the Camacho-Ortiz law [21].

A reversible triangular model with uncoupled normal and tangential forces

This model depends on the opening and prescribes uncoupled normal and tangential interface forces. It relies on two parameters: σ_c, the maximal cohesive force, and d_c, the critical

opening. It can be represented by a set-valued map $R : \mathbb{R}^d \to \mathcal{P}(\mathbb{R}^d)$ whose components are independent. The normal component $R_1 : \mathbb{R} \to \mathcal{P}(\mathbb{R})$ is such that

$$R_1(p) := \begin{cases} (-\infty, \sigma_c] & \text{if } p = 0, \\ \sigma_c \left(1 - \frac{p}{d_c}\right) & \text{if } 0 < p \leq d_c, \\ 0 & \text{if } d_c < p, \\ \emptyset & \text{if } p < 0. \end{cases}$$

For simplicity, in the definition of cohesive zone models, a singleton $\{x\}$ is simply denoted by x. The tangential components $R_2 : \mathbb{R} \to \mathcal{P}(\mathbb{R})$ and $R_3 : \mathbb{R} \to \mathcal{P}(\mathbb{R})$ are such that

$$R_2(p) = R_3(p) := \begin{cases} 0 & \text{if } p < -d_c, \\ -\sigma_c \left(1 + \frac{p}{d_c}\right) & \text{if } -d_c \leq p < 0, \\ [-\sigma_c, \sigma_c] & \text{if } p = 0, \\ \sigma_c \left(1 - \frac{p}{d_c}\right) & \text{if } 0 < p \leq d_c, \\ 0 & \text{if } d_c < p. \end{cases}$$

This model is represented in Figure 5.1. It is easy to check that this model satisfies Assumption 1 with $c_s = \sigma_c/d_c$. Moreover, energies $\Psi_1 : \mathbb{R}^+ \to \mathbb{R}$, $\Psi_2 : \mathbb{R} \to \mathbb{R}$, and $\Psi_3 : \mathbb{R} \to \mathbb{R}$ can be associated with this model, namely

$$\Psi_1(p) := \begin{cases} \sigma_c p \left(1 - \frac{p}{2d_c}\right) & \text{if } 0 \leq p \leq d_c, \\ \frac{1}{2}\sigma_c d_c & \text{if } d_c < p, \end{cases}$$

and

$$\Psi_2(p) = \Psi_3(p) := \begin{cases} \frac{1}{2}\sigma_c d_c & \text{if } p < -d_c, \\ -\sigma_c p \left(1 + \frac{p}{2d_c}\right) & \text{if } -d_c \leq p < 0, \\ \sigma_c p \left(1 - \frac{p}{2d_c}\right) & \text{if } 0 \leq p \leq d_c, \\ \frac{1}{2}\sigma_c d_c & \text{if } d_c < p. \end{cases}$$

An irreversible triangular model with only normal force

This model depends on the normal opening p and maximal normal opening δ and prescribes only the normal force. Moreover, it is irreversible with a linear unloading. As the previous model, it involves two parameters: σ_c, the maximal cohesive force, and d_c, the critical opening. It can be represented by the set-valued map $R_1^{irr} : \mathbb{R} \times \mathbb{R} \to \mathcal{P}(\mathbb{R})$ such that

$$R_1^{irr}(\delta, p) := \begin{cases} (-\infty, \sigma_c] & \text{if } \delta = p = 0 \\ (-\infty, 0] & \text{if } 0 = p < \delta \\ \sigma_c \left(1 - \frac{\delta}{d_c}\right) \frac{p}{\delta} & \text{if } 0 < p \leq \delta \leq d_c \\ \sigma_c \left(1 - \frac{p}{d_c}\right) & \text{if } 0 < \delta < p \leq d_c \\ 0 & \text{if } d_c < p,\ 0 \leq \delta \\ 0 & \text{if } d_c < \delta, 0 \leq p \\ \emptyset & \text{otherwise} \end{cases}$$

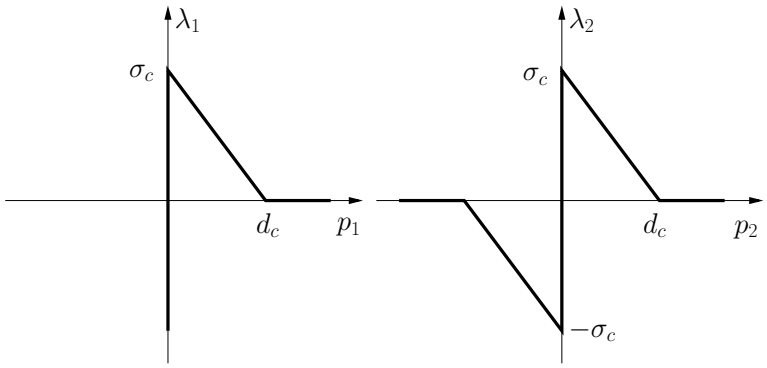

Fig. 5.1. Triangular model with uncoupled normal and tangential forces. Normal force (left). Tangential force (right).

This model is represented in Figure 5.2, left. It satisfies Assumption 1 with $c_s = \sigma_c/d_c$. A common variant of this model consists in replacing the linear unloading with a rigid unloading (Figure 5.2, right). An energy $\Psi_1^{irr} : \mathbb{R}^+ \times \mathbb{R}^+ \to \mathbb{R}$ and a dissipated energy $\tilde{\Psi}_1^{irr} : \mathbb{R}^+ \to \mathbb{R}$ can be associated with the irreversible model with linear unloading. One define them as follows :

$$\Psi_1^{irr}(\delta, p) := \begin{cases} \sigma_c \left(-\frac{\delta}{2} + p - \frac{p^2}{2d_c} \right) & \text{if } 0 < \delta < p \leq d_c \\ \sigma_c \left(1 - \frac{\delta}{d_c} \right) \frac{p^2}{2\delta} & \text{if } 0 < p \leq \delta \leq d_c \\ \frac{1}{2}\sigma_c d_c & \text{if } d_c < p,\ \delta = 0 \\ 0 & \text{if } d_c < \delta, 0 \leq p \end{cases},$$

$$\tilde{\Psi}_1^{irr}(\delta) := \begin{cases} \frac{1}{2}\sigma_c \delta & \text{if } 0 \leq \delta \leq d_c \\ \frac{1}{2}\sigma_c d_c & \text{if } d_c < \delta \end{cases}.$$

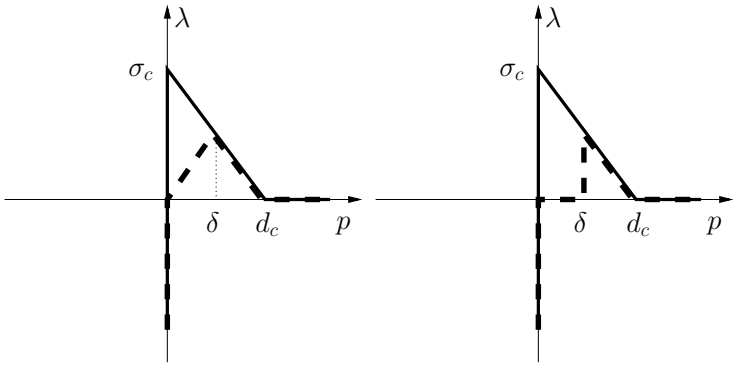

Fig. 5.2. An irreversible triangular model with only normal force. Linear unloading (left). Rigid unloading (right).

A rate-dependent triangular model with only normal force [126]

This model depends on the normal opening p and the normal opening rate z, and prescribes only the normal interface force. It relies on three parameters: σ_c, the maximal cohesive force, d_c,

the critical opening, and η, a viscosity parameter. It can be represented by the set-valued map $R_1^{visc} : \mathbb{R} \times \mathbb{R} \to \mathcal{P}(\mathbb{R}^d)$ such that

$$R_1^{visc}(z,p) := \begin{cases} (-\infty, \sigma_c] & \text{if } p = 0 \\ \sigma_c \left(1 - \frac{p}{d_c(1+\eta z^+)}\right) & \text{if } 0 < p < d_c(1+\eta z^+) \\ 0 & \text{if } d_c(1+\eta z^+) \leq p \\ \emptyset & \text{otherwise} \end{cases},$$

where z^+ denotes the positive part of z. This model is represented in Figure 5.3. It satisfies Assumption 1 with $c_s = \sigma_c/d_c$.

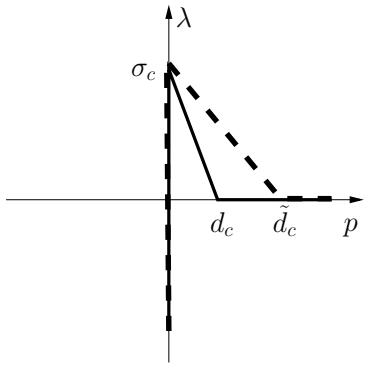

Fig. 5.3. A rate-dependent triangular model with only normal force ($\tilde{d}_c := d_c(1+\eta z^+)$).

5.2.3 Link with Griffith's model

It is possible to make a link between cohesive zone models and Griffith's models. When cohesive forces act over a sufficiently short range, the stress fields near the crack tip are equivalent in both models. Furthermore, the material parameter used in Griffith's model, the fracture toughness G_c, is equal to the energy needed to completely open the crack in the cohesive zone model. A formal argument for this asymptotic analysis can be found in [123] and a rigorous proof for a simple model in [95]. The fracture toughness corresponding to the rate-independent triangular models (presented above) is

$$G_c = \frac{1}{2}\sigma_c d_c.$$

In the rate-dependent triangular model, the fracture toughness increases with the opening rate.

5.3 Continuous problem

We now formulate the governing equations of the dynamic fracture problem.

5.3.1 Geometry

We consider a domain $\Omega \subset \mathbb{R}^d$ ($d = 2$ or $d = 3$) and we assume that the crack can only appear on a $(d-1)$-dimensional smooth surface Γ (see Figure 5.4). We call Γ the fracture interface. We set $\tilde{\Omega} := \Omega \setminus \overline{\Gamma}$. We can fix an orientation and define two sides for Γ, a positive side and a negative side. The trace of u on the positive side is denoted by u^+, the trace on the negative side is denoted by u^-. We denote by ν the unit normal vector to Γ pointing to the positive side. We define two tangential unit vectors τ_1 and τ_2, so that (ν, τ_1, τ_2) forms a local direct orthonormal basis. The displacement jump at the interface is defined as

$$[\![u]\!] = u^+ - u^-. \tag{5.2}$$

To define the interface forces, we take into account the local orientation of the interface by introducing the rotation matrix Q transforming the canonical basis of $\mathbb{R}^d$ into (ν, τ_1, τ_2).

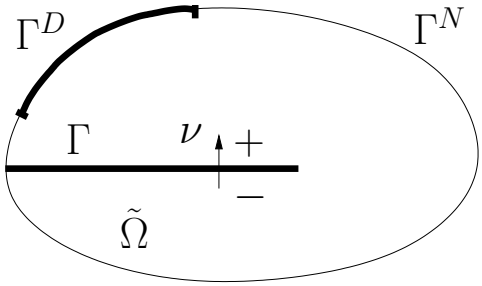

Fig. 5.4. Geometric setup.

5.3.2 Governing equations

The material is supposed to be linear isotropic elastic with Young modulus E, Poisson ratio ν_P, and mass density ρ. The elasticity tensor is denoted by $\mathcal{A}$. An external load f is applied to the body. Let $u : \Omega \times (0,T) \to \mathbb{R}^d$, $\epsilon(u) : \Omega \times (0,T) \to \mathbb{R}^{d,d}$, and $\sigma(u) : \Omega \times (0,T) \to \mathbb{R}^{d,d}$ be the displacement field, the linearized strain tensor, and the stress tensor, respectively. Denoting time-derivatives by dots, the momentum conservation equation reads

$$\rho\ddot{u} - \operatorname{div}\sigma = f, \qquad \sigma = \mathcal{A} : \epsilon, \qquad \epsilon = \frac{1}{2}(\nabla u +^{\mathrm{T}} \nabla u) \quad \text{in } \tilde{\Omega} \times (0,T). \tag{5.3}$$

The boundary $\partial\Omega$ of Ω is partitioned into two disjoint subsets Γ^D and Γ^N. Dirichlet and Neumann conditions are prescribed on Γ^D and Γ^N, respectively,

$$u = u_D \quad \text{on } \Gamma^D \times (0,T), \qquad \sigma \cdot \nu = f_N \quad \text{on } \Gamma^N \times (0,T). \tag{5.4}$$

On Γ, the cohesive law is enforced

$$\sigma(u^-) \cdot \nu = -\sigma(u^+) \cdot \nu =: \lambda, \qquad \lambda \in^{\mathrm{T}} QR(\delta, Q[\![\dot{u}]\!], Q[\![u]\!]). \tag{5.5}$$

The maximal effective opening δ is defined, for $t > 0$, as

$$\delta(t) = \sup_{s\in[0,t)} \bar{\delta}(Q[\![u(s)]\!]). \tag{5.6}$$

At the initial time, the displacement, the velocity, and the maximal effective opening are prescribed:

$$u(0) = u^0, \quad \dot{u}(0) = \mathrm{v}^0, \quad \delta(0) = \delta^0. \tag{5.7}$$

Equations (5.3)-(5.5) can be written in a variational form : seek u such that for all test function v,

$$\int_{\tilde{\Omega}} \rho\ddot{u}\cdot v + \int_{\tilde{\Omega}} \epsilon(u) : \mathcal{A} : \epsilon(v) = \int_{\tilde{\Omega}} f(t)\cdot v + \int_{\Gamma^N} f_N(t)\cdot v - \int_{\Gamma} \lambda\cdot[\![v]\!], \tag{5.8}$$

where $\lambda \in^{\mathrm{T}} QR(\delta, Q[\![\dot{u}]\!], Q[\![u]\!])$.

5.3.3 Mathematical aspects

The mathematical analysis of Problem (5.3)-(5.7) is beyond the scope of the present work. However, let us mention some related results.

- In the quasi-static case with a reversible cohesive zone model (with perfect adhesion or not), the existence is proven. The solution is in general not unique [37].
- In the quasi-static case with an irreversible cohesive zone model, the existence of a solution is proven in [30, 20].
- In the dynamic case, it should be possible to prove, using compactness arguments, existence for a visco-elastic material and a reversible cohesive law with perfect adhesion, and even to prove existence and uniqueness for an elastic material and a regularized cohesive law.

5.3.4 Length and time scales

In order to capture accurately a phenomenon with numerical simulations, it is important to choose a time step and a mesh size which resolve its time and length scales. In a dynamic fracture problem, the relevant length scale is the length of the cohesive zone (part of the interface which is not completely cracked and where cohesive forces act). The relevant time scale is the crack tip speed divided by the cohesive zone length. For an isotropic linear elastic material and a triangular cohesive zone model, in the quasi-static setting, the estimated cohesive zone length is [108]

$$l_{coh} = \frac{9\pi}{32}\frac{E}{1-\nu_P^2}\frac{G_c}{\sigma_c^2}. \tag{5.9}$$

For an isotropic linear elastic material and a Griffith model of fracture, a theoretical analysis predicts that the limiting crack tip speed for a mode I fracture is the Rayleigh wave speed [51, 17]. For mode II and mode III fractures, the limiting speeds are the dilatational wave speed and the shear wave speed, respectively [51, 17]. The dilatational and shear wave speeds are given by the following formulae:

$$c_d = \sqrt{\frac{E(1-\nu_P)}{\rho(1+\nu_P)(1-2\nu_P)}}, \qquad c_s = \sqrt{\frac{E}{2\rho(1+\nu_P)}}. \tag{5.10}$$

The Rayleigh wave speed can be estimated by the following expression [51]

$$c_R \approx c_s \frac{0.862 + 1.14\nu_P}{1+\nu_P}. \tag{5.11}$$

5.4 Finite element discretization

In this section, we describe the space approximation of the dynamic fracture problem. Linear finite elements are used together with lumping of the mass term and the interface forces.

5.4.1 Finite element spaces

In 2D (resp. in 3D), we approximate the domain Ω by a polygon (resp. a polyhedron) Ω_h and the interface Γ by a polygonal curve (resp. a polygon) Γ_h. We mesh Ω_h with triangles (resp. tetrahedra) conforming to the interface Γ_h. Let $\mathcal{T}_h$ denote the mesh over Ω_h and let $\mathcal{F}_h$ collect the faces located on Γ_h. Let $\tilde{\Omega}_h = \Omega_h \setminus \overline{\Gamma_h}$. Let $\{x_i\}_{i\in\mathcal{N}}$ be the nodes of the mesh $\mathcal{T}_h$. We denote by $\mathcal{N}^D$ the indices of nodes where a Dirichlet condition is enforced and by $\mathcal{N}^c$ the indices of nodes lying on Γ_h. We approximate the displacements with P_1 finite elements:

$$\mathcal{V}_h = \{v_h \in C^0(\tilde{\Omega}_h)^d \cap L^\infty(\Omega_h)^d;\ v_{h|T} \in (\mathbb{P}_1)^d,\ \forall T \in \mathcal{T}_h,\ \text{and } v_h(x_i) = 0,\ \forall i \in \mathcal{N}^D\}.$$

Note that functions in $\mathcal{V}_h$ can be discontinuous across Γ_h. We consider the Lagrange nodes of $\mathcal{V}_h$ and denote them by $\{\xi_i\}_{i\in\mathcal{N}^L}$. The Lagrange nodes are not exactly the mesh nodes $\{x_i\}_{i\in\mathcal{N}}$ because of the discontinuity at the interface. Specifically, for each mesh node x_i lying on Γ_h, there are two Lagrange nodes ξ_{i^+} and ξ_{i^-}. For all $i \in \mathcal{N}^c$, for all $v_h \in \mathcal{V}_h$, we set

$$v_h(\xi_{i^+}) := v_h^+(x_i), \qquad v_h(\xi_{i^-}) := v_h^-(x_i). \tag{5.12}$$

The cohesive forces are also approximated by P_1 finite elements,

$$\mathcal{L}_h = \{\lambda_h \in C^0(\overline{\Gamma_h})^d;\ \lambda_{h|F} \in (\mathbb{P}_1)^d,\ \forall F \in \mathcal{F}_h\}.$$

At each node x_i lying on $\overline{\Gamma_h}$, we define normal and tangential unit vectors $(\nu_i, \tau_{1i}, \tau_{2i})$ forming a local direct orthonormal basis. Let Q_i be the associated rotation matrix. We define also the set-valued operator R_i:

$$R_i(\cdot,\cdot,\cdot) = {}^{\mathrm{T}}Q_i R(\cdot, Q_i\cdot, Q_i\cdot). \tag{5.13}$$

5.4.2 Lumping of the mass term and the cohesive term

We lump the mass term and the cohesive forces term. Mass lumping is usual with explicit time-integration schemes. It yields an easy-to-invert mass matrix at each time step, while improving the CFL condition [70]. A way of lumping the mass term is to evaluate it with an

approximate quadrature whose Gauss points are the nodes of the finite element space. Of course, this quadrature must be of sufficiently high order to avoid deteriorating the global accuracy of the method. For P_1 finite elements, it is usual to use the following quadrature formula (in dimension d)

$$\int_T f \approx \sum_{i=1}^{d+1} \frac{|T|}{d+1} f(\alpha_i), \tag{5.14}$$

where $|T|$ is the measure of the simplex T and $\{\alpha_i\}_{1\le i\le d+1}$ its vertices. This quadrature is second-order accurate. The lumped mass term $\hat{m}_h : \mathcal{V}_h \times \mathcal{V}_h \to \mathbb{R}$ is built with this quadrature by setting

$$\hat{m}_h(v_h, w_h) = \sum_{i\in\mathcal{N}^L} \mu_i v_h(\xi_i) \cdot w_h(\xi_i), \tag{5.15}$$

where

$$\mu_i = \sum_{T\in\mathcal{T}_i} \rho|T|/(d+1), \tag{5.16}$$

$\mathcal{T}_i$ being the set of elements for which ξ_i is a vertex. The lumped cohesive term $\hat{b}_h : \mathcal{L}_h \times \mathcal{V}_h \to \mathbb{R}$ is such that

$$\hat{b}_h(\lambda_h, w_h) = \sum_{i\in\mathcal{N}^c} \beta_i \lambda_h(x_i) \cdot \left(v_h^-(x_i) - v_h^+(x_i)\right), \tag{5.17}$$

where

$$\beta_i = \sum_{F\in\mathcal{F}_i} |F|/d, \tag{5.18}$$

$\mathcal{F}_i$ being the set of faces for which x_i is a vertex. Finally, the stiffness term $a_h : \mathcal{V}_h \times \mathcal{V}_h \to \mathbb{R}$ and the external force term $l_h : [0,T] \times \mathcal{V}_h \to \mathbb{R}$ are built in a standard way, namely

$$a_h(v_h, w_h) := \int_{\tilde{\Omega}_h} \epsilon(v_h) : \mathcal{A} : \epsilon(w_h), \tag{5.19}$$

$$l_h(t, v_h) := \int_{\tilde{\Omega}_h} f(t) \cdot v_h + \int_{\Gamma^N} f_N(t) \cdot v_h, \tag{5.20}$$

up to quadratures. We define the matrices $\hat{M}_h$, K_h, and $\hat{B}_h$ associated with the bilinear forms $\hat{m}_h$, a_h, and $\hat{b}_h$, respectively. We also define $L_h(t)$ to be the column vector associated with the linear form $l_h(t,\cdot)$. For $u_h \in \mathcal{V}_h$, we define U_h as the column vector whose components are the coordinates of u_h in the finite element basis. We denote by N_V the size of U_h. We denote by $U_{h,i}$ the d-dimensional sub-vector associated with the Lagrange node ξ_i. Similarly, for $\lambda_h \in \mathcal{L}_h$, we define Λ_h as the column vector whose components are the coordinates of λ_h in the finite element basis. We denote by N_Λ the size of Λ_h. We denote by $\Lambda_{h,i}$ the d-dimensional sub-vector associated with the node x_i. Finally, we define for all $i \in \mathcal{N}^c$,

$$[\![U_h]\!]_i = U_{h,i^+} - U_{h,i^-} \quad \text{and} \quad \{U_h\}_i = \frac{U_{h,i^+} + U_{h,i^-}}{2}. \tag{5.21}$$

For each $i \in \mathcal{N}^L$, we denote respectively by $\hat{M}_{h,i}$ and $K_{h,i}$ the $d \times d$ sub-matrices of $\hat{M}_h$ and K_h associated with the Lagrange node ξ_i. For each $i \in \mathcal{N}^c$, we denote by $\hat{B}_{h,i}$ the $d \times d$ sub-matrix of $\hat{B}_h$ associated with the node x_i. We define the set-valued operator $R_h : \mathbb{R}^{N_\Lambda} \times \mathbb{R}^{N_\Lambda} \times \mathbb{R}^{N_\Lambda} \to \mathcal{P}(\mathbb{R}^{N_\Lambda})$ such that for all $\Delta_h \in \mathbb{R}^{N_\Lambda}$, $Z_h \in \mathbb{R}^{N_\Lambda}$, $P_h \in \mathbb{R}^{N_\Lambda}$,

$$\Lambda_h \in R_h(\Delta_h, Z_h, P_h) \Longleftrightarrow \Lambda_{h,i} \in R_i(\Delta_{h,i}, Z_{h,i}, P_{h,i}) \ \forall i \in \mathcal{N}^c. \tag{5.22}$$

The space semi-discrete problem takes the form

$$\hat{M}_h \ddot{U}_h(t) + K_h U_h(t) = L_h(t) + \hat{B}_h \Lambda_h(t), \tag{5.23}$$

$$\Lambda_h(t) \in R_h(\Delta_h(t), [\![\dot{U}_h(t)]\!], [\![U_h(t)]\!]), \tag{5.24}$$

$$\Delta_{h,i}(t) = \sup_{s\in[0,t)} \bar{\delta}(Q_i [\![U_h(s)]\!]_i), \qquad \forall i \in \mathcal{N}^c. \tag{5.25}$$

Remark 5.1. *In the present work, we consider P_1 finite elements. Other types of finite elements can be used, provided an accurate lumping technique is available. For instance, this is the case for Q_1 elements (see [70]). For P_k and Q_k elements with $k \geq 2$, the lumping techniques are more subtle (see for instance [28] and references therein).*

5.5 Time-integration schemes

It remains now to discretize the problem in time. The time-integration schemes we propose are based on the central difference scheme. To begin with, we recall the main properties of this scheme in the linear elastodynamic case. We then describe and analyze two schemes for the dynamic fracture problem.

5.5.1 Central differences

For simplicity, the interval $[0, T]$ is divided into equal subintervals of length Δt. We set $t^n = n\Delta t$ and denote by U_h^n the approximation of U_h at time t^n. For the central difference scheme, the discrete velocity and the discrete acceleration are defined respectively as

$$\dot{U}_h^n := \frac{U_h^{n+1} - U_h^{n-1}}{2\Delta t} \quad \text{and} \quad \ddot{U}_h^n := \frac{U_h^{n+1} - 2U_h^n + U_h^{n-1}}{\Delta t^2}. \tag{5.26}$$

At each time step of the central difference scheme, one seeks U_h^{n+1} such that

$$\frac{1}{\Delta t^2} \hat{M}_h (U_h^{n+1} - 2U_h^n + U_h^{n-1}) + K_h U_h^n = L_h(t^n). \tag{5.27}$$

The central difference scheme exhibits a stability condition (CFL condition) of the form

$$c_d \Delta t \leq O(h_{min}), \tag{5.28}$$

where h_{min} is the size of the smallest mesh element. An admissible value of the constant in the CFL condition can be specified in 1D and for structured meshes in higher dimension. We define the elastic energy, the kinetic energy, and the total energy of the discrete system at time t^n respectively as

$$E_{el}^n := \frac{1}{2} \left(K_h U_h^n, U_h^n\right), \qquad E_{kin}^n := \frac{1}{2} \left(\hat{M}_h \dot{U}_h^n, \dot{U}_h^n\right), \qquad E^n := E_{el}^n + E_{kin}^n. \tag{5.29}$$

In linear elastodynamics, the central difference scheme does not preserve the energy. Nevertheless, the scheme preserves the following quadratic form, referred to as a shifted energy,

$$\mathcal{E}^n := E^n - \frac{\Delta t^2}{8}\left(\hat{M}_h\ddot{U}_h^n, \ddot{U}_h^n\right). \tag{5.30}$$

In particular, the following shifted energy balance holds true :

$$\mathcal{E}^{n+1} - \mathcal{E}^n = \frac{1}{2}(L_h(t^{n+1}) + L_h(t^n), U_h^{n+1} - U_h^n). \tag{5.31}$$

5.5.2 Scheme A (fully implicit interface forces)

We combine a central difference scheme with an implicit enforcement of the interface forces. More precisely, the interface forces are implicit in the opening, while they are explicit in the opening rate and in the maximal effective opening.

Scheme A. *Seek $U_h^{n+1} \in \mathbb{R}^{N_V}$ and $\Lambda_h^{n+1} \in \mathbb{R}^{N_\Lambda}$ such that*

$$\frac{1}{\Delta t^2}\hat{M}_h(U_h^{n+1} - 2U_h^n + U_h^{n-1}) + K_h U_h^n = L_h(t^n) + \hat{B}_h\Lambda_h^{n+1}, \tag{5.32}$$

$$\Lambda_h^{n+1} \in R_h(\Delta_h^n, Z_h^n, [\![U_h^{n+1}]\!]), \tag{5.33}$$

where, for all $i \in \mathcal{N}^c$,

$$Z_{h,i}^n = \frac{[\![U_h^n]\!]_i - [\![U_h^{n-1}]\!]_i}{\Delta t}, \qquad \Delta_{h,i}^n = \max(\Delta_{h,i}^{n-1}, \bar{\delta}(Q_i[\![U_h^n]\!]_i)). \tag{5.34}$$

A way of implementing this scheme will be described in Section 5.6.1. We now prove that, at each time step, the problem is well-posed under a mild restriction on the time step.

Proposition 5.1 (Well-posedness). *Problem (5.32)-(5.34) has a unique solution under the conditions*

$$\frac{\mu_{i^+}}{\Delta t^2} > 2c_s\beta_i \quad \text{and} \quad \frac{\mu_{i^-}}{\Delta t^2} > 2c_s\beta_i, \qquad \forall i \in \mathcal{N}^c, \tag{5.35}$$

where the coefficients μ_i and β_i are defined by (5.16) and (5.18). For a quasi-uniform mesh, the above condition can be rewritten as

$$\frac{\Delta t^2}{h_c} < C, \tag{5.36}$$

where h_c is the mesh size at the interface and C a constant independent of the mesh size.

Proof. The relations (5.32)-(5.33) can be recast as an inclusion : seek $U_h^{n+1} \in \mathbb{R}^{N_V}$ such that

$$\frac{1}{\Delta t^2}\hat{M}_h U_h^{n+1} - \hat{B}_h R_h^n(U_h^{n+1}) \ni F_h^n \tag{5.37}$$

where $F_h^n := (1/\Delta t^2)\hat{M}_h(2U_h^n - U_h^{n-1}) - K_h U_h^n + L_h(t^n)$ and $R_h^n(U_h^{n+1}) := R_h(\Delta_h^n, Z_h^n, [\![U_h^{n+1}]\!])$. We are now going to prove that the set-valued operator involved in this inclusion is strongly

monotone for Δt small enough. Let $U_h \in \mathbb{R}^{N_V}$ and let $V_h \in \mathbb{R}^{N_V}$. Let $\Lambda_h \in R_h^n(U_h)$ and $\Theta_h \in R_h^n(V_h)$. We observe that

$$-(\hat{B}_h\Lambda_h - \hat{B}_h\Theta_h, U_h - V_h) = \sum_{i\in\mathcal{N}^c} \beta_i(B_{h,i}\Lambda_{h,i} - B_{h,i}\Theta_{h,i}, [\![U_h]\!]_i - [\![V_h]\!]_i).$$

Using the one-sided Lipschitz condition (5.1) and the properties of the rotation matrices Q_i,

$$\begin{aligned} -(\hat{B}_h\Lambda_h - \hat{B}_h\Theta_h, U_h - V_h) &\geq -\sum_{i\in\mathcal{N}^c} \beta_i c_s |[\![U_h]\!]_i - [\![V_h]\!]_i|^2, \\ &\geq -\sum_{i\in\mathcal{N}^c} 2\beta_i c_s (|U_{h,i^+} - V_{h,i^+}|^2 + |U_{h,i^-} - V_{h,i^-}|^2). \end{aligned} \tag{5.38}$$

By definition of the mass matrix,

$$(\hat{M}_h U_h - \hat{M}_h V_h, U_h - V_h) \geq \sum_{i\in\mathcal{N}^L} \mu_i |U_{h,i} - V_{h,i}|^2. \tag{5.39}$$

Collecting inequalities (5.38) and (5.39) yields

$$\begin{aligned} \frac{1}{\Delta t^2}(\hat{M}_h U_h - \hat{M}_h V_h, U_h - V_h) - (\hat{B}_h\Lambda_h - \hat{B}_h\Theta_h, U_h - V_h) \geq \\ \sum_{i\in\mathcal{N}^L} \frac{\mu_i}{\Delta t^2} |U_{h,i} - V_{h,i}|^2 - \sum_{i\in\mathcal{N}^c} 2\beta_i c_s (|U_{h,i^+} - V_{hi^+}|^2 + |U_{h,i^-} - V_{h,i^-}|^2). \end{aligned} \tag{5.40}$$

Therefore, a sufficient condition for the set-valued operator to be strongly monotone is given by (5.35). For a quasi-uniform mesh, we can rewrite the condition as (5.36).

It is straightforward to derive the energy balance for Scheme A.

Proposition 5.2 (Energy balance).

$$\mathcal{E}^{n+1} - \mathcal{E}^n = \frac{1}{2}\left(\hat{B}_h\Lambda_h^{n+2} + \hat{B}_h\Lambda_h^{n+1}, U_h^{n+1} - U_h^n\right) + \frac{1}{2}\left(L_h(t^{n+1}) + L_h(t^n), U_h^{n+1} - U_h^n\right). \tag{5.41}$$

With this scheme, the work of the interface forces can be positive or negative. As a consequence, we cannot prove the same CFL condition as in the linear elastodynamic case, although we do observe numerically the same CFL condition (see Section 5.7.1). Perhaps, more importantly, it tourns out (see again Section 5.7.1) that decentering in time the interface forces can have an unfavorable impact on the energy behavior and the accuracy of the time-integration scheme. To remedy this, we propose another time-integration scheme in the next section.

5.5.3 Scheme B (implicit set-valued part)

The key idea is to split the interface forces into a set-valued monotone part and a single-valued softening part. The former is treated in an implicit way, the latter in an explicit way.

Assumption 5.2. *There exist* $P : \mathbb{R}^d \times \mathbb{R}^d \times \mathbb{R}^d \to \mathcal{P}(\mathbb{R}^d)$ *and* $\chi : \mathbb{R}^d \times \mathbb{R}^d \times \mathbb{R}^d \to \mathbb{R}^d$ *such that*

$$R = P + \chi. \tag{5.42}$$

Moreover, the operator P *is monotone with respect to the opening: for all* $\delta \in \mathbb{R}^d$, $z \in \mathbb{R}^d$, $p_1 \in \mathbb{R}^d$, $p_2 \in \mathbb{R}^d$,

$$(\lambda_1 - \lambda_2, p_1 - p_2) \geq 0, \quad \forall \lambda_1 \in P(\delta, z, p_1),\ \forall \lambda_2 \in P(\delta, z, p_2), \tag{5.43}$$

and the function χ *is Lipschitz continuous with respect to the opening : there exists* $c_s \in \mathbb{R}^+$ *such that for all* $\delta \in \mathbb{R}^d$, $z \in \mathbb{R}^d$, $p_1 \in \mathbb{R}^d$, $p_2 \in \mathbb{R}^d$,

$$|\chi(\delta, z, p_1) - \chi(\delta, z, p_2)| \leq c_s |p_1 - p_2|. \tag{5.44}$$

Of course, the decomposition (5.42) of R is not unique. In Figures 5.5, 5.7, and 5.6, we present examples of the decomposition (5.42) for the cohesive zone models presented in Section 5.2.2. Similarly to (5.13), we define the set-valued operator P_i and the single-valued function χ_i as

$$P_i(\cdot,\cdot,\cdot) = {}^{\mathrm{T}} Q_i P(\cdot, Q_i\cdot, Q_i\cdot), \qquad \chi_i(\cdot,\cdot,\cdot) = {}^{\mathrm{T}} Q_i \chi(\cdot, Q_i\cdot, Q_i\cdot). \tag{5.45}$$

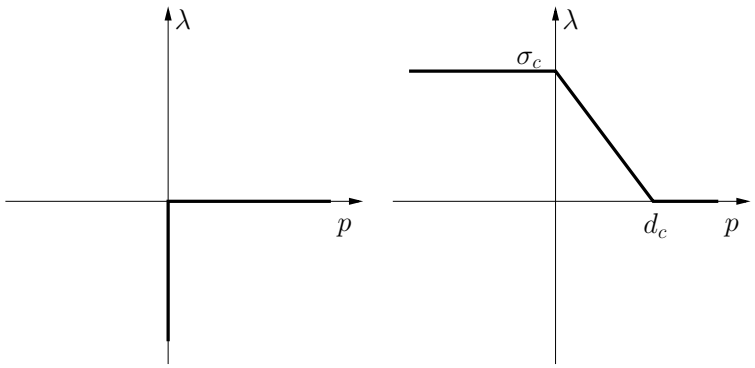

Fig. 5.5. A decomposition of R_1. P_1 (left) and χ_1 (right).

Scheme B. *Seek* $U_h^{n+1} \in \mathbb{R}^{N_V}$ *and* $\Lambda_h^{n+1} \in \mathbb{R}^{N_\Lambda}$ *such that*

$$\frac{1}{\Delta t^2} \hat{M}_h (U_h^{n+1} - 2U_h^n + U_h^{n-1}) + K_h U_h^n = L_h(t^n) + \hat{B}_h \Lambda_h^{n+1} + \hat{B}_h \Theta_h^n, \tag{5.46}$$

$$\Lambda_h^{n+1} \in P_h(\Delta_h^n, Z_h^n, [\![U_h^{n+1}]\!]). \tag{5.47}$$

where, for all $i \in \mathcal{N}^c$,

$$\Theta_{h,i}^n = \chi_i(\Delta_{h,i}^n, Z_{h,i}^n, [\![U_h^n]\!]_i), \forall i \in \mathcal{N}^c, \tag{5.48}$$

while Z_h^n *and* Δ_h^n *are defined by (5.34).*

Proposition 5.3 (Well-posedness). *Problem (5.46)-(5.48) has a unique solution.*

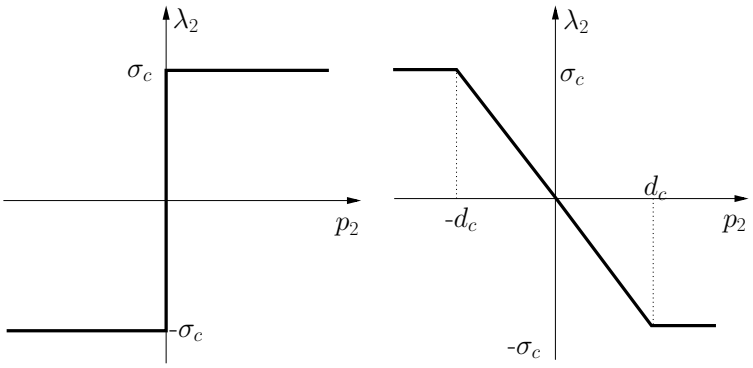

Fig. 5.6. A decomposition of R_2. P_2 (left) and χ_2 (right).

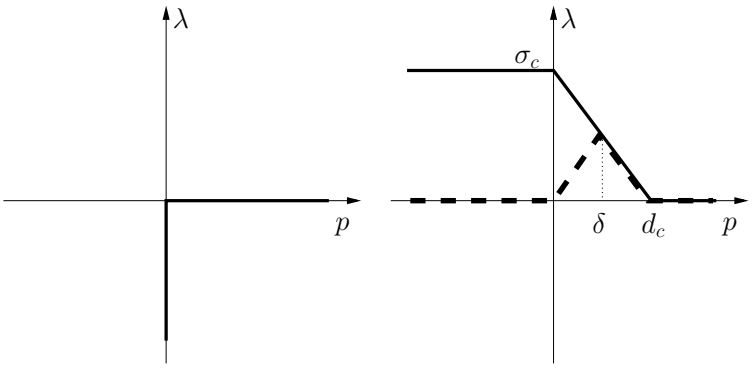

Fig. 5.7. A decomposition of R_1^{irr}. P_1^{irr} (left) and χ_1^{irr} (right).

Proof. As in the proof of Proposition 5.3, we recast the problem as a differential inclusion with a strongly monotone operator. Since the operator P is monotone, contrary to the operator R, there is no condition on the time step to prove the strong monotonicity.

It is straightforward to derive the energy balance for Scheme B.

Proposition 5.4 (Energy balance).

$$\begin{aligned}\mathcal{E}^{n+1} - \mathcal{E}^n =& \frac{1}{2}\left(\hat{B}_h \Lambda_h^{n+2} + \hat{B}_h \Lambda_h^{n+1}, U_h^{n+1} - U_h^n\right) \\ &+ \frac{1}{2}\left(\hat{B}_h \Theta_h^{n+1} + \hat{B}_h \Theta_h^n, U_h^{n+1} - U_h^n\right) + \frac{1}{2}\left(L_h(t^{n+1}) + L_h(t^n), U_h^{n+1} - U_h^n\right).\end{aligned} \tag{5.49}$$

5.6 Numerical implementation

This section briefly describes the main steps to implement Schemes A and B.

5.6.1 Scheme A

Step 1 : Computation of the interior components of U_h^{n+1} (explicit step).
Owing to the lumping of the mass matrix, the components of U_h^{n+1} corresponding to the interior nodes and the components corresponding to the interface nodes can be computed independently. We begin by seeking U_h^{n+1} such that

$$\frac{1}{\Delta t^2}\hat{M}_h(U_h^{n+1} - 2U_h^n + U_h^{n-1}) + KU_h^n = L_h(t^n). \tag{5.50}$$

This is the standard step in the central difference scheme. Since the mass matrix is lumped, it only requires a matrix-vector multiplication and vector additions. After this step, the interface components of U_h^{n+1} are not correct, they will be corrected in the next step. Note that this step uses the standard data structures.

Step 2 : Computation of the interface components of U_h^{n+1} (implicit step).
Owing to the lumping of the cohesive forces, the computation of the interface displacements can performed independantly at each node. For each $i \in \mathcal{N}^c$, we seek U_{h,i^+}^{n+1} and U_{h,i^-}^{n+1} such that

$$\frac{1}{\Delta t^2}M_{h,i^+}U_{h,i^+}^{n+1} + F_{h,i^+}^n = \hat{B}_{h,i}\Lambda_{h,i}^{n+1}, \tag{5.51}$$

$$\frac{1}{\Delta t^2}M_{h,i^-}U_{h,i^-}^{n+1} + F_{h,i^+}^n = -\hat{B}_{h,i}\Lambda_{h,i}^{n+1}, \tag{5.52}$$

$$\Lambda_{h,i}^{n+1} \in R_i^n([\![U]\!]_{h,i}^{n+1}), \tag{5.53}$$

where $R_i^n(\cdot) = R_i(\Delta_{h,i}^n, Z_{h,i}^n, \cdot)$ and $F_h^n := (1/\Delta t^2)\hat{M}_h(2U_h^n - U_h^{n-1}) - K_hU_h^n + L_h(t^n)$. Problem (5.51)-(5.53) amounts to seeking $[\![U_h^{n+1}]\!]_i$ and $\{U_h^{n+1}\}_i$ such that

$$\frac{1}{\Delta t^2}[\![U_h^{n+1}]\!]_i + M_{h,i^+}^{-1}F_{h,i^+}^n - M_{h,i^-}^{-1}F_{h,i^-}^n \in (M_{h,i^+}^{-1} + M_{h,i^-}^{-1})\hat{B}_{h,i}R_i^n([\![U_h^{n+1}]\!]_i), \tag{5.54}$$

$$\frac{1}{\Delta t^2}M_{h,i^+}M_{h,i^-}\{U_h^{n+1}\}_i + \frac{1}{2}(M_{h,i^+}F_{h,i^-}^n + M_{h,i^-}F_{h,i^+}^n) = 0. \tag{5.55}$$

The inclusion can generally be solved in an analytical way. For instance, for the normal component of an irreversible triangular model, we have to solve, at each node, a scalar inclusion of the form: seek $x \in \mathbb{R}$ such that

$$-\frac{a}{\Delta t^2}x + b \in R_1(x), \tag{5.56}$$

where a and b are given real numbers. Since R_1 is non-monotone, this problem may have in general several solutions (Figure 5.8, left). However, for a time step satisfying the condition (5.35), the solution is unique (Figure 5.8, right).

Step 3 : Update of Δ_h^{n+1} and Z_h^{n+1} by computing Z_h^{n+1} and Δ_h^{n+1} with the explicit formulae (5.34).

5.6.2 Scheme B

Step 1 : Computation of the interior components of U_h^{n+1} (explicit step).
We begin by seeking U_h^{n+1} such that

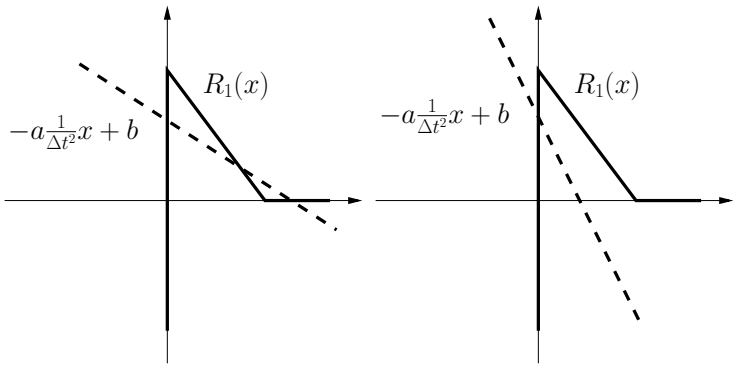

Fig. 5.8. Computation of the interface components for Scheme A.

$$\frac{1}{\Delta t^2}\hat{M}_h(U_h^{n+1}-2U_h^n+U_h^{n-1})+KU_h^n=L_h(t^n)+\hat{B}_h\Theta_h^n. \tag{5.57}$$

Step 2 : Computation of the interface components of U_h^{n+1} (implicit step).
For each $i\in\mathcal{N}^c$, we have to seek U_{h,i^+}^{n+1} and U_{h,i^-}^{n+1} such that

$$\frac{1}{\Delta t^2}M_{h,i^+}U_{h,i^+}^{n+1}+F_{h,i^+}^n=\hat{B}_{h,i}\Lambda_{h,i}^{n+1}, \tag{5.58}$$

$$\frac{1}{\Delta t^2}M_{h,i^-}U_{h,i^-}^{n+1}+F_{h,i^+}^n=-\hat{B}_{h,i}\Lambda_{h,i}^{n+1}, \tag{5.59}$$

$$\Lambda_{h,i}^{n+1}\in P_i^n([\![U_h]\!]_i). \tag{5.60}$$

where $P_i^n(\cdot)=P_i(\Delta_{h,i}^n,Z_{h,i}^n,\cdot)$ and $F_h^n:=(1/\Delta t^2)\hat{M}_h(2U_h^n-U_h^{n-1})-K_hU_h^n+L_h(t^n)+\hat{B}_h\Theta_h^n$. Problem (5.58)-(5.60) amounts to seeking $[\![U_h^{n+1}]\!]_i$ and $\{U_h^{n+1}\}_i$ such that

$$\frac{1}{\Delta t^2}[\![U_h^{n+1}]\!]_i+M_{h,i^+}^{-1}F_{h,i^+}^n-M_{h,i^-}^{-1}F_{h,i^-}^n\in(M_{h,i^+}^{-1}+M_{h,i^-}^{-1})\hat{B}_{h,i}P_i^n([\![U_h^{n+1}]\!]_i), \tag{5.61}$$

$$\frac{1}{\Delta t^2}M_{h,i^+}M_{h,i^-}\{U_h^{n+1}\}_i+\frac{1}{2}(M_{h,i^+}F_{h,i^-}^n+M_{h,i^-}F_{h,i^+}^n)=0. \tag{5.62}$$

The inclusion can generally be solved in an analytical way. For instance, for the normal component of an irreversible triangular model (decomposed as in Figure 5.5), we have to solve, at each node, a scalar inclusion of the form: seek $x\in\mathbb{R}$ such that

$$-\frac{a}{\Delta t^2}x+b\in P_1(x), \tag{5.63}$$

where a and b are given real numbers. Since P_1 is monotone, there is a unique solution to this problem (Figure 5.9).

Step 3 : Update of Δ_h^{n+1} and Z_h^{n+1} by computing Z_h^{n+1} and Δ_h^{n+1} with the explicit formulae (5.48).

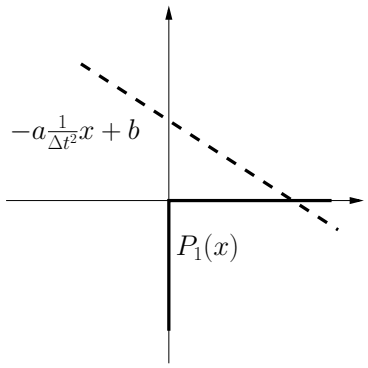

Fig. 5.9. Computation of the interface components for Scheme B.

5.7 Numerical simulations

We perform numerical simulations on 2D examples with the purpose to illustrate the effectiveness of the quasi-explicit time-integration schemes and to investigate their properties (stability condition on the time step, accuracy). For the first problem, we test the quasi-explicit time-integration schemes A and B, and a fully explicit scheme with a regularized cohesive zone model. For the other problems, we only test Scheme B, which appears as the most efficient scheme on the first problem. All the simulations have been performed using FreeFem++ [65].

5.7.1 Mode I fracture

We consider a mode I fracture problem (Figure 5.10). The domain is the rectangle $\Omega = (0, L_x) \times (-L_y, L_y)$. The fracture interface is the line $\Gamma = (0, L_x) \times \{0\}$. The cohesive zone model is a reversible triangular model with fracture toughness G_c and critical stress σ_c. A constant displacement load is prescribed at the bottom and top edges ($u_y = u_D$ at the top edge and $u_y = -u_D$ at the bottom edge, with $u_D = \epsilon L_y$). At the initial time, a precrack of length L_{pre} is inserted at mid-height on the left edge. Unless otherwise specified, the parameters are L_x =100 mm, $L_y = 10$ mm, $L_{pre} = 10$ mm, $\epsilon = 0.003$, $T = 14$ μs, $E = 200$ GPa, $\nu_P = 0$, $\rho = 7800$ kg·m^{-3}, $\sigma_c = 1.2$ GPa, and $G_c = 16\,000$ N·m^{-1}. The material parameters are representative of those of a steel (except the Poisson ratio which is taken to be zero). The wave speeds associated with the above parameters are $c_d = 5064$ m·s^{-1}, $c_s = 3581$ m·s^{-1}, and $c_R = 3086$ m·s^{-1}. The estimated cohesive zone length and the critical opening are l_{coh}= 1.963 mm and d_c= 0.0267 mm.

Owing to symmetry, numerical simulations are performed only on the upper half part of the domain. This half-domain is uniformly meshed with half-square triangles. We denote by n_{mesh} the number of elements on the large edge of the domain and by Δx the length of the elements on this edge. The time step is then determined by fixing a value for the Courant number defined as $\nu_C := c_d\sqrt{2}\frac{\Delta t}{\Delta x}$. We are interested in the following quantities: crack length, crack tip speed, energy. We denote by $l_{cr}(t)$ the length of the crack at time t and by $v_{cr}(t_1, t_2)$ the average crack tip speed between times t_1 and t_2. To localize the crack tip, we consider that the interface is cracked when the opening exceeds $0.1d_c$. We denote by $E_{el}(t)$, $E_{kin}(t)$, $E_{coh}(t)$, and $E_{tot}(t)$, the elastic energy, the kinetic energy, the cohesive energy, and the total energy at time t, respectively.

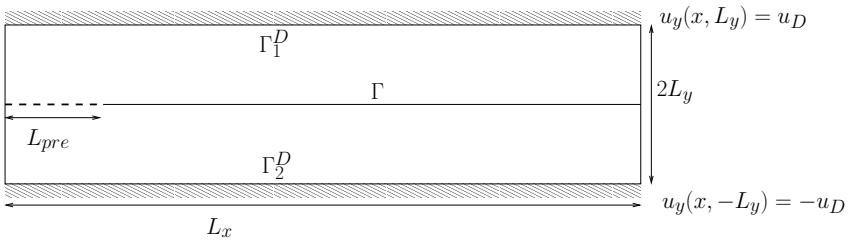

Fig. 5.10. Mode I fracture. Geometric setup.

The cohesive energy is defined as follows:

$$E_{coh}(t) := \sum_{i \in \mathcal{N}^c} \beta_i \Psi_1([\![U_h(t)]\!]_{i,1}), \tag{5.64}$$

where The total energy is defined as the sum of the elastic energy, the kinetic energy and the cohesive energy. In the continuous problem, the total energy is expected to be constant (although there is no rigorous proof of this fact). In the different simulations, we observe the following qualitative behavior: the precrack opens, and there is a stress concentration around the precrack tip; as soon as this stress reaches the cohesive critical stress, the crack starts growing; the crack tip speed quickly reaches a limit value (lower than the Rayleigh wave speed). This behavior is illustrated in Figure 5.11 (crack tip advance and energy evolution) and Figures 5.12 and 5.13 (deformation and stress fields at time T).

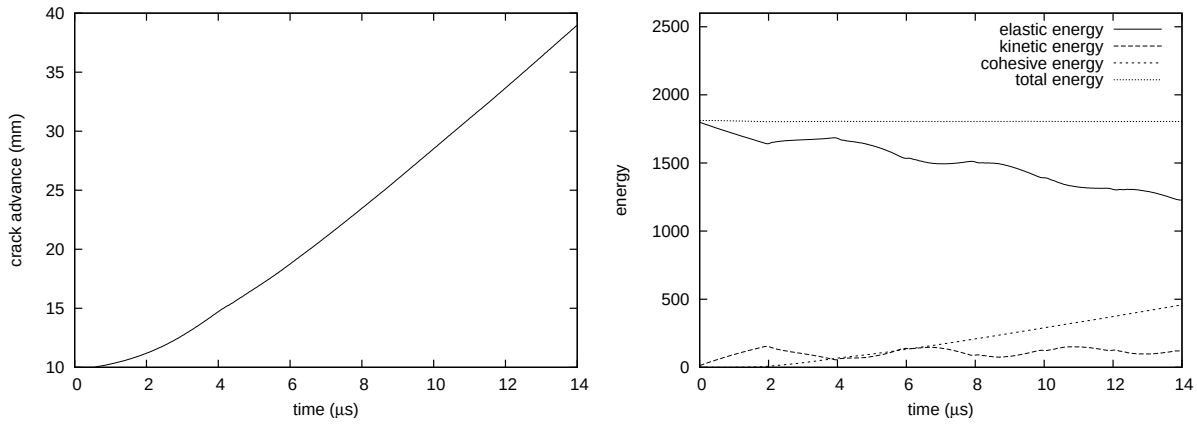

Fig. 5.11. Mode I fracture. Crack tip advance (left) and energy evolution (right). Scheme B ($n_{mesh} = 800$, $\nu_C = 1$).

We investigate the properties of the quasi-explicit time-integration schemes A and B, and a fully explicit scheme with a regularized cohesive zone model (the penalty parameter for the regularization of the non-interpenetration condition is denoted by p_c). First of all, we examine the stability condition. We observe numerically that Schemes A and B exhibit the same CFL condition as the central difference scheme on the problem without cohesive zone, namely $\nu_C \lesssim 1$. On the contrary, a fully explicit treatment of a regularized cohesive zone model deteriorates the CFL condition (Table 5.1).

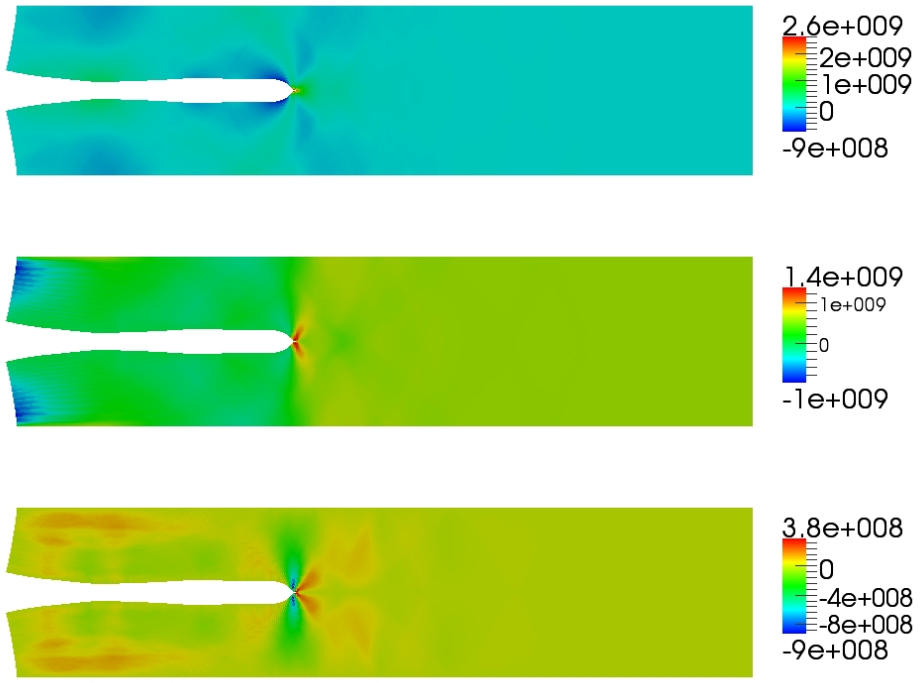

Fig. 5.12. Mode I fracture. Deformed configuration (enlarged 50 times) and stresses σ_{xx} (top), σ_{yy} (middle), and σ_{yy} (bottom) at time T. Scheme B ($n_{mesh} = 800$, $\nu_C = 1$).

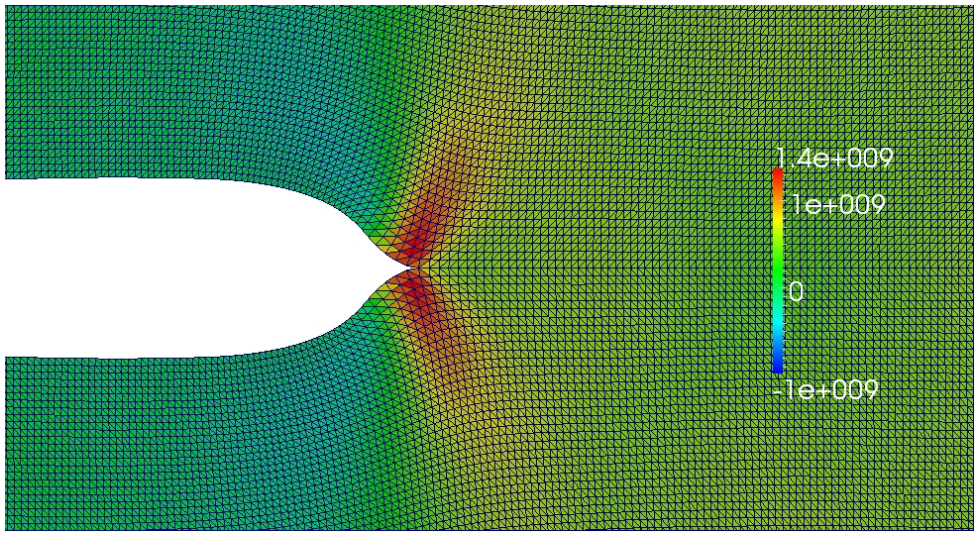

Fig. 5.13. Mode I fracture. Deformed configuration (enlarged 50 times) and stress σ_{yy} around the crack tip at time T. Scheme B ($n_{mesh} = 800$, $\nu_C = 1$).

p_c/c_s	10	100	1000
stability condition	$\nu_C \lesssim 0.88$	$\nu_C \lesssim 0.33$	$\nu_C \lesssim 0.11$

Table 5.1. Mode I fracture. Observed stability condition for a fully explicit scheme with regularized cohesive zone model ($n_{mesh} = 200$).

Now we compare the accuracy of the different schemes. We choose a mesh size equivalent or finer than the estimated cohesive length. With $\nu_C = 1$, we observe that Scheme A is not very accurate (Table 5.2). In particular, the energy balance is quite poor. By taking a smaller Courant number, the results are improved. In contrast to Scheme A, Scheme B yields accurate results with $\nu_C = 1$ (Table 5.3). The results of the fully explicit scheme with regularized cohesive zone model are relatively accurate (Table 5.4). However, in addition to a more restrictive stability condition than Scheme B, this scheme does not enforce a perfect adhesion on the sound part of the interface (Figure 5.14).

n_{mesh}	ν_C	$l_{coh}/\Delta x$	$l_{cr}(T)$	$v_{cr}(T/2,T)$	$E_{el}(T)$	$E_{kin}(T)$	$E_{coh}(T)$	$E_{tot}(T)$
100	1	1.963	0.04495	2930	1388	352.3	560.1	2301
200	1	3.927	0.04376	2956	1301	275.1	537.3	2113
400	1	7.854	0.04197	2845	1239	194.6	510.4	1944
800	1	15.71	0.04052	2723	1226	148.7	485.7	1860
n_{mesh}	ν_C	$l_{coh}/\Delta x$	$l_{cr}(T)$	$v_{cr}(T/2,T)$	$E_{el}(T)$	$E_{kin}(T)$	$E_{coh}(T)$	$E_{tot}(T)$
200	0.4	3.927	0.04071	2737	1240	163.8	488.9	1892
200	0.2	3.927	0.0395	2619	1233	133.2	472.3	1839
200	0.1	3.927	0.03897	2581	1232	120.3	464.1	1817

Table 5.2. Mode I fracture. Numerical results. Scheme A.

n_{mesh}	ν_C	$l_{coh}/\Delta x$	$l_{cr}(T)$	$v_{cr}(T/2,T)$	$E_{el}(T)$	$E_{kin}(T)$	$E_{coh}(T)$	$E_{tot}(T)$
100	1	1.963	0.03645	2282	1274	132.2	418.1	1825
200	1	3.927	0.03844	2528	1235	123.3	454.4	1813
400	1	7.854	0.03877	2556	1231	116.7	457.2	1805
800	1	15.71	0.03876	2556	1231	113.8	456.5	1801

Table 5.3. Mode I fracture. Numerical results. Scheme B.

p_c/c_s	ν_C	$l_{cr}(T)$	$v_{cr}(T/2,T)$	$E_{el}(T)$	$E_{kin}(T)$	$E_{coh}(T)$	$E_{tot}(T)$
10	0.88	0.03918	2561	1294	146.3	465.3	1905
100	0.33	0.03944	2593	1229	149.2	470.3	1848
1000	0.11	0.03942	2594	1216	138.8	468.9	1824

Table 5.4. Mode I fracture. Numerical results. Fully explicit scheme with regularized cohesive zone model ($n_{mesh} = 200$).

Finally, we investigate the influence of the parameters. The crack tip speed depends on the displacement load and the fracture toughness. It increases with the displacement load and

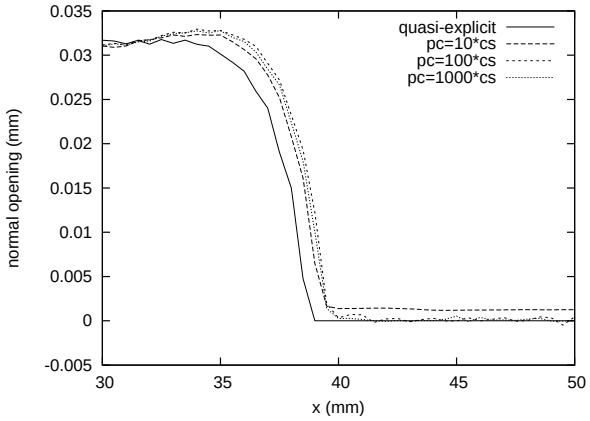

Fig. 5.14. Normal opening around the crack tip at time T. Quasi-explicit scheme B and fully explicit schemes with regularized cohesive zone model ($n_{mesh} = 200$).

decreases with the fracture toughness. If the load displacement is too small or the fracture toughness too large, the crack does not propagate. We observe that, with about 4-8 elements in the cohesive zone, the crack tip speed is accurate to about 1% (Table 5.6).

n_{mesh}	ν_C	$l_{coh}/\Delta x$	$l_{cr}(T)$	$v_{cr}(T/2,T)$	$E_{el}(T)$	$E_{kin}(T)$	$E_{coh}(T)$	$E_{tot}(T)$
100	1	1.963	0.04196	2720	1690	281.8	512.2	2484
200	1	3.927	0.04341	2823	1660	273.1	535	2468
400	1	7.854	0.04373	2860	1647	273.1	538.8	2458
800	1	15.71	0.04371	2862	1646	270.4	537.4	2454
n_{mesh}	ν_C	$l_{coh}/\Delta x$	$l_{cr}(T)$	$v_{cr}(T/2,T)$	$E_{el}(T)$	$E_{kin}(T)$	$E_{coh}(T)$	$E_{tot}(T)$
200	1	3.927	0.02112	493.7	1242	54.16	167.5	1464
400	1	7.854	0.02209	618.2	1230	44.45	181.8	1457
800	1	15.71	0.02229	639	1228	40.55	184.7	1453

Table 5.5. Mode I fracture. Numerical results for different displacement loads. Scheme B. $\epsilon = 0.0035$ (top). $\epsilon = 0.0027$ (bottom).

n_{mesh}	ν_C	$l_{coh}/\Delta x$	$l_{cr}(T)$	$v_{cr}(T/2,T)$	$E_{el}(T)$	$E_{kin}(T)$	$E_{coh}(T)$	$E_{tot}(T)$
100	1	0.9817	0.04195	2686	1308	253	256	1817
200	1	1.963	0.04494	2865	1266	266.8	280	1813
400	1	3.927	0.04614	2944	1240	276.5	288.4	1805
800	1	7.854	0.04648	2969	1230	281.5	291.7	1803
1600	1	15.71	0.04654	2982	1226	283.6	292.1	1802
n_{mesh}	ν_C	$l_{coh}/\Delta x$	$l_{cr}(T)$	$v_{cr}(T/2,T)$	$E_{el}(T)$	$E_{kin}(T)$	$E_{coh}(T)$	$E_{tot}(T)$
50	1	1.963	0.03326	1922	2336	237.2	722.2	3296
100	1	3.927	0.03516	2089	2258	195.7	771.7	3225
200	1	7.854	0.03554	2157	2247	168.4	784.4	3199
400	1	15.71	0.0357	2168	2246	153.7	787	3187

Table 5.6. Mode I fracture. Numerical results for different fracture toughness. Scheme B. $\sigma_c = 1.2$, $G_c = 8000$, $\epsilon = 0.004$ (top). $\sigma_c = 1.2$, $G_c = 32000$, $\epsilon = 0.004$ (bottom).

We still consider the same mode I fracture problem except that the cohesive zone model is now a triangular rate-dependent cohesive zone model with only normal force (the viscosity parameter is denoted by η). The notation and the parameters are the same. As expected, the introduction of a viscosity parameter slows down the crack tip (Figure 5.15 right, and Table 5.7). We observe a certain variation in the crack tip speed for $\eta = 0.01$ and $\eta = 0.02$. Indeed, in these cases, the crack tip speed is so low that the mechanical waves generated by the crack growth and reflected on the boundary perturb the crack tip advance. Note that the total energy is not preserved in this problem since the rate-dependent cohesive zone model is dissipative.

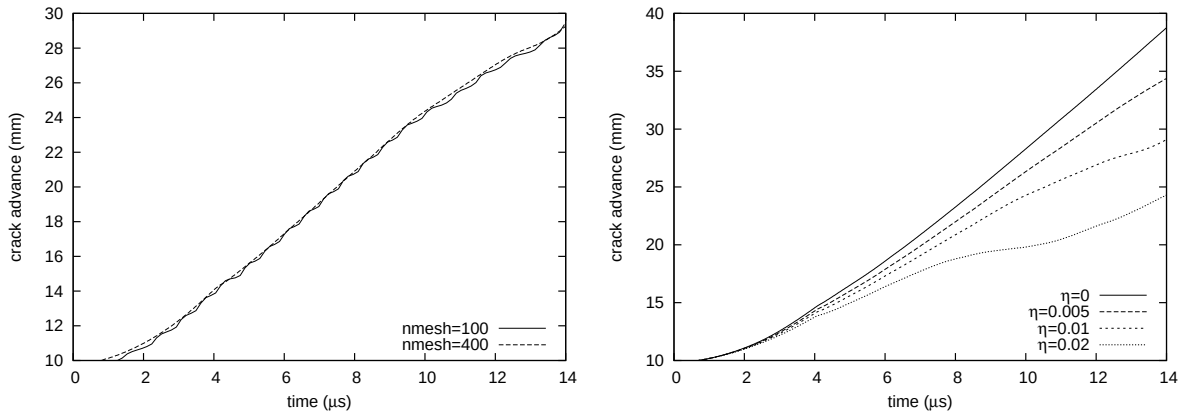

Fig. 5.15. Mode I fracture with a rate-dependent cohesive zone model. Crack tip advance for a fine and a coarse discretization (left). Crack tip advance for different viscosity parameters (right).

η	$l_{cr}(T)$	$v_{cr}(T/2,T)$	$E_{el}(T)$	$E_{kin}(T)$	$E_{coh}(T)$	$E(T)$
0	0.03877	2556	1231	116.7	457.2	1805
0.005	0.0345	2083	1289	83.43	384.6	1757
0.01	0.02926	1453	1379	74.61	299.7	1754
0.02	0.0244	953	1471	60.24	220	1751

Table 5.7. Mode I fracture with a rate-dependent cohesive zone model. Numerical results for different viscosity parameters (Scheme B, $n_{mesh} = 400$, $\nu_C = 1$).

The rate dependence of the cohesive zone model introduces a new time scale in the problem, linked to the opening rate. This time scale is smaller than the time scale linked to the crack tip speed and requires therefore smaller time steps to be resolved (compare Table 5.8 with Table 5.3). For instance, we observe small oscillations on the crack tip advance when a too coarse discretization is used (Figure 5.15, left).

5.7.2 Mode II fracture

In this section, we consider an example of mode II fracture (Figure 5.16). The domain is the rectangle $\Omega = (0, L_x) \times (-L_y, L_y)$. The fracture interface is the line $\Gamma = (0, L_x) \times \{0\}$. The cohesive zone model is a reversible uncoupled triangular model with a fracture toughness G_c

n_{mesh}	ν_C	$l_{coh}/\Delta x$	$l_{cr}(T)$	$v_{cr}(T/2,T)$	$E_{el}(T)$	$E_{kin}(T)$	$E_{coh}(T)$	$E(T)$
100	1	1.963	0.02936	1502	1377	103.9	305.1	1786
200	1	3.927	0.02951	1485	1374	84.6	304.6	1763
400	1	7.854	0.02926	1453	1379	74.61	299.7	1754
800	1	15.71	0.0291	1434	1382	70.64	296.3	1749

Table 5.8. Mode I fracture with a rate-dependent cohesive zone model. Numerical results. Scheme B.

and a critical stress σ_c. A constant shear force is prescribed at the sides of the interface ($f_s e_x$ is enforced at the top side and $-f_s e_x$ at the bottom side, with $f_s = \sigma_c/2$). At the interface, the normal opening is enforced to zero, so that the fracture is in pure mode II. At the initial time, a precrack of length L_{pre} is inserted at mid-height on the left edge.

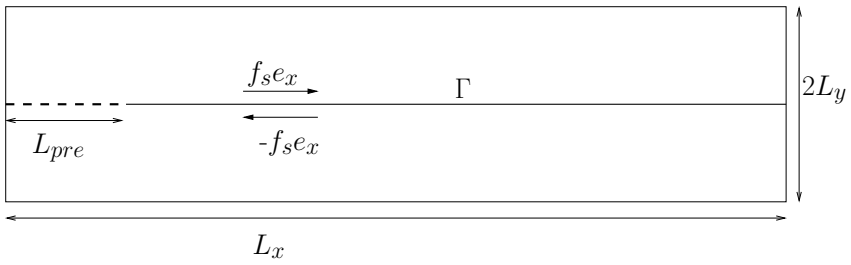

Fig. 5.16. Mode II fracture. Geometric setup.

Owing to antisymmetry, numerical simulations are performed only on the upper half part of the domain. This half-domain is uniformly meshed with half-square triangles. The parameters and the notation are the same as in the previous problems. We just change the definition of the cohesive energy:

$$E_{coh}(t) := \sum_{i \in \mathcal{N}^c} \beta_i \Psi_2([\![U_h(t)]\!]_{i,2}). \tag{5.65}$$

The sum of the kinetic energy, the elastic energy and the cohesive energy is expected to be equal to the work of the shear force (denoted by W_{ext}).

This simulation of mode II fracture exhibits the same kind of behavior as the simulation of mode I fracture. The precrack opens by sliding and there is a stress concentration around the precrack tip; as soon as this stress reaches the cohesive critical stress, the crack starts growing; the crack tip speed reaches quickly a limit value, slightly lower than the dilatational wave speed. This behavior is illustrated in Figure 5.17 (crack tip advance and energy evolution) and Figures 5.18 and 5.19 (deformation and stress fields at time T).

The observed stability condition is $\nu_C \lesssim 0.98$. With a mesh resolving the estimated cohesive zone length and $\nu_C = 0.98$, the numerical results obtained with Scheme B are very accurate (Table 5.9).

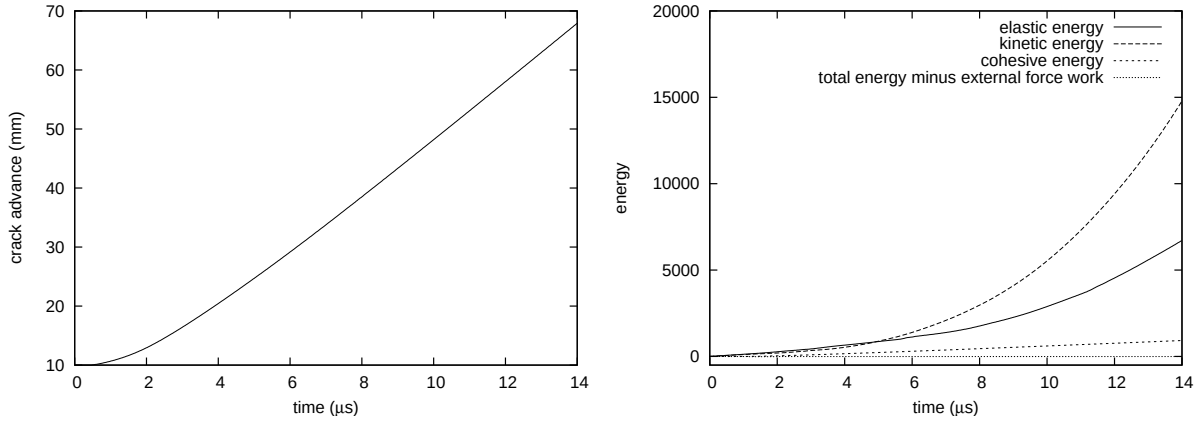

Fig. 5.17. Mode II fracture. Crack tip advance (left) and energy evolution (right). Scheme B ($n_{mesh} = 800$, $\nu_C = 0.98$).

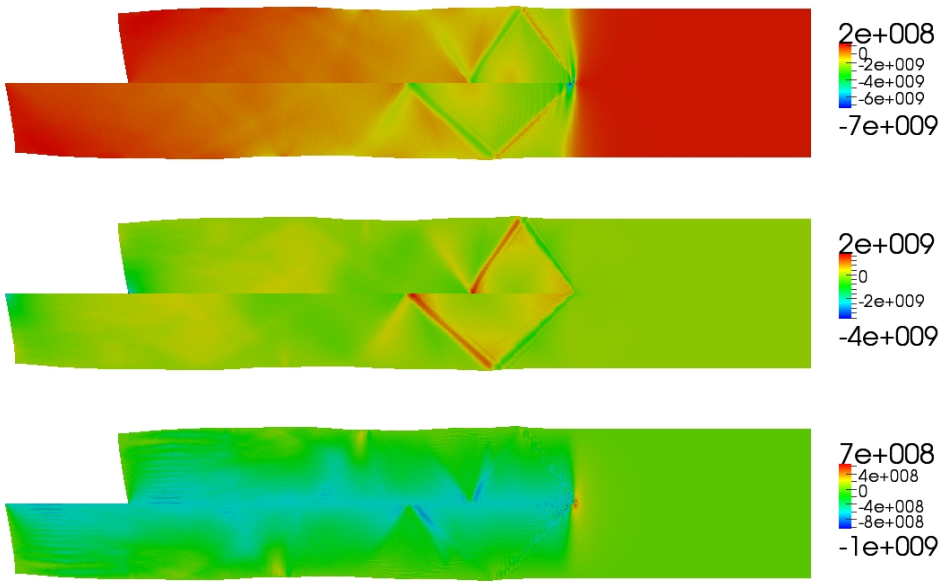

Fig. 5.18. Mode II fracture. Deformed configuration (enlarged 20 times) and and stresses σ_{xx} (top), σ_{yy} (middle), and σ_{yy} (bottom) at time T. Scheme B ($n_{mesh} = 800$, $\nu_C = 0.98$).

n_{mesh}	ν_C	$l_{coh}/\Delta x$	$l_{cr}(T)$	$v_{cr}(T/2,T)$	$E_{el}(T)$	$E_{kin}(T)$	$E_{coh}(T)$	$E_{tot}(T) - W_{ext}(T)$
100	0.98	1.964	0.06542	4721	6637	13383	881.9	-18.6
200	0.98	3.93	0.06687	4804	6686	14267	907.3	-8.8
400	0.98	7.86	0.06765	4852	6714	14675	920.7	-4.8
800	0.98	15.71	0.06789	4878	6706	14768	923.8	-2.9

Table 5.9. Mode II fracture. Numerical results. Scheme B.

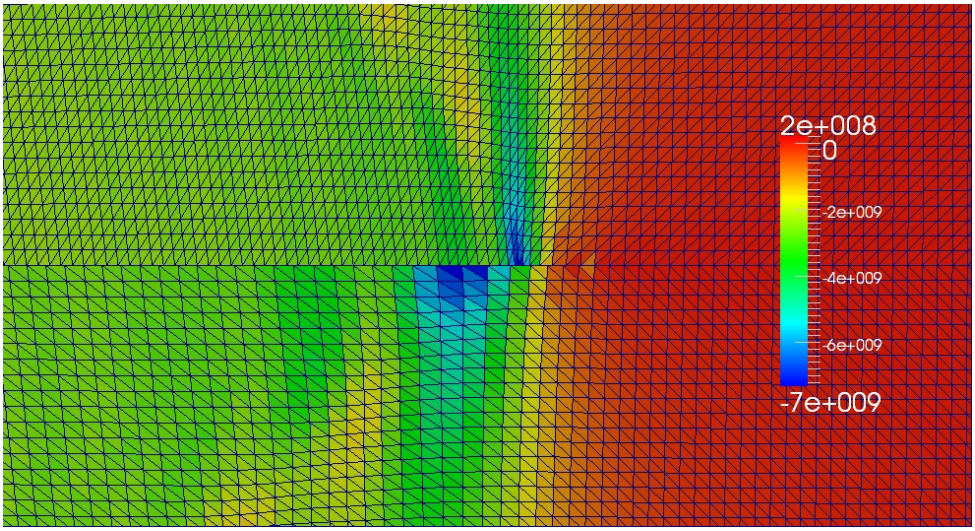

Fig. 5.19. Mode II fracture. Deformed configuration (enlarged 20 times) and stress σ_{xx} around the crack tip at time T. Scheme B ($n_{mesh} = 800$, $\nu_C = 0.98$).

5.7.3 Mode I fracture with contact

This last problem involves mode I fracture and contact (Figure 5.20). The domain is the rectangle $\Omega = (0, L_x) \times (-L_y, L_y)$. The fracture interface is the line $\Gamma = (0, L_x) \times \{0\}$. There is a precrack of length L_{pre} at mid-height on the left edge. The cohesive zone model is an irreversible triangular model with linear unloading. A constant displacement load is prescribed at the upper left edge and lower left edge ($u_y = u_d$ at the upper edge and $u_y = -u_d$ at the lower edge, with $u_d = \epsilon L_y$). The initial state corresponds to the static equilibrium with Neumann condition on the precrack and Dirichlet condition on the rest of Γ (Figure 5.22, top).

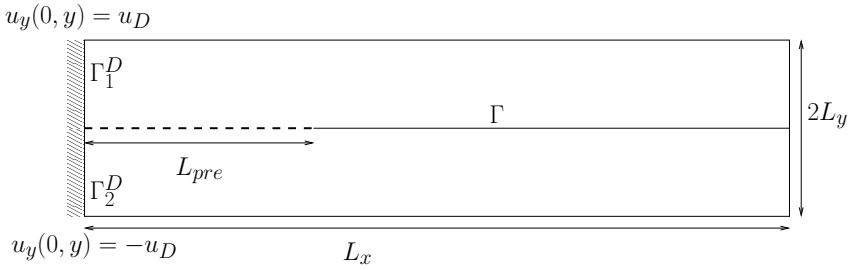

Fig. 5.20. Mode I fracture with contact. Geometric setup.

Owing to symmetry, numerical simulations are performed only on the upper half part of the domain. We use en unstructured triangular mesh. The parameters are the same as in the previous problems except the precrack length ($L_{pre} = 40$ mm), the displacement load ($\epsilon = 0.09$), and the time of simulation ($T = 100$ μs). The notation are also essentially the same. We change the definition of the cohesive energy and define a dissipated cohesive energy :

$$E_{coh}(t) := \sum_{i \in \mathcal{N}^c} \beta_i \Psi_1^{irr}(\Delta(t)_{h,i,1}, [\![U_h(t)]\!]_{i,1}), \tag{5.66}$$

$$\tilde{E}_{coh}(t) := \sum_{i \in \mathcal{N}^c} \beta_i \tilde{\Psi}_1^{irr}(\Delta(t)_{h,i,1}). \tag{5.67}$$

The total energy is defined as the sum of the elastic energy, the kinetic energy, the cohesive energy and the dissipated cohesive energy. In the continuous problem, the total energy is expected to be constant.

For this problem, we observe the following behavior. At the initial time, there is a stress concentration around the precrack tip so the crack starts immediately growing (not uniformly). After a while, the crack stops growing and contact phenomena occur near the crack tip. This behavior is illustrated in Figure 5.21 (crack tip advance and energy evolution) and Figure 5.22 (deformation and stress fields at time $T/2$).

The observed stability condition is $\nu_C \lesssim 0.8$. With a mesh resolving the estimated cohesive zone length and $\nu_C = 0.8$, the numerical results obtained with Scheme B are again very accurate (Table 5.10).

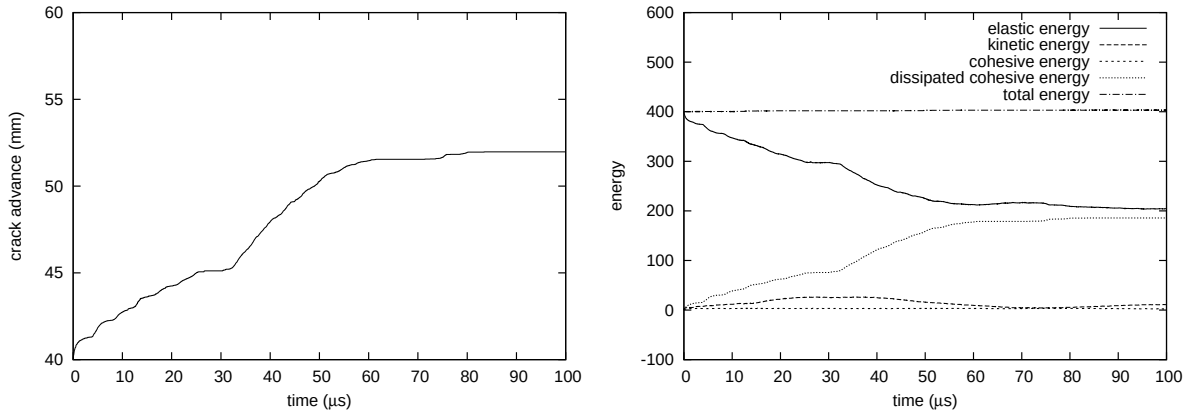

Fig. 5.21. Mode I fracture with contact. Crack tip advance (left) and energy evolution (right). Scheme B (n_{mesh} = 800, ν_C = 0.8).

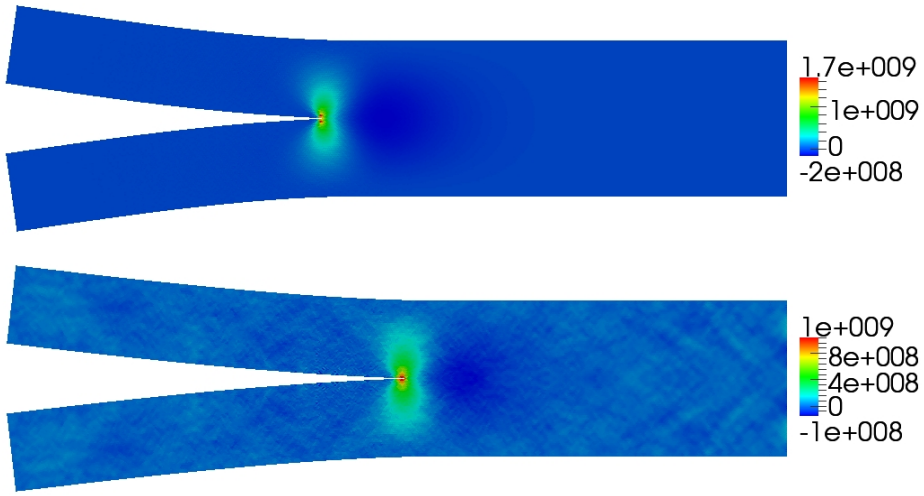

Fig. 5.22. Mode I fracture with contact. Deformed configuration (enlarged 5 times) and stress σ_{xx} at initial time (top) and time $T/2$ (bottom). Scheme B (n_{mesh} = 800, ν_C = 0.8).

n_{mesh}	ν_C	$l_{coh}/\Delta x$	$l_{cr}(T)$	$E_{el}(T)$	$E_{kin}(T)$	$E_{coh}(T)$	$\tilde{E}_{coh}(T)$	$E_{tot}(T)$
100	0.8	1.963	0.05364	199.9	11	1.66	208.7	421.3
200	0.8	3.93	0.05257	202	13.7	2.073	194.8	412.5
400	0.8	7.86	0.05197	204.6	10.82	1.988	185.8	403.2
800	0.8	15.71	0.0519	205.1	10.67	1.86	184.9	402.5

Table 5.10. Mode I fracture with contact. Numerical results. Scheme B.

6

A three-field augmented Lagrangian formulation of unilateral contact problems with cohesive forces

This chapter has been published in *ESAIM: Mathematical Modelling and Numerical Analysis* [37].

6.1 Introduction

The purpose of this work is to analyze augmented Lagrangian methods for solving static unilateral contact problems with cohesive forces. Problems of this kind arise in fracture mechanics, such as crack initiation and growth in brittle and ductile materials as well as delamination of composite materials [50, 12]. Unilateral contact problems without cohesive forces have been widely studied from both theoretical and numerical standpoints; see, for instance, [61, 76]. They can be formulated as the minimization of a convex functional or, equivalently, as a monotone variational inequality. The presence of cohesive forces in addition to the unilateral contact makes the functional to be minimized possibly nonconvex or, equivalently, the operator in the variational inequality possibly non-monotone. This complicates substantially the problem.

Consider a prototypical unilateral contact problem with cohesive forces, as illustrated in Fig. 6.1. The domain $\Omega \subset \mathbb{R}^d$ ($d = 2$ or $d = 3$) represents a deformable body. The material is assumed to be linear isotropic elastic, with Lamé coefficients λ and μ. Let $u : \Omega \to \mathbb{R}^d$ be the displacement field. The linearized strain tensor and stress tensor, $\epsilon(u) : \Omega \to \mathbb{R}^{d,d}$ and $\sigma(u) : \Omega \to \mathbb{R}^{d,d}$, are respectively defined as

$$\epsilon(u) = \frac{1}{2}\left(\nabla u + \nabla u^T\right) \qquad \text{and} \qquad \sigma(u) = \lambda \operatorname{tr} \epsilon(u) I + 2\mu\epsilon(u).$$

An external load f is applied to the body. The boundary $\partial\Omega$ is partitioned into three disjoint open subsets $\partial\Omega_D$, $\partial\Omega_N$, and Γ (the measure of $\partial\Omega_D$ is supposed to be positive). An homogeneous Dirichlet condition and a Neumann condition are prescribed on $\partial\Omega_D$ and $\partial\Omega_N$, respectively. The normal load on $\partial\Omega_N$ is denoted by g.

On Γ, we impose a unilateral contact condition with cohesive forces. The cohesive forces depend on the displacement on Γ. The present model belongs to the class of so-called cohesive zone models; see, e.g., [50, 12]. For the sake of simplicity, we restrict ourselves to the case where the cohesive forces are normal and depend only on the normal displacement. Let n be the

outward normal to Ω and let $v_\Gamma := -v|_\Gamma \cdot n$ and $\sigma_\Gamma := n \cdot \sigma|_\Gamma \cdot n$ respectively denote the normal displacement and the normal stress on Γ. Then, (i) v_Γ cannot be negative; (ii) if v_Γ is zero, σ_Γ must be lower than a yield σ_c; and (iii) if v_Γ is positive, σ_Γ obeys the cohesive law $\sigma_\Gamma = t(v_\Gamma)$. Hence, the cohesive law is a function $t : \mathbb{R}^+ \to \mathbb{R}$, and we define a cohesive energy $\psi : \mathbb{R}^+ \to \mathbb{R}$ such that $\psi' = t$ and, say, $\psi(0) = 0$. For later convenience, we extend the domain of ψ to $\mathbb{R}$ by setting for $s \geq 0$, $\psi(-s) = -\psi(s)$. There is a large variety of cohesive laws. Their common feature is a softening behavior: when the displacement increases, the cohesive force decreases. Consequently, the boundary condition is non-monotone and the cohesive energy is nonconvex. Typical functions t and ψ are represented on the left part of Fig. 6.2. The boundary condition is represented on the right part of Fig. 6.2.

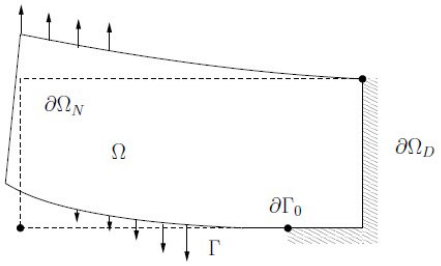

Fig. 6.1. Example of unilateral contact problem with cohesive forces.

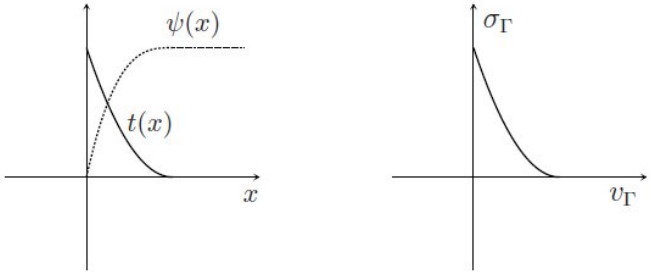

Fig. 6.2. Example of cohesive law.

Let V and H be function spaces on Ω and Γ, respectively, defined in Section 2 below. Consider the functionals

$$W : V \ni v \longmapsto W(v) := \frac{1}{2}\int_\Omega \sigma(v) : \epsilon(v) - \int_\Omega f \cdot v - \int_{\partial\Omega_N} g \cdot v \in \mathbb{R}, \tag{6.1}$$

$$\Psi : H \ni q \longmapsto \Psi(q) := \int_\Gamma \psi\,(q) \in \mathbb{R}, \tag{6.2}$$

and the linear operator

$$B : V \ni v \longmapsto Bv := v|_\Gamma \cdot n \in H. \tag{6.3}$$

The unilateral contact problem with cohesive forces can be expressed in the abstract variational form

$$\begin{cases} \min\limits_{v \in V} W(v) + \Psi(Bv) \\ \text{subject to } Bv \in H^+ \end{cases} \tag{6.4}$$

where $H^+ := \{q \in H; q \geq 0\}$.

Problem (6.4) is a constrained minimization problem. For solving numerically such a problem, the main techniques are penalty methods, feasible direction methods, linear programming methods, and Lagrangian methods. These techniques are thoroughly discussed in [11]. The main drawbacks of the first three methods can be summarized in this way: penalty methods generally yield ill-conditioned problems, feasible direction methods are often expensive due to the projection step, and linear programming methods are limited to linear constraints and quadratic objective functions. In contrast, Lagrangian methods are based on a reformulation of the constrained minimization problem. The new problem consists in seeking a saddle-point (or a stationary point) of a Lagrangian. This can be achieved efficiently by Uzawa algorithms or Newton methods. Uzawa algorithms generally feature good global convergence properties (in the sense that they do not need an initialization value close to the optimum), but their speed of convergence is only linear. Newton methods feature a quadratic speed of convergence, but this is achieved only locally (that is, if the initialization is close to the optimum). Furthermore, augmenting the Lagrangian offers some additional advantages. Whenever the objective function is actually convex, this augmentation improves the performance of the algorithms. In the nonconvex case, the ordinary Lagrangian formulation is not necessarily well-posed and the augmentation enables to recover well-posedness. More details on augmented Lagrangian methods can be found in [10, 11].

In the present work, we analyze two augmented Lagrangian methods for the problem of unilateral contact with cohesive forces: a decomposition-coordination method and a nonsmooth Newton's method. These two methods are based on the same three-field augmented Lagrangian formulation. The decomposition-coordination method has been proposed by Fortin and Glowinski [49] as a general method for solving nonlinear problems. The idea is to solve separately the linear and nonlinear parts of the problem at each iteration. This method can be seen as an Uzawa-like algorithm. It is closely related to the so-called Latin method [84] and also to splitting operator methods. Such methods have been applied to various unilateral contact problems, as for instance in [23, 52]. In the case of a convex functional split into two convex parts, the convergence of the algorithm has been proved in [49]. Furthermore, Newton's method is a standard method for solving nonlinear systems of equations and, as such, can be used to find a stationary point of the augmented Lagrangian. In the case of unilateral constraints, the resulting system is only piecewise continuously differentiable and Newton's method can be extended to this class of nonsmooth systems [104]. Newton's method for unilateral contact problems has been used for instance in [1, 83]. In particular, it has been applied to the problem of unilateral contact with cohesive forces in [93].

This paper is organized as follows. In Section 6.2, we specify the mathematical structure of the original constrained minimization problem (6.4) and investigate its well-posedness. In particular, we establish an existence result where the lack of convexity is compensated by a compactness argument. In Section 6.3, we introduce the three-field augmented Lagrangian formulation and study its well-posedness, namely the existence of a local saddle-point of the augmented Lagrangian. This result is well-known in the convex case [42]. In the nonconvex case,

a result is available only in a finite-dimensional setting [10]. Here, we extend this latter approach to the (infinite-dimensional) problem of unilateral contact with cohesive forces, assuming the surjectivity of the operator B defined by (6.3) and using a compactness argument in the (closure of the) cone of feasible directions. Sections 6.2 and 6.3 are set in a general framework encompassing the particular case of unilateral contact problems with cohesive forces. In Section 6.4, we analyze mixed finite element approximations of the augmented Lagrangian formulation of unilateral contact problems with cohesive forces. Since a nonlinear problem needs to be solved for the normal displacement on Γ, it is convenient to use a collocation method. In the same way, numerical integration can be employed to build the Jacobian matrix in Newton's method. A key point is the use of discontinuous finite element spaces leading to a collocation method, while ensuring an inf-sup condition which is the discrete counterpart of the surjectivity of the operator B. The resulting mixed finite element approximation is nonconforming. Numerous works have been devoted to the error analysis of mixed formulations for unilateral contact problems, especially for two-field formulations (bulk displacement-displacement on Γ or bulk displacement-normal stress on Γ). To our knowledge, the only work dealing with the three-field augmented Lagrangian formulation is [24] in a conforming and consistent case. Here, we prove *a priori* error estimates in the present nonconforming setting for various finite element spaces under the simplifying assumption that the cohesive forces are mild enough. In Section 6.5, we describe the algorithms. We prove the convergence of the decomposition-coordination method in the particular case of a convex functional split into a convex part and a nonconvex part. Finally, numerical simulations illustrating the theoretical results are presented in Section 6.6.

6.2 Well-posedness of the continuous problem

The main result of this section is the existence of a minimizer for problem (6.4). The lack of convexity is compensated by a compactness argument. We also specify a sufficient condition for uniqueness based on α-convexity and give some hints on the regularity of the solution.

We make the following assumptions on the mathematical structure of problem (6.4).

(H1) V and H are Hilbert spaces and $B \in \mathcal{L}(V,H)$ (the continuity constant is denoted by c_B);

(H2) W is α-convex on V (the α-convexity constant is denoted by α_W);

(H3) H^+ is a nonempty closed convex subset of H;

(H4) There is a Hilbert space $M \equiv M'$ with scalar product $(\cdot,\cdot)_M$ such that $H \hookrightarrow M$ with compact imbedding (the continuity constant of the imbedding is denoted by c_M) and $\Psi : M \to \mathbb{R}$ is bounded and continuous;

(H5) W and Ψ are continuously differentiable on V and M respectively, and Ψ' is Lipschitz continuous on M (the Lipschitz constant of Ψ' is denoted by $k_{\Psi'}$).

Let $V^+ := \{v \in V; Bv \in H^+\}$, observe that V^+ is a closed convex subset of V, and define the functional

$$J : V \ni v \longmapsto J(v) := W(v) + \Psi(Bv) \in \mathbb{R}. \tag{6.5}$$

Problem (6.4) can be rewritten as

$$\min_{v \in V^+} J(v). \tag{6.6}$$

Theorem 6.1. *Assume* (H1)-(H4). *Then, there exists a solution to problem (6.4).*

Proof. Let $(v_n)_{n\in\mathbb{N}}$ be a minimizing sequence of J in V^+. Since the functional J is coercive (W is α-convex and Ψ is bounded), the sequence $(v_n)_{n\in\mathbb{N}}$ is bounded in V. Hence, we can extract a subsequence, still denoted by $(v_n)_{n\in\mathbb{N}}$, which converges weakly to v_∞ in V. The limit v_∞ belongs to V^+ since a strongly closed convex set is weakly closed. Moreover, owing to the continuity of B from V to H and the compactness of the imbedding $H \hookrightarrow M$, the sequence $(Bv_n)_{n\in\mathbb{N}}$ strongly converges to Bv_∞ in M. Using the continuity of Ψ on M, we conclude that $\lim_{n\to\infty}\Psi(Bv_n) = \Psi(Bv_\infty)$. Furthermore, since the functional W is convex and continuous on V, $\liminf_{n\to\infty} W(v_n) \geq W(v_\infty)$. Thus, $v_\infty \in V^+$ is a global minimizer of J in V^+.

Proposition 6.1. *Assume* (H1)-(H5). *Then, J is differentiable on V so that a solution u to (6.4) satisfies*

$$\langle J'(u), v-u\rangle_{V',V} \geq 0, \qquad \forall v \in V^+. \tag{6.7}$$

Furthermore, if

$$\alpha_W - k_{\Psi'} c_M^2 c_B^2 > 0, \tag{6.8}$$

then J is α-convex on V and the solution to (6.4) is unique.

Proof. The first statement is evident. Concerning the second one, observe that for all $(v,w) \in V\times V$,

$$\begin{aligned}
\big\langle J'(v) - J'(w), v-w\big\rangle_{V',V} &\geq \big\langle W'(v) - W'(w), v-w\big\rangle_{V',V} + (\Psi'(Bv) - \Psi'(Bw), Bv - Bw)_M \\
&\geq \alpha_W \|v-w\|_V^2 - k_{\psi'}\|Bv-Bw\|_M^2 \\
&\geq \alpha_W \|v-w\|_V^2 - k_{\psi'} c_M^2 \|Bv-Bw\|_H^2 \\
&\geq (\alpha_W - k_{\Psi'} c_M^2 c_B^2)\|v-w\|_V^2,
\end{aligned}$$

which proves the α-convexity of J under the condition (6.8), and hence the uniqueness of the solution.

Remark 6.1. *Relation (6.7) links problem (6.4) to the theory of variational inequalities. When J is convex, the operator J' is monotone. In the general case, the proof of Theorem 6.1 shows that J' is pseudo-monotone.*

We now verify that the unilateral contact problem with cohesive forces defined in the introduction fits the above abstract framework. Recalling the definitions (6.1)-(6.3) of W, Ψ, and B, we also set

$$V := \{v \in H^1(\Omega)^d;\ v|_{\partial\Omega_D} = 0\}, \qquad H := H_{00}^{\frac12}(\Gamma, \partial\Gamma_0), \qquad M := L^2(\Gamma),$$

where $\partial\Gamma_0 := \overline{\partial\Omega_D} \cap \overline{\Gamma}$ (see Fig. 6.1). The space $H_{00}^{\frac12}(\Gamma,\partial\Gamma_0)$ is the space of functions of $H^{\frac12}(\Gamma)$ that are zero in a certain sense on $\partial\Gamma_0$. It can be built by interpolation between $L^2(\Gamma)$ and $H_0^1(\Gamma,\partial\Gamma_0)$; see [92] for more details. Furthermore, $H^+ := \{q \in H; q \geq 0 \text{ a.e. in } \Gamma\}$ and observe that with the above notation,

$$\Psi(q) = (\psi(q), 1)_M. \tag{6.9}$$

Finally, for further use, we set $M^+ = \{q \in M; q \geq 0 \text{ a.e. in } \Gamma\}$.

Proposition 6.2. *Assumptions* (H1)-(H3) *hold. If ψ is continuous and bounded on $\mathbb{R}$, Assumption* (H4) *holds. If ψ' is Lipschitz continuous on $\mathbb{R}$ with Lipschitz constant $k_{\psi'}$, Assumption* (H5) *holds with $k_{\Psi'} = k_{\psi'}$.*

Proof. Assumption (H1) holds by construction. Assumption (H2) is a direct consequence of Korn's first inequality [25]. Assumption (H3) is readily verified. Concerning assumptions (H4) and (H5), we first observe that, by construction, $H^{\frac{1}{2}}_{00}(\Gamma, \partial\Gamma_0)$ is compactly imbedded in $L^2(\Gamma)$. Furthermore, to prove the regularity of Ψ, we use a basic result of nonlinear analysis [32]; see Lemma 6.1 below. Using this lemma with $\phi = \psi$, $p = 2$, and $q = 1$ along with the boundedness of ψ to verify condition (6.10), we infer that $\mathcal{S}_\psi$ is continuous from $L^2(\Gamma)$ into $L^1(\Gamma)$. Since for all $q \in L^2(\Gamma)$, $\Psi(q) = (\mathcal{S}_\psi(q), 1)_M$, the operator Ψ is continuous on M. Moreover, since for all $q, r \in L^2(\Gamma)$,

$$\begin{aligned}\Psi(q+r) - \Psi(q) - (\mathcal{S}_{\psi'}(q), r)_M &= \int_\Gamma \left(\int_0^1 (\psi'(q(x) + tr(x)) - \psi'(q(x)))dt \right) r(x)dx \\ &\leq \frac{1}{2} k_{\psi'} \int_\Gamma |r(x)|^2 dx,\end{aligned}$$

owing to the Lipschitz continuity of ψ', Ψ is differentiable on M with $(\Psi'(q), r)_M = (\mathcal{S}_{\psi'}(q), r)_M$. Using Lemma 6.1 with $\phi = \psi'$ and $p = q = 2$ along with the Lipschitz continuity of ψ' readily shows that Ψ' is Lipschitz continuous on M with Lipschitz constant $k_{\psi'}$. Finally, the differentiability of W is obvious.

Lemma 6.1. *Let $\phi : \mathbb{R} \to \mathbb{R}$ be a continuous function. Consider a measurable function $q : \Gamma \subset \mathbb{R}^n \to \mathbb{R}$. The superposition operator (or Nemitsky operator) $\mathcal{S}_\phi$ maps q to $\phi \circ q$. If q and r are measurable functions that coincide almost everywhere on Γ, then $\mathcal{S}_\phi(q)$ and $\mathcal{S}_\phi(r)$ are measurable functions that coincide almost everywhere on Γ. Moreover, if ϕ satisfies the growth condition,*

$$\exists a, b \in \mathbb{R}, \quad \forall x \in \mathbb{R}, \qquad |\phi(x)| \leq a + b|x|^{p/q}, \tag{6.10}$$

then the superposition operator maps $L^p(\Gamma)$ into $L^q(\Gamma)$ and is strongly continuous ($p, q \in [1; +\infty[$).

Remark 6.2. *The α-convexity condition (6.8) can be interpreted in terms of the problem parameters. The constant α_W is proportional to the Young modulus of the material. The constant $k_{\psi'}$ is larger when the cohesive forces decrease fast. By a scaling argument, it can be seen that $c_M c_B$ decreases to zero with the $(d-1)$-dimensional measure $|\Gamma|$. Thus, condition (6.8) is more likely to be met when the Young modulus is large, the cohesive force decreases slowly, or $|\Gamma|$ is small.*

A detailed study of the regularity of the solution to the minimization problem (6.4) is beyond the scope of the present work. However, let us mention some results in particular cases. For a unilateral contact problem without cohesive forces under body forces in $L^2(\Omega)^d$, the displacement is in $H^2_{loc}(\Omega \cup \Gamma)^d$ [77]. Furthermore, for a scalar elliptic problem in 2D with unilateral contact and homogeneous Dirichlet condition, the regularity of the solution has been studied near the junction between these boundary conditions [98]. Under body forces in $L^2(\Omega)$ and for a smooth junction, the solution is in $H^{\frac{3}{2}}(\Omega)$. For an angular junction (of internal angle ω), the

solution is in $H^2(\Omega)$ if $\omega \leq \pi/2$, and in $H^{1+\frac{\pi}{2\omega}}(\Omega)$ otherwise. With a sufficiently smooth cohesive law, it seems reasonable to expect at least the same kind of regularity. Furthermore, cohesive zone models have been designed to avoid unphysical infinite stresses at the crack tip. Yet, the question whether an appropriate choice of cohesive interface and law can lead to more regular solutions is still mathematically open.

6.3 A three-field augmented Lagrangian formulation

We introduce a new unknown q representing the normal displacement on Γ. The decomposed problem is

$$\begin{cases} \min\limits_{(v,q)\in V\times H^+} W(v)+\Psi(q) \\ \text{subject to } Bv = q \end{cases} \tag{6.11}$$

The decomposed problem (6.11), which is obviously equivalent to the initial minimization problem (6.4), is a minimization problem under a linear equality constraint. We treat this constraint by an augmented Lagrangian method. Introduce the space $Y := V \times H$ (equipped with its natural norm) and the convex set $K := V \times H^+$. Define

$$\begin{aligned} &J_0 : Y \ni y := (v,q) \longmapsto J_0(y) := W(v)+\Psi(q) \in \mathbb{R}, \\ &\tilde{B} : Y \ni y := (v,q) \longmapsto \tilde{B}y := Bv - q \in H, \end{aligned}$$

so that (6.11) amounts to

$$\min_{y\in K\cap \ker \tilde{B}} J_0(y). \tag{6.12}$$

The augmented Lagrangian associated with the decomposed problem is

$$L_r : Y \times H' \ni (y,\lambda) \longmapsto L_r(y,\lambda) := J_0(y) + \langle \lambda, \tilde{B}y\rangle_{H',H} + \frac{r}{2}\|\tilde{B}y\|_M^2 \in \mathbb{R}, \tag{6.13}$$

where r is an arbitrary non-negative constant. For $y \in Y$, set

$$J_r(y) := J_0(y) + \frac{r}{2}\|\tilde{B}y\|_M^2. \tag{6.14}$$

A couple $(x,\theta) \in K \times H'$ is said to be a local saddle-point of the augmented Lagrangian if it satisfies

$$\forall \lambda \in H', \qquad L_r(x,\lambda) \leq L_r(x,\theta) \leq L_r(y,\theta), \qquad \forall y \in U, \tag{6.15}$$

where $U \subset K$ is a neighborhood of x. The introduction of the augmented Lagrangian is motivated by the following proposition whose proof is straightforward.

Proposition 6.3. *If $(x,\theta) \in K \times H'$ is a local saddle-point of the augmented Lagrangian, then x is a local minimizer of the decomposed problem (6.11).*

The converse of this statement is more difficult to establish. We first prove, under the key assumption that B is surjective from V to H, that if $x \in K \cap \ker \tilde{B}$ is a local minimizer of J_0, there is (a unique) $\theta \in H'$ such that (x,θ) is a stationary point of the augmented Lagrangian

L_r. Then, we prove, under an additional assumption, that such a stationary point is a local saddle-point of L_r. A couple $(x,\theta) \in K \times H'$ is said to be a stationary point of L_r if it satisfies

$$\langle \partial_y L_r(x,\theta), y-x\rangle_{Y',Y} \equiv \big\langle J_r'(x), y-x\big\rangle_{Y',Y} + \langle \theta, \tilde{B}(y-x)\rangle_{H',H} \geq 0, \qquad \forall y \in K, \tag{6.16}$$

$$\langle \partial_\lambda L_r(x,\theta), \lambda\rangle_{H,H'} \equiv \langle \lambda, \tilde{B}x\rangle_{H',H} = 0, \qquad \forall \lambda \in H'. \tag{6.17}$$

Observe that being a stationary point of the augmented Lagrangian is a property independent of r since (6.17) implies $\tilde{B}x = 0$ so that $J_r'(x) = J_0'(x)$. Notice also that (6.16) can be rewritten for $x := (u,p)$ as

$$\langle W'(u), v\rangle_{V',V} + \langle \theta, Bv\rangle_{H',H} = 0, \qquad \forall v \in V, \tag{6.18}$$

$$(\psi'(p), q-p)_M - \langle \theta, q-p\rangle_{H',H} \geq 0, \qquad \forall q \in H^+. \tag{6.19}$$

Proposition 6.4. *Let $x \in K \cap \ker \tilde{B}$ be a local minimizer of the decomposed problem (6.11). If B is surjective from V to H, there exists a unique $\theta \in H'$ such that (x,θ) is a stationary point of the augmented Lagrangian.*

Proof. Let $x \in K \cap \ker \tilde{B}$ be a local minimizer of the decomposed problem. Then, $\tilde{B}x = 0$ and (6.17) obviously holds. Let us now prove (6.16). For all $r \geq 0$, x minimizes J_r over $K \cap \ker \tilde{B}$ and hence it satisfies

$$\langle J_r'(x), y-x\rangle_{Y',Y} \geq 0, \qquad \forall y \in K \cap \ker \tilde{B}.$$

For all $v \in \ker B$, $y := x + (v,0)$ belongs to $K \cap \ker \tilde{B}$ so that $\langle J_r'(x), (v,0)\rangle_{Y',Y} = 0$. Since B is surjective, $(\ker B)^\perp = \operatorname{im} B^*$ by the closed range theorem. As a consequence, there exists $\theta \in H'$ such that

$$\langle J_r'(x), (v,0)\rangle_{Y',Y} + \langle \theta, Bv\rangle_{H',H} = 0, \qquad \forall v \in V.$$

Since $J_r'(x) = J_0'(x)$, θ does not depend on r. Now let $y := (v,q) \in K$ and let $w \in V$ be such that $Bw = q$. Then,

$$\begin{aligned}\langle J_r'(x), y-x\rangle_{Y',Y} + \langle \theta, \tilde{B}(y-x)\rangle_{H',H} &= \langle J_r'(x), y-x\rangle_{Y',Y} + \langle \theta, B(v-w)\rangle_{H',H} \\ &= \langle J_r'(x), (w,q)-x\rangle_{Y',Y} \geq 0,\end{aligned}$$

since (w,q) is by construction in $K \cap \ker \tilde{B}$. Hence, (6.16) also holds. Finally, the relation $\langle J_r'(x), (v,0)\rangle_{Y',Y} + \langle \theta, Bv\rangle_{H',H} = 0$ for all $v \in V$ and the surjectivity of B from V to H imply that θ is unique.

Remark 6.3. *In the context of unilateral contact problems, the Lagrange multiplier θ can be interpreted as the normal stress on Γ, namely $\theta = \sigma(u)_\Gamma$ where $x := (u, u_\Gamma)$. This results from the relation (6.16).*

Remark 6.4. *A more general existence result for mixed linear variational inequalities can be found in [113].*

We now examine whether a stationary point of the augmented Lagrangian is a local saddle-point. The cone of feasible directions at the point $x := (u,p) \in K$ can be defined as $(V \times C_+(x)) \cap \ker \tilde{B}$ where

$$C_+(x) := \{d \in H;\ \exists \alpha > 0,\ p + \alpha d \in H^+\}. \tag{6.20}$$

Proposition 6.5. *Assume that W and Ψ are of class C^2. Let $(x,\theta) \in K \times H'$ be a stationary point of the augmented Lagrangian. Assume that (x,θ) satisfies the following second-order condition (indices on brackets are dropped for second-order derivatives)*

$$\langle J_0''(x),(d,d)\rangle > 0, \qquad \forall d \in (V \times \overline{C_+(x)}) \cap \ker \tilde{B} \setminus \{0\}. \tag{6.21}$$

Then, there exists $r_0 \geq 0$ such that (x,θ) is a local saddle-point of the augmented Lagrangian L_{r_0}. Furthermore, for all $r \geq r_0$, (x,θ) is a local saddle-point of the augmented Lagrangian L_r.

Proof. The left inequality in (6.15) is obvious for all $r \geq 0$. If the right inequality holds for $r_0 \geq 0$, then it holds also for $r \geq r_0$. Now we shall prove by contradiction that there exist $r_0 \geq 0$ and a neighborhood U of x such that $L_r(x,\theta) \leq L_r(y,\theta),\ \forall y \in U,\ \forall r \geq r_0$. Suppose there exists a sequence of positive reals $(r_k)_{k\in\mathbb{N}}$ tending to infinity and a sequence $(x_k)_{k\in\mathbb{N}}$ of elements of K tending to x such that

$$L_{r_k}(x_k,\theta) \leq L_{r_k}(x,\theta). \tag{6.22}$$

Consider the sequence $(e_k)_{k\in\mathbb{N}}$ such that $e_k := (e_k^v, e_k^q) := \varrho_k^{-1}(x_k - x)$ where $\varrho_k := \|x_k - x\|_Y$. Since this sequence is bounded in Y, there exists a subsequence, still denoted by $(e_k)_{k\in\mathbb{N}}$, weakly converging to $e := (e^v, e^q)$ in Y. To obtain a contradiction, we shall now prove that $e \in (V \times \overline{C_+(x)}) \cap \ker \tilde{B}$ and that $\langle J_0''(x),(e,e)\rangle \leq 0$. A second-order Taylor expansion of $L_0(\cdot,\theta)$ at x in the Y-norm yields

$$L_0(x_k,\theta) = L_0(x,\theta) + \langle \partial_y L_0(x,\theta), x_k - x\rangle_{Y',Y} + \frac{1}{2}\langle J_0''(x),(x_k-x,x_k-x)\rangle + o(\varrho_k^2).$$

Since $x_k = x + \varrho_k e + \varrho_k(e_k - e)$,

$$\begin{aligned} L_0(x_k,\theta) = L_0(x,\theta) &+ \langle \partial_y L_0(x,\theta), x_k - x\rangle_{Y',Y} + \alpha_k^2\langle J_0''(x),(e_k-e,e)\rangle \\ &+ \frac{\alpha_k^2}{2}\langle J_0''(x),(e,e)\rangle + \frac{\alpha_k^2}{2}\langle J_0''(x),(e_k-e,e_k-e)\rangle + o(\varrho_k^2). \end{aligned} \tag{6.23}$$

Since (x,θ) is a stationary point of the augmented Lagrangian, $\langle \partial_y L_0(x,\theta), x_k - x\rangle_{Y',Y} \geq 0$. Now observe that $\tilde{B}x_k = \tilde{B}x + \varrho_k \tilde{B}e_k = \varrho_k \tilde{B}e_k$. Hence, substituting (6.23) into (6.22), it is inferred that

$$\alpha_k^2\langle J_0''(x),(e_k-e,e)\rangle + \frac{\alpha_k^2}{2}\langle J_0''(x),(e,e)\rangle + \frac{\alpha_k^2}{2}\langle J_0''(x),(e_k-e,e_k-e)\rangle + \frac{r_k}{2}\varrho_k^2\|\tilde{B}e_k\|_M^2 + o(\varrho_k^2) \leq 0. \tag{6.24}$$

Since the sequence $(e_k)_{k\in\mathbb{N}}$ converges weakly to e in Y, $\langle J_0''(x),(e_k-e,e)\rangle$ tends to 0. By convexity $\langle W''(x),(e_k^v - e^v, e_k^v - e^v)\rangle \geq 0$ and by compactness, e_k^q tends to e^q in M so that $\langle \Psi''(x),(e_k^q - e^q, e_k^q - e^q)\rangle$ tends to 0. Hence, $\liminf_k \langle J_0''(x),(e_k-e,e_k-e)\rangle \geq 0$. By compactness, the sequence $(\tilde{B}e_k)_{k\in\mathbb{N}}$ converges strongly to $\tilde{B}e$ in M. Dividing (6.24) by $\varrho_k^2 r_k$ and passing to the limit, we obtain $\|\tilde{B}e\|_M^2 \leq 0$ and thus $e \in \ker \tilde{B}$. Moreover, since $x_k = x + \varrho_k e_k$, it is clear that for all $k \geq 0$, $e_k^q \in C_+(x)$. Observing that $C_+(x)$ is convex, it is inferred that $e^q \in \overline{C_+(x)}$. Hence, $e \in (V \times \overline{C_+(x)}) \cap \ker \tilde{B}$; furthermore, by construction, $e \neq 0$. Finally, dividing (6.24) by ϱ_k^2, dropping the positive terms, and passing to the limit leads to $\langle J_0''(x),(e,e)\rangle \leq 0$.

6.4 Approximation by mixed finite elements

In this section, we discretize the augmented Lagrangian formulation of unilateral contact problems with cohesive forces by a Galerkin method with finite element spaces. The augmented Lagrangian formulation is a three-field formulation: the bulk displacement, the normal displacement on Γ, and the Lagrange multiplier (which can be interpreted as the normal stress on Γ). The two key ideas in the design of the mixed finite element approximation are the following. Firstly, we want to solve the nonlinear part of the problem concerning the normal displacement on Γ by a collocation method. This leads to the use of discontinuous finite element spaces spanned by nodal basis functions for approximating this quantity. Secondly, a surjectivity condition in the form of a discrete inf-sup condition must be satisfied, linking the discrete spaces for the bulk displacement and the Lagrange multiplier. In the sequel, we refer to a 3D/2D setting when Ω is 3D and Γ is 2D, and to a 2D/1D setting when Ω is 2D and Γ is 1D. Moreover, $A \lesssim B$ means the inequality $A \le cB$ with a positive constant c independent of the mesh-size. Henceforth, the minimal regularity requirement for ψ is that ψ' is Lipschitz continuous.

6.4.1 The discrete setting

Let $\{\mathcal{T}_h\}_{h>0}$ be a shape-regular family of affine meshes covering exactly Ω, where the parameter h stands for the maximum size of the elements in $\mathcal{T}_h$. Without loss of generality, we assume $h \le 1$. Let $\mathcal{F}_h$ collect the mesh faces located on Γ. To alleviate technicalities, the mesh family $\{\mathcal{F}_h\}_{h>0}$ is assumed to be quasi-uniform on Γ, but this assumption can be relaxed. Let V_h, M_h, and Λ_h respectively denote the finite element approximation spaces for the bulk displacement, the normal displacement on Γ, and the Lagrange multiplier. Henceforth, we assume that

$$V_h \subset V, \qquad \text{and} \qquad \Lambda_h \subset M_h \subset M. \tag{6.25}$$

Thus, the approximation is conforming for the bulk displacement and the Lagrange multiplier, but not for the normal displacement on Γ since in general $M_h \not\subset H$. In fact, motivated by the use of a collocation method, we will choose M_h as a discontinuous finite element space spanned by nodal basis functions; see Remark 6.6 below for further insight. Let Π_{Λ_h} denote the L^2-orthogonal projection from M onto Λ_h and define the operator

$$B_h : V \ni v \longmapsto B_h v := \Pi_{\Lambda_h} B v \in \Lambda_h. \tag{6.26}$$

The choice for the spaces V_h and Λ_h is linked by the following discrete inf-sup condition

$$\exists \beta_h > 0, \qquad \forall \lambda_h \in \Lambda_h, \qquad \beta_h h^{1/2} \|\lambda_h\|_M \le \sup_{v_h \in V_h} \frac{(B_h v_h, \lambda_h)_M}{\|v_h\|_V}. \tag{6.27}$$

This means that the restriction of the operator B_h to V_h is surjective onto Λ_h. Henceforth, we assume that this condition holds.

Remark 6.5. *The scaling factor $h^{1/2}$ has been introduced since the natural norm for λ_h is the $H^{-\frac{1}{2}}$-norm.*

Consider the following finite element spaces

$$\mathcal{P}_{\rm c}^k(\mathcal{T}_h) = \{v_h \in C^0(\Omega); \forall T \in \mathcal{T}_h, v_h|_T \in \mathbb{P}_k\}, \tag{6.28}$$

$$\mathcal{P}_{\rm d}^k(\mathcal{F}_h) = \{q_h \in L^2(\Gamma); \forall F \in \mathcal{F}_h, q_h|_F \in \mathbb{P}_k\}, \qquad \mathcal{P}_{\rm c}^k(\mathcal{F}_h) = \mathcal{P}_{\rm d}^k(\mathcal{F}_h) \cap C^0(\Gamma), \tag{6.29}$$

where for an integer k, $\mathbb{P}_k$ denotes the space of polynomials with total degree $\le k$. We are interested in analyzing the following situations

$$M_h = \mathcal{P}_{\rm d}^0(\mathcal{F}_h), \qquad \Lambda_h = M_h, \qquad V_h \supset \mathcal{P}_{\rm c}^1(\mathcal{T}_h)^d, \tag{6.30}$$

$$M_h = \mathcal{P}_{\rm d}^1(\mathcal{F}_h), \qquad \Lambda_h = M_h, \qquad V_h \supset \mathcal{P}_{\rm c}^2(\mathcal{T}_h)^d, \tag{6.31}$$

$$M_h = \mathcal{P}_{\rm d}^1(\mathcal{F}_h), \qquad \Lambda_h = \mathcal{P}_{\rm c}^1(\mathcal{F}_h), \qquad V_h = \mathcal{P}_{\rm c}^2(\mathcal{T}_h)^d. \tag{6.32}$$

In (6.30) and (6.31), the most robust choice is to take for V_h, respectively, the continuous first-order and second-order finite element spaces augmented with suitable face bubbles on Γ, leading to an inf-sup constant β_h in (6.27) *independent of* h in both 2D/1D and 3D/2D settings; see [8, 64]. In 2D/1D whenever at least one of the endpoints of Γ is free, it is also possible to take $V_h = \mathcal{P}_{\rm c}^1(\mathcal{T}_h)^d$ in (6.30) or $V_h = \mathcal{P}_{\rm c}^2(\mathcal{T}_h)^d$ in (6.31); then, the discrete inf-sup condition (6.27) still holds, but the constant β_h is of order h. The choice (6.32) has been introduced in [93] and differs from the two previous choices in the fact that $\Lambda_h \neq M_h$. The idea is to avoid the use of face bubbles on Γ by simply taking $V_h = \mathcal{P}_{\rm c}^2(\mathcal{T}_h)^d$, to ensure a robust discrete inf-sup condition (with β_h independent of h) by restricting Λ_h to $\mathcal{P}_{\rm c}^1(\mathcal{F}_h)$, and to keep M_h as a discontinuous finite element space to be able to use a collocation method.

In all cases resulting from (6.30)–(6.32), there holds $M_h = \mathcal{P}_{\rm d}^k(\mathcal{F}_h)$ with $k \in \{0,1\}$, and it is readily verified that there is a family of nodes $(\xi_i^F)_{1\le i\le n_q, F\in\mathcal{F}_h}$ such that

- the associated shape functions form a basis of M_h (in 2D/1D, $n_q = k+1$ and the usual Gauss nodes are used; in 3D/2D, if $k=0$, $n_q = 1$ and the barycenter of each $F \in \mathcal{F}_h$ is used, while if $k=1$, $n_q = 3$ and the midpoints of the three edges of each $F \in \mathcal{F}_h$ are used);
- there are *positive* weights $(\omega_i^F)_{1\le i\le n_q, F\in\mathcal{F}_h}$ such that for all $q_h, r_h \in M_h$,

$$(q_h, r_h)_M = \sum_{F\in\mathcal{F}_h} \sum_{i=1}^{n_q} \omega_i^F q_h(\xi_i^F) r_h(\xi_i^F). \tag{6.33}$$

In other words, on all $F \in \mathcal{F}_h$, the quadrature with nodes $(\xi_i^F)_{1\le i\le n_q}$ and weights $(\omega_i^F)_{1\le i\le n_q}$ is at least of degree $2k$. For further use, it is convenient to define the bilinear form

$$C^0(\mathcal{F}_h)\times C^0(\mathcal{F}_h) \ni (q_h, r_h) \longmapsto (q_h, r_h)_{M_h} := \sum_{F\in\mathcal{F}_h} \sum_{i=1}^{n_q} \omega_i^F q_h(\xi_i^F) r_h(\xi_i^F) \in \mathbb{R}, \tag{6.34}$$

where $C^0(\mathcal{F}_h)$ denotes the space of functions whose restriction to every $F \in \mathcal{F}_h$ is continuous.

6.4.2 The discrete augmented Lagrangian formulation

Set $Y_h = V_h \times M_h$ and $K_h = V_h \times M_h^+$ where

$$M_h^+ := \{q_h \in M_h;\ \forall F \in \mathcal{F}_h,\ \forall 1 \le i \le n_q,\ q_h(\xi_i^F) \ge 0\}. \tag{6.35}$$

Observe that $M_h^+ \subset M^+$ if $k = 0$ (that is, functions in M_h^+ are indeed non-negative), whereas this is no longer the case if $k = 1$, thereby introducing an additional source of nonconformity in the approximation. Let

$$\tilde{B}_h : Y_h \ni y_h := (v_h, q_h) \longmapsto \tilde{B}_h y_h := \Pi_{\Lambda_h}(Bv_h - q_h) \in \Lambda_h. \tag{6.36}$$

Whenever $\Lambda_h \neq M_h$, we will also need the operator

$$\tilde{B}_h^\sharp : Y_h \ni y_h := (v_h, q_h) \longmapsto \tilde{B}_h^\sharp y_h := \Pi_{M_h} Bv_h - q_h \in M_h, \tag{6.37}$$

where Π_{M_h} denotes the L^2-orthogonal projection from M onto M_h. We define the discrete augmented Lagrangian as

$$L_{r,h} : Y_h \times \Lambda_h \ni (y_h, \lambda_h) \longmapsto L_{r,h}(y_h, \lambda_h) := J_{0,h}(y_h) + (\lambda_h, \tilde{B}_h y_h)_M + \frac{r}{2}\|\tilde{B}_h^\sharp y_h\|_M^2 \in \mathbb{R}, \tag{6.38}$$

where r is a non-negative parameter. Here, for $y_h := (v_h, q_h) \in Y_h$,

$$J_{0,h}(y_h) := W(v_h) + (\psi(q_h), 1)_{M_h}, \tag{6.39}$$

that is, the energy associated with the cohesive forces is evaluated using a quadrature, and it is convenient to set

$$J_{r,h}(y_h) := J_{0,h}(y_h) + \frac{r}{2}\|\tilde{B}_h^\sharp y_h\|_M^2. \tag{6.40}$$

Observe that the penalty term in (6.38) and in (6.40) is stronger than the usual penalty term associated with the constraint $\tilde{B}_h y_h = 0$ in Λ_h; indeed, owing to the fact that $\Lambda_h \subset M_h$, there holds

$$\forall y_h \in Y_h, \qquad \|\tilde{B}_h y_h\|_M \le \|\tilde{B}_h^\sharp y_h\|_M. \tag{6.41}$$

The discrete decomposed problem takes the following form

$$\min_{y_h \in K_h \cap \ker \tilde{B}_h} J_{r,h}(y_h). \tag{6.42}$$

Proposition 6.6. *There exists a solution to the discrete decomposed problem* (6.42).

Proof. The functional $J_{r,h}$ is coercive and continuous, and the set $K_h \cap \ker \tilde{B}_h$ is nonempty and closed. In finite dimension, this suffices for the existence of a global minimizer.

We now investigate sufficient conditions for the functional $J_{r,h}$ to be α-convex over $K_h \cap \ker \tilde{B}_h$ (and thus the solution of (6.42) to be unique). Since we are working in a nonconforming framework ($M_h \subset M$, but $M_h \not\subset H$), it is convenient to equip $Y_h \subset Z := V \times M$ with the natural norm of Z and to formulate duality products using Z. We first treat the simpler case $\Lambda_h = M_h$.

Proposition 6.7. *Assume* $\alpha_W - k_{\psi'} c_M^2 c_B^2 > 0$ *and* $\Lambda_h = M_h$. *Then, the functional* $J_{r,h}$ *is* α*-convex on* $K_h \cap \ker \tilde{B}_h$, *namely there is* $\alpha > 0$ *such that for all* $r \ge 0$,

$$\forall y_h, z_h \in K_h \cap \ker \tilde{B}_h, \qquad \langle J'_{r,h}(y_h) - J'_{r,h}(z_h), y_h - z_h\rangle_{Z',Z} \ge \alpha \|y_h - z_h\|_Z^2. \tag{6.43}$$

Proof. Let $y_h, z_h \in K_h \cap \ker \tilde{B}_h$ with $y_h := (v_h, q_h)$ and $z_h := (w_h, r_h)$. Set $A = \langle J'_{r,h}(y_h) - J'_{r,h}(z_h), y_h - z_h\rangle_{Z',Z}$.
Since $\Lambda_h = M_h$, the penalty term in (6.40) vanishes for $y_h, z_h \in \ker \tilde{B}_h$. As a result,

$$\begin{aligned} A &= \langle W'(v_h) - W'(w_h), v_h - w_h\rangle_{V',V} + (\psi'(q_h) - \psi'(r_h), q_h - r_h)_{M_h} \\ &\geq \alpha_W \|v_h - w_h\|_V^2 - k_{\psi'} \sum_{F\in\mathcal{F}_h} \sum_{i=1}^{n_q} \omega_i^F (q_h(\xi_i^F) - r_h(\xi_i^F))^2, \end{aligned}$$

where we have used the α-convexity of W, the Lipschitz continuity of ψ', and the fact that the weights ω_i^F are positive. Moreover, since the quadrature is at least of degree $2k$, since $\Pi_{\Lambda_h} B(v_h - w_h) = q_h - r_h$ by assumption, and owing to the conformity of V_h, it is inferred that

$$\begin{aligned} A &\geq \alpha_W \|v_h - w_h\|_V^2 - k_{\psi'} \|q_h - r_h\|_M^2 \\ &= \alpha_W \|v_h - w_h\|_V^2 - k_{\psi'} \|\Pi_{\Lambda_h} B(v_h - w_h)\|_M^2 \\ &\geq \alpha_W \|v_h - w_h\|_V^2 - k_{\psi'} \|B(v_h - w_h)\|_M^2 \\ &\geq (\alpha_W - k_{\psi'} c_M^2 c_B^2) \|v_h - w_h\|_V^2, \end{aligned}$$

whence the conclusion readily follows since $\|q_h - r_h\|_M \leq c_M c_B \|v_h - w_h\|_V$.

Proposition 6.8. *Assume $\alpha_W - 2k_{\psi'} c_M^2 c_B^2 > 0$. Then, (6.43) still holds if $r > 4k_{\psi'}$ and if h is small enough.*

Proof. Proceeding as above leads to

$$\begin{aligned} A &\geq \alpha_W \|v_h - w_h\|_V^2 - k_{\psi'} \|q_h - r_h\|_M^2 + r \|\tilde{B}_h^\sharp (y_h - z_h)\|_M^2 \\ &\geq \alpha_W \|v_h - w_h\|_V^2 - 2k_{\psi'} \|\Pi_{\Lambda_h} B(v_h - w_h)\|_M^2 - 2k_{\psi'} \|(I - \Pi_{\Lambda_h})(q_h - r_h)\|_M^2 + r \|\tilde{B}_h^\sharp (y_h - z_h)\|_M^2 \\ &= (\alpha_W - 2k_{\psi'} c_M^2 c_B^2) \|v_h - w_h\|_V^2 - 2k_{\psi'} \|(I - \Pi_{\Lambda_h})(q_h - r_h)\|_M^2 + r \|\Pi_{M_h} B(v_h - w_h) - (q_h - r_h)\|_M^2, \end{aligned}$$

since $\Pi_{\Lambda_h} B(v_h - w_h) = \Pi_{\Lambda_h}(q_h - r_h)$. The last term in the right-hand side can be transformed into

$$\begin{aligned} \|\Pi_{M_h} B(v_h - w_h) - (q_h - r_h)\|_M^2 &= \|\Pi_{M_h} B(v_h - w_h) - \Pi_{\Lambda_h} B(v_h - w_h) - (I - \Pi_{\Lambda_h})(q_h - r_h)\|_M^2 \\ &\geq \frac{1}{2} \|(I - \Pi_{\Lambda_h})(q_h - r_h)\|_M^2 - \|\Pi_{M_h} B(v_h - w_h) - \Pi_{\Lambda_h} B(v_h - w_h)\|_M^2 \\ &\geq \frac{1}{2} \|(I - \Pi_{\Lambda_h})(q_h - r_h)\|_M^2 - \|(I - \Pi_{\Lambda_h}) B(v_h - w_h)\|_M^2 \end{aligned}$$

since $\Lambda_h \subset M_h$. Moreover, in all cases for Λ_h,

$$\|(I - \Pi_{\Lambda_h}) B(v_h - w_h)\|_M \lesssim h^{1/2} \|B(v_h - w_h)\|_H \lesssim h^{1/2} \|v_h - w_h\|_V.$$

To conclude, observe that $\|\Pi_{\Lambda_h}(q_h - r_h)\|_M = \|\Pi_{\Lambda_h} B(v_h - w_h)\|_M \leq c_M c_B \|v_h - w_h\|_V$.

As in the continuous case, the discrete decomposed problem (6.42) is tackled by solving the stationarity conditions for the discrete augmented Lagrangian $L_{r,h}$, that is, we seek $x_h := (u_h, p_h) \in V_h \times M_h^+$ and $\theta_h \in \Lambda_h$ such that

$$\langle W'(u_h), v_h\rangle_{V',V} + (\theta_h, Bv_h)_M + r(\Pi_{M_h} Bu_h - p_h, Bv_h)_M = 0, \qquad \forall v_h \in V_h, \tag{6.44}$$

$$(\psi'(p_h), q_h - p_h)_{M_h} - (\theta_h, q_h - p_h)_M - r(Bu_h - p_h, q_h - p_h)_M \geq 0, \qquad \forall q_h \in M_h^+, \tag{6.45}$$

$$(\lambda_h, Bu_h - p_h)_M = 0, \qquad \forall \lambda_h \in \Lambda_h. \tag{6.46}$$

By proceeding as in the continuous case (and using additional simplifications due to the finite-dimensional setting), the following equivalence result is readily verified.

Proposition 6.9. *If (x_h, θ_h) is a local saddle-point of $L_{r,h}$ on $K_h \times \Lambda_h$, then $x_h \in K_h \cap \ker \tilde{B}_h$ is a local minimizer of the discrete decomposed problem (6.42). Conversely, let $x_h \in K_h \cap \ker \tilde{B}_h$ be a local minimizer of the discrete decomposed problem (6.42). Then, there exists a unique $\theta_h \in \Lambda_h$ such that (x_h, θ_h) is a stationary point of $L_{r,h}$ on $K_h \times \Lambda_h$. Moreover, if the following second-order condition holds,*

$$\langle J''_{0,h}(x_h), (d_h, d_h)\rangle > 0, \qquad \forall d_h \in (V_h \times \overline{C_{+,h}(x_h)}) \cap \ker \tilde{B}_h \setminus \{0\}, \tag{6.47}$$

where $C_{+,h}(x_h) = \{d_h \in M_h; \exists \alpha > 0,\ p_h + \alpha d_h \in M_h^+\}$, then (x_h, θ_h) is a local saddle-point of the augmented Lagrangian on $K_h \times \Lambda_h$ for r large enough.

Remark 6.6. *In the decomposition-coordination method or when assembling the Jacobian matrix in Newton's method (see Section 6.5), the variational inequality (6.45) has to be solved with fixed u_h and θ_h. This amounts to a nonlinear problem of size the dimension of M_h, namely of size $n_q \times N_\Gamma$ where n_q is defined above and where N_Γ stands for the cardinal number of the set $\mathcal{F}_h$. The key point is that since the underlying quadrature is at least of degree $2k$, (6.45) is equivalent to*

$$(\psi'(p_h), q_h - p_h)_{M_h} - (\theta_h, q_h - p_h)_{M_h} - r(Bu_h - p_h, q_h - p_h)_{M_h} \geq 0, \qquad \forall q_h \in M_h^+, \tag{6.48}$$

and using the nodal basis of M_h, this leads to $n_q \times N_\Gamma$ uncoupled one-dimensional nonlinear problems. Note that (6.48) amounts to the minimization problem

$$\min_{q_h \in M_h^+} (\psi_h(q_h), 1)_{M_h} - (\theta_h, q_h)_M + \frac{r}{2} \|\tilde{B}_h^\sharp(y_h, q_h)\|_M^2. \tag{6.49}$$

It is readily verified that for $r \geq k_{\psi'}$, the above functional is convex so that the minimization problem (6.49) has a unique solution.

6.4.3 Error analysis

This section is devoted to the error analysis for the three choices (6.30)–(6.32) of discrete spaces V_h, M_h, and Λ_h. Their analysis is of increasing complexity. In (6.30) and (6.31), $\Lambda_h = M_h$, while $M_h^+ \subset M^+$ in (6.30), but $M_h^+ \not\subset M^+$ in (6.31); finally, in (6.32), $\Lambda_h \neq M_h$ and $M_h^+ \not\subset M^+$. In all cases, the goal is to obtain error estimates with (quasi)optimal convergence rates in the mesh-size h under the assumption that the exact solution is unique and smooth enough. We assume for the sake of simplicity that the functional $J_{r,h}$ is α-convex on $K_h \cap \ker \tilde{B}_h$ so that the discrete solution is also unique. Sufficient conditions for α-convexity and uniqueness are given by Propositions 6.7 and 6.8 above. In the sequel, (x, θ) with $x := (u, p)$ denotes the exact solution

and (x_h, θ_h) with $x_h := (u_h, p_h)$ denotes the approximate solution. Henceforth, we assume that $\theta \in M$. Then, using the density of H^+ in M^+, (6.19) yields $(\psi'(p) - \theta, q - p)_M \geq 0$ for all $q \in M^+$, whence it is classically deduced that $\psi'(p) - \theta \in M^+$ and that $\mathrm{supp}(\psi'(p) - \theta) \cap \mathrm{supp}(p)$ has zero measure.

We introduce an additional regularity assumption regarding the topology of the subset of Γ where the unilateral constraint $p \geq 0$ is actually active, namely, letting

$$\Gamma_0(p) := \{x \in \Gamma; p(x) = 0\}, \qquad \text{and} \qquad \Gamma_+(p) := \Gamma \setminus \Gamma_0(p), \tag{6.50}$$

we assume that the set $\overline{\mathring{\Gamma_0}(p)} \cap \overline{\Gamma_+(p)}$ is

– in 2D/1D, a finite union of points;

– in 3D/2D, a finite union of Lipschitz curves.

Under this assumption, henceforth referred to as A[p], a sharper error estimate can be obtained by using the modified Lagrange interpolate introduced by Hüeber and Wohlmuth [69] in the piecewise affine case or its piecewise quadratic extension in 2D/1D introduced in Lemma 6.4 below.

Since we are working in a nonconforming framework ($M_h \not\subset H$ and possibly $M_h^+ \not\subset M^+$) and recalling that we have set $Z := V \times M$, it is convenient to redefine the operator $\tilde{B}$ as $Z \ni y := (v, q) \mapsto Bv - q \in M$ and to extend the domain of the functional J_r to Z. Moreover, taking advantage that for the exact solution $\theta \in M$, the augmented Lagrangian is now redefined as

$$L_r : Z \times M \ni (y, \lambda) \longmapsto L_r(y, \lambda) := J_r(y) + (\lambda, \tilde{B}y)_M \in \mathbb{R}. \tag{6.51}$$

An abstract error estimate

The proof of the following key abstract error estimate is postponed to Appendix 6.7. Observe that the error $(x - x_h)$ is measured in the $\|\cdot\|_Z$-norm, that is the $H^1(\Omega)^d$-norm for the bulk displacement and the $L^2(\Gamma)$-norm for the normal displacement on Γ, while the error $(\theta - \theta_h)$ on the Lagrange multiplier is measured in the $L^2(\Gamma)$-norm scaled by the factor $h^{1/2}$.

Lemma 6.2. *For all $y_h := (v_h, q_h) \in K_h \cap \ker \tilde{B}_h^\sharp$ and for all $q \in M^+$, letting*

$$\eta_{\mathrm{unil}}(q) := (\psi'(p) - \theta, q - p_h)_M, \tag{6.52}$$

$$\eta_{\mathrm{unil}}(q_h) := (\psi'(p) - \theta, q_h - p)_M, \tag{6.53}$$

$$\eta_{\mathrm{quad}}(q_h) := \sup_{r_h \in M_h, \|r_h\|_M = 1} |(\psi'(q_h), r_h)_M - (\psi'(q_h), r_h)_{M_h}|, \tag{6.54}$$

there holds

$$\|x - x_h\|_Z^2 \lesssim \|x - y_h\|_Z^2 + \eta_{\mathrm{unil}}(q_h) + \eta_{\mathrm{quad}}(q_h)^2 + \eta_{\mathrm{unil}}(q) + h^s \|\theta - \Pi_{\Lambda_h} \theta\|_M^2, \tag{6.55}$$

$$\beta_h h^{1/2} \|\theta - \theta_h\|_M \lesssim h^{1/2} \|\theta - \Pi_{\Lambda_h} \theta\|_M + \|x - x_h\|_Z, \tag{6.56}$$

where $s = 1$ if $\Lambda_h = M_h$ and $s = 0$ otherwise.

Remark 6.7. *$\eta_{\mathrm{unil}}(q)$ measures the nonconformity error resulting from $M_h^+ \not\subset M^+$; indeed, if $p_h \in M^+$, taking $q = p_h$ yields $\eta_{\mathrm{unil}}(q) = 0$. $\eta_{\mathrm{quad}}(q_h)$ measures the quadrature error when evaluating the cohesive energy. Finally, $\|x - y_h\|_Z + \eta_{\mathrm{unil}}(q_h)$ measures the interpolation error while accounting for the unilateral constraint.*

The case $M_h = \mathcal{P}^0_{\rm d}(\mathcal{F}_h)$, $\Lambda_h = M_h$, and $V_h \supset \mathcal{P}^1_{\rm c}(\mathcal{T}_h)^d$

Theorem 6.2. *Let $M_h = \mathcal{P}^0_{\rm d}(\mathcal{F}_h)$, $\Lambda_h = M_h$, and $V_h \supset \mathcal{P}^1_{\rm c}(\mathcal{T}_h)^d$. Assume $u \in H^{3/2+\nu}(\Omega)$ with $0 < \nu \le \frac{1}{2}$, so that $p \in H^{1+\nu}(\Gamma)$ and $\theta \in H^\nu(\Gamma)$. Then, in the above framework, there holds*

$$\|x - x_h\|_Z + \beta_h h^{1/2} \|\theta - \theta_h\|_M \lesssim h^{1/2+\nu}. \tag{6.57}$$

Proof. We apply Lemma 6.2 in the setting $\Lambda_h = M_h$ and $\tilde{B}_h^\sharp = \tilde{B}_h$. Since $M_h^+ \subset M^+$ because $M_h = \mathcal{P}^0_{\rm d}(\mathcal{F}_h)$, we can take $q = p_h$ to obtain $\eta_{\rm unil}(q) = 0$. Moreover, it is readily verified that for piecewise constant functions, $\eta_{\rm quad}(q_h) = 0$. It remains to select $y_h := (v_h, q_h) \in K_h \cap \ker \tilde{B}_h$ to estimate $\eta_{\rm unil}(q_h)$ and $\|x - y_h\|_Z$. Let $\mathcal{I}^1_{\rm HW}$ be the piecewise affine interpolation operator introduced by Hüeber and Wohlmuth; see [69] and also the left panel of Fig. 6.3. Recall that $\mathcal{I}^1_{\rm HW} p \ge 0$ on Γ and that $\mathrm{supp}(\mathcal{I}^1_{\rm HW} p) \subset \mathrm{supp}(p)$. In particular, since $\mathrm{supp}(\psi'(p) - \theta) \cap \mathrm{supp}(p)$ has zero measure, it is inferred that $(\psi'(p) - \theta, \mathcal{I}^1_{\rm HW} p)_M = 0$. Hence, setting $q_h := \Pi_{M_h} \mathcal{I}^1_{\rm HW} p$, it is clear that $q_h \in M_h^+$ since $M_h = \mathcal{P}^0_{\rm d}(\mathcal{F}_h)$. Moreover, observing that q_h and $\mathcal{I}^1_{\rm HW} p$ have the same support yields

$$\eta_{\rm unil}(q_h) = 0.$$

Now, let $\mathcal{I}^1_{\rm Lag}$ be the usual piecewise affine Lagrange interpolation operator (the same notation is used for interpolating vector-valued functions in Ω and scalar-valued functions on Γ). Define $v_h \in \mathcal{P}^1_{\rm c}(\mathcal{T}_h)^d$ from $\mathcal{I}^1_{\rm Lag} u$ by just modifying the normal component of the nodal values located on Γ so that $B v_h = \mathcal{I}^1_{\rm HW} p$ on Γ. Then, by construction, $y_h := (v_h, q_h) \in K_h \cap \ker \tilde{B}_h$. In addition, since $u \in H^{3/2+\nu}(\Omega)$, standard interpolation properties (see, e.g., [44]) lead to

$$\|u - \mathcal{I}^1_{\rm Lag} u\|_V \lesssim h^{1/2+\nu},$$

and using an inverse inequality, the triangle inequality, standard approximation properties of $\mathcal{I}^1_{\rm Lag}$, and the fact that $p \in H^{1+\nu}(\Gamma)$ yields

$$\|\mathcal{I}^1_{\rm Lag} u - v_h\|_V \lesssim h^{-1/2} \|\mathcal{I}^1_{\rm Lag} p - \mathcal{I}^1_{\rm HW} p\|_M \le h^{-1/2} (h^{1+\nu} + \|p - \mathcal{I}^1_{\rm HW} p\|_M).$$

Assumption A[p] is now used to infer that $\|p - \mathcal{I}^1_{\rm HW} p\|_M \lesssim h^{1+\nu}$; see [69]. Collecting the above estimates yields $\|u - v_h\|_V \lesssim h^{1/2+\nu}$ and since

$$\|p - q_h\|_M \le \|p - \Pi_{M_h} p\|_M + \|\Pi_{M_h}(p - \mathcal{I}^1_{\rm HW} p)\|_M \le \|p - \Pi_{M_h} p\|_M + \|p - \mathcal{I}^1_{\rm HW} p\|_M \lesssim h,$$

and recalling that $\nu \le \frac{1}{2}$, it is inferred that

$$\|x - y_h\|_Z \lesssim h^{1/2+\nu}.$$

Finally, since $\theta \in H^\nu(\Gamma)$, $\|\theta - \Pi_{\Lambda_h} \theta\|_M \lesssim h^\nu$, whence the conclusion is straightforward.

Remark 6.8. *Without assumption A[p], $\eta_{\rm unil}(q_h)$ can be estimated by taking $q_h = \Pi_{M_h} \mathcal{I}^1_{\rm Lag} p$. Since ψ' is Lipschitz continuous and $\nu \le \frac{1}{2}$, $\zeta := \psi'(p) - \theta \in H^\nu(\Gamma)$. Hence, $\eta_{\rm unil}(q_h) \le \|\zeta - \Pi_{M_h} \zeta\|_M \|p - \Pi_{M_h} \mathcal{I}^1_{\rm Lag} p\|_M \lesssim h^\nu \|p - \Pi_{M_h} \mathcal{I}^1_{\rm Lag} p\|_M \lesssim h^{1+\nu}$, so that the upper bound in* (6.57) *becomes $h^{1/2+\nu/2}$.*

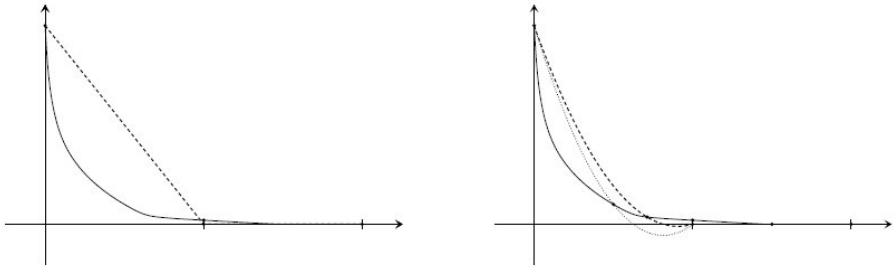

Fig. 6.3. Principle of the Hüeber–Wohlmuth interpolate; left: piecewise affine case; right: piecewise quadratic case.

The case $M_h = \mathcal{P}^1_{\rm d}(\mathcal{F}_h)$, $\Lambda_h = M_h$, and $V_h \supset \mathcal{P}^2_{\rm c}(\mathcal{T}_h)^d$

Theorem 6.3. *Let $M_h = \mathcal{P}^1_{\rm d}(\mathcal{F}_h)$, $\Lambda_h = M_h$, and $V_h \supset \mathcal{P}^2_{\rm c}(\mathcal{T}_h)^d$. Assume $u \in H^{2+\nu}(\Omega)$ with $0 < \nu \le \frac{1}{2}$, so that $p \in H^{3/2+\nu}(\Gamma)$ and $\theta \in H^{1/2+\nu}(\Gamma)$. Then, in the above framework, there holds in 3D/2D,*

$$\|x - x_h\|_Z + \beta_h h^{1/2} \|\theta - \theta_h\|_M \lesssim h^{3/4+\nu/2}. \tag{6.58}$$

Moreover, in 2D/1D, if ψ is of class $C^n 2$ with ψ'' Lipschitz continuous,

$$\|x - x_h\|_Z + \beta_h h^{1/2} \|\theta - \theta_h\|_M \lesssim h^{1+\nu}. \tag{6.59}$$

Proof. Again, we apply Lemma 6.2 in the setting $\Lambda_h = M_h$ and $\tilde{B}_h^\sharp = \tilde{B}_h$. Consider first $\eta_{\rm unil}(q)$. Take $q = \Pi_0 p_h$, where Π_0 denotes the M-orthogonal projection onto $\mathcal{P}^0_{\rm d}(\mathcal{F}_h)$, and observe that $q \in M^+$. Letting $\zeta := \psi'(p) - \theta$, this yields

$$\begin{aligned}
\eta_{\rm unil}(q) &= (\zeta, \Pi_0 p_h - p_h)_M = (\zeta - \Pi_0\zeta, \Pi_0 p_h - p_h)_M \\
&= (\zeta - \Pi_0\zeta, \Pi_0 p_h - \Pi_0 p + \Pi_0 p - p + p - p_h)_M \\
&\lesssim \|\zeta - \Pi_0\zeta\|_M (h^{1/2}\|p - p_h\|_H + \|\Pi_0 p - p\|_M),
\end{aligned}$$

where the H-stability of Π_0 has been used owing to the quasi-uniformity of the mesh on Γ and since $\|\zeta - \Pi_0\zeta\|_{H'} \lesssim h^{1/2}\|\zeta - \Pi_0\zeta\|_M$. Moreover,

$$\begin{aligned}
\|p - p_h\|_H = \|Bu - \Pi_{\Lambda_h} Bu_h\|_H &\le \|Bu - \Pi_{\Lambda_h} Bu\|_H + \|\Pi_{\Lambda_h}(Bu - Bu_h)\|_H \\
&\lesssim \|Bu - \Pi_{\Lambda_h} Bu\|_H + \|Bu - Bu_h\|_H \lesssim h^{1+\nu} + \|u - u_h\|_V.
\end{aligned}$$

Since ψ' is Lipschitz continuous and $\nu \le \frac{1}{2}$, classical properties of superposition operators [94] yield $\zeta \in H^{1/2+\nu}(\Gamma)$, so that $\|\zeta - \Pi_0\zeta\|_M \lesssim h^{1/2+\nu}$. Moreover, $\|\Pi_0 p - p\|_M \lesssim h$ since $p \in H^1(\Gamma)$. Hence,

$$\eta_{\rm unil}(q) \lesssim h^{1+\nu}\|u - u_h\|_V + h^{3/2+\nu}.$$

Consider now $\eta_{\rm quad}(q_h)$ for $q_h \in M_h$. Since the quadrature is at least of degree two, letting $\mathcal{I}^1_\xi$ be the (discontinuous) interpolation operator at the Gauss nodes, there holds

$$\eta_{\rm quad}(q_h) \le \|\psi'(q_h) - \mathcal{I}^1_\xi(\psi'(q_h))\|_M.$$

Since ψ' is Lipschitz continuous, $\psi'(q_h)$ is in $H^1(\mathcal{F}_h)$, the usual broken Sobolev space on the mesh $\mathcal{F}_h$, and there holds $\|\psi'(q_h)\|_{H^1(\mathcal{F}_h)} \lesssim \|q_h\|_{H^1(\mathcal{F}_h)}$. Hence,

$$\eta_{\rm quad}(q_h) \lesssim h\|q_h\|_{H^1(\mathcal{F}_h)}.$$

Consider now $\eta_{\rm unil}(q_h)$ and $\|x - y_h\|_Z$. In 3D/2D, we set $v_h = \mathcal{I}^2_{\rm Lag}u$, the piecewise quadratic Lagrange interpolate of u, and $q_h = \Pi_{M_h}\mathcal{I}^2_{\rm Lag}p$. Then, $q_h \in M_h^+$; see Lemma 6.3 below. Moreover,

$$\eta_{\rm unil}(q_h) \lesssim \|p - q_h\|_M \lesssim h^{3/2+\nu},$$

and $\|x - y_h\|_Z \lesssim h^{1+\nu}$. Finally, $\|\theta - \Pi_{\Lambda_h}\theta\|_M \lesssim h^{1/2+\nu}$. Collecting the above estimates yields (6.58).

In 2D/1D, we consider the piecewise quadratic extension, $\mathcal{I}^2_{\rm HW}$, of the Hüeber–Wohlmuth interpolation operator; see Lemma 6.4 below. Then, we set $q_h = \Pi_{M_h}\mathcal{I}^2_{\rm HW}p$ and v_h is obtained from $\mathcal{I}^2_{\rm Lag}u$ by just modifying the normal component of the nodal values located on Γ so that $Bv_h = \mathcal{I}^2_{\rm HW}p$. Then, proceeding as in the proof of Theorem 6.2 yields $\eta_{\rm unil}(q_h) = 0$, and $\|x - y_h\|_Z \lesssim h^{1+\nu}$. Furthermore, owing to the assumption on ψ and observing that $(\psi'(q_h))' = \psi''(q_h)q_h'$, it is readily seen using inverse inequalities and the fact that q_h is piecewise affine that $\|\psi'(q_h)\|_{H^{3/2}(\mathcal{F}_h)} \lesssim h^{-1/2}\|q_h\|^2_{H^1(\mathcal{F}_h)}$. Hence,

$$\eta_{\rm quad}(q_h) \lesssim h^{3/2}\|q_h\|^2_{H^1(\mathcal{F}_h)}.$$

Finally, still using assumption A[p], the above estimate on $\eta_{\rm unil}(q)$ can be sharpened using the fact that (see [66, Theorem 4.4]) $(\zeta - \Pi_0\zeta, \Pi_0 p - p)_M \lesssim h^{2+2\nu}$ yielding

$$\eta_{\rm unil}(q) \lesssim h^{1+\nu}\|u - u_h\|_V + h^{2+2\nu}.$$

Collecting the above estimates yields (6.59).

Lemma 6.3. *Let F be a triangle, let $u \in \mathbb{P}_2(F)$, and assume that u is non-negative at the six interpolation nodes of $\mathcal{I}^2_{\rm Lag}$ in F. Let $\Pi_1 u$ be the L^2-orthogonal projection of u onto $\mathbb{P}_1(F)$. Let $(\xi_i^F)_{1\le i\le 3}$ be the midpoints of the three edges of F. Then, for all $1 \le i \le 3$, $\Pi_1 u(\xi_i^F) \ge 0$.*

Proof. Let $(\phi_i^F)_{1\le i\le 3}$ be the (Crouzeix–Raviart) basis functions associated with the nodes $(\xi_i^F)_{1\le i\le 3}$. Observe that for all $1 \le i \le 3$,

$$\frac{1}{3}\Pi_1 u(\xi_i^F) = \frac{1}{|F|}\int_F u\phi_i^F.$$

Moreover, using the classical 7-point quadrature of degree 3 yields

$$\int_F u\phi_1^F = \frac{3}{20}u(\gamma^F) + \frac{2}{15}u(\xi_1^F) + \frac{1}{20}(u(\sigma_2^F) + u(\sigma_3^F) - u(\sigma_1^F)),$$

where γ^F denotes the barycenter of F and σ_i^F is the vertex of F opposite the edge containing ξ_i^F. Furthermore, since $u \in \mathbb{P}_2(F)$,

$$u(\gamma^F) = \frac{1}{3}(u(\sigma_1^F) + u(\sigma_2^F) + u(\sigma_3^F)) + \frac{4}{9}(u(\xi_1^F) + u(\xi_2^F) + u(\xi_3^F)),$$

so that $\int_F u\phi_1^F$ is a linear combination of non-negative terms. The same holds for $i \in \{2, 3\}$.

Lemma 6.4. *Assume $\Omega \subset \mathbb{R}^2$. Then, there exists an interpolation operator $\mathcal{I}^2_{\mathrm{HW}} : H^1(\Gamma) \to \mathcal{P}^2_{\mathrm{c}}(\mathcal{F}_h)$ such that*

(i) *if $q \geq 0$, then $\mathcal{I}^2_{\mathrm{HW}} q(\xi_i^F) \geq 0$ for all $1 \leq i \leq n_q$ and for all $F \in \mathcal{F}_h$;*

(ii) $\mathrm{supp}(\mathcal{I}^2_{\mathrm{HW}} q) \subset \mathrm{supp}(q)$;

(iii) *if $p \in H^{3/2+\nu}(\Gamma)$, $\nu \leq \frac{3}{2}$, satisfies Assumption* A[p], *then $\|p - \mathcal{I}^2_{\mathrm{HW}} p\|_M \lesssim h^{3/2+\nu}$.*

Proof. Consider first the usual, piecewise quadratic Lagrange interpolate of q, say $\mathcal{I}^2_{\mathrm{Lag}} q$. Since $\Omega \subset \mathbb{R}^2$, each $F \in \mathcal{F}_h$ is a segment and the restriction of $\mathcal{I}^2_{\mathrm{Lag}} q$ to F can be specified by its values at the endpoints and the midpoint of F. Two modifications need to be implemented. Firstly, as for $\mathcal{I}^1_{\mathrm{HW}}$, if for $F \in \mathcal{F}_h$, $F \cap \{x \in \Gamma; q(x) = 0\}$ has nonzero measure, the three nodal values of $\mathcal{I}^2_{\mathrm{HW}} q$ are set to zero on F. This suffices to guarantee Property (ii). However, contrary to the construction of $\mathcal{I}^1_{\mathrm{HW}}$, this does not suffice to guarantee Property (i). To this purpose a further modification is needed. Let $F \in \mathcal{F}_h$ and assume that $\mathcal{I}^2_{\mathrm{Lag}} q$ is negative at one quadrature node (it cannot take negative values at the two quadrature nodes since it takes non-negative values at the interval endpoints and midpoint and can have only one minimizer). Then, instead of interpolating at the midpoint, we interpolate at this quadrature node; see the right panel of Fig. 6.3. To verify that the resulting quadratic interpolate is still non-negative at the other quadrature node, consider the reference interval $[0,1]$ with $\xi_\pm = \frac{1}{2}(1 \pm \frac{1}{\sqrt{3}})$. Let $\lambda_0(t) = 1 - t$, $\lambda_1(t) = t$, and $b(t) = 4t(1-t)$ so that the usual quadratic Lagrange interpolate of a non-negative function q takes the form

$$\alpha\lambda_0(t) + \beta\lambda_1(t) + (\gamma - \tfrac{1}{2}(\alpha+\beta))b(t),$$

with non-negative coefficients $\alpha = q(0)$, $\beta = q(1)$, and $\gamma = q(\frac{1}{2})$. If this interpolate is negative at, say, ξ_+, this yields $\frac{1}{6}(\alpha+\beta) + \frac{2}{3}\gamma - \frac{1}{2\sqrt{3}}(\alpha-\beta) \leq 0$, so that $\alpha \geq \beta$. Now, the Lagrange interpolate using the two endpoints and the node ξ_+ takes the form

$$\alpha\lambda_0(t) + \beta\lambda_1(t) + \frac{3}{2}(\delta - \alpha\lambda_0(\xi_+) - \beta\lambda_1(\xi_+))b(t),$$

with $\delta = q(\xi_+)$ and evaluating this expression at ξ_- yields $\delta + \frac{1}{\sqrt{3}}(\alpha - \beta) \geq 0$. This proves Property (i). Finally, Property (iii) is established as in [69] using Assumption A[p] and the fact that a possible interpolation at a quadrature node and not at a midpoint does not alter the asymptotic accuracy of the quadratic Lagrange interpolate.

Remark 6.9. *Similar error estimates have been obtained for quadratic approximations of two-field formulations of unilateral contact problems in [66]. Estimate* (6.58) *is suboptimal and does not use assumption A[p]. Instead, estimate* (6.59) *is optimal and relies, in particular, on this latter assumption. Without this assumption, estimate* (6.58) *holds in 2D/1D; the only modification of the above proof in 3D/2D is in the choice of $q_h \in M_h^+$ to estimate $\eta_{\mathrm{unil}}(q_h)$, where the Lagrange interpolation can be performed at a quadrature node instead of at the edge midpoint, similarly to the proof of Lemma 6.4. This remark also applies to the conclusions of Theorem 6.4 below.*

The case $M_h = \mathcal{P}^1_{\mathrm{d}}(\mathcal{F}_h)$, $\Lambda_h = \mathcal{P}^1_{\mathrm{c}}(\mathcal{F}_h)$, and $V_h = \mathcal{P}^2_{\mathrm{c}}(\mathcal{T}_h)^d$

Theorem 6.4. *Let $M_h = \mathcal{P}^1_{\mathrm{d}}(\mathcal{F}_h)$, $\Lambda_h = \mathcal{P}^1_{\mathrm{c}}(\mathcal{F}_h)$, and $V_h = \mathcal{P}^2_{\mathrm{c}}(\mathcal{T}_h)^d$. Assume $u \in H^{2+\nu}(\Omega)$ with $0 < \nu \leq \frac{1}{2}$, so that $p \in H^{3/2+\nu}(\Gamma)$, and also assume $\theta \in H^{1+\nu}(\Gamma)$. Then, in the above framework, there holds in 3D/2D,*

$$\|x - x_h\|_Z + \beta_h h^{1/2} \|\theta - \theta_h\|_M \lesssim h^{3/4+\nu/2}. \tag{6.60}$$

Moreover, in 2D/1D, if ψ is of class $C^n 2$ with ψ'' Lipschitz continuous,

$$\|x - x_h\|_Z + \beta_h h^{1/2} \|\theta - \theta_h\|_M \lesssim h^{1+\nu}. \tag{6.61}$$

Proof. We apply Lemma 6.2 in the setting $\Lambda_h \neq M_h$. We proceed as above, except for the interpolation error on the Lagrange multiplier for which there holds $\|\theta - \Pi_{\Lambda_h}\theta\|_M \lesssim h^{1+\nu}$ since $\theta \in H^{1+\nu}(\Gamma)$.

6.5 Algorithms

In this section, we present two iterative algorithms for solving the discrete problem (6.44)–(6.46), namely a decomposed version of a classical Uzawa algorithm and a nonsmooth Newton's method.

6.5.1 A decomposed Uzawa algorithm

The first algorithm we propose is a decomposed version of a classical iterative Uzawa algorithm. Each iteration of the decomposed algorithm consists of the following steps:

$$u_h^{n+1} \leftarrow \arg \min_{v_h \in V_h} L_{r,h}(v_h, p_h^n; \theta_h^n), \tag{6.62}$$

$$p_h^{n+1} \leftarrow \arg \min_{q_h \in M_h^+} L_{r,h}(u_h^{n+1}, q_h; \theta_h^n), \tag{6.63}$$

$$\theta_h^{n+1} \leftarrow \theta_h^n + \rho \Pi_{\Lambda_h}(\Pi_{M_h} B_h u_h^{n+1} - p_h^{n+1}), \tag{6.64}$$

where ρ is an arbitrary positive parameter. Instead of minimizing directly the Lagrangian with respect to the couple (u_h^n, p_h^n), the Lagrangian is minimized with respect to u_h^n and then with respect to p_h^n. This is the difference with the classical Uzawa algorithm.

Step (6.62) amounts to the solution of a linear system. Moreover, at each iteration, only the right-hand side changes. Hence, this step can be efficiently solved once a factorization method has been initially performed (LU factorization for instance). Step (6.63) is solved by the collocation method described in Section 4.1. Finally, Step (6.64) is straightforward if $\Lambda_h = M_h$ since it can be performed elementwise. Otherwise, it requires a projection onto Λ_h by inverting a global mass matrix.

Remark 6.10. *This algorithm corresponds to ALG2 in [49], where a slightly different version called ALG3, equivalent to the LATIN method [84], is also proposed.*

We now prove a global convergence result for the decomposed Uzawa algorithm in the case where $\Lambda_h = M_h$ and under the convexity condition (6.8). Recall that this condition implies the α-convexity of the discrete functional $J_{r,h}$ and thus the uniqueness of the discrete solution (u_h, p_h, θ_h). The following proposition yields sufficient conditions on the parameters r and ρ for global convergence. Its proof is postponed to Appendix 6.8.

Proposition 6.10. *Assume $\Lambda_h = M_h$ and the convexity condition $\alpha_W - 2k_{\psi'}c_M^2 c_B^2 > 0$. If the parameters r and ρ are such that*

$$r \geq \rho \geq 4k_{\psi'}, \tag{6.65}$$

Algorithm (6.62)–(6.64) *is well-defined and converges to the discrete solution (u_h, p_h, θ_h) for any initialization.*

Remark 6.11. *When the functional is nonconvex, a convergence result exists for the classical Uzawa algorithm [10]. We did not try to extend it to the decomposed version described here.*

6.5.2 A nonsmooth Newton's method

Let (u_h, p_h, θ_h) solve (6.44)–(6.46). Given u_h and θ_h, the variational inequality (6.45) is equivalent to the minimization problem (6.49). Recall that for $r \geq k_{\psi'}$, this problem has a unique solution. Hence, p_h can be expressed as a function of u_h and θ_h in the form $p_h := \pi(u_h, \theta_h)$. Equations (6.44) and (6.46) can then be recast as a nonlinear system of equations

$$\left\langle W'(u_h), v_h \right\rangle_{V',V} + (\theta_h, v_h)_M + r(Bu_h - \pi(u_h, \theta_h), Bv_h)_M = 0, \quad \forall v_h \in V_h, \tag{6.66}$$

$$(\lambda_h, Bu_h - \pi(u_h, \theta_h))_M = 0, \qquad \forall \lambda_h \in \Lambda_h, \tag{6.67}$$

or in a compact form with $z_h := (u_h, \theta_h)$,

$$F(z_h) = 0, \tag{6.68}$$

where F maps $V_h \times \Lambda_h$ onto $V_h \times \Lambda_h$. Equation (6.68) can be solved using a Newton's method. However, the function F is continuous but non-differentiable owing to the unilateral constraint. F is locally Lipschitz continuous though, so that, according to Rademacher's theorem, it is differentiable almost everywhere. Denote by $D_F \subset V_h \times \Lambda_h$ the set where F is differentiable. For the points where F is non-differentiable, we introduce the generalized Jacobian as defined in [26],

$$\partial F(z) = co\left\{ \lim_{z_i \to z,\ z_i \in D_F} \nabla F(z_i) \right\}, \tag{6.69}$$

where *co* stands for the convex hull of a set. The nonsmooth Newton's method consists of the step

$$z_h^{n+1} \leftarrow z_h^n - G_n^{-1} F(z_h^n), \tag{6.70}$$

where $G_n \in \partial F(z_h^n)$.

Proposition 6.11. *Let (u_h, θ_h) solve* (6.68). *Assume that all $G \in \partial F(u_h, \theta_h)$ are nonsingular. Then, if $r \geq k_{\psi'}$, Newton's method* (6.70) *is well-defined and converges to (u_h, θ_h) for any initialization sufficiently close to (u_h, θ_h).*

Proof. The function F is said to be semi-smooth at a point $z \in V_h \times \Lambda_h$ if F is locally Lipschitz at z and

$$\lim_{G \in \partial F(z+td),\, d \to e,\, t \to 0^+} Gd \text{ exists for all } e \in V_h \times \Lambda_h. \tag{6.71}$$

We can verify that F is semi-smooth on $V_h \times \Lambda_h$ and conclude using a convergence result [104] on Newton's method for semi-smooth functions.

Remark 6.12. *Newton's method is a local method. To globalize it, a line-search technique with the augmented Lagrangian as merit function can be used.*

6.6 Numerical results

To investigate numerically the proposed methodology, we build a 2D benchmark problem with analytical solution. Let $\Omega :=]0, L_x[\times]0, L_y[$, $\partial\Omega_D := \{L_x\}\times]0, L_y[$ and $\Gamma :=]0, L_x[\times\{0\}$. Consider the cohesive law

$$t(\delta) = \begin{cases} \sigma_c \frac{(\delta - d_c)^2}{d_c^2} & \text{if } \delta \in [0, d_c], \\ 0 & \text{if } \delta > d_c. \end{cases} \tag{6.72}$$

Let $n \geq 2$ and let $L_0 \in \mathbb{R}$ be such that $0 < L_0 < L_x$. Introducing the functions

$$s(x) = \begin{cases} d_c(1 - \frac{x}{L_0})^n & \text{if } x \in [0, L_0], \\ 0 & \text{if } x \in [L_0, L_x], \end{cases} \quad \text{and} \quad \phi(x) = \begin{cases} t(s(x)) & \text{if } x \in [0, L_0], \\ \sigma_c & \text{if } x \in [L_0, L_x], \end{cases} \tag{6.73}$$

the bulk displacement in the analytical solution is set to

$$u(x, y) := \begin{pmatrix} -y s'(x) \\ s(x) + y\phi(x) \end{pmatrix}. \tag{6.74}$$

This solution is built to satisfy the boundary condition of unilateral contact with cohesive forces on Γ. The normal displacement on Γ is given by the function s, and the contact zone corresponds to the interval $[L_0, L_x]$. To complete the specification of the test case, it remains to choose suitable external load and boundary conditions on $\partial\Omega \setminus (\Gamma \cup \partial\Omega_D)$ according to (6.74). We can readily verify that $u \in H^{n-1}(\Omega)$. We also observe that u_Γ does not exceed d_c so that the regularity of t at d_c does not limit the regularity of u.

First, we study the convergence rates for two choices of finite element spaces, namely $V_h = \mathcal{P}^1_{\mathrm{c}}(\mathcal{T}_h)^d$ and $M_h = \Lambda_h = \mathcal{P}^0_{\mathrm{d}}(\mathcal{F}_h)$ (referred to as $\mathbb{P}_1/\mathbb{P}_0$ case) and $V_h = \mathcal{P}^2_{\mathrm{c}}(\mathcal{T}_h)^d$ and $M_h = \Lambda_h = \mathcal{P}^1_{\mathrm{d}}(\mathcal{F}_h)$ (referred to as $\mathbb{P}_2/\mathbb{P}_1$ case). The simulations are performed with the decomposed Uzawa algorithm. The Young modulus and the Poisson ratio are $E = 2 \cdot 10^5$ and $\nu = 0.2$. Further parameters are $L_x = 20$, $L_y = 6$, $L_0 = 10$, $\sigma_c = 0.001$, and $d_c = 0.1$. Observe that the Young modulus is very large so that the continuous and discrete functionals are expected to be convex. The analytical solution is chosen to be in $H^3(\Omega)$ ($n = 4$). The results are summarized in Tables 6.1 and 6.2. Optimal convergence rates are observed in both cases. In the $\mathbb{P}_1/\mathbb{P}_0$ case, this result matches the estimate of Theorem 6.2. In the $\mathbb{P}_2/\mathbb{P}_1$ case, the numerical result improves on the estimate of Theorem 6.3 which is suboptimal. Moreover, in both cases, the Lagrange multiplier super-converges although in the present setting for V_h, the discrete inf-sup condition is not robust with respect to mesh-size.

We now address the convergence of the decomposed Uzawa algorithm. We consider that convergence is reached when the difference between the exact solution and the approximate solution is below a given tolerance. The simulations are performed with $V_h = \mathcal{P}^1_{\mathrm{c}}(\mathcal{T}_h)$ and $M_h = \Lambda_h = \mathcal{P}^0_{\mathrm{d}}(\mathcal{F}_h)$. The numbers of iterations to reach convergence for various couples of parameters (r, ρ) are collected in Table 6.3. The two criteria $r \geq \rho$ and $r > 2k_{\psi'}$ derived in Proposition 6.10 appear to be rather sharp.

h	$\|u-u_h\|_{H^1}$		$\|p-p_h\|_{L^2}$		$\|\theta-\theta_h\|_{L^2}$	
2.83	6.42e-2	-	2.95e-2	-	1.04e-2	-
1.54	2.49e-2	1.55	1.51e-2	1.09	5.93e-3	0.92
0.80	1.02e-2	1.36	7.60e-3	1.04	1.17e-3	2.46
0.40	4.98e-3	1.04	3.80e-3	1.01	2.50e-4	2.25
0.21	2.33e-3	1.13	1.90e-3	1.04	5.35e-5	2.31

Table 6.1. Errors and convergence rates with $V_h = \mathcal{P}^1_{\rm c}(\mathcal{T}_h)^d$ and $M_h = \Lambda_h = \mathcal{P}^0_{\rm d}(\mathcal{F}_h)$.

h	$\|u-u_h\|_{H^1}$		$\|p-p_h\|_{L^2}$		$\|\theta-\theta_h\|_{L^2}$	
2.83	4.12e-3	-	3.53e-3	-	2.94e-4	-
1.54	8.60e-4	2.57	8.87e-4	2.26	1.10e-5	5.38
0.80	1.90e-4	2.29	2.22e-4	2.10	2.95e-6	2.00
0.40	5.31e-5	1.86	5.59e-5	2.01	7.52e-7	1.99
0.21	1.60e-5	1.80	1.48e-5	1.99	1.93e-7	2.03

Table 6.2. Errors and convergence rates with $V_h = \mathcal{P}^2_{\rm c}(\mathcal{T}_h)^d$ and $M_h = \Lambda_h = \mathcal{P}^1_{\rm d}(\mathcal{F}_h)$.

ρ/r	$r = k_{\psi'}$	$r = 2k_{\psi'}$	$r = 10k_{\psi'}$	$r = 20k_{\psi'}$	$r = 100k_{\psi'}$
0.5	∞	13	12	9	5
1.0	∞	32	7	6	3
1.5	∞	∞	11	7	5
2.0	∞	∞	∞	∞	∞

Table 6.3. Number of iterations in the decomposed Uzawa algorithm for various couples (r, ρ).

Remark 6.13. *Numerical results with Newton's method and the choice $V_h = \mathcal{P}^2_{\rm c}(\mathcal{T}_h)$, $M_h = \mathcal{P}^1_{\rm d}(\mathcal{F}_h)$, and $\Lambda_h = \mathcal{P}^1_{\rm c}(\mathcal{F}_h)$ are presented in [93], where optimal convergence rates are reported.*

6.7 Proof of Lemma 6.2

Proof. Let $y_h := (v_h, q_h) \in K_h \cap \ker \tilde{B}_h^\sharp$. Since $\ker \tilde{B}_h^\sharp \subset \ker \tilde{B}_h$ (because $\Lambda_h \subset M_h$), $y_h \in \ker \tilde{B}_h$. As a result, it is inferred from (6.44)–(6.46) that

$$\begin{aligned} 0 &\le \langle J'_{r,h}(x_h), y_h - x_h\rangle_{Z',Z} + (\theta_h, \tilde{B}_h(y_h - x_h))_M \\ &= \langle J'_{r,h}(x_h), y_h - x_h\rangle_{Z',Z}. \end{aligned}$$

Set $\delta_h = x_h - y_h := (\delta_h^v, \delta_h^p)$ and observe that $\delta_h \in \ker \tilde{B}_h$. Then, since $y_h \in \ker \tilde{B}_h^\sharp$,

$$\begin{aligned} \langle J'_{r,h}(x_h) - J'_{r,h}(y_h), \delta_h\rangle_{Z',Z} &\le \langle -J'_{r,h}(y_h), \delta_h\rangle_{Z',Z} = \langle -J'_{0,h}(y_h), \delta_h\rangle_{Z',Z} \\ &= \langle -J'_0(y_h), \delta_h\rangle_{Z',Z} + \langle J'_0(y_h) - J'_{0,h}(y_h), \delta_h\rangle_{Z',Z} \\ &= \langle -J'_0(x), \delta_h\rangle_{Z',Z} + \langle J'_0(x) - J'_0(y_h), \delta_h\rangle_{Z',Z} + \langle J'_0(y_h) - J'_{0,h}(y_h), \delta_h\rangle_{Z',Z} \\ &= \langle -J'_0(x), \delta_h\rangle_{Z',Z} + \langle J'_0(x) - J'_0(y_h), \delta_h\rangle_{Z',Z} + (\psi'(q_h), \delta_h^q)_M - (\psi'(q_h), \delta_h^q)_{M_h} \\ &\lesssim \langle -J'_0(x), \delta_h\rangle_{Z',Z} + (\|x - y_h\|_Z + \eta_{\rm quad}(q_h))\|\delta_h\|_Z, \end{aligned}$$

using the Lipschitz-continuity of J'_0 and the definition (6.54). Focusing on the first term in the right-hand side, we observe that for all $y := (v, q) \in K$,

$$\begin{aligned}\langle -J_0'(x),\delta_h\rangle_{Z',Z} &= \langle -J_0'(x), y-y_h\rangle_{Z',Z} + \langle -J_0'(x), x_h - y\rangle_{Z',Z}\\ &= \langle -J_0'(x), y-y_h\rangle_{Z',Z} + (\theta, \tilde{B}(x_h-y))_M - \langle \partial_y L_0(x,\theta), x_h-y\rangle_{Z',Z}\\ &= \langle -J_0'(x), y-x\rangle_{Z',Z} + \langle -J_0'(x), x-y_h\rangle_{Z',Z} + (\theta,\tilde{B}(x_h-y))_M - \langle \partial_y L_0(x,\theta), x_h-y\rangle_{Z',Z}\\ &\le (\theta,\tilde{B}(x_h-x))_M + \langle -J_0'(x), x-y_h\rangle_{Z',Z} - \langle \partial_y L_0(x,\theta), x_h-y\rangle_{Z',Z}\\ &= (\theta,\tilde{B}(x_h-y_h))_M - \langle \partial_y L_0(x,\theta), x-y_h\rangle_{Z',Z} - \langle \partial_y L_0(x,\theta), x_h-y\rangle_{Z',Z},\end{aligned}$$

where we have used the fact that $\langle -J_0'(x), y-x\rangle_{Z',Z} \le (\theta,\tilde{B}(y-x))_M$ since (x,θ) is the exact solution and $y\in K$. Furthermore, using the definitions (6.52) and (6.53) and the fact that $V_h\subset V$, it is readily seen that

$$\langle \partial_y L_0(x,\theta), y_h - x\rangle_{Z',Z} = (\psi'(p)-\theta, q_h-p)_M = \eta_{\mathrm{unil}}(q_h),$$

and

$$\langle \partial_y L_0(x,\theta), y - x_h\rangle_{Z',Z} = (\psi'(p)-\theta, q-p_h)_M = \eta_{\mathrm{unil}}(q),$$

so that

$$\langle -J_0'(x),\delta_h\rangle_{Z',Z} \le (\theta,\tilde{B}(x_h-y_h))_M + \eta_{\mathrm{unil}}(q_h) + \eta_{\mathrm{unil}}(q).$$

Since H^+ is dense in M^+, the above estimate can be extended by continuity to $q\in M^+$. Furthermore, observing that $(x_h-y_h)\in\ker\tilde{B}_h$, there holds

$$\begin{aligned}\langle -J_0'(x),\delta_h\rangle_{Z',Z} &\le (\theta-\Pi_{\Lambda_h}\theta,\tilde{B}(x_h-y_h))_M + \eta_{\mathrm{unil}}(q_h)+\eta_{\mathrm{unil}}(q)\\ &\le \|\theta-\Pi_{\Lambda_h}\theta\|_M\|\tilde{B}(x_h-y_h)\|_M + \eta_{\mathrm{unil}}(q_h)+\eta_{\mathrm{unil}}(q).\end{aligned}$$

Moreover, if $\Lambda_h = M_h$,

$$\|\tilde{B}(x_h-y_h)\|_M = \|(I-\Pi_{\Lambda_h})B(u_h-v_h)\|_M \lesssim h^{1/2}\|B(u_h-v_h)\|_H \lesssim h^{1/2}\|u_h-v_h\|_V,$$

while $\|\tilde{B}(x_h-y_h)\|_M \lesssim \|x_h-y_h\|_Z$ if $\Lambda_h\neq M_h$. Thus, in all cases, $\|\tilde{B}(x_h-y_h)\|_M\lesssim h^{s/2}\|x_h-y_h\|_Z$ with $s=1$ if $\Lambda_h=M_h$ and $s=0$ if $\Lambda_h\neq M_h$, and this yields

$$\langle -J_0'(x),\delta_h\rangle_{Z',Z} \lesssim h^{s/2}\|\theta-\Pi_{\Lambda_h}\theta\|_M\|x_h-y_h\|_Z + \eta_{\mathrm{unil}}(q_h)+\eta_{\mathrm{unil}}(q).$$

Collecting the above estimates and using (6.43) together with a Young inequality, it is inferred that

$$\|x_h-y_h\|_Z^2 \lesssim \|x-y_h\|_Z^2 + \eta_{\mathrm{unil}}(q_h) + \eta_{\mathrm{quad}}(q_h)^2 + \eta_{\mathrm{unil}}(q) + h^s\|\theta-\Pi_{\Lambda_h}\theta\|_M^2,$$

whence the bound on $\|x-x_h\|_Z$ follows using a triangle inequality. Finally, to derive the bound on $h^{1/2}\|\theta-\theta_h\|_M$, observe that for $v_h\in V_h$ and since $V_h\subset V$,

$$\begin{aligned}(\theta_h-\Pi_{\Lambda_h}\theta, B_h v_h)_M &= (\theta_h-\Pi_{\Lambda_h}\theta, Bv_h)_M\\ &= (\theta_h-\theta, Bv_h)_M + (\theta-\Pi_{\Lambda_h}\theta, Bv_h)_M\\ &= \langle W'(u)-W'(u_h), v_h\rangle_{V',V} + r(\tilde{B}_h^{\natural}(u-u_h), Bv_h)_M + (\theta-\Pi_{\Lambda_h}\theta, Bv_h-\Pi_{\Lambda_h}Bv_h)_M\\ &\lesssim \|x-x_h\|_Z\|v_h\|_V + \|\theta-\Pi_{\Lambda_h}\theta\|_M\|Bv_h-\Pi_{\Lambda_h}Bv_h\|_M\\ &\lesssim (\|x-x_h\|_Z + h^{1/2}\|\theta-\Pi_{\Lambda_h}\theta\|_M)\|v_h\|_V,\end{aligned}$$

whence the desired estimate results from the discrete inf-sup condition and a triangle inequality.

6.8 Proof of Proposition 6.10

Proof. The couple $(u_h, p_h) \in V_h \times M_h^+$ is such that

$$\left\langle W'(u_h), v_h \right\rangle_{V',V} + (\theta_h, Bv_h)_M + r(Bu_h - p_h, Bv_h)_M = 0, \qquad \forall v_h \in V_h, \tag{6.75}$$

$$(\psi'(p_h), q_h - p_h)_{M_h} - (\theta_h, q_h - p_h)_M - r(Bu_h - p_h, q_h - p_h)_M \geq 0, \quad \forall q_h \in M_h^+, \tag{6.76}$$

$$\theta_h = \theta_h + \rho\left(\Pi_{M_h} Bu_h - p_h\right). \tag{6.77}$$

The couple $(u_h^n, p_h^n) \in V_h \times M_h^+$ is such that

$$\left\langle W'(u_h^n), v_h \right\rangle_{V',V} + (\theta_h^{n-1}, Bv_h)_M + r(Bu_h^n - p_h^{n-1}, Bv_h)_M = 0, \qquad \forall v_h \in V_h, \tag{6.78}$$

$$(\psi'(p_h^n), q_h - p_h^n)_{M_h} - (\theta_h^{n-1}, q_h - p_h^n)_M - r(Bu_h^n - p_h^n, q_h - p_h^n)_M \geq 0, \quad \forall q_h \in M_h^+, \tag{6.79}$$

$$\theta_h^n = \theta_h^{n-1} + \rho\left(\Pi_{M_h} Bu_h^n - p_h^n\right). \tag{6.80}$$

Set $\bar\theta_h^n := \theta_h^n - \theta_h$, $\bar p_h^n := p_h^n - p_h$, and $\bar u_h^n := u_h^n - u_h$. Applying (6.75) and (6.78) to $v_h = \bar u_h^n$ and subtracting yields

$$\left\langle W'(\bar u_h^n), \bar u_h^n \right\rangle_{V',V} + (\bar\theta_h^{n-1}, B\bar u_h^n)_M + r\|B\bar u_h^n\|_M^2 - r(\bar p_h^{n-1}, B\bar u_h^n)_M = 0, \tag{6.81}$$

where the linearity of W' has been used. Similarly, using (6.76) with $q_h = p_h^n$ and (6.79) with $q_h = p_h$ and subtracting leads to

$$(\psi'(p_h^n) - \psi'(p_h), p_h^n - p_h)_{M_h} - (\bar\theta_h^{n-1}, \bar p_h^n)_M + r\|\bar p_h^n\|_M^2 - r(\bar p_h^n, B\bar u_h^n)_M \leq 0. \tag{6.82}$$

Adding (6.81) and (6.82) and setting $\alpha := \alpha_W - 2k_{\psi'} c_M^2 c_B^2$ and $\beta := r - 2k_{\psi'}$ yields

$$\begin{aligned}
-(\bar\theta_h^{n-1}, B\bar u_h^n - \bar p_h^n)_M &\geq \left\langle W'(\bar u_h^n), \bar u_h^n \right\rangle_{V',V} + (\psi'(p_h^n) - \psi'(p_h), p_h^n - p_h)_{M_h} \\
&\quad + r\|B\bar u_h^n - \bar p_h^n\|_M^2 + r(\bar p_h^n - \bar p_h^{n-1}, B\bar u_h^n)_M \\
&\geq \alpha_W \|\bar u_h^n\|_V^2 - k_{\psi'}\|\bar p_h^n\|_M^2 + r\|B\bar u_h^n - \bar p_h^n\|_M^2 + r(\bar p_h^n - \bar p_h^{n-1}, B\bar u_h^n)_M \\
&\geq \alpha_W \|\bar u_h^n\|_V^2 - 2k_{\psi'}\|B\bar u_h^n\|_M^2 - 2k_{\psi'}\|B\bar u_h^n - \bar p_h^n\|_M^2 + r\|B\bar u_h^n - \bar p_h^n\|_M^2 \\
&\quad + r(\bar p_h^n - \bar p_h^{n-1}, B\bar u_h^n)_M \\
&\geq \alpha\|\bar u_h^n\|_V^2 + \beta\|B\bar u_h^n - \bar p_h^n\|_M^2 + r(\bar p_h^n - \bar p_h^{n-1}, B\bar u_h^n)_M.
\end{aligned} \tag{6.83}$$

Adding (6.79) written at iteration $n-1$ with $q_h = p_h^n$ and (6.79) written at iteration n with $q_h = p_h^{n-1}$ and since $\bar p_h^n - \bar p_h^{n-1} = p_h^n - p_h^{n-1}$ and so on, yields

$$\begin{aligned}
-(\bar\theta_h^{n-2} - \bar\theta_h^{n-1}, \bar p_h^n - \bar p_h^{n-1})_M &\geq (\psi'(p_h^n) - \psi'(p_h^{n-1}), p_h^n - p_h^{n-1}) + r\|\bar p_h^n - \bar p_h^{n-1}\|_M^2 \\
&\quad - r(\bar p_h^n - \bar p_h^{n-1}, B\bar u_h^n - B\bar u_h^{n-1})_M \\
&\geq (r - k_{\psi'})\|\bar p_h^n - \bar p_h^{n-1}\|_M^2 - r(\bar p_h^n - \bar p_h^{n-1}, B\bar u_h^n - B\bar u_h^{n-1})_M.
\end{aligned} \tag{6.84}$$

Owing to (6.77) and (6.80) at iteration $(n-1)$,

$$\bar\theta_h^{n-1} = \bar\theta_h^{n-2} + \rho\left(\Pi_{M_h} B\bar u_h^{n-1} - \bar p_h^{n-1}\right), \tag{6.85}$$

whence, owing to (6.84),

$$r(\bar{p}_h^n - \bar{p}_h^{n-1}, B\bar{u}_h^n - B\bar{u}_h^{n-1})_M \geq \beta\|\bar{p}_h^n - \bar{p}_h^{n-1}\|_M^2 - \rho(B\bar{u}_h^{n-1} - \bar{p}_h^{n-1}, \bar{p}_h^n - \bar{p}_h^{n-1})_M. \tag{6.86}$$

This equation can be reorganized as

$$\begin{aligned} r(B\bar{u}_h^n, \bar{p}_h^n - \bar{p}_h^{n-1})_M \geq \beta\|\bar{p}_h^n - \bar{p}_h^{n-1}\|_M^2 + (r-\rho)(B\bar{u}_h^{n-1} - \bar{p}_h^{n-1}, \bar{p}_h^n - \bar{p}_h^{n-1})_M \\ + r(\bar{p}_h^{n-1}, \bar{p}_h^n - \bar{p}_h^{n-1})_M. \end{aligned}$$

Using the identity $2(\bar{p}_h^{n-1}, \bar{p}_h^n - \bar{p}_h^{n-1})_M = \|\bar{p}_h^n\|_M^2 - \|\bar{p}_h^{n-1}\|_M^2 - \|\bar{p}_h^n - \bar{p}_h^{n-1}\|_M^2$, we turn (6.86) into

$$\begin{aligned} 2r(B\bar{u}_h^n, \bar{p}_h^n - \bar{p}_h^{n-1})_M \geq (2\beta - r)\|\bar{p}_h^n - \bar{p}_h^{n-1}\|_M^2 + r(\|\bar{p}_h^n\|_M^2 - \|\bar{p}_h^{n-1}\|_M^2) \\ + 2(r-\rho)(B\bar{u}_h^{n-1} - \bar{p}_h^{n-1}, \bar{p}_h^n - \bar{p}_h^{n-1})_M. \end{aligned} \tag{6.87}$$

Squaring (6.85) at iteration n leads to

$$\|\bar{\theta}_h^{n-1}\|_M^2 - \|\bar{\theta}_h^n\|_M^2 \geq -2\rho(\bar{\theta}_h^{n-1}, B\bar{u}_h^n - \bar{p}_h^n)_M - \rho^2\|B\bar{u}_h^n - \bar{p}_h^n\|_M^2.$$

Finally, collecting (6.83) and (6.87) and using $r \geq \rho$ yields

$$\begin{aligned} \|\bar{\theta}_h^{n-1}\|_M^2 - \|\bar{\theta}_h^n\|_M^2 \geq\ & 2\rho\alpha\|\bar{u}_h^n\|_V^2 + \rho(2\beta-\rho)\|B\bar{u}_h^n - \bar{p}_h^n\|_M^2 + \rho(2\beta - r)\|\bar{p}_h^n - \bar{p}_h^{n-1}\|_M^2 \\ & + r\rho(\|\bar{p}_h^n\|_M^2 - \|\bar{p}_h^{n-1}\|_M^2) + 2\rho(r-\rho)(B\bar{u}_h^{n-1} - \bar{p}_h^{n-1}, \bar{p}_h^n - \bar{p}_h^{n-1})_M \\ \Leftrightarrow (\|\bar{\theta}_h^{n-1}\|_M^2 + r\rho\|\bar{p}_h^{n-1}\|_M^2) - (\|\bar{\theta}_h^n\|_M^2 + r\rho\|\bar{p}_h^n\|_M^2) \geq\ & 2\rho\alpha\|\bar{u}_h^n\|_V^2 + \rho(2\beta-\rho)\|B\bar{u}_h^n - \bar{p}_h^n\|_M^2 \\ & + \rho(2\beta - r)\|\bar{p}_h^n - \bar{p}_h^{n-1}\|_M^2 + 2\rho(r-\rho)(B\bar{u}_h^{n-1} - \bar{p}_h^{n-1}, \bar{p}_h^n - \bar{p}_h^{n-1})_M \\ \Rightarrow (\|\bar{\theta}_h^{n-1}\|_M^2 + r\rho\|\bar{p}_h^{n-1}\|_M^2) - (\|\bar{\theta}_h^n\|_M^2 + r\rho\|\bar{p}_h^n\|_M^2) \geq\ & 2\rho\alpha\|\bar{u}_h^n\|_V^2 + \rho(2\beta-\rho)\|B\bar{u}_h^n - \bar{p}_h^n\|_M^2 \\ & + \rho(2\beta - r)\|\bar{p}_h^n - \bar{p}_h^{n-1}\|_M^2 - \rho(r-\rho)(\|B\bar{u}_h^{n-1} - \bar{p}_h^{n-1}\|_M^2 + \|\bar{p}_h^n - \bar{p}_h^{n-1}\|_M^2). \end{aligned} \tag{6.88}$$

Set $\epsilon^n = \|\bar{\theta}_h^n\|_M^2 + r\rho\|\bar{p}_h^n\|_M^2 + \rho(r-\rho)\|B\bar{u}_h^n - \bar{p}_h^n\|_M^2$ so that (6.88) can be rewritten as

$$\epsilon^{n-1} - \epsilon^n \geq\ 2\rho\alpha\|\bar{u}_h^n\|_V^2 + \rho(2\beta - r)\|B\bar{u}_h^n - \bar{p}_h^n\|_M^2 + \rho(2\beta - 2r + \rho)\|\bar{p}_h^n - \bar{p}_h^{n-1}\|_M^2. \tag{6.89}$$

By assumption, $\alpha > 0$, $2\beta - r > 0$, and $2\beta - 2r + \rho = \rho - 4k_{\psi'} \geq 0$. Hence, the sequence $(\epsilon^n)_{n\in\mathbb{N}}$, which is clearly nonnegative, is decreasing; thus it converges. As a consequence, the right-hand side of (6.89) converges to zero, implying that the sequences $(u_h^n)_{n\in\mathbb{N}}$ and $(p_h^n)_{n\in\mathbb{N}}$ converge to u_h and p_h respectively. Finally, the sequence $(\theta_h^n)_{n\in\mathbb{N}}$ is bounded. According to the Bolzano–Weierstrass theorem, there exists a converging subsequence. By uniqueness of the discrete solution (u_h, p_h, θ_h), the whole sequence $(\theta_h^n)_{n\in\mathbb{N}}$ converges to θ_h.

7

Conclusion et perspectives

Dans cette thèse, nous avons proposé et analysé des méthodes numériques pour des problèmes de contact et de fissuration en dynamique. Pour les problèmes de contact, nous avons d'abord comparé les principales méthodes proposées dans la littérature. Nous nous sommes ensuite concentrés sur la méthode de masse modifiée. Celle-ci élimine les oscillations parasites, offre un bon comportement énergétique et peut s'adapter à n'importe quel schéma en temps. De plus, elle se programme relativement facilement et ne nécessite ni d'étape de calcul supplémentaire ni de paramètres supplémentaires. La méthode de masse modifiée apparaît donc comme une des meilleures méthodes pour les problèmes de contact en dynamique. Dans cette thèse, nous avons contribué à son analyse (convergence vers une solution continue dans le cas viscoélastique, analyse des formulations semi-discrètes et discrètes dans le cas du frottement de Coulomb) et proposé une variante semi-explicite. Plusieurs développements sont encore envisageables. Premièrement, la méthode semi-explicite que nous avons proposée dans le cas du contact sans frottement, pourrait être étendue au cas du frottement de Coulomb. Deuxièmement, dans un article récent [107], Y. Renard propose une extension de la méthode de masse modifiée à une structure mince, en l'occurence une membrane avec obstacle. Il serait donc intéressant d'appliquer cette approche à d'autres structures minces (plaques, coques). Enfin, l'application de la méthode de masse modifiée à des problèmes en grandes déformations ou en grands déplacements n'est pas immédiate. En effet, l'orientation des conditions de contact peut évoluer au cours de la simulation. S'il s'agit d'un problème de contact sans frottement, l'utilisation de la méthode de masse modifiée ne pose pas de problèmes puisqu'on peut retirer toute la masse associée aux nœuds de la frontière. En revanche, s'il s'agit d'un problème avec frottement de Coulomb, il faut garder la masse associée aux déplacements tangentiels et donc modifier la matrice de masse au cours de la simulation, ce qui pourrait poser des problèmes numériques. Concernant l'analyse de la méthode, en 2D et en 3D, dans le cas d'un solide viscoélastique, nous avons montré un résultat de convergence de la méthode de masse modifiée. En 1D, il doit être possible d'obtenir des résultats plus précis (convergence forte, taux de convergence). Il serait également intéressant d'établir des résultats de convergence pour les structures minces.

Dans la deuxième partie de cette thèse, nous avons étudié un modèle de fissuration dynamique combinant un chemin de fissuration pré-défini et des zones cohésives. Nous avons proposé et analysé des schémas en temps quasi-explicites pour ce modèle. Ce type de modèle permet de représenter un comportement assez riche de la fissure (différents modes de rupture, contact et frottement après décohésion, etc...). En revanche, il ne permet pas de prédire le trajet de fissura-

tion, le branchement d'une fissure ou la multi-fissuration. Il est certes possible d'insérer une zone cohésive entre tous les éléments du maillage. Mais cette approche s'avère très sensible au maillage (voir les exemples de simulations dans [120]). De plus, on se sait pas bien quel modèle continu on tente d'approcher en insérant une zone cohésive entre tous les éléments du maillage. L'approche variationnelle proposée par G. Francfort et J.-J. Marigo est, à notre avis, une meilleure approche pour prédire le trajet, le branchement ou la multi-fissuration. Cette approche a été initialement développée pour des problèmes quasi-statiques. Des travaux récents proposent une extension au cas dynamique (Bourdin, Larsen & Richardson [13] Larsen [85], Larsen, Ortner & Süli [86]). Les premiers résultats numériques sont prometteurs. Il serait intéressant d'explorer cette voie, tant sur le plan de la modélisation (modèles intégrant une viscosité) que de l'analyse mathématique ou de la résolution numérique (choix des schémas d'intégration en temps notamment).

References

[1] P. Alart and A. Curnier. A mixed formulation for frictional contact problems prone to Newton like solution methods. *Comput. Methods Appl. Mech. Engrg.*, 92(3):353–375, 1991.

[2] F. Armero and E. Petocz. Formulation and analysis of conserving algorithms for frictionless dynamic contact/impact problems. *Comput. Methods Appl. Mech. Engrg.*, 158(3-4):269 – 300, 1998.

[3] J.-P. Aubin and H. Frankowska. *Set-valued analysis*, volume 2 of *Systems & Control: Foundations & Applications*. Birkhäuser Boston Inc., Boston, MA, 1990.

[4] Y. Ayyad, M. Barboteu, and J. Fernandez. A frictionless viscoelastodynamic contact problem with energy consistent properties: Numerical analysis and computational aspects. *Comput. Methods Appl. Mech. Engrg.*, 198(5-8):669 – 679, 2009.

[5] P. Ballard and S. Basseville. Existence and uniqueness for dynamical unilateral contact with Coulomb friction: a model problem. *M2AN Math. Model. Numer. Anal.*, 39(1):59–77, 2005.

[6] G. Barenblatt. The formation of brittle cracks during brittle fracture. General ideas and hypotheses. Axially-symmetric cracks. *Appl. Math. Mech*, 23:1273–1282, 1959.

[7] G. Barenblatt. The mathematical theory of equilibrium cracks in brittle fracture. *Advances in applied mechanics*, 7(2):55–129, 1962.

[8] K. J. Bathe and F. Brezzi. Stability of finite element mixed interpolations for contact problems. *Atti Accad. Naz. Lincei Cl. Sci. Fis. Mat. Natur. Rend. Lincei (9) Mat. Appl.*, 12:167–183 (2002), 2001.

[9] T. Belytschko and M. Neal. Contact-impact by the pinball algorithm with penalty and lagrangian methods. *International Journal for Numerical Methods in Engineering*, 31(3):547–572, MAR 1991.

[10] D. P. Bertsekas. *Constrained Optimization and Lagrange Multiplier Methods*. Athena Scientific, 1982.

[11] D. P. Bertsekas. *Nonlinear Programming*. Athena Scientific, 1999.

[12] B. Bourdin, G. A. Francfort, and J.-J. Marigo. The variational approach to fracture. *J. Elasticity*, 91(1-3):5–148, 2008.

[13] B. Bourdin, C. J. Larsen, and C. L. Richardson. A time-discrete model for dynamic fracture based on crack regularization. Technical report, 2009.

[14] H. Brézis. *Opérateurs maximaux monotones et semi-groupes de contractions dans les espaces de Hilbert*. North-Holland Publishing Co., Amsterdam, 1973.

[15] H. Brezis. *Analyse fonctionnelle: théorie et applications*. Masson, 1983.

[16] H. Brézis and J.-L. Lions. Sur certains problèmes unilatéraux hyperboliques. *C. R. Acad. Sci. Paris Sér. A-B*, 264:A928–A931, 1967.

[17] K. Broberg. *Cracks and fracture*. Academic Pr, 1999.

[18] B. Brogliato. *Nonsmooth impact mechanics*, volume 220 of *Lecture Notes in Control and Information Sciences*. Springer-Verlag London Ltd., London, 1996. Models, dynamics and control.

[19] H. Bui and P. Germain. *Mécanique de la rupture fragile*. Masson Paris, 1978.

[20] F. Cagnetti. A vanishing viscosity approach to fracture growth in a cohesive zone model with prescribed crack path. *Math. Models Methods Appl. Sci.*, 18(7):1027–1071, 2008.

[21] G. T. Camacho and M. Ortiz. Computational modelling of impact damage in brittle materials. *International Journal of Solids and Structures*, 33(20-22):2899 – 2938, 1996.

[22] N. Carpenter, R. Taylor, and M. Katona. Lagrange constraints for transcient finite element surface contact. *Int. J. Numer. Meth. Engng*, 32:103–128, 1991.

[23] L. Champaney, J.-Y. Cognard, and P. Ladevèze. Modular analysis of assemblages of three-dimensional structures with unilateral contact conditions. *Computers & Structures*, 73:249–266, 1999.

[24] Z. Chen. On the augmented Lagrangian approach to Signorini elastic contact problem. *Numer. Math.*, 88(4):641–659, 2001.

[25] P. G. Ciarlet. *Mathematical elasticity. Vol. I*, volume 20 of *Studies in Mathematics and its Applications*. North-Holland Publishing Co., Amsterdam, 1988. Three-dimensional elasticity.

[26] F. H. Clarke. *Optimization and nonsmooth analysis*, volume 5 of *Classics in Applied Mathematics*. Society for Industrial and Applied Mathematics (SIAM), Philadelphia, PA, second edition, 1990.

[27] M. Cocou. Existence of solutions of a dynamic Signorini's problem with nonlocal friction in viscoelasticity. *Z. Angew. Math. Phys.*, 53(6):1099–1109, 2002. Dedicated to Eugen Soós.

[28] G. Cohen, P. Joly, J. Roberts, and N. Tordjman. Higher order triangular finite elements with mass lumping for the wave equation. *SIAM Journal on Numerical Analysis*, 38(6):2047–2078, 2001.

[29] R. Courant and D. Hilbert. *Methods of mathematical physics. Vol. I*. Interscience Publishers, Inc., New York, N.Y., 1953.

[30] G. Dal Maso and C. Zanini. Quasi-static crack growth for a cohesive zone model with prescribed crack path. *Proc. Roy. Soc. Edinburgh Sect. A*, 137(2):253–279, 2007.

[31] K. Deimling. *Multivalued differential equations*, volume 1 of *de Gruyter Series in Nonlinear Analysis and Applications*. Walter de Gruyter & Co., Berlin, 1992.

[32] Z. Denkowski, S. Migórski, and N. S. Papageorgiou. *An introduction to nonlinear analysis: applications*. Kluwer Academic Publishers, Boston, MA, 2003.

[33] P. Deuflhard, R. Krause, and S. Ertel. A contact-stabilized Newmark method for dynamical contact problems. *Int. J. Numer. Methods Engrg.*, 73(9):1274–1290, 2008.

[34] D. Doyen and A. Ern. Analysis of the modified mass method for the dynamic Signorini problem with Coulomb friction. *submitted*.

[35] D. Doyen and A. Ern. Convergence of a space semi-discrete modified mass method for the dynamic Signorini problem. *Commun. Math. Sci.*, 7(4):1063–1072, 2009.

[36] D. Doyen, A. Ern, and S. Piperno. Time-integration schemes for the finite element dynamic Signorini problem. *submitted*.

[37] D. Doyen, A. Ern, and S. Piperno. A three-field augmented Lagrangian formulation of unilateral contact problems with cohesive forces. *ESAIM, Math. Model. Numer. Anal.*, 44(2):323–346, 2010.

[38] D. Doyen, A. Ern, and S. Piperno. A semi-explicit modified mass method for dynamic contact problems. Lectures Notes in Applied and Computational Mechanics. Springer, 2010.

[39] D. S. Dugdale. Yielding of steel sheets containing slits. *Journal of the Mechanics and Physics of Solids*, 8(2):100 – 104, 1960.

[40] G. Duvaut and J.-L. Lions. *Inequalities in mechanics and physics*. Springer-Verlag, Berlin, 1976. Translated from the French by C. W. John, Grundlehren der Mathematischen Wissenschaften, 219.

[41] C. Eck, J. Jarušek, and M. Krbec. *Unilateral contact problems*, volume 270 of *Pure and Applied Mathematics (Boca Raton)*. Chapman & Hall/CRC, Boca Raton, FL, 2005. Variational methods and existence theorems.

[42] I. Ekeland and R. Témam. *Convex analysis and variational problems*, volume 28 of *Classics in Applied Mathematics*. Society for Industrial and Applied Mathematics (SIAM), Philadelphia, PA, english edition, 1999. Translated from the French.

[43] M. Elices, G. Guinea, J. Gomez, and J. Planas. The cohesive zone model: advantages, limitations and challenges. *Engineering Fracture Mechanics*, 69(2):137–163, 2002.

[44] A. Ern and J.-L. Guermond. *Theory and Practice of Finite Elements*, volume 159 of *Applied Mathematical Sciences*. Springer-Verlag, New York, 2004.

[45] L. C. Evans and R. F. Gariepy. *Measure theory and fine properties of functions*. Studies in Advanced Mathematics. CRC Press, Boca Raton, FL, 1992.

[46] M. Falk, A. Needleman, and J. Rice. A critical evaluation of cohesive zone models of dynamic fractur. *Le Journal de Physique IV*, 11(PR5), 2001.

[47] G. Fichera. Problemi elastostatici con vincoli unilaterali: Il problema di Signorini con ambigue condizioni al contorno. *Atti Accad. Naz. Lincei Mem. Cl. Sci. Fis. Mat. Natur. Sez. I (8)*, 7:91–140, 1963/1964.

[48] A. F. Filippov. *Differential equations with discontinuous righthand sides*, volume 18 of *Mathematics and its Applications (Soviet Series)*. Kluwer Academic Publishers Group, Dordrecht, 1988. Translated from the Russian.

[49] M. Fortin and R. Glowinski. *Augmented Lagrangian methods*, volume 15 of *Studies in Mathematics and its Applications*. North-Holland Publishing Co., Amsterdam, 1983.

[50] M. Frémond. Contact with adhesion. In *Topics in nonsmooth mechanics*, pages 157–185. Birkhäuser, Basel, 1988.

[51] L. B. Freund. *Dynamic fracture mechanics*. Cambridge Monographs on Mechanics and Applied Mathematics. Cambridge University Press, Cambridge, 1990.

[52] R. Glowinski and P. Le Tallec. *Augmented Lagrangian and operator-splitting methods in nonlinear mechanics*, volume 9 of *SIAM Studies in Applied Mathematics*. Society for Industrial and Applied Mathematics (SIAM), Philadelphia, PA, 1989.

[53] R. Glowinski, J.-L. Lions, and R. Trémolières. *Numerical analysis of variational inequalities*, volume 8 of *Studies in Mathematics and its Applications*. North-Holland Publishing Co., Amsterdam, 1981.

[54] R. Glowinski, L. Shiau, Y. M. Kuo, and G. Nasser. The numerical simulation of friction constrained motions. I. One degree of freedom models. *Appl. Math. Lett.*, 17(7):801–807, 2004.

[55] R. Glowinski, L. Shiau, Y. M. Kuo, and G. Nasser. The numerical simulation of friction constrained motions. II. Multiple degrees of freedom models. *Appl. Math. Lett.*, 18(10):1108–1115, 2005.

[56] E. Grosu and I. Harari. Stability of semidiscrete formulations for elastodynamics at small time steps. *Finite Elements in Analysis and Design*, 43(6-7):533 – 542, 2007.

[57] C. Hager, S. Hüeber, and B. I. Wohlmuth. A stable energy-conserving approach for frictional contact problems based on quadrature formulas. *Internat. J. Numer. Methods Engrg.*, 73(2):205–225, 2008.

[58] C. Hager and B. I. Wohlmuth. Analysis of a space-time discretization for dynamic elasticity problems based on mass-free surface elements. *SIAM J. Numer. Anal.*, 47(3):1863–1885, 2009.

[59] E. Hairer, C. Lubich, and G. Wanner. *Geometric numerical integration*, volume 31 of *Springer Series in Computational Mathematics*. Springer-Verlag, Berlin, 2002. Structure-preserving algorithms for ordinary differential equations.

[60] W. Han and M. Sofonea. *Quasistatic contact problems in viscoelasticity and viscoplasticity*, volume 30 of *AMS/IP Studies in Advanced Mathematics*. American Mathematical Society, Providence, RI, 2002.

[61] J. Haslinger, I. Hlaváček, and J. Nečas. Numerical methods for unilateral problems in solid mechanics. In *Handbook of numerical analysis, Vol. IV*, Handb. Numer. Anal., IV, pages 313–485. North-Holland, Amsterdam, 1996.

[62] P. Hauret. Mixed interpretation and extensions of the Khenous-Laborde-Renard mass lumping approach for elastodynamics with contact. Technical report, 2010.

[63] P. Hauret and P. Le Tallec. Energy-controlling time integration methods for nonlinear elastodynamics and low-velocity impact. *Comput. Methods Appl. Mech. Engrg.*, 195(37-40):4890–4916, 2006.

[64] P. Hauret and P. Le Tallec. A discontinuous stabilized mortar method for general 3d elastic problems. *Computer Methods in Applied Mechanics and Engineering*, 196:4881–4900, 2007.

[65] F. Hecht and O. Pironneau. Freefem++. www.freefem.org.

[66] P. Hild and P. Laborde. Quadratic finite element methods for unilateral contact problems. *Appl. Numer. Math.*, 41(3):401–421, 2002.

[67] P. Hild and Y. Renard. Local uniqueness and continuation of solutions for the discrete Coulomb friction problem in elastostatics. *Quart. Appl. Math.*, 63(3):553–573, 2005.

[68] J.-B. Hiriart-Urruty and C. Lemaréchal. *Fundamentals of convex analysis*. Grundlehren Text Editions. Springer-Verlag, Berlin, 2001.

[69] S. Hüeber and B. I. Wohlmuth. An optimal a priori error estimate for nonlinear multibody contact problems. *SIAM J. Numer. Anal.*, 43(1):156–173 (electronic), 2005.

[70] T. J. R. Hughes. *The finite element method*. Prentice Hall Inc., Englewood Cliffs, NJ, 1987. Linear static and dynamic finite element analysis, With the collaboration of Robert M. Ferencz and Arthur M. Raefsky.

[71] P. Jaillet, D. Lamberton, and B. Lapeyre. Variational inequalities and the pricing of american options. *Acta Applicandae Mathematicae*, 21:263–289, 1990. 10.1007/BF00047211.

[72] C. Kane, E. A. Repetto, M. Ortiz, and J. E. Marsden. Finite element analysis of nonsmooth contact. *Comput. Methods Appl. Mech. Engrg.*, 180(1-2):1–26, 1999.

[73] H. Khenous. *Problèmes de contact unilatéral avec frottement de Coulomb en élastostatique et élastodynamique. Etude mathématique et résolution numérique.* PhD thesis, INSA de Toulouse, 2005.

[74] H. B. Khenous, P. Laborde, and Y. Renard. Comparison of two approaches for the discretization of elastodynamic contact problems. *Comptes Rendus Mathematique*, 342(10):791 – 796, 2006.

[75] H. B. Khenous, P. Laborde, and Y. Renard. Mass redistribution method for finite element contact problems in elastodynamics. *Eur. J. Mech. A Solids*, 27(5):918–932, 2008.

[76] N. Kikuchi and J. T. Oden. *Contact problems in elasticity: a study of variational inequalities and finite element methods*, volume 8 of *SIAM Studies in Applied Mathematics*. Society for Industrial and Applied Mathematics (SIAM), Philadelphia, PA, 1988.

[77] D. Kinderlehrer. Remarks about Signorini's problem in linear elasticity. *Ann. Scuola Norm. Sup. Pisa Cl. Sci. (4)*, 8(4):605–645, 1981.

[78] D. Kinderlehrer and G. Stampacchia. *An introduction to variational inequalities and their applications*. Society for Industrial Mathematics, 2000.

[79] C. Klapproth, A. Schiela, and P. Deuflhard. Consistency results for the contact-stabilized Newmark method. *Numer. Math.*, 116(1):65–94, 2010.

[80] R. Krause and M. Walloth. Presentation and comparison of selected algorithms for dynamic contact based on the Newmark scheme. Technical report, ICS.

[81] A. S. Kravchuk and P. J. Neittaanmäki. *Variational and quasi-variational inequalities in mechanics*, volume 147 of *Solid Mechanics and its Applications*. Springer, Dordrecht, 2007.

[82] S. Krenk. Energy conservation in Newmark based time integration algorithms. *Comput. Methods Appl. Mech. Engrg.*, 195(44-47):6110–6124, 2006.

[83] K. Kunisch and G. Stadler. Generalized Newton methods for the 2D-Signorini contact problem with friction in function space. *M2AN Math. Model. Numer. Anal.*, 39(4):827–854, 2005.

[84] P. Ladevèze. *Nonlinear Computational Structural Mechanics - New Approaches and Non-Incremental Methods of Calculation*. Springer-Verlag, 1999.

[85] C. J. Larsen. Models for dynamic fracture based on griffith's criterion. IUTAM Symposium on Variational Concepts with Applications to the Mechanics of Materials. Springer, 2010.

[86] C. J. Larsen, C. Ortner, and E. Süli. Existence of solutions to a regularized model of dynamic fracture. *Math. Models Methods Appl. Sci.*, 20(7):1021–1048, 2010.

[87] T. A. Laursen. *Computational contact and impact mechanics*. Springer-Verlag, Berlin, 2002. Fundamentals of modeling interfacial phenomena in nonlinear finite element analysis.

[88] T. A. Laursen and V. Chawla. Design of energy conserving algorithms for frictionless dynamic contact problems. *Internat. J. Numer. Methods Engrg.*, 40(5):863–886, 1997.

[89] T. A. Laursen and G. R. Love. Improved implicit integrators for transient impact problems—geometric admissibility within the conserving framework. *Internat. J. Numer. Methods Engrg.*, 53(2):245–274, 2002.

[90] B. Lawn. *Fracture of brittle solids*. Cambridge Univ Pr, 1993.

[91] G. Lebeau and M. Schatzman. A wave problem in a half-space with a unilateral constraint at the boundary. *J. Differential Equations*, 53(3):309–361, 1984.

[92] J.-L. Lions and E. Magenes. *Non-homogeneous boundary value problems and applications. Vol. I*. Springer-Verlag, New York, 1972.

[93] E. Lorentz. A mixed interface finite element for cohesive zone models. *Computer Methods in Applied Mechanics and Engineering*, 198:302–317, 2008.

[94] M. Marcus and V. J. Mizel. Every superposition operator mapping one Sobolev space into another is continuous. *J. Funct. Anal.*, 33(2):217–229, 1979.

[95] J.-J. Marigo and L. Truskinovsky. Initiation and propagation of fracture in the models of Griffith and Barenblatt. *Contin. Mech. Thermodyn.*, 16(4):391–409, 2004.

[96] J. Mazars. Application de la mécanique de l'endommagement au comportement non linéaire et à la rupture du béton de structure. *These de Doctorat d'Etat*.

[97] J. J. Moreau. Numerical aspects of the sweeping process. *Comput. Methods Appl. Mech. Engrg.*, 177(3-4):329–349, 1999. Computational modeling of contact and friction.

[98] M. Moussaoui and K. Khodja. Régularité des solutions d'un problème mêlé Dirichlet-Signorini dans un domaine polygonal plan. *Comm. Partial Differential Equations*, 17(5-6):805–826, 1992.

[99] R. H. Nochetto and L. B. Wahlbin. Positivity preserving finite element approximation. *Math. Comp.*, 71(240):1405–1419 (electronic), 2002.

[100] N. Nsiampa, J.-P. Ponthot, and L. Noels. Comparative study of numerical explicit schemes for impact problems. *International Journal of Impact Engineering*, 35(12):1688 – 1694, 2008.

[101] A. Pandolfi, P. R. Guduru, M. Ortiz, and A. J. Rosakis. Three dimensional cohesive-element analysis and experiments of dynamic fracture in c300 steel. *International Journal of Solids and Structures*, 37(27):3733 – 3760, 2000.

[102] L. Paoli and M. Schatzman. A numerical scheme for impact problems. I. The one-dimensional case. *SIAM J. Numer. Anal.*, 40(2):702–733 (electronic), 2002.

[103] L. Paoli and M. Schatzman. A numerical scheme for impact problems. II. The multidimensional case. *SIAM J. Numer. Anal.*, 40(2):734–768 (electronic), 2002.

[104] L. Q. Qi and J. Sun. A nonsmooth version of Newton's method. *Math. Programming*, 58(3, Ser. A):353–367, 1993.

[105] K. Ravi-Chandar and W. Knauss. An experimental investigation into dynamic fracture: III. On steady-state crack propagation and crack branching. *International Journal of Fracture*, 26(2):141–154, 1984.

[106] P.-A. Raviart and J.-M. Thomas. *Introduction à l'analyse numérique des équations aux dérivées partielles*. Collection Mathématiques Appliquées pour la Maîtrise. [Collection of Applied Mathematics for the Master's Degree]. Masson, Paris, 1983.

[107] Y. Renard. The singular dynamic method for constrained second order hyperbolic equations: application to dynamic contact problems. *J. Comput. Appl. Math.*, 234(3):906–923, 2010.

[108] J. Rice. The mechanics of earthquake rupture. *Physics of the Earthï¿½s Interior*, pages 555–649, 1980.

[109] W. Rudin. *Real and complex analysis*. McGraw-Hill Book Co., New York, third edition, 1987.

[110] O. Samudrala, Y. Huang, and A. J. Rosakis. Subsonic and intersonic mode ii crack propagation with a rate-dependent cohesive zone. *Journal of the Mechanics and Physics of Solids*, 50(6):1231 – 1268, 2002.

[111] M. Schatzman and M. Bercovier. Numerical approximation of a wave equation with unilateral constraints. *Math. Comp.*, 53(187):55–79, 1989.

[112] E. Sharon, S. Gross, and J. Fineberg. Energy dissipation in dynamic fracture. *Physical review letters*, 76(12):2117–2120, 1996.

[113] L. Slimane, A. Bendali, and P. Laborde. Mixed formulations for a class of variational inequalities. *M2AN Math. Model. Numer. Anal.*, 38(1):177–201, 2004.

[114] G. V. Smirnov. *Introduction to the theory of differential inclusions*, volume 41 of *Graduate Studies in Mathematics*. American Mathematical Society, Providence, RI, 2002.

[115] M. Sofonea, W. Han, and M. Shillor. *Analysis and approximation of contact problems with adhesion or damage*, volume 276 of *Pure and Applied Mathematics (Boca Raton)*. Chapman & Hall/CRC, Boca Raton, FL, 2006.

[116] D. E. Stewart. Rigid-body dynamics with friction and impact. *SIAM Rev.*, 42(1):3–39 (electronic), 2000.

[117] C. Talon and A. Curnier. A model of adhesion coupled to contact and friction. *European Journal of Mechanics - A/Solids*, 22(4):545 – 565, 2003.

[118] R. Taylor and P. Papadopoulos. On a finite element method for dynamic contact/impact problems. *Int. J. Numer. Meth. Engng*, 36:2123–2140, 1993.

[119] R. Temam. *Navier-Stokes equations. Theory and numerical analysis*. North-Holland Publishing Co., Amsterdam, 1977. Studies in Mathematics and its Applications, Vol. 2.

[120] M. G. A. Tijssens, B. L. J. Sluys, and E. van der Giessen. Numerical simulation of quasi-brittle fracture using damaging cohesive surfaces. *European Journal of Mechanics - A/Solids*, 19(5):761 – 779, 2000.

[121] D. Vola, E. Pratt, M. Jean, and M. Raous. Consistent time discretization for dynamical contact problems and complementarity techniques. *Rev. Europ. Elém. Finis*, 7(1-3):149–162, 1998.

[122] T. Warburton and J. S. Hesthaven. On the constants in *hp*-finite element trace inverse inequalities. *Comput. Methods Appl. Mech. Engrg.*, 192(25):2765–2773, 2003.

[123] J. R. Willis. A comparison of the fracture criteria of griffith and barenblatt. *Journal of the Mechanics and Physics of Solids*, 15(3):151 – 162, 1967.

[124] P. Wriggers. *Computational Contact Mechanics*. John Wiley & Sons Ltd., 2002.

[125] X.-P. Xu and A. Needleman. Numerical simulations of fast crack growth in brittle solids. *Journal of the Mechanics and Physics of Solids*, 42(9):1397 – 1434, 1994.

[126] F. Zhou, J.-F. Molinari, and T. Shioya. A rate-dependent cohesive model for simulating dynamic crack propagation in brittle materials. *Engineering Fracture Mechanics*, 72(9):1383 – 1410, 2005.